75-17,507

CAMISA, Raymond Louis, 1942-
MICROWAVE METAL-INSULATOR-SEMICONDUCTOR VARACTORS.

The City University of New York, Ph.D., 1975
Engineering, electrical

Xerox University Microfilms, Ann Arbor, Michigan 48106

MICROWAVE METAL-INSULATOR-SEMICONDUCTOR VARACTORS

by

Raymond L. Camisa

A dissertation submitted to the Graduate Faculty in Electrical Engineering in partial fulfillment of the requirements for the degree of Doctor of Philosophy, the City University of New York.

1975

This manuscript has been read and accepted for the Graduate Faculty in Engineering in satisfaction of the dissertation requirement for the degree of Doctor of Philosophy.

3/13/75
Date

Chairman of Examining Committee

3/13/75
Date

Executive Officer

S. J. Oh

J. S. Nadan

P. Karmel

M. Ettenberg
Supervisory Committee

City University of New York

ABSTRACT

MICROWAVE METAL-INSULATOR-SEMICONDUCTOR VARACTORS

By

Raymond L. Camisa

Advisor: Professor Morris Ettenberg

In this dissertation the characteristics of Metal-Insulator-Semiconductor (MIS) varactors are studied theoretically and experimentally. A numerical model for the small signal impedance of a one dimensional MIS structure is developed. The solution is valid for non-degenerate semiconductors with arbitrary impurity profiles. The solution proceeds by first solving for the steady state electrostatic potential everywhere in the structure. Laplace's equation is specified in the insulator, Poisson's equation in the semiconductor, and boundary conditions at the ends and interface point. The resulting mathematical formulation is a mixed linear - nonlinear boundary value problem and a quasilinearization algorithm is used to obtain a numerical solution. Once the electrostatic problem is solved the microwave impedance may be calculated by perturbing the d.c. solution with a small sinusoidal signal. The basic equations are linearized about the d.c. operating point resulting in three coupled linear second order differential equations. The sinusoidal steady state problem is set up as a linear boundary value problem which may be solved for without iteration.

The numerical program developed is then used to study MIS varactors made on epitaxial substrates. Silicon MIS varactors are fabricated and compared to theoretical calculations. It is shown that high Q varactors are possible using this technology but also MIS varactors have unique characteristics which may be exploited in certain microwave applications. The use of MIS varactors in microwave digital phase shifters and low noise parametric amplifiers is further investigated. Microwave circuits using silicon MIS varactors are developed and studied.

ACKNOWLEDGMENTS

I gratefully acknowledge the influence of Professor Morris Ettenberg on my career as a student and practicing microwave engineer. It was his sound understanding of basic principles and eagerness to teach which gave me direction. He also believed in me when others doubted and for this I will always be indebted.

I would like to thank Professor Joseph Nadan for encouraging me to enter the Doctoral program and for providing an ear when it was needed.

I would also like to thank Demos and Elaine Eitzer for being there when Judy and I needed them. I believe they love us for what we are unselfishly. Demos taught me many things, but most of all he taught me to see the beauty when I didn't feel beautiful. I am proud of his many accomplishments, and if I am not truly his friend it is because I am envious of him.

To my wife, who shares this life with me, if this work is any accomplishment it is equally yours. I thank you for your love and I pledge to continue to strive for growth with you.

To Mom and Dad, thank you for encouraging me to go to school, but most of all for your patience and loving support.

I wish to acknowledge S. Yuan, Ben Hitch and Dr. Pan of the RCA Advance Communications Laboratory, Somerville, N.J. Ben did much of the circuit work on the phase shifter and paramp. Steve provided interest and encouragement for my ideas and generated the enthusiasm to sell them. Dr. Pan believed in me enough to hire me as a consultant for the last three years of graduate study.

This work was supported in part by grants from RCA (F30602-73-C-0107), C.U.N.Y. Research Foundation (R.F. 1265), and the National Science Foundation (GK 13160).

TABLE OF CONTENTS

TABLE OF CONTENTS (CONT'D)

LIST OF TABLES

LIST OF ILLUSTRATIONS

LIST OF ILLUSTRATIONS (CONT'D)

LIST OF ILLUSTRATIONS (CONT'D)

LIST OF ILLUSTRATIONS (CONT'D)

LIST OF ILLUSTRATIONS (CONT'D)

CHAPTER 1

INTRODUCTION TO METAL INSULATOR SEMICONDUCTOR VARACTORS

1.1 Basic Structure

Figure 1.1 shows a metal-insulator-semiconductor (MIS) varactor one dimensional cross section. Embodied in this sketch are two similar but distinctive varactors described in the literature:

(a) surface varactor

(b) space charge varactor

The surface varactor operates in a depletion mode and corresponds to the case of a low resistivity epitaxial layer. When a d.c. reverse bias is applied, the surface of the semiconductor at the insulator-semiconductor (I-S) interface is depleted of majority carriers forming a series connection of a fixed insulator capacitance and variable depletion capacitance. The space charge varactor operates in an accumulation or carrier injection mode, corresponding to the case of a high resistivity epitaxial layer. The capacitance of this device is varied by forward biasing and injecting carriers from the substrate into the epitaxial (semi-insulating region). In both modes of operation, very little direct current flows because of the insulating barrier.

The physical picture for both structures is actually more complicated because for no d.c. current the product of holes and electrons at every point in the semiconductor must equal a constant (n_i^2). Therefore, when the surface of a semiconductor is depleted of majority carriers, there will be a build-up of minority carriers. For a strong reverse bias the minority carriers will dominate and the resulting charge layer is called an inversion layer. For the N type semiconductor shown in Figure 1.1 the inversion layer would be a thin layer of holes at the

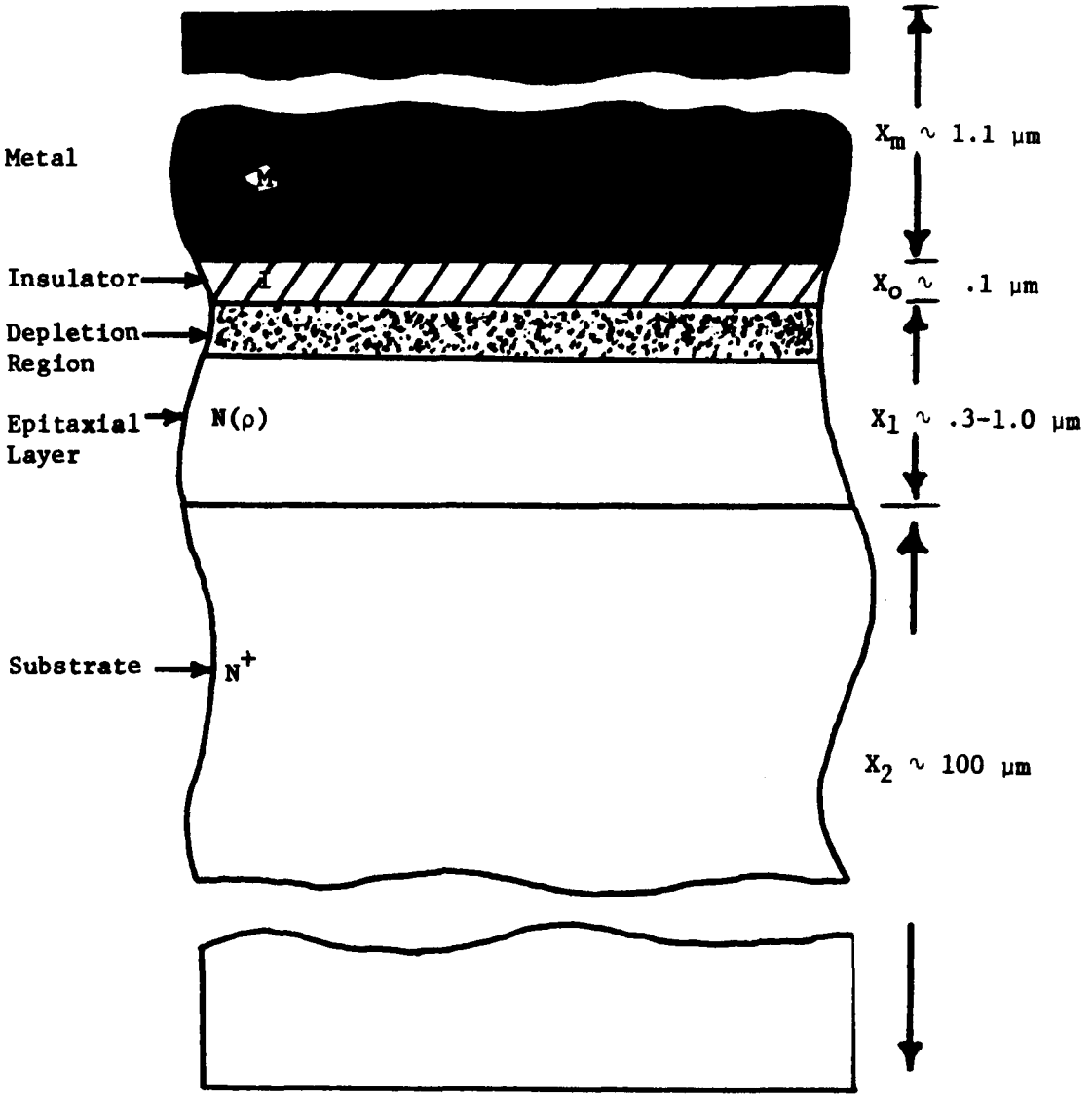

Figure 1.1 Metal insulator semiconductor varactor - one dimensional cross section:
(a) surface varactor ρ - low resistivity.
(b) space charge varactor ρ - high resistivity.

S-I interface. Once the inversion layer forms, any further reverse bias increases the density of minority carriers in the inversion layer and the depletion thickness no longer increases. The inversion layer response to applied signals is important in that it determines MIS terminal characteristics. Figure 1.2 describes MIS capacitance versus voltage characteristics. At zero bias there is no depletion layer and the total capacitance is the insulator capacitance. When a depletion layer is formed the capacitance decreases until a maximum depletion depth is reached due to inversion. For further reverse bias the path that the capacitance characteristic takes depends on the type of measuring signal. For a very low frequency small signal (<100 Hz) the inversion layer responds to variations in the small signal and, since it appears at the S-I interface, the capacitance curve relaxes to the insulator value (C_H). For a high frequency small signal the inversion layer cannot follow since the minority carriers are generated thermally, which is a very slow process. But, the d.c. inversion layer is still there preventing further depletion into the semiconductor and therefore the capacitance stays at C_L. For a large high frequency signal the inversion layer is never formed because the instantaneous value of potential required to generate the minority carriers is not present long enough. Therefore, as reverse bias is applied, the semiconductor depletes further and further, similar to a conventional varactor. The resistance characteristics for MIS structures are similar to the capacitance curves. The resistance corresponds to ohmic losses from the edge of the depletion layer to the substrate. Losses in the substrate should be negligible because of its low resistivity ($\tilde{\sim}$ .005 Ω-cm).

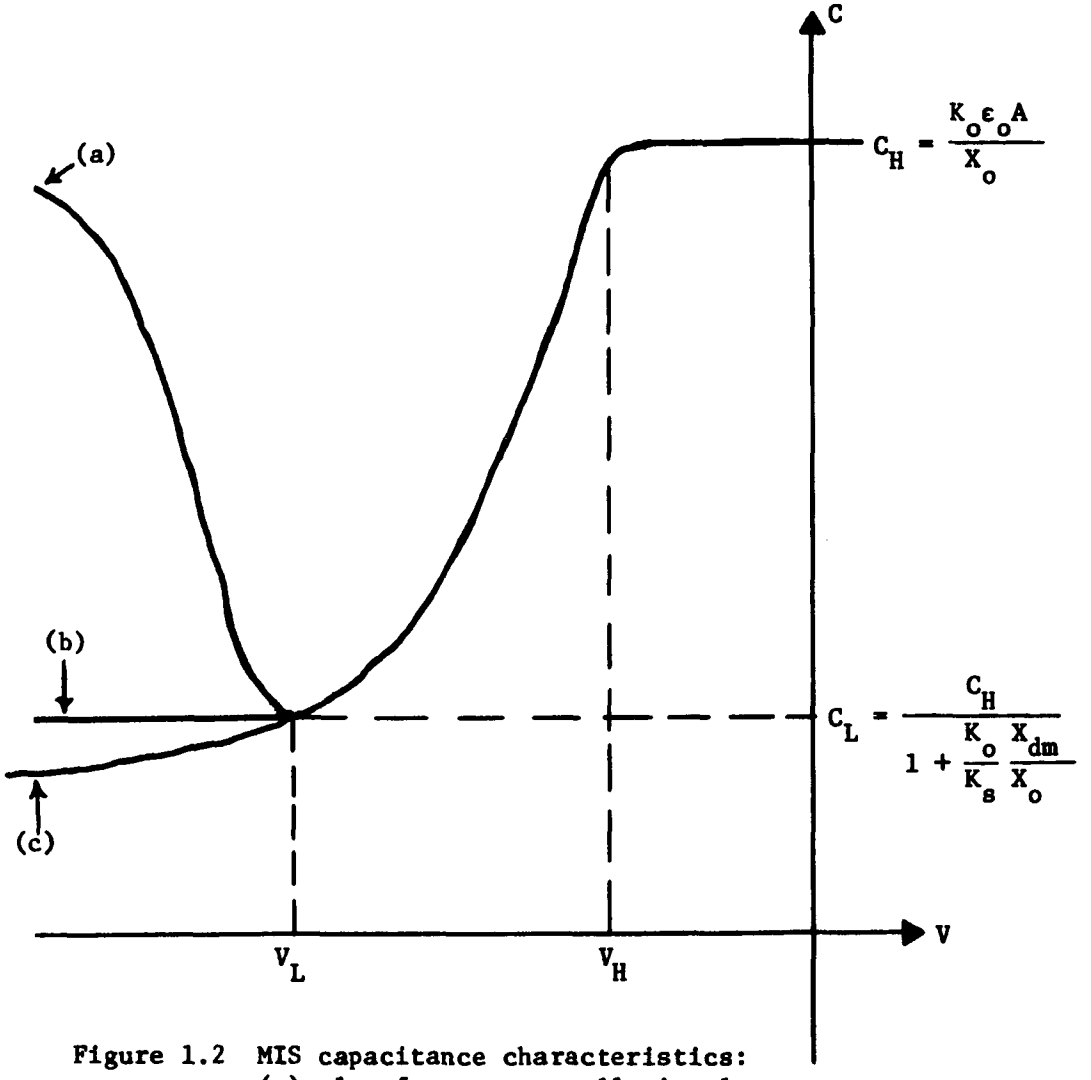

Figure 1.2 MIS capacitance characteristics:
(a) low frequency small signal
(b) high frequency small signal
(c) large high frequency signal

1.2 Pertinent Literature

In 1959 J. L. Moll[1] and Pfann and Garrett[2] proposed an MIS varactor structure. The device was called a surface varactor because it used surface space charge layers to vary the capacitance. The differential capacitance versus voltage characteristic was derived, based upon the depletion approximation, and was compared favorably with the abrupt $P^{+}N$ junction varactor. Frankl[3] and Lindner[4] investigated material parameter effects on the design of surface varactors. Lindner also compared the MIS varactor and junction varactors on the basis of cutoff frequency and total capacity change. Feursanger and Frankl[5] built surface varactors consisting of epitaxially grown silicon and germanium wafers with titanium dioxide films as a dielectric. Measurements were made up to 9 GHz and were in good agreement with existing theories[3,4]. High quality devices with zero bias cutoff frequencies above 100 GHz were described. Grove[6] did a detailed investigation of thermally oxidized silicon surfaces consolidating many of the ideas of previous researches. He modeled and measured in detail the effects of measurement frequency, illumination and temperature on the space charge capacitance of an inverted surface. This capacitance was shown to follow one of three simple models depending on the measurement frequency and rate of generation of minority carriers.

In 1965 Howson, Owen and Wright[7] described the space charge varactor, which consisted of a high resistivity epitaxial structure. This device was analyzed by characterizing the epitaxial layer as a semi-insulator (no thermally generated carriers). The differential capacitance was derived and shown to be more abrupt than the surface varactor. Silicon space charge varactors were built and measurements

confirmed their low frequency theory. In 1970 Nigrin[9] presented a small signal theory for the space charge varactor. His theory again neglects thermally generated carriers and predicts transit time effects. UHF measurements carried out on structures using high resistivity silicon epitaxial layers for the semi-insulator and a silicon dioxide insulator qualitatively verified the theory. Good high frequency devices could not be made. The thin high resistivity layers required on an N^+ substrate could not be fabricated because it was found that significant out-diffusion or autodoping effects predominated.

Numerical simulation of semiconductor devices has progressed with the development of large high speed digital computers and with the need for more detailed device performance models. A one-dimension computer simulation of a semiconductor device proceeds by first solving the d.c. steady state problem for the electrostatic potential throughout the structure and then using pertubation techniques to solve the sinusoidal steady state problem. Previously, the d.c. electrostatic problem has been treated as an initial value problem[11] by making simplifying assumptions at the boundaries. It has also been treated as a boundary value problem by dynamic programming methods ("shooting" methods)[12,14]. A regional approach[13] may also be used where closed form solutions are joined by numerical solutions. The small signal steady state problem has been solved by developing small signal equivalent circuits [11,13] and using matrix analyses [13,22] to solve for the impedance of the device. These models have never been tested at microwave frequencies.

Both the surface varactor and the space charge varactor theoretically have performance advantages in microwave circuit applications[4,7,8]. None of these advantages were ever realized at microwave frequencies

because high Q varactors were never available. Recently, a high Q surface varactor was reported[2,3] and potential new microwave applications explored. With this success, many researchers are reinvestigating their potential advantages. In 1971 Muller[23] built an MIS Upper-Sideband Upconverter and compared its performance to a charge storage diode. Marquart and Schick[8] showed how one could achieve decreased pump sensitivity by using MIS varactors. Other authors[24,25,26] showed how MIS varactors may be used in unique computer-controlled microwave networks such as digitally tuned oscillators and digital phase shifters. MIS varactors in such applications are voltage-controlled devices which require very low steady state drive power. This makes them attractive for electronically scanned antennas which require a large number of phase shifters and must be controlled by a computer.

1.3 Dissertation Research Summary

This research studies the possible use of metal-insulator-semiconductor varactors as a microwave voltage variable circuit element. A unified theory for MIS varactors using thin epitaxially grown semiconductors is developed. Silicon MIS varactors are built using silicon dioxide insulators.* These devices were mounted in ceramic pill packages and characterized at microwave frequencies. Selected devices were then used to build a four-bit digital phase shifter at 3.5 GHz and a microwave (2 GHz signal circuit) low noise parametric amplifier. Both circuits were built using a microwave integrated circuit format. The phase shifter showed potential for filling low power drain phase shifter

*Later in the research, mixtures of silicon dioxide, silicon nitride, and aluminum oxide were used as insulators successfully.

needs. The paramp was the first of its kind built at microwave frequencies, and showed decrease pump sensitivity over conventional parametric amplifiers. Both applications require further study in order to realize optimized devices.

In Chapter 2 the solution for the d.c. electrostatic potential in a one-dimensional MIS structure is treated as a two-point boundary value problem which is solved iteratively by the "η"[15] or quasilinearization[16] procedure. This method is a generalized Newton-Raphson approach for nonlinear boundary value problems and, therefore, converges quadradically when it converges at all. This method has been used in the study of bipolar transistors [17]. Once the electrostatic potential is solved for, it is shown that the differential capacitance may be determined by storing the potential at the I-S interface for a given externally applied potential. The low frequency characteristics of MIS varactors are then studied for a wide range of material parameters and device dimensions. The low frequency computer simulation is performed by fitting a capacitance curve to an experimentally measured device. The two curves were fitted by varying impurity profiles and surface state charge density.

In Chapter 3 a small signal theory valid at microwave frequencies is developed. The solution proceeds by superimposing small signal sinusoidal terms on the d.c. solution. The exact equations are linearized and combined into three coupled second order linear differential equations. The coefficients of the linearized equations are terms involving the previously derived d.c. solution. All derivatives are expanded using finite difference approximations resulting in a seven-band matrix. This system of equations is solved for by a specialized Gauss-elimination

routine for band matrices. In this procedure, the small signal sinusoidal electrostatic potential (V_1) and quasipotentials (V_{n1},V_{p1}) are solved for at every point in the semiconductor knowing the externally applied electrostatic potential. The small signal current is solved for and the current and voltage may then be used to determine the small signal impedance. The surface varactor is simulated at microwave frequencies and compared with experiments. It should be noted that the small signal problem is solved without iteration once the d.c. coefficients are known.

Chapter 4 is an applications chapter in which a digital phase shifter and a parametric amplifier are designed and tested. The phase shifter is of the reflection type and uses a Lange[31] hybrid to separate input and output. Phase stretching techniques are developed for realization of large phase shifts using varactors with limited capacitance ratio. These networks are simulated on COSMIC (Computer Simulation of Microwave Integrated Circuit), an RCA analysis program. A four-bit phase shifter is fabricated and tested. It is shown that switching speed and phase shift are power sensitive. The MIS parametric amplifier is shown to be less sensitive to pump power variations than conventional varactor paramps.

Chapter 5 summarizes the work performed. It also outlines further research which could be performed in this area.

1.4 Basic Equations

In general, the following set of equations must be satisfied in a semiconductor[27,28].

Transport Model

$$\bar{J}_p = -q\mu_p P \nabla V_p \tag{1-1}$$

$$\bar{J}_n = -q\mu_n N \nabla V_n \tag{1-2}$$

$$P = n_i \exp(V_p - V)/V_T \tag{1-3}$$

$$N = n_i \exp(V - V_n)/V_T \tag{1-4}$$

where P,N correspond to hole and electron densities, μ is particle mobility, n_i is the intrinsic carrier concentration, V_T is thermal potential (KT/q), V_p and V_n are the hole and electron quasi-Fermi potentials, and $\bar{J}$ is the particle current density.

Continuity

$$\nabla \cdot \bar{J}_p + q \frac{\partial P}{\partial t} + qU_p = 0 \tag{1-5}$$

$$\nabla \cdot \bar{J}_n - q \frac{\partial N}{\partial E} - qU_n = 0 \tag{1-6}$$

where, in general, the recombination model (U_n,U_p) is of the Schottky-Hall-Read type[29,30].

$$U_p = U_n = \frac{P \cdot N - n_i^2}{\Gamma_n (P + P_r) + \Gamma_p (N + N_r)} \tag{1-7}$$

$$N_r P_r = n_i^2 \tag{1-8}$$

$$P_r = n_i \exp \frac{V_r - V}{V_T} \tag{1-9}$$

Γ_r, Γ_p are carrier lifetimes for holes and electrons, V is the electrostatic potential, and V_r is the trap potential.

Poissons' Equations

$$\nabla \cdot \bar{D} = q[P-N+G(X)] \tag{1-10}$$

where G(X) is the impurity concentration profile and $\bar{D}$ is the electric flux density.

$\bar{D}$ may be related to the electrostatic potential by

$$\bar{D} = -\varepsilon \nabla V \tag{1-11}$$

And, finally, the total current may be expressed as the sum of displacement current and individual particle currents

$$\bar{J}_T = \frac{\partial \bar{D}}{\partial_t} + \bar{J}_n + \bar{J}_p \tag{1-12}$$

CHAPTER 2

D. C. SIMULATION OF METAL INSULATOR SEMICONDUCTOR VARACTORS

In order to characterize the performance of MIS varactors at microwave frequencies one must first solve for the d.c. steady state electrostatic potential everywhere in the structure. Once this is done the microwave impedance may be calculated by perturbing the d.c. solution with a small sinusoidal signal. In addition to being necessary for high frequency calculations, the d.c. solution, especially near the insulator-semiconductor interface, may be used to calculate differential capacitance ($C_d = \partial Q/\partial V$). This quantity may be measured experimentally and used to check the d.c. solution. Also, differential capacitance versus voltage curves may be used to study interface properties of semiconductors and impurity profile effects. The differential capacitance is also calculated here so as to compare it later with the imaginary part of the impedance solved for directly. This is of particular interest since they are commonly used interchangeably in the literature.

The problem is approached by specifying Laplace's equation in the insulator, Poisson's equation in the semiconductor and boundary conditions at the ends and interface point. The resulting mathematical formulation is a mixed linear and nonlinear boundary value problem. A closed form solution for this problem is not possible for arbitrary doping profiles and this chapter is confined to a computer solution. The solution proceeds by linearizing the system about a present guess, $V_o^i(X)$. The linearized system is then solved for the error $[\delta(1),\delta(2)...\delta(n)]$ at every grid point. The solution of the linear problem involves the inversion of a tridiagonal matrix of the band type. The maximum error

DMAX is then found and compared with an allowable bound (.01*VT). If the error is not small enough, the initial guess is updated by the error and the linearization process is continued. The program stops iterating when the maximum error is within the error bound. The analysis program (MIS) using this procedure is then used to analyze MIS structures with various doping profiles.

2.1 Mathematical Formulation (D.C.)

2.1.1 D.C. Equations

Since only a one dimension solution is considered, all vector quantities will be understood to have a single component in the $\hat{X}$ direction. Therefore, vector equations may be written as scalar equations and subscript, o, will be used to denote a d.c. quantity.

A sketch of a one-dimensional MIS structure is shown in Figure 2.1. In the insulator, Laplace's equation is assumed to hold for the d.c. potential, V_o.

$$\frac{d^2V_o}{dX^2} = 0 \qquad (2\text{-}1)$$

The above equation implies an ideal insulator with no injected carriers or distributed ionic contamination. In the semiconductor the basic equations (1-1) to (1-12) may be further simplified with the assumption of no d.c. convection current (J_{no}, J_{po}) flow.

$$J_{no} = J_{po} = 0 \qquad (2\text{-}2)$$

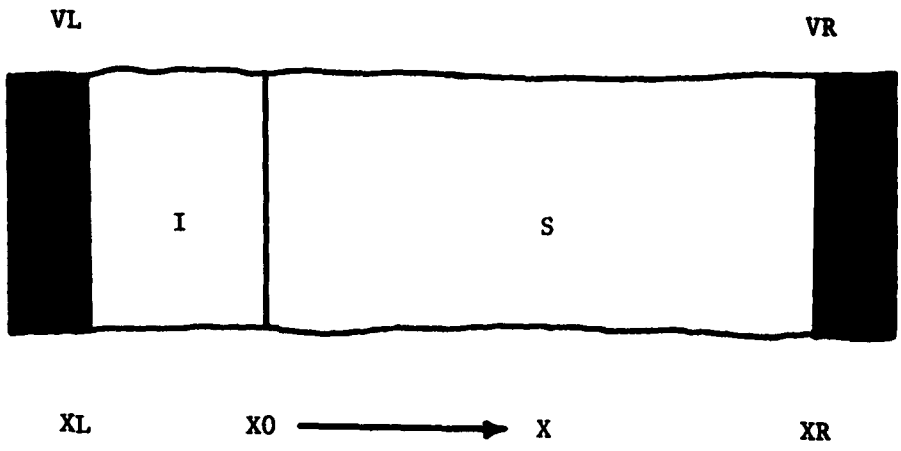

Region I:
$$\frac{d^2V_o}{dX^2} = 0$$

Region S:
$$\frac{d^2V_o}{dX^2} = -\frac{q}{\varepsilon_s}\left\{G(X) - 2n_i \sinh\frac{V_o}{V_T}\right\}$$

Boundary Conditions:

$$V_o(XL) = VL$$

$$V_o(XR) = V_T \operatorname{Sinh}^{-1}\left(\frac{G(XR)}{2n_i}\right)$$

$$V_o(XO^-) = V(XO^+)$$

$$K_s \frac{dV_o}{dX}\Big]_s - K_I \frac{dV_o}{dX}\Big]_I = -\frac{Q_{ss}}{\varepsilon_o}$$

Figure 2.1 Summary of one dimensional D.C. boundary value problem.

From Eq. (1-1), (1-2), and (2-2) it is seen that the d.c. quasipotentials (V_{no}, V_{po}) must be constants independent of distance and, in fact, by definition, must be equal to the equilibrium Fermi potential, V_F.

$$V_{no} = V_{po} = V_F = \text{constant} \tag{2-3}$$

Since V_F is a constant independent of distance, it is chosen as the reference or ground potential.

$$V_{no} = V_{po} = V_F = 0 \tag{2-4}$$

Substituting Eq. (1-3), (1-4), (1-11), and (2-4) into (1-10) a specialized form of Poisson's equation results:

$$\frac{d^2V_o}{dX^2} = -\frac{q}{K_s\varepsilon_o}\left\{G(X) - 2n_i \text{Sinh}\,\frac{V_o}{V_T}\right\} \tag{2-5}$$

2.1.2 Boundary Conditions

The contact at the metal-insulator boundary is considered an ideal metal maintained with respect to the Fermi potential in the semiconductor at an electrostatic potential, VL. The metal semiconductor contact is considered ohmic[17] which implies the following two assumptions:

(A) - infinite surface recombination velocity

(B) - space charge neutrality

An infinite surface recombination velocity implies for finite hole and electron current densities at the contacts that hole and electron densities must be equal to the d.c. quantities; i.e.,

$$P = P_o \text{ and } N = N_o \tag{2-6}$$

This may be deduced from the definition of surface recombination velocity.

$$q(P-P_o)\big|_{\text{ohmic contact}} = \lim_{S_{RP}\to\infty} (J_p/S_{RP}) = 0 \tag{2-7a}$$

$$q(N-N_o) = \lim_{S_{RN}\to\infty} (J_N/S_{RN}) = 0 \tag{2-7b}$$

The second assumption (B) may be expressed using Eq. (2-6) as

$$P_o - N_o + G(XR) = 0 \tag{2-8}$$

which may be solved for $V_o(XR)$ assuming Boltzmann's statistics, Eq. (1-3), (1-4), and (2-4).

$$V_o(XR) = V_T \, \text{Sinh}^{-1} \left(\frac{G(XR)}{2n_i}\right) \tag{2-9a}$$

This equation may be rewritten in the following form, which is easier to handle on the computer.

$$V_o(XR) = V_T \, \ell n \left\{ \frac{G(XR)}{2n_i} + \left(\left(\frac{G(XR)}{2n_i}\right)^2 + 1 \right)^{1/2} \right\} \tag{2-9b}$$

Note that n_i is a function of temperature and the type of material used. For silicon[18]

$$n_i(T) = (3.73 \times 10^{16}) * T^{3/2} \exp \left(-\frac{7014}{T}\right) (cm^{-3}) \tag{2-10}$$

At the semiconductor insulator interface the normal component of electric flux density is discontinuous.

$$D_S - D_I = Q_{SS} \tag{2-11}$$

Q_{SS} is any surface state or interface charge which may exist. The electric flux densities may be expressed in terms of electrostatic potential:

$$D = \varepsilon E = - \varepsilon \frac{dV_o}{dX} \tag{2-12}$$

A summary of the mathematical formulation is presented in Figure 2.1, including structure, d.c. equations and boundary conditions.

2.2 Numerical Solution of the D.C. Steady State Problem

2.2.1 Quasilinearization

First, the structure is divided into three section in each of which a uniform grid is set up as described in Figure 2.2. The mesh sizes (XH1, XH2, XH3) need not be the same size and, in general, they are not. At each point it is assumed that the electrostatic potential consists of a present value (V_o^i) plus an error (δ).

$$V_o = V_o^i + \delta \tag{2-13}$$

Substituting Eq. (2-13) into Eq. (2-1)

$$\frac{d^2(\delta + V_o^i)}{dX^2} = 0 \tag{2-14}$$

Solving for the error term, a second order linear differential equation results where the right side is known since V_o^i is known.

$$\frac{d^2\delta}{dX^2} = - \frac{d^2V_o^i}{dX} \tag{2-15}$$

Substituting Eq. (2-13) into (2-5), and similarly separating error terms, a second order nonlinear differential equation in δ results.

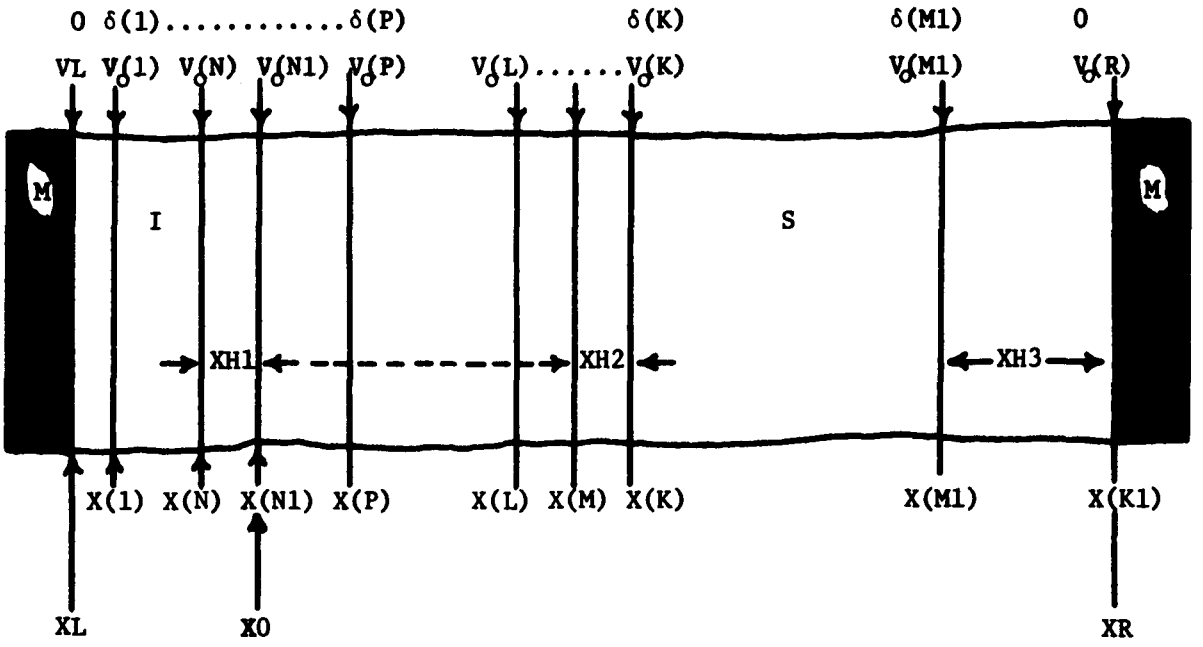

N1 = Number of Increments in Insulator

N2,N3 = Number of Increments in Grid 1 and Grid 2 in the Semiconductor

X(I) = Mesh Coordinate

δ,V = Error and Exact Value of Electrostatic Potential

K = N1 + N2

K1 = N1 + N2 + N3

Figure 2.2 Finite difference grid and associated variables.

$$\frac{d^2(V_o^i+\delta)}{dX^2} = -\frac{q}{\varepsilon_s}\left\{G(X) - 2n_i \sinh\frac{(V_o^i+\delta)}{V_T}\right\} \tag{2-16}$$

$$\sinh\left(\frac{V_o^i}{V_T} + \frac{\delta}{V_T}\right) = \sinh\frac{V_o^i}{V_T}\cosh\frac{\delta}{V_T} + \cosh\frac{V_o^i}{V_T}\sinh\frac{\delta}{V_T} \tag{2-17}$$

It is assumed here that V_o^i is close to the exact solution such that $\delta/V_T << 1$. This may be justified on the grounds that this problem is a physical one to which under certain conditions a good approximation is known. Therefore, under these assumptions, the nonlinear boundary value problem in V_o may be converted to a linear problem in δ, which may be solved directly without iteration. Expanding the terms cosh δ/V_T and sinh δ/V_T and keeping only first order terms, Eq. (2-17) may be expressed as

$$\sinh\left(\frac{V_o^i}{V_T} + \frac{\delta}{V_T}\right) \cong \sinh\frac{V_o^i}{V_T} + \frac{\delta}{V_T}\cosh\frac{V_o^i}{V_T} \tag{2-18}$$

Substituting Eq. (2-18) into (2-16) and collecting error terms

$$\frac{d^2\delta}{dX^2} - \alpha\delta + \beta = 0 \tag{2-19}$$

$$\alpha = \frac{q}{\varepsilon}\frac{2n_i}{V_T}\cosh\frac{V_o^i}{V_T} \tag{2-20}$$

$$\beta = \frac{d^2V_o^i}{dX^2} + \frac{q}{\varepsilon}\left(G(X) + 2n_i \sinh\frac{V_o^i}{V_T}\right) \tag{2-21}$$

At the interface point between insulator and semiconductor, the boundary condition on the error may be determined by substituting Eq. (2-13) into (2-11) and (2-12)

$$K_S \left.\frac{d\delta}{dX}\right]_S - K_I \left.\frac{d\delta}{dX}\right]_I = - Q_{SS} - K_S \left.\frac{dV_o^i}{dX}\right]_S + K_I \left.\frac{dV_o^i}{dX}\right]_I \tag{2-22}$$

The subscripts S and I denote derivatives evaluated from the semiconductor or insulator sides, respectively. At the metal contacts, the electrostatic potential is assumed known, and therefore error at these points is always zero.

$$\delta(XL) = 0 \tag{2-23}$$

$$\delta(XR) = 0 \tag{2-24}$$

A summary of the linearized boundary value problem is shown in Figure 2.3. It should be noted that the coefficients of the linearized second order problem are in terms of the presently known V_o^i and other known constants.

The solution proceeds now by approximating all derivatives by finite difference approximations and obtaining a system of equations of the form

$$\overline{J} \cdot \overline{\delta} = \overline{D} \tag{2-25}$$

The matrix $\overline{J}$ is a tridiagonal band matrix as shown in Figure 2.4. The matrices $\overline{\delta}$ and $\overline{D}$ are column vectors. The elements (a,b,c) of $\overline{J}$ may be derived in the insulator by using centered difference approximations to second derivatives of δ and V_o^i. Therefore, if we let

$$\frac{d^2V_o^i}{dX^2}(I) = D2V(I) = \frac{V_o^i(I-1) - 2V_o^i(I) + V_o^i(I+1)}{(XH1)^2} \tag{2-26}$$

and if the second derivative of δ with respect to X is expressed similarly, the following set of equations result in the insulator.

$$V = V_o^i + \delta$$

Region I:
$$\frac{d^2\delta}{dX^2} = - \frac{d^2V_o^i}{dX^2}$$

Region S:
$$\frac{d^2\delta}{dX^2} - \alpha\delta + \beta = 0$$

$$\alpha = \frac{q}{\epsilon_s} \frac{2n_i}{V_T} \text{Cosh} \frac{V_o^i}{V_T}$$

$$\beta = \frac{d^2V_o^i}{dX^2} + \frac{q}{\epsilon_s} \left\{ G(X) - 2n_i \text{ Sinh} \frac{V_o^i}{V_T} \right\}$$

Boundary Conditions:

$$\delta(XL) = 0$$

$$\delta(XR) = 0$$

At X=XO,

$$K_s \frac{d\delta}{dX}\Big]_s - K_I \frac{d\delta}{dX}\Big]_I = - \frac{Q_{ss}}{\epsilon_o} - K_s \frac{dV_o^i}{dX}\Big]_s + K_I \frac{dV_o^i}{dX}\Big]_I$$

Figure 2.3 Linearized boundary value problem.

$$\overline{J} \cdot \overline{\delta} = \overline{D}$$

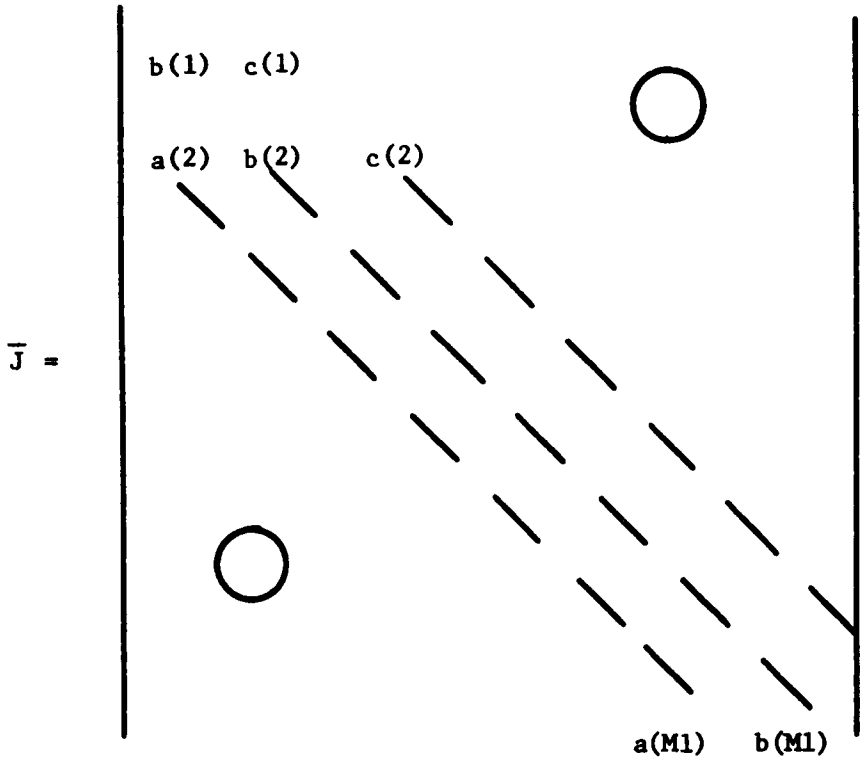

Figure 2.4 Tridiagonal system of equations.

$$\text{At} \quad X = X(1) \qquad -2\delta(1) + \delta(2) = -(XH1)^2 D2V(1) \tag{2-27}$$

$$\vdots \qquad\qquad \vdots$$

$$X = X(I) \qquad \delta(I-1) - 2\delta(I) + \delta(I+1) = -(XH1)^2 D2V(I),$$

$$I = 2,N \tag{2-28}$$

At the interface point X=XO=X(N1), Equation (2-22) must be satisfied. At this point, derivatives evaluated from the right are determined using the forward difference approximation

$$\left.\frac{d\delta}{dX}\right]_S = \frac{\delta(P) - \delta(N1)}{(XH2)} \tag{2-29}$$

Similarly, derivatives evaluated from the left are determined by backward difference approximations

$$\left.\frac{d\delta}{dX}\right]_I = \frac{\delta(N1) - \delta(N)}{XH1} \tag{2-30}$$

Collecting similar terms, the following is valid at the interface point.

$$\delta(N) - \left(1 + \frac{K_S}{K_I}\,\frac{XH1}{XH2}\right)\delta(N1) + \frac{K_S}{K_I}\,\frac{XH1}{XH2}\,\delta(P)$$

$$= -\frac{XH1\,Q_{SS}}{K_I \varepsilon_o} - V_o^i(N) + \left(1 + \frac{K_S}{K_I}\,\frac{XH1}{XH2}\right) V_o^i(N1)$$

$$- \frac{K_S}{K_I}\,\frac{XH1}{XH2}\,V_o^i(P) \tag{2-31}$$

In the semiconducting region of grid 2, centered difference approximations are again used yielding

$$\delta(I-1) - \Big(2 + (XH2)^2\,\alpha(I)\Big)\delta(I) + \delta(I+1) = -(XH2)^2\,\beta(I) \tag{2-32}$$

$$\alpha(I) = \frac{q}{\varepsilon}\frac{2n_i}{V_T}\cosh\frac{V_o^i(I)}{V_T} \tag{2-33}$$

$$\beta(I) = D2V(I) + \frac{q}{\varepsilon}\left(G(I) - 2n_i \sinh\frac{V_o^i(I)}{V_T}\right) \tag{2-34}$$

$$I = P,M \tag{2-35}$$

At the interface point between two grids (point K), the centered difference approximation for second derivative (Appendix A1) is used resulting in Eq. (2-36).

$$\delta(M) - \left\{1 + \frac{XH2}{XH3} + \alpha(K)\ \frac{(XH2)(XH2+XH3)}{2}\right\}\delta(K) + \frac{XH2}{XH3}\,\delta(P1)$$
$$= -\beta(K)\ \frac{XH2(XH2+XH3)}{2} \tag{2-36}$$

Note that Eq. (2-36) reduces to (2-32) for XH2=XH3. Similarly, in grid 3: $I = P1, M1$.

$$\delta(I-1) - \left(2+(XH3)^2\right)\delta(I) + \delta(I+1) = -(XH3)^2\beta(I) \tag{2-37}$$

Comparing Eq. (2-27) to (2-37) with the elements of $\bar{J}$, a,b,c at every point may be determined and is summarized in Figure 2.5. Figure 2.6 is a flow diagram of the program (MIS) pertinent to this chapter.

2.2.2 Inversion Algorithm for a Tridiagonal Band Matrix

The M1 system of equations may be solved for the M1 unknown δ's by a Gauss elimination routine[19,20]. Expanding Eq. (2-25) into component form, the system may be written as

$$b(1)\delta(1)+c(1)\delta(2) = d(1) \tag{2-38}$$

$$a(2)\delta(1)+b(2)\delta(2)+c(2)\delta(3) = d(2) \tag{2-39}$$

$$a(3)\delta(2)+b(3)\delta(3)+c(3)\delta(4) = d(3) \tag{2-40}$$

. . .
. . .
. . .

$$a(I) = 1, \qquad I = 2, M1$$

$$\left.\begin{aligned} b(I) &= -2 \\ c(I) &= 1 \\ d(I) &= -(XH1)^2\ D2V(I) \end{aligned}\right\} \qquad I = 1,N$$

$$b(N1) = -\left(1 + \frac{K_s}{K_I}\ \frac{XH1}{XH2}\right)$$

$$c(N1) = \frac{K_s}{K_I}\ \frac{XH1}{XH2}$$

$$d(N1) = -\frac{XH1}{K_I}\ \frac{Q_{ss}}{\varepsilon_o} - V_o^i(N) + \left(1 + \frac{K_s}{K_I}\ \frac{XH1}{XH2}\right)V_o^i(N1) - \frac{K_s}{K_I}\ \frac{XH1}{XH2}\ V_o^i(P)$$

$$\left.\begin{aligned} b(I) &= -\left(2 + (XH2)^2\alpha(I)\right) \\ c(I) &= 1 \\ d(I) &= -\ (XH2)^2\beta(I) \end{aligned}\right\} \qquad I = P,M$$

$$\alpha(I) = \frac{q}{\varepsilon_s}\ \frac{2n_i}{V_T}\ \cosh\ \frac{V_o^i(I)}{V_T}$$

$$\beta(I) = D2V(I) + \frac{q}{\varepsilon_s}\left(G(I) - 2n_i\ \sinh\ \frac{V_o^i(I)}{V_T}\right)$$

$$b(K) = -\left\{1 + \frac{XH2}{XH3} + \alpha(K)\left(\frac{XH2(XH2+XH3)}{2}\right)\right\}$$

$$c(K) = \frac{XH2}{XH3}$$

$$d(K) = \beta(K)\ \frac{XH2(XH2+XH3)}{2}$$

$$\left.\begin{aligned} b(I) &= -\left(2+(XH3)^2\right)\alpha(I) \\ d(I) &= -\ (XH3)^2\beta(I) \end{aligned}\right\} \qquad I = P1,M1$$

$$c(I) = 1, \quad I = P1,L1 \text{ where } L1 = M1-1.$$

Figure 2.5 Summary of matrix elements abcd.

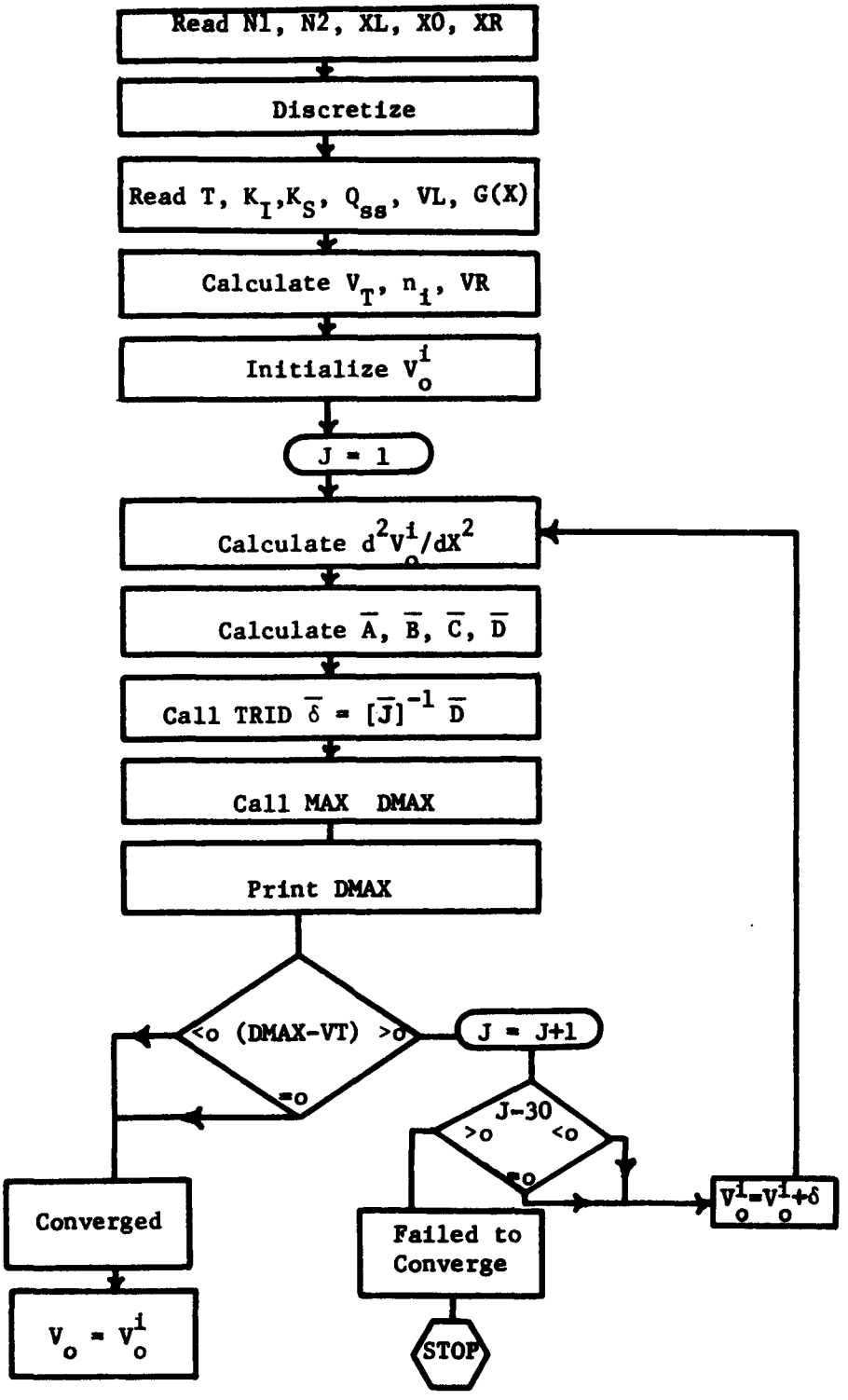

Figure 2.6 MIS flow diagram.

$$\vdots \qquad \vdots \qquad \vdots \qquad \vdots$$

$$a(M1-1)\delta(M1-2)+b(M1-1)\delta(M1-1)+c(M1-1)\delta(M1) = d(M1-1) \tag{2-41}$$

$$a(M1-1)\delta(M1-1)+b(M1)\delta(M1) = d(M1) \tag{2-42}$$

Multiplying Eq. (2-38) by a(2)/b(1), and using the resulting equation to eliminate $\delta(1)$ from Eq. (2-39)

$$b'(2)\delta(2)+c(2)\delta(3) = d'(2) \tag{2-43}$$

$$b'(2) = b(2) - \frac{a(2)c(1)}{b(1)} \tag{2-44}$$

$$d'(2) = d(2) - \frac{a(2)d(1)}{b(1)} \tag{2-45}$$

Multiplying Eq. (2-39) by a(3)/b'(2) and subtracting the resulting equation from Eq. (2-40)

$$b'(3)\delta(3)+c(3)\delta(4) = d'(3) \tag{2-46}$$

where

$$b'(3) = b(3) - \frac{a(3)c(2)}{b'(2)} \tag{2-47}$$

$$d'(3) = d(3) - \frac{a(3)d'(2)}{b'(2)} \tag{2-48}$$

Also, eliminating $\delta(M1-2)$ from Eq. (2-41)

$$b'(M1-1)\delta(M1-1) + c(M1-1)\delta(M1) = d'(M1-1) \tag{2-49}$$

$$b'(M1-1) = b(M1-1) - \frac{a(M1-1)c(M1-2)}{b'(M1-2)} \tag{2-50}$$

$$d'(M1-1) = d(M1-1) - \frac{a(M1-1)d(M1-2)}{b'(M1-2)} \tag{2-51}$$

Similarly, eliminating $\delta(M1-1)$ from Eq. (2-42)

$$b'(M1)\delta(M1) = d'(M1) \tag{2-52}$$

$$b'(M1) = b(M1) - \frac{a(M1)c(M1-1)}{b'(M1-1)} \tag{2-53}$$

$$d'(M1) = d(M1) - \frac{a(M1)d(M1-1)}{b'(M1-1)} \tag{2-54}$$

Solving Eq. (2-52) for $\delta(M1)$

$$\delta(M1) = \frac{d'(M1)}{b'(M1)} \tag{2-55}$$

Back substituting into Eq. (2-49)

$$\delta(M1-1) = \frac{d'(M1-1)-c(M1-1)\delta(M1)}{b'(M1-1)} \tag{2-56}$$

or

$$\delta(R) = \frac{d'(R) - c(R)\ \delta(R+1)}{b'(R)} \tag{2-57}$$

$$R = M1-1 \text{ to } R = 1 \tag{2-58}$$

Algorithm Summary

1. If b(1) ≠ 0, then calculate Ratio
2. Ratio = $\frac{a(2)}{b(1)}$

   Then for I = 2, M1, do steps 3,4,5,6.
3. b(I) = b(I) - Ratio * c(I-1)
4. d(I) = d(I) - Ratio * d(I-1)
5. If b(I) ≠ 0, calculate Ratio.
6. Ratio = $\frac{a(I+1)}{b(I)}$

Note that the array $\overline{B}$, $\overline{D}$ is destroyed in the process of solving the system. This feature reduces the numbers of arrays required by two. The

algorithm now proceeds by back substituting and solving for the solution vector $\bar{\delta}$.

7. $\delta(M1) = \frac{d(M1)}{b(M1)}$

8. $\delta(R) = \frac{d(R) - c(R) * \delta(R)}{b(R)}$ $\quad R = M-1$ to $R = 1$

2.2.3 Calculation of Low Frequency Capacitance

By definition the differential capacitance of a semiconductor structure is

$$C(v) = \frac{dQ}{dV} \tag{2-59}$$

where

V = voltage variation across the structure.

VL = applied electrostatic potential relative to the Fermi potential within the semiconductor.

VR = contact potential relative to the Fermi potential.

Q = charge per unit area at the interface between metal and insulator.

The surface charge (Q) may be related to the electric field (E_I) in the insulator by knowing that the electric flux density (D) is discontinuous across the boundary and that the electric field in the metal is zero.

$$D_I - D_M = Q \tag{2-60}$$

$$D_M = 0 \tag{2-61}$$

$$Q = \epsilon_o K_I E_I \tag{2-62}$$

where

ε_o = permittivity of free space.

K_I = relative permittivity of the insulator.

E_I = electric field in the insulator.

The electric field may be related to the electrostatic potential by

$$E_I = \frac{VL - V(XO)}{XO} \tag{2-63}$$

Substituting Eq. (2-63) into (2-62) a relationship between Q and electrostatic potentials results.

$$Q = C_o \left(VL - V(XO)\right) \tag{2-64}$$

where

$$C_o = \frac{\varepsilon_o K_I}{X_o} \tag{2-65}$$

$$dQ = C_o \left(dVL - dV(XO)\right) \tag{2-66}$$

$$dV = dVL \tag{2-67}$$

Substituting Eq. (2-66) and (2-67) in the capacitance definition (2-59)

$$C = C_o \left(1 - \frac{dV(XO)}{d(VL)}\right) \tag{2-68}$$

Approximating the first derivative by a forward difference

$$\frac{dV(X_o)}{dVL} = \frac{V(X_o)_{I+1} - V(X_o)_I}{(VL)_{I+1} - (VL)_I} \tag{2-69}$$

If increments in applied voltage are defined as DV where

$$DV = (VL)_{I+1} - (VL)_I \tag{2-70}$$

then the final expression for differential capacitance may be expressed in terms of DV and the change in voltage at the semiconductor insulator interface.

$$C(I) = C_o\left(1 - \frac{V(X_o)_{I+1} - V(X_o)_I}{DV}\right) \tag{2-71}$$

$$VL = VR + DV * I \tag{2-72}$$

$$I = 1, NP \tag{2-73}$$

NP - number of points of interest.

2.2.4 Assumed Impurity Profile for Ideal Epitaxial Material

The impurity profile most used in calculations will be that of a hyperbolic tangent function of the following form:

$$G(X) = A\tanh\,(X-X_1)/BX + C \tag{2-74}$$

where

$$A = (NS-NE)/2 \tag{2-75}$$

BX = slope parameter

$$C = (NS+NE)/2 \tag{2-76}$$

NS and NE are substrate and epitaxial layer densities, respectively.

X_1 = break point of the abrupt junction

The function can simulate an abrupt junction if the slope parameter is made small enough. This function is also continuous everywhere and is bounded, which makes numerical computation simple. Figure 2.7 plots Eq. (2-74) for two epi layer densities and two different slope parameters. In general, we will be interested in doping profiles corresponding to the surface varactor and the space charge varactor.

The parameters of the impurity profile [Eq. (2-74)] for the surface varactor are assumed to be

$$NS = 1.0 \times 10^{20}\ (1/cm^3)$$

$$NE = 0.5 \times 10^{16}\ (1/cm^3)$$

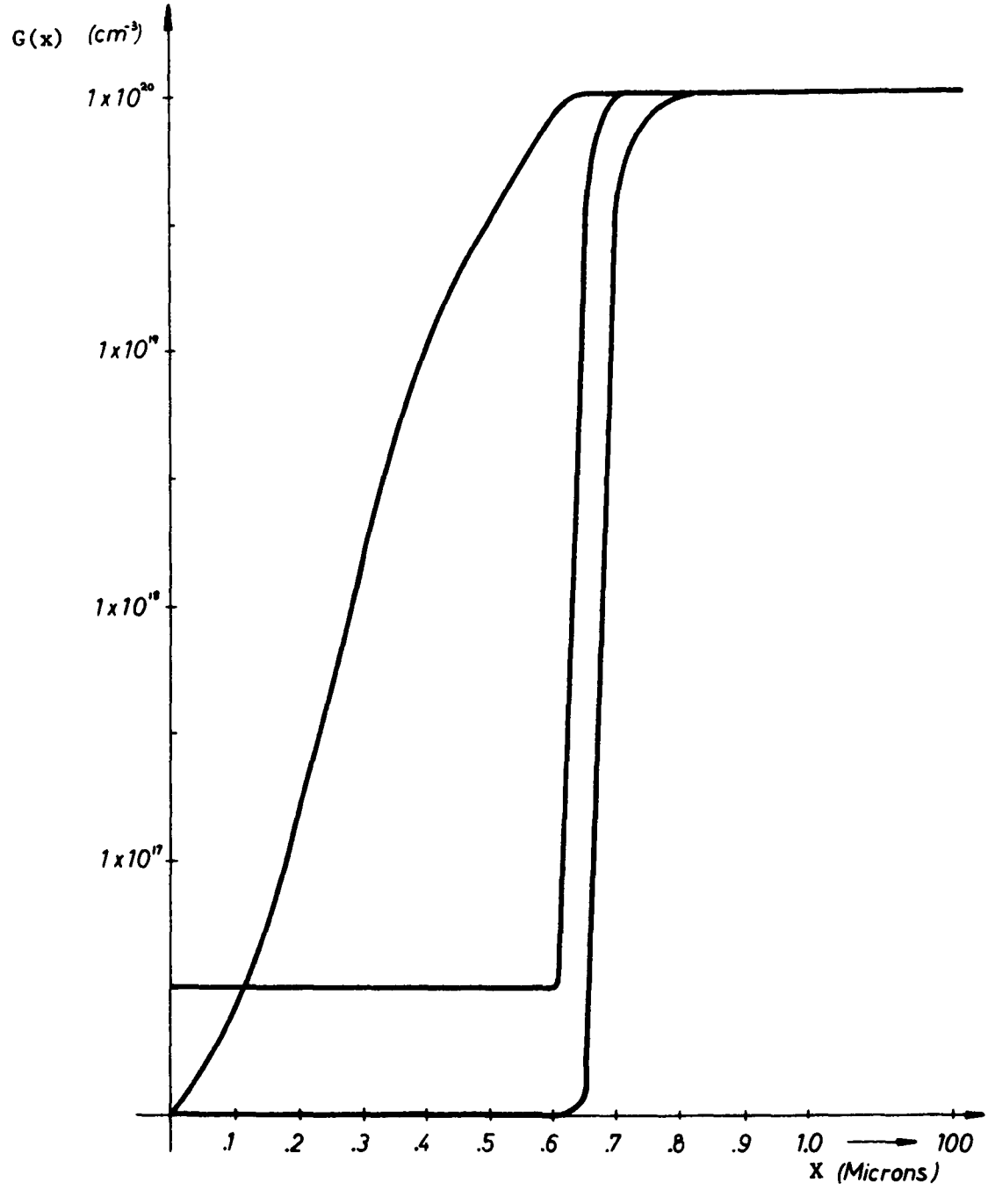

Figure 2.7 G(x) versus distance x.

$$X1 = 0.7 \text{ (microns)}$$

$$BX = 1.0 \times 10^{-3} \text{ (microns)}$$

In addition to the above parameters referring to Figure 2.1, the rest of the dimensions are:

$$XL = 0$$

$$XO = 0.1 \text{ (microns)}$$

$$XR = 101.3 \text{ (microns)}$$

For the space charge varactor all dimensions and densities are the same except for NE. For the space charge varactor an intrinsic material is assumed

$$NE = 0$$

2.3 Solution for Electrostatic Potential

Figure 2.8 is a plot of electrostatic potential at the insulator semiconductor interface. As is shown in the plot:

$$VL = -2.47 \text{ volts}$$

$$VR = 0.53 \text{ volts}$$

$$Q_{SS} = 0.34 \times 10^{-3} \text{ coul/m}^2$$

The doping profile corresponds to that of the surface varactor. In the insulator, since there is no charge density, the electrostatic potential is a linear function versus distance. At the insulator-semiconductor interface ($X = XO = 0.1$ μm) there is a change in slope due to the change in relative dielectric constant and also due to the surface charge density. The potential decays into the semiconductor, approximately 0.3 micron until charge neutrality ($\rho = 0$) is valid and the electrostatic potential is independent of distance. It should be noted that there is a region near the interface where $V_o = 0$. At this point ($X = 0.18$ μm) according to Eq. (1-3), (1-4), and (2-4)

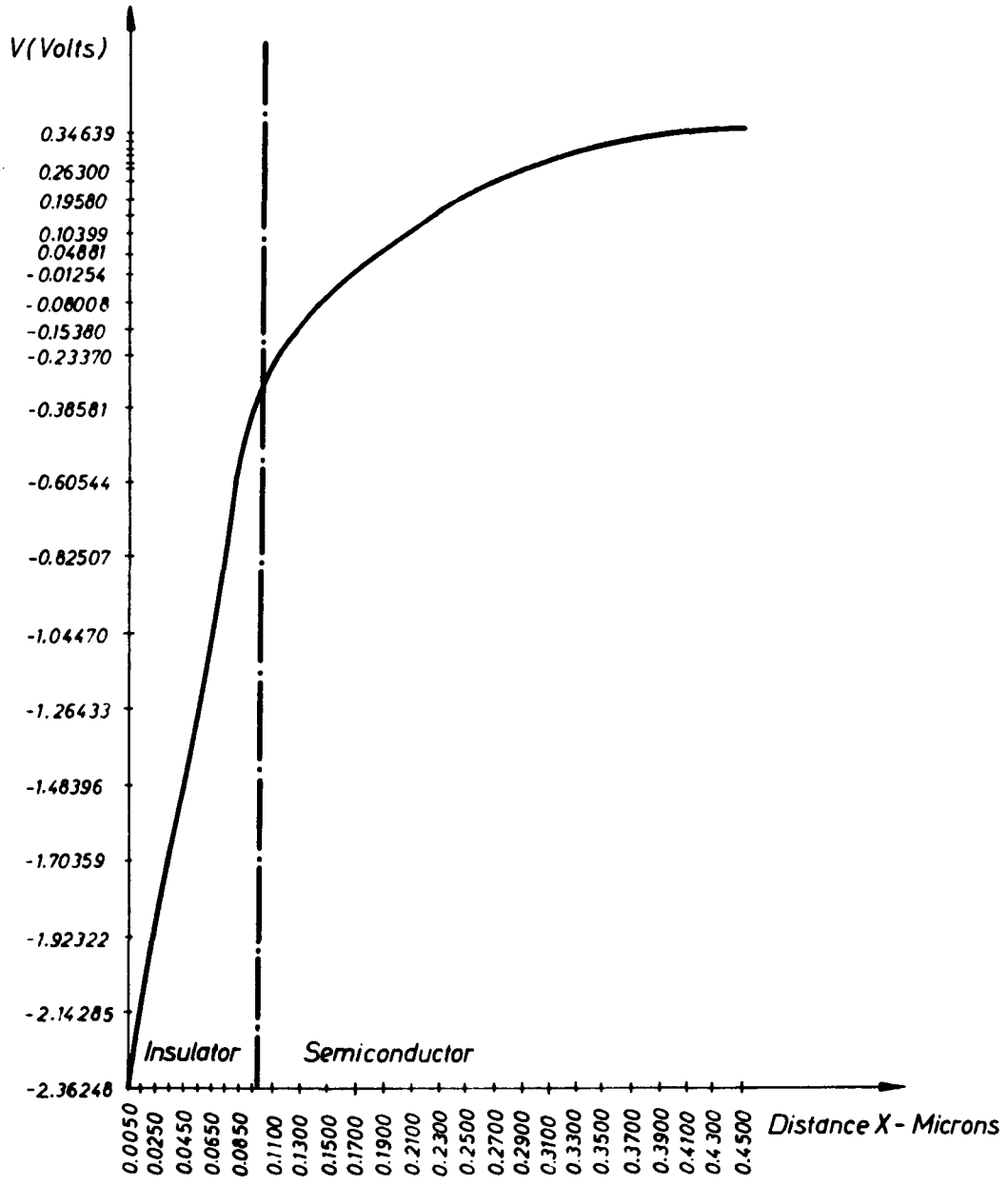

Figure 2.8 Computer simulation of potential at the insulator-semiconductor interface.

$$P_o = n_i \exp - V_o/V_T \tag{2-77}$$

$$N_o = n_i \exp V_o/V_T \tag{2-78}$$

$$P_o = N_o = n_i \tag{2-79}$$

and $\rho = q(P_o - N_o + G(X) = qG(X)$ (2-80)

At approximately X = 0.18 μm there is essentially a depletion region where there is a positive background charge density. At the I-S interface there is a large negative potential which, according to Eq. (2-77) and (2-78) corresponds to a large hole concentration and a small electron concentration. Since holes are minority carriers, this is called an inversion layer.

Figure 2.9 shows a plot of the N/N+ interface (X = 0.7 μm). To the left and right of this interface are charge neutral regions where no electric fields exist. But, right at the interface an electric field exists corresponding to an electron accumulation. This charge is an out-diffusion of electrons from the more heavily doped substrate into the lower impurity epitaxial region. This charge accumulation or injection becomes important in the space charge varactor which works on a charge injection principle.

2.4 MIS Differential Capacitance Simulation

Using equation (2-71) differential capacitance versus voltage, plots may be used to study MIS properties. It should be noted that the capacitance characteristic resulting will be the low frequency curve. This is because the total charge including minority carriers is used to calculate capacitance. Figure 2.10 shows a C(v) plot for an abrupt surface varactor with surface charge as a parameter. As the surface

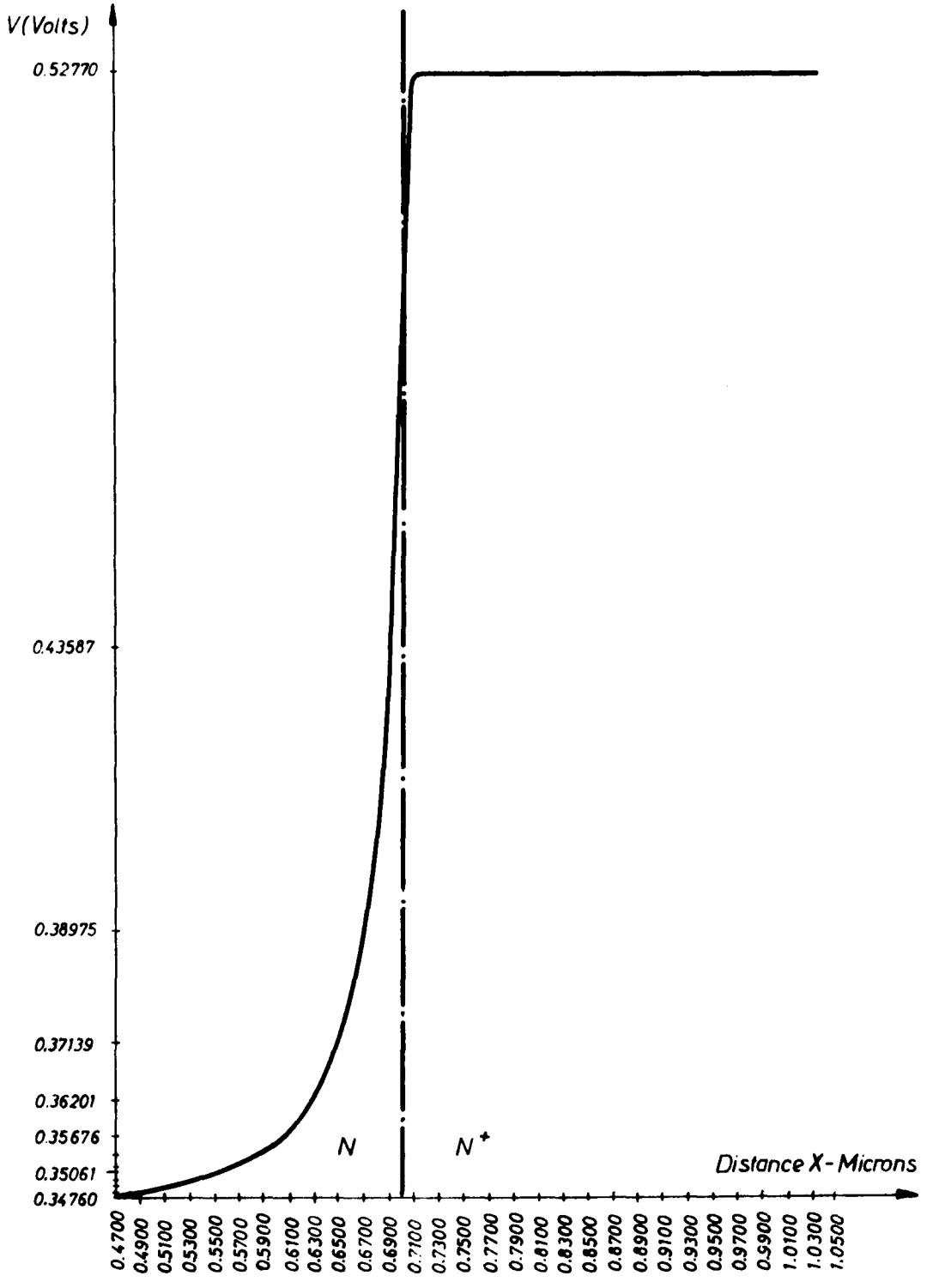

Figure 2.9 Computer simulation of potential at the N/N^+ interface.

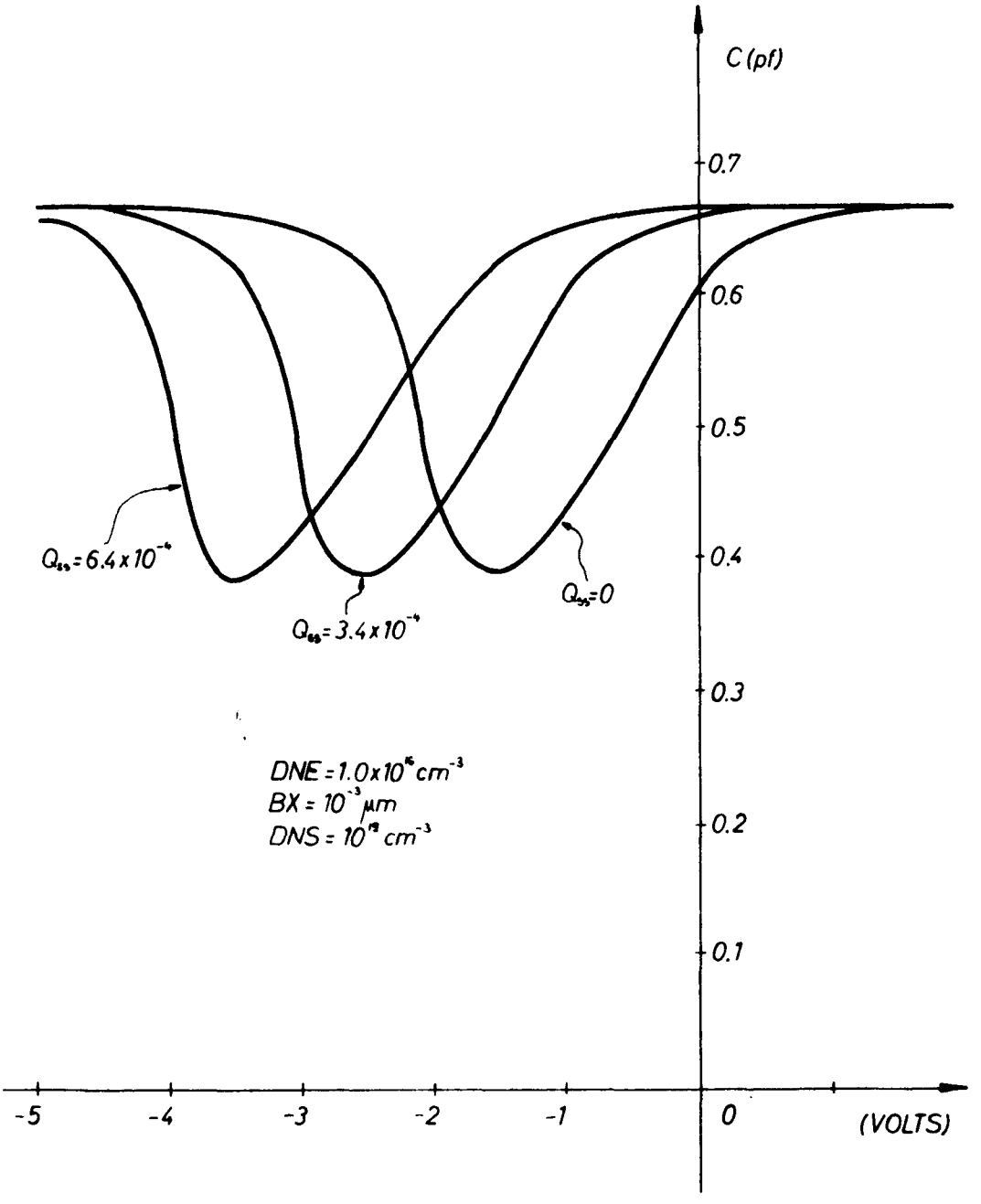

Figure 2.10 Differential capacitance versus voltage with Q_{ss} as a parameter.

charge is increased the C(V) curve is displaced along the voltage axis. Grove[6] shows that a reasonable number for surface state charge density is $Q_{ss} \sim 10^{-4}$ coul/m^2 for an annealed silicon-silicon dioxide interface. Figure 2.11 shows the effect of varying the epitaxial layer density. The lower the density the larger the maximum depletion depth and the greater the maximum to minimum capacitance ratio. The curve DNE=0 corresponds to the space charge varactor case. Also, changing the slope BX affects the capacitance plot as shown in Figure 2.12. A slope parameter is necessary because in thin epitaxial material there is an autodoping effect in which it takes a finite distance to go from a high density to a low density of impurities. Autodoping is a function of temperature and occurs within a micron of the substrate surface. Material for microwave varactors will have effective epitaxial layer thicknesses less than one micron.

Figure 2.13 shows an experimental curve and a computer simulation plotted on the same set of coordinates. The purchased material used had the following given parameters:

epi thickness = 0.6 micron DNE = 1.0×10^{16} cm^{-3}

substrate thickness = 100 microns ONS = 1×10^{19} cm^{-3}

In matching the experimental curve to the computer predicted curve DNE, Q_{ss} and BX were perturbed slightly about initial guesses based on manufacturers' data and information supplied by other authors[6]. The final values used are listed in Figure 2.13 and are not very different from the initial data. Also, the experimental curve is a high frequency plot because the lowest measurement frequency available out of the Boonton bridge was 100 kHz. In order to see the low frequency plot, a measurement below 100 Hz is necessary.

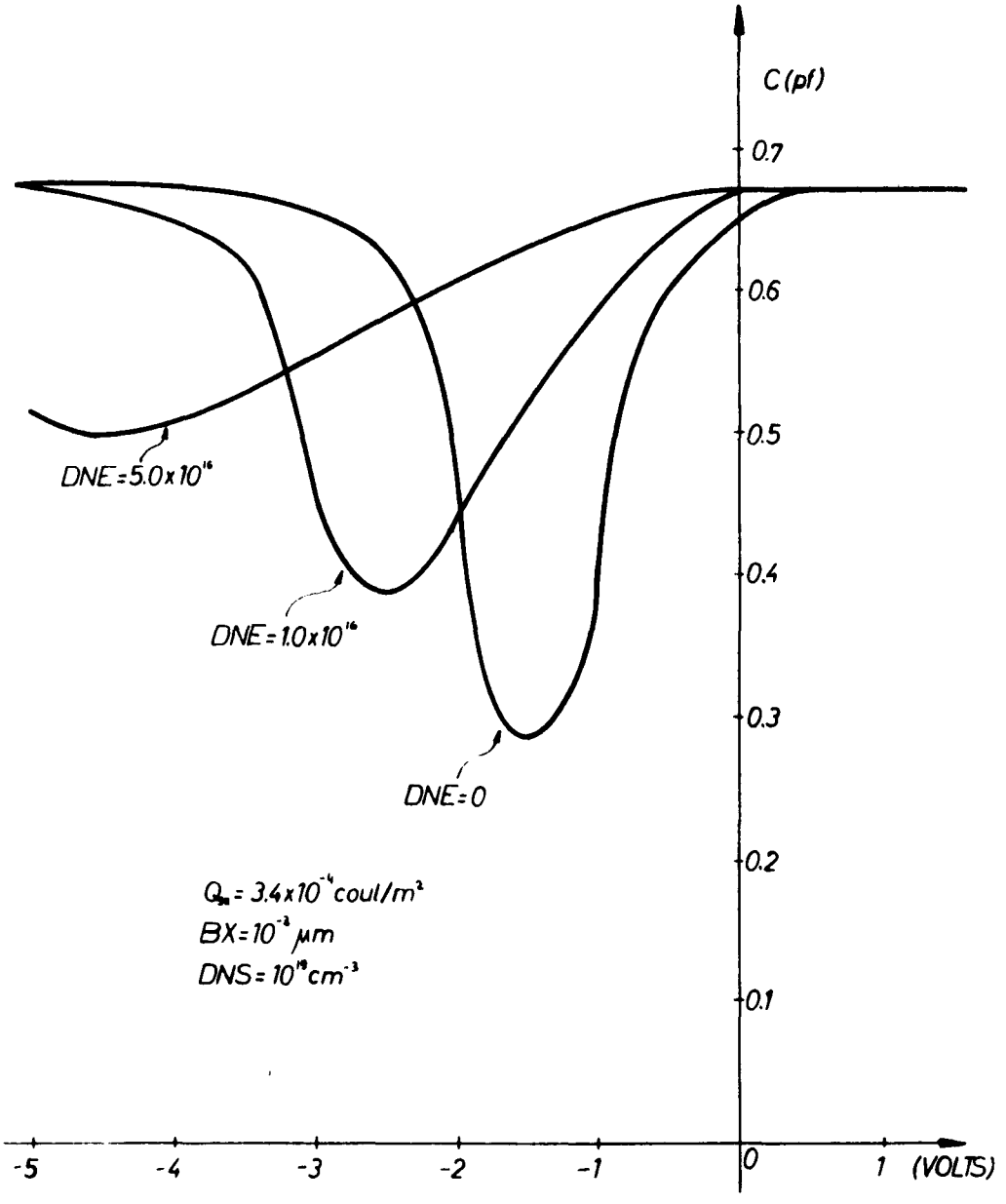

Figure 2.11 Differential capacitance versus voltage with DNE as a parameter.

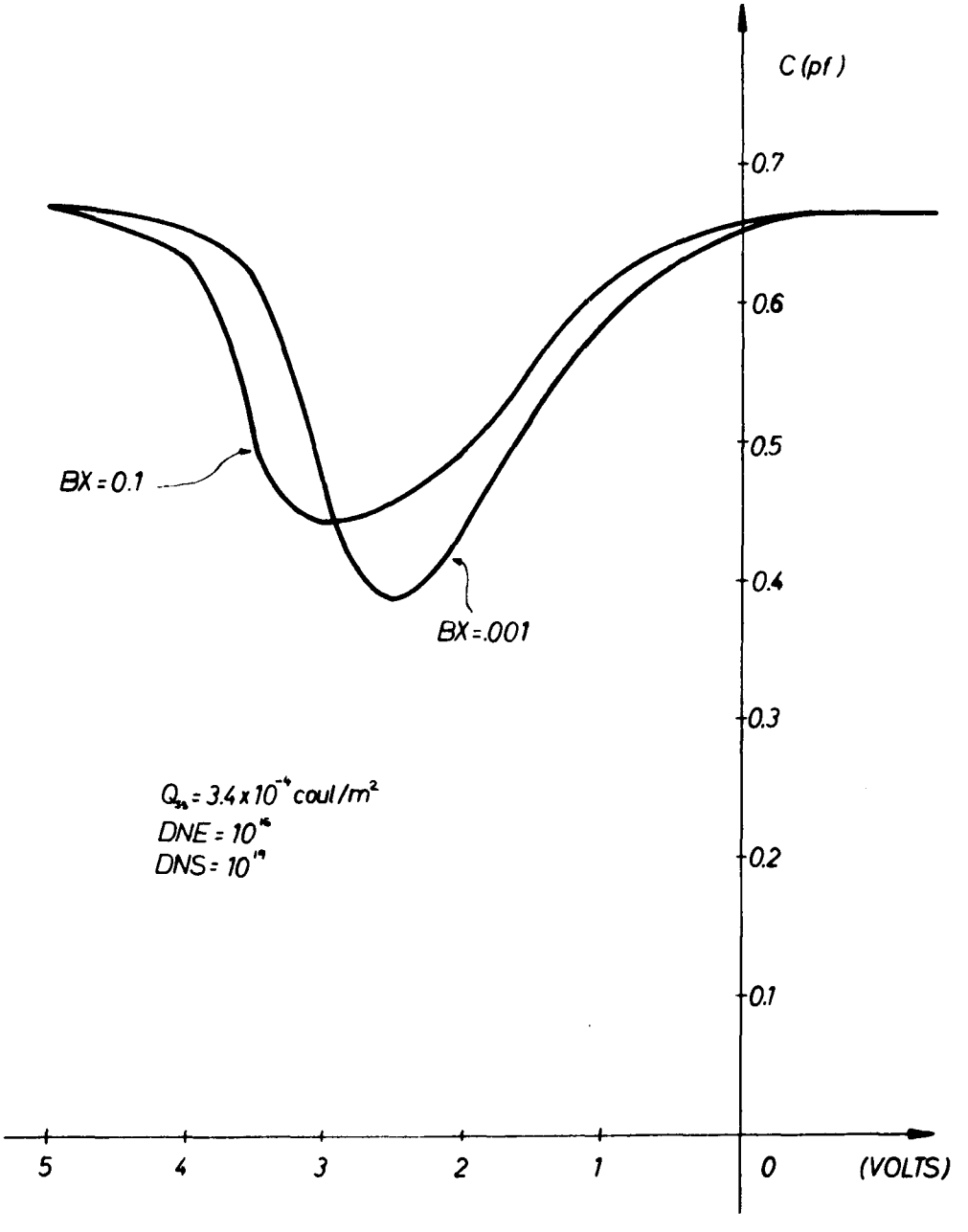

Figure 2.12 Differential capacitance versus voltage with BX as a parameter.

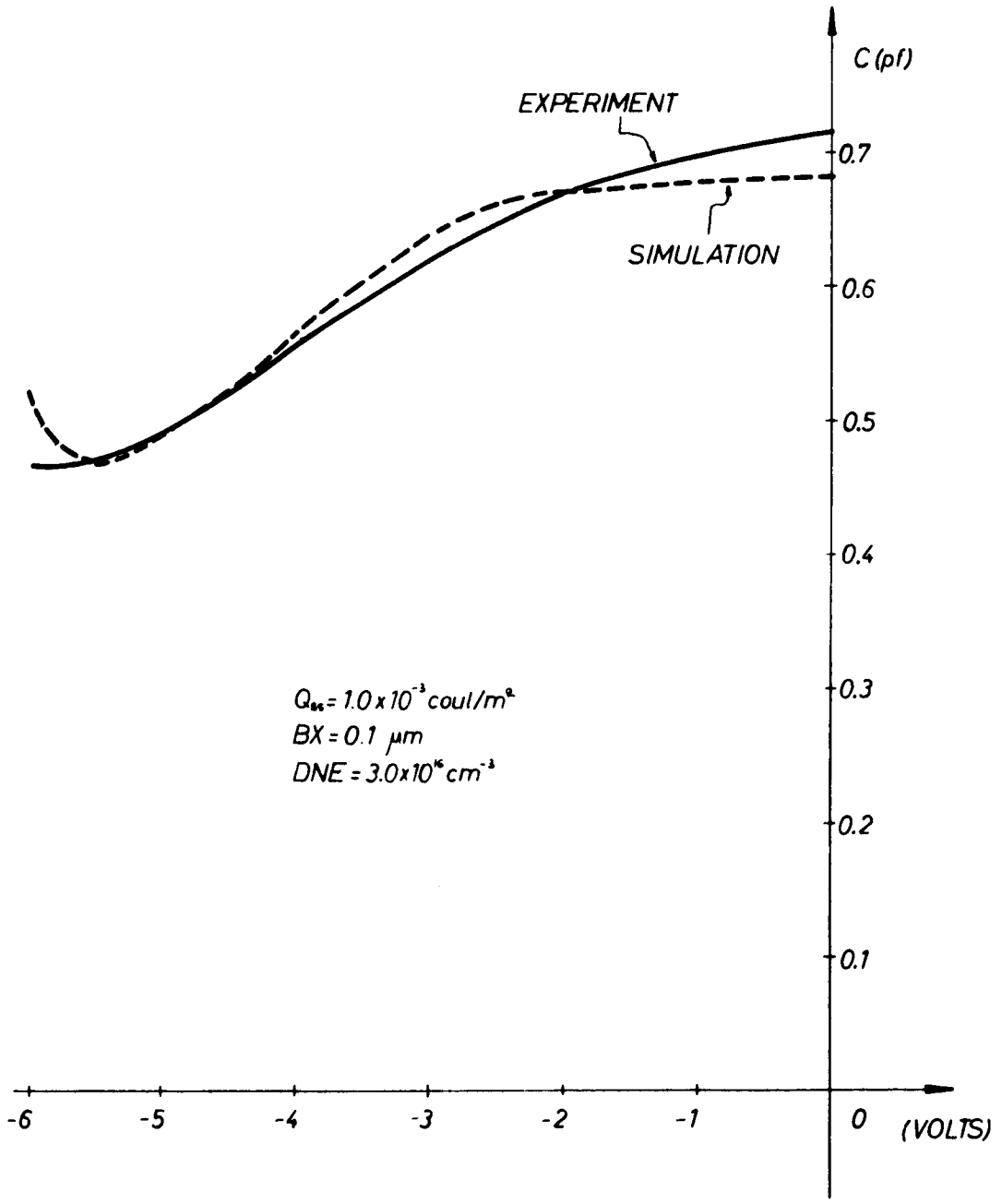

Figure 2.13 Simulation and correlation of SO-100-1000.

CHAPTER 3

MICROWAVE SMALL SIGNAL SIMULATION OF MIS VARACTORS

3.1 Derivation of a Small Signal Mathematical Model

In this section a small signal sinusoidal steady state model of an MIS varactor is developed. This involves the linearization and manipulation of the basic equations (1-1 to 1-12) into three coupled second order linear differential equations. The basic equations are linearized about a d.c. operating point (V_o) previously determined at every point in the semiconductor by the quasilinearization procedure described in Chapter 2. The coefficients of the microwave differential equations are terms involving only the d.c. solution. Boundary conditions are derived at the I-S interface and at an ohmic contact. The problem is set up as a linear boundary value problem and it is shown in later sections how these equations may be solved directly without iteration.

3.1.1 Small Signal Microwave Equations Valid in the Semiconductor

Combining Eq. (1-3), (1-4), (1-10) and (1-11), Poisson's equation may be written again in the form

$$\nabla^2 V = -\frac{q}{\varepsilon_s}\left(P-N+G(X)\right) \tag{3-1}$$

Also neglecting bulk recombination the continuity equations (1-5) and (1-6) may be rewritten as

$$\nabla\cdot\bar{J}_p + q\frac{\partial P}{\partial t} = 0 \tag{3-2}$$

$$\nabla\cdot\bar{J}_N - q\frac{\partial N}{\partial t} = 0 \tag{3-3}$$

It has been shown by others[13] that neglecting bulk recombination will predominantly have an effect on the minority carrier low frequency response. At microwaves neglecting recombination will increase calculated device Q. The current expressions (1-1) and (1-2) and the definitions of particle densities in terms of quasi-potentials are repeated here for completeness.

$$\bar{J}_p = -q\mu_p P \nabla V_p \tag{3-4}$$

$$\bar{J}_n = -q\mu_n N \nabla V_n \tag{3-5}$$

$$P = n_i \exp \frac{V_p - V}{V_T} \tag{3-6}$$

$$N = n_i \exp \frac{V - V_n}{V_T} \tag{3-7}$$

It should be noted that the three equations (3-1) to (3-3) form a set of nonlinear equations in V, V_p and V_n when the expressions (3-4) to (3-7) are used.

In the analysis that follows it is assumed that all terms are of the form

$$\bar{H} = \bar{H}_0 + \bar{H}_1 \exp j\omega t \tag{3-8}$$

where the subscripts 0 and 1 correspond to the d.c. small signal sinusoidal amplitudes, respectively. It is again assumed, as in the d.c. chapter, that no d.c. hole and electron current can flow.

$$\bar{J}_{no} = \bar{J}_{po} = 0 \tag{3-9}$$

This assumption is made since the insulator acts as a barrier to hole and electron movement. Starting with Eq. (3-4), the linearization process may begin.

$$\bar{J}_p = \bar{J}_{po}+\bar{J}_{p1}\exp j\omega t = -q\mu_p(P_o+P_1\exp j\omega t)\ \nabla\ (V_{po}+V_{p1}\exp j\omega t) \tag{3-10}$$

Expanding Eq. (3-10)

$$\bar{J}_p = -q\mu_p P_o \nabla\ (V_{po}+V_{p1}\exp j\omega t) - q\mu_p P_1 \exp j\omega t\ \ (V_{po}+V_{p1}\exp j\omega t) \tag{3-11}$$

Equating like terms on either side of the equation, and neglecting higher order terms

$$\bar{J}_{po} = -q\mu_p P_o \nabla V_{po} \tag{3-12}$$

$$\bar{J}_{p1} = -q\mu_p P_o \nabla V_{p1} - q\mu_p P_1 \nabla V_{po} \tag{3-13}$$

Using assumption (3-9)

$$\nabla V_{po} = 0 \tag{3-14}$$

and therefore

$$\bar{J}_{p1} = -q\mu_p P_o \nabla V_{p1} \tag{3-15}$$

Similarly, for electrons it may be shown that

$$\bar{J}_{n1} = -q\mu_n N_o \nabla V_{n1} \tag{3-16}$$

As in Chapter 2, if the Fermi potential is chosen as a reference, then

$$V_{no} = V_{po} = V_F = 0 \tag{3-17}$$

Expanding the hole density equation (3-6)

$$P_o+P_1\exp j\omega t = n_i\exp\left\{\frac{(V_{po}+V_{p1}\exp j\omega t)-(V_o+V_1\exp j\omega t)}{V_T}\right\} \tag{3-18}$$

$$P_o+P_1\exp j\omega t = n_i\exp\frac{V_{po}-V_o}{V_T}\exp\left\{\frac{(V_{p1}-V_1)\exp j\omega t}{V_T}\right\} \tag{3-19}$$

Expanding and neglecting higher order terms

$$P_o+P_1\exp j\omega t \cong n_i\exp\frac{V_{po}-V_o}{V_T}\left\{1+\frac{V_{p1}-V_1}{V_T}\exp j\omega t\right\} \tag{3-20}$$

Equating like terms and using Eq. (3-17)

$$P_o = n_i\exp-\frac{V_o}{V_T} \tag{3-21}$$

$$P_1 = P_o\left(\frac{V_{p1}-V_1}{V_T}\right) \tag{3-22}$$

Similarly, it may be shown for electrons

$$N_o = n_i\exp+\frac{V_o}{V_T} \tag{3-23}$$

$$N_1 = N_o\left(\frac{V_1-V_{n1}}{V_T}\right) \tag{3-24}$$

Poisson's equation and the two continuity equations may also be linearized in a like manner.

$$\nabla^2V_1+\frac{q}{\varepsilon_s}(P_1-N_1) = 0 \tag{3-25}$$

$$\nabla\cdot\bar{J}_{p1}+j\omega qP_1 = 0 \tag{3-26}$$

$$\nabla\cdot\bar{J}_{n1}-j\omega qN_1 = 0 \tag{3-27}$$

Note that $\frac{\partial}{\partial t}$ has been replaced by $j\omega$ since the assumed form of the solution is sinusoidal.

Substituting Eq. (3-22) and (3-24) into (3-25)

$$\nabla^2 V_1 + \frac{q}{\varepsilon_s}\left\{\frac{P_o}{V_T}(V_{p1}-V_1) - \frac{N_o}{V_T}(V_1-V_{n1})\right\} = 0 \tag{3-28}$$

Collecting like terms

$$\nabla^2 V_1 + \frac{q}{\varepsilon_s V_T}\left\{P_o V_{p1} - P_o V_1 - N_o V_1 + N_o V_{n1}\right\} = 0 \tag{3-29}$$

$$\nabla^2 V_1 + \frac{q}{\varepsilon_s V_T}\left\{P_o V_{p1} - (P_o+N_o)V_1 + N_o V_{n1}\right\} = 0 \tag{3-30}$$

or

$$\nabla^2 V_1 - \frac{q(P_o+N_o)}{\varepsilon_s V_T} V_1 + \frac{qN_o}{\varepsilon_s V_T} V_{n1} + \frac{qP_o}{\varepsilon_s V_T} V_{p1} = 0 \tag{3-31}$$

Substituting Eq. (3-15), (3-22) into (3-26)

$$\nabla\cdot\left\{-q\mu_p P_o \nabla V_{p1}\right\} + j\omega q P_o\left(\frac{V_{p1}-V_1}{V_T}\right) = 0 \tag{3-32}$$

but

$$\nabla(P_o \nabla V_{p1}) = P_o \nabla^2 V_{p1} + \nabla P_o \cdot \nabla V_{p1} \tag{3-33}$$

and

$$\nabla P_o = \nabla\left\{n_i \exp - \frac{V_o}{V_T}\right\} \tag{3-34}$$

$$\nabla P_o = n_i \nabla\left\{\exp - \frac{V_o}{V_T}\right\} \tag{3-35}$$

$$\nabla P_o = \underbrace{n_i \exp - \frac{V_o}{V_T}}_{P_o}\left(-\frac{1}{V_T}\right)\nabla V_o \tag{3-36}$$

but also

$$\bar{E}_o = -\nabla V_o \tag{3-37}$$

$$\therefore \quad \nabla P_o = \frac{P_o \bar{E}_o}{V_T} \tag{3-38}$$

Substituting Eq. (3-38) and (3-33) into (3-32)

$$P_o \nabla^2 V_{p1} + \frac{P_o \bar{E}_o}{V_T} \cdot \nabla V_{p1} - \frac{j\omega P_o}{V_T \mu_p} (V_{p1} - V_1) = 0 \tag{3-39}$$

and dividing through by P_o

$$\nabla^2 V_{p1} + \frac{\bar{E}_o}{V_T} \cdot \nabla V_{p1} - \frac{j\omega}{V_T \mu_p} (V_{p1} - V_1) = 0 \tag{3-40}$$

or

$$\nabla^2 V_{p1} + \frac{\bar{E}_o}{V_T} \cdot \nabla V_{p1} + \frac{j\omega}{V_T \mu_p} (V_1 - V_{p1}) = 0 \tag{3-41}$$

A similar equation may be derived using Eq. (3-27), (3-24) and (3-16).

$$\nabla^2 V_{n1} - \frac{\bar{E}_o}{V_T} \cdot \nabla V_{n1} + \frac{j\omega}{\mu_n V_T} (V_1 - V_{n1}) = 0 \tag{3-42}$$

Therefore, in order to solve the small signal r.f. problem, three coupled linear equations must be solved self-consistently for V_1, V_{n1}, and V_{p1} at every point in the semiconductor. The three pertinent equations are repeated here in summary.

$$\nabla^2 V_1 - \frac{q(P_o + N_o)}{\epsilon_s V_T} V_1 + \frac{qN_o}{\epsilon_s V_T} V_{n1} + \frac{qP_o}{\epsilon_s V_T} V_{p1} = 0 \tag{3-31}$$

$$\nabla^2 V_{n1} - \frac{\bar{E}_o}{V_T} \cdot \nabla V_{n1} + \frac{j\omega}{V_T \mu_n} (V_1 - V_{n1}) = 0 \tag{3-41}$$

$$\nabla^2 V_{p1} + \frac{\bar{E}_o}{V_T} \cdot \nabla V_{p1} + \frac{j\omega}{V_T \mu_p} (V_1 - V_{p1}) = 0 \tag{3-42}$$

Note that the coefficients involve d.c. solutions for hole and electron densities and electric field, which have previously been solved for in the d.c. problem:

$$\bar{E}_o = - \nabla V_o \tag{3-37}$$

$$P_o = n_i \exp - \frac{V_o}{V_T} \tag{3-21}$$

$$N_o = n_i \exp + \frac{V_o}{V_T} \tag{3-23}$$

3.1.2 Boundary Conditions at the Insulator-Semiconductor Interface (Ideal Surface)

Boundary conditions, at the I-S interface, will be derived for the variables V_1, V_{n1}, and V_{p1}. An ideal surface will be assumed with no fast surface states. This assumption is justified since this work deals exclusively with the silicon-silicon dioxide interface and annealing techniques have been worked out[6, others] for the minimization of fast states. Also, in a sufficiently high frequency range below the dielectric relaxation frequency of the majority carriers, but above the relaxation or characteristic frequencies of the surface states, the surface state impedance may be neglected[11,13].

At any point in the semiconductor or insulator the total current density is continuous. In the insulator, since no charged particles are allowed to exist the total current consists only of displacement current. In the insulator:

$$\bar{J}_1 = j\omega \bar{D}_1 \tag{3-43}$$

since

$$\bar{J}_{p1} = \bar{J}_{n1} = 0 \tag{3-44}$$

Taking the hole continuity equation (3-14) and integrating over the volume of the pillbox shown in Figure 3.1, a boundary condition on $\bar{J}_{p1}$ may be obtained.

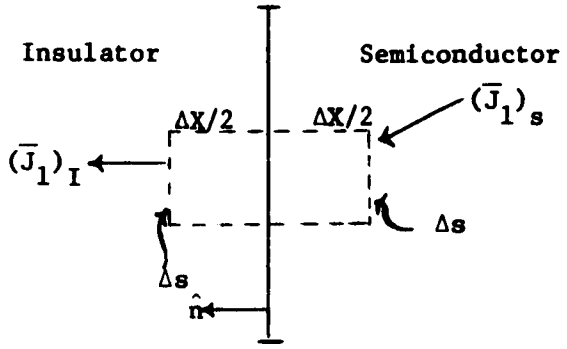

Figure 3.1 Insulator-semiconductor Interface.

$$\int_{\Delta V} (\nabla \cdot \bar{J}_{p1} + j\omega P_1)\, dV = 0 \tag{3-45}$$

where

$$\nabla V = \nabla s \cdot \nabla X \tag{3-46}$$

$$\int_{\Delta V} \nabla \cdot \bar{J}_{p1}\, dV + j\omega q \int_{\Delta V} P_1 dV = 0 \tag{3-47}$$

Using the divergence theorem on the first integral of Eq. (3-47)

$$I = \int_{\Delta V} \nabla \cdot \bar{J}_{p1} dv = \int_{\Delta V} \bar{J}_{p1} \cdot \hat{n}\, ds \tag{3-48}$$

where $s_{\nabla V}$ = surface of the volume ∇V.

$\hat{n}$ = unit vector normal to the I-S interface.

If we assume the pillbox is small enough so that the hole current may be consideree constant over the surface of the pillbox, then Eq. (3-47) may be written as

$$J_{p1}(X0+\Delta X/2)\Delta s - J_{p1}(X0-\Delta X/2)\Delta s + j\omega q P_1 \Delta s \Delta X = 0 \tag{3-49}$$

where all magnitudes are in the normal ($\hat{n}$) direction. Using Eq. (3-44) and dividing by Δs

$$J_{p1}(X0+\Delta X/2) + j\omega q P_1 \Delta X = 0 \tag{3-50}$$

The r.f. hold current may be defined by Eq. (3-50) in the limit as the pillbox volume goes to zero.

$$J_{p1}(X0) = \lim_{\Delta X \to 0} J_{p1}(X0+\Delta X/2) = \lim_{\Delta X \to 0} (-j\omega q P_1 \Delta X) \tag{3-51}$$

$$\therefore \quad J_{p1}(X0) = 0 \tag{3-52}$$

But, if the hole current is zero at the surface, the gradient of the quasi-hole potential must be zero by Eq. (3-15).

$$\therefore \quad \nabla_s V_{p1} = 0 \tag{3-53}$$

where it is understood that the gradient is in the normal direction. Similarly, it may be shown that

$$J_{n1}(X0) = \lim_{\Delta X \to 0} J_{n1}(X0+\Delta X/2) = \lim_{\Delta X \to 0} j\omega q n_1 \Delta X \tag{3-54}$$

$$\therefore \quad J_{n1}(\text{surface}) = 0 \tag{3-55}$$

and by Eq. (3-26)

$$\nabla_s V_{n1} = 0 \tag{3-56}$$

Now all that is required is a boundary condition on V_1. This may be obtained from the r.f. divergence equation

$$\nabla\cdot\bar{D}_1 = q(P_1-N_1) \tag{3-57}$$

Integrating again over the pillbox of Figure 3.1:

$$\int_{\Delta V} \nabla\cdot\bar{D}_1 \, dV = q\int_{\Delta V} (P_1-N_1) \, dV \tag{3-58}$$

Again using the divergence theorem

$$\int_{\Delta V} \nabla\cdot\bar{D}_1 \, dv = \int_{S_{\Delta V}} (\bar{D}_1\cdot\bar{n}ds) \tag{3-59}$$

$$\therefore \quad (D_1(X0+\Delta X/2) - D_1(X0-\Delta X/2)\Delta s = q(P_1-N_1)\Delta s\Delta X \tag{3-60}$$

$$(D_1-D_{I1})_{surface} = \lim_{\Delta X\to 0} q(P_1-N_1)\Delta X = 0 \tag{3-61}$$

Therefore, at the surface, in the normal direction

$$(D_{S1}-D_{I1}) = 0 \tag{3-62}$$

Note this boundary condition may be written in terms of r.f. electrostatic potentials since

$$D_1 = \varepsilon E_1 = -\varepsilon\nabla V_1 \tag{3-63}$$

$$\varepsilon_s\nabla_s V_1 - \varepsilon_I\nabla_I V_1 = 0 \tag{3-64}$$

It should also be noted that the boundary condition (3-64) may be obtained once results (3-52) and (3-55) have been established by realizing that the total current in the insulator is displacement current.

$$\bar{J}_I = j\omega\varepsilon_I \bar{E}_I = -j\omega\varepsilon_I \nabla_I V_1 \tag{3-65}$$

The total current at the semiconductor surface is displacement current by Eq. (3-52) and (3-55).

$$\bar{J}_s = j\omega\varepsilon_s \bar{E}_s = j\omega\varepsilon_s(-\nabla_s V_1) \tag{3-66}$$

But the total current must be continuous. Therefore,

$$j\omega\varepsilon_s(-\nabla_s V_1) = j\omega\varepsilon_I(-\nabla_I V_1) \tag{3-67}$$

$$\boxed{\varepsilon_s \nabla_s V_1 - \varepsilon_I \nabla_I V_1 = 0} \tag{3-64}$$

In summary, an ideal insulator-semiconductor interface has three boundary conditions which must be satisfied on the three unknowns: V_1, V_{p1}, and V_{n1}.

Summary of R.F. Boundary Conditions at I-S Interface

$$\varepsilon_s \nabla_s V_1 - \varepsilon_I \nabla_I V_1 = 0 \tag{3-64}$$

$$\nabla_s V_{n1} = 0 \tag{3-56}$$

$$\nabla_s V_{p1} = 0 \tag{3-53}$$

3.1.3 Boundary Conditions at an Ohmic Contact

At an ohmic contact the definition of surface recombination velocity is used.

$$\bar{J}_{p1} = S_{RP}(P-P_o) = S_{RP}P_1 \tag{3-68}$$

or

$$P_1 = \frac{\bar{J}_{p1}}{S_{RP}} \tag{3-69}$$

At an ohmic contact an infinite surface recombination velocity is often assumed[17].

$$P_1 = \lim_{S_{RP}\to\infty}\left(\frac{\bar{J}_{p1}}{S_{RP}}\right) = 0 \tag{3-70}$$

But by equation (3-22), Eq. (3-70) implies that

$$P_o\left(\frac{V_{p1}-V_1}{V_T}\right) = 0 \tag{3-71}$$

which in turn implies

$$V_{p1} = V_1 \tag{3-72}$$

Similarly, for electrons at an ohmic contact,

$$N_1 = \lim\left(\frac{J_{n1}}{S_{RN}}\right) = 0 \tag{3-73}$$

which by Eq. (3-24) implies that

$$V_1 = V_{n1} \tag{3-74}$$

Therefore, by Eq. (3-71) and (3-73), at an ohmic contact,

$$V_{n1} = V_{p1} = V_1 \tag{3-75}$$

and if the ohmic contact is r.f. grounded

$$V_{n1} = V_{p1} = V_1 = 0 \tag{3-76}$$

3.2 Finite Difference Approximation of MIS Small Signal Equations

Figure 3.2 summarizes the small signal, sinusoidal steady state mathematical model. As is shown by this figure, in this formulation a linear boundary value problem results in which three coupled linear equations in three unknowns must be solved. In the insulator Laplace's equation must be solved since no charge distribution is allowed to exist (fixed or mobile). The sinusoidal steady state solution requires first the solution for the d.c. electrostatic potential (V_o) throughout the semiconductor. The d.c. electrostatic potential is then used to calculate the coefficients of the linearized sinusoidal steady state differential equations. Once these coefficients are known, the system differential equations may be approximated by a system of algebraic equations which may be solved for uniquely.

The solution proceeds by setting up within the insulator and semiconductor a nonuniform grid of points. Figure 3.3 depicts a one-dimensional MIS structure with a uniform grid for the insulator, epitaxial layer, and substrate. Each grid step size may be varied by varying the number of points (N1,N2,N3) in each region. At each grid point the first and second derivatives are approximate by finite differences. The form of the expressions depends upon whether the region of interest is a uniform or nonuniform grid. In general, for a uniform grid the following two approximations may be used for first and second derivatives:

$$\left.\frac{dY}{dX}\right]_I = \frac{Y(I+1) - Y(I-1)}{2\Delta X} \qquad (3\text{-}77)$$

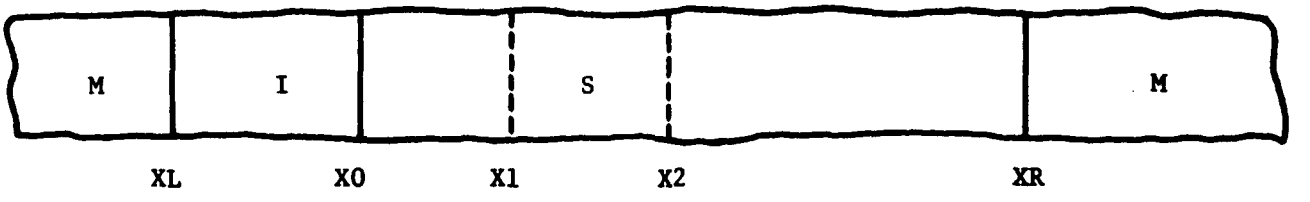

1. Insulator $$\frac{d^2V_1}{dX^2} = 0$$

2. Semiconductor

$$\nabla^2 V_1 + \frac{q}{\varepsilon_s V_T} \left[-(P_o + n_o)V_1 + n_o V_{n1} + P_o V_{p1} \right] = 0$$

$$\nabla^2 V_{n1} - \frac{\bar{E}_o}{V_T} \cdot \nabla V_{n1} + \frac{j\omega}{V_T \mu_n} (V_1 - V_{n1}) = 0$$

$$\nabla^2 V_{p1} + \frac{\bar{E}_o}{V_T} \cdot \nabla V_{p1} + \frac{j\omega}{V_T \mu_p} (V_1 - V_{p1}) = 0$$

3. Boundary Conditions

(3-a) $V_1(XL) = V1L$ at $X = XL$

(3-b) I-S Interface ($X = X_o$)

$$\varepsilon_s \nabla_s V_1 - \varepsilon_I \nabla_I V_1 = 0$$

$$\nabla_s V_{n1} = 0$$

$$\nabla_s V_{p1} = 0$$

(3-c) OHMIC CONTACT (Assuming infinite surface recombination)

$$V_1 = V_{n1} = V_{p1} = 0 \qquad \text{at } X = XR$$

Figure 3.2 Summary of small signal sinusoidal steady state mathematical model of an MIS varactor.

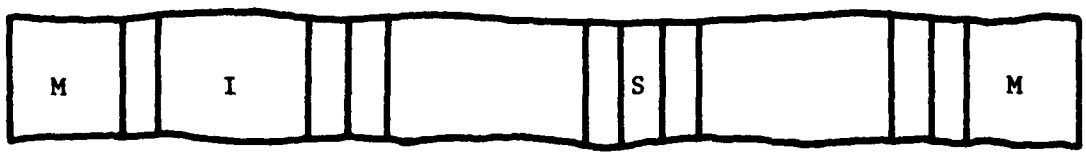

(1) N M1 P · L M K P1 L1 M1 K1

XL XO X1 X2 XR

XL, XO, XR - Are Metal-Insulator, Insulator-Semiconductor, and ohmic contacts, respectively.

X1 - Corresponds to transition point between N/NT

X2 - Corresponds to transition point between two uniform grids.

N1, N2, N3 - Are the number of increments in the insulator, semiconductor and substrate, respectively.

$K = N1 + N2$

$K1 = N1 + N2 + N3$

$XH1 = (XO-XL)/N1$

$XH2 = (X2-XO)/N2$

$XH3 = (XR-X2)/N3$

Figure 3.3 Grid point locations for numerical model.

$$\left.\frac{d^2Y}{dX^2}\right]_I = \frac{Y(I+1) - 2Y(I) + Y(I-1)}{\Delta X^2} \tag{3-78}$$

At point K in the semiconductor, special expressions for the first and second derivatives must be derived (Appendix I) since that point is the junction between two regions with different grid sizes. Therefore, at point K

$$\left.\frac{dY}{dX}\right]_K = \frac{Y(P1)}{(1+RS)XH3} + \frac{(RS-1)}{XH3}\,Y(K) - \frac{RS}{(1+RS)XH2}\,Y(M) \tag{3-79}$$

$$\left.\frac{d^2Y}{dX^2}\right]_K = \frac{2Y(M)}{H2(1+RS)} - \frac{2Y(K)}{(H2)(RS)} + \frac{2Y(P1)}{(H2)(RS)(1+RS)} \tag{3-80}$$

where XH2 and XH3 are the grid sizes in the epitaxial layer and substrate, respectively, and are defined in Figure 3.3.

$$H2 = (XH2)^2 \tag{3-81}$$

$$RS = (XH3)/(XH2) \tag{3-82}$$

Note that when the grid is uniform

$$XH2 = XH3 = \Delta X \tag{3-83}$$

$$RS = 1 \tag{3-84}$$

Eq. (3-79) and (3-80) reduce to Eq. (3-77) and (3-78) where

$$I = K \tag{3-85}$$

$$I+1 = P1 \tag{3-86}$$

$$I-1 = M \tag{3-87}$$

3.2.1 Finite Difference Approximation of Boundary Conditions at the I-S Interface

In one dimension, the boundary conditions at the I-S interface may be expressed as:

$$\varepsilon_s \left.\frac{dV_1}{dX}\right]_S - \varepsilon_I \left.\frac{dV_1}{dX}\right]_I = 0 \tag{3-88}$$

$$\left.\frac{dV_{n1}}{dX}\right]_S = 0 \tag{3-89}$$

$$\left.\frac{dV_{p1}}{dX}\right]_S = 0 \tag{3-90}$$

where again the subscripts S and I refer to derivatives evaluated from the semiconductor or insulator side of the interface. Using forward and backward approximations to the derivatives in Eq. (3-88) we get

$$\varepsilon_s \left(\frac{V1(P) - V1(N1)}{XH2}\right) - \varepsilon_I \left(\frac{V1(N1) - V1L}{X_o}\right) = 0 \tag{3-91}$$

Dividing Eq. (3-91) by ε_I/X_o and noting that

$$\frac{\varepsilon_s}{\varepsilon_I} = \frac{DKS}{DKI} \tag{3-92}$$

where DKS and DKI are relative permittivity of S and I

$$\frac{DKS}{DKI}\ \frac{XO}{XH2}\ \left(V1(P) - V1(N1)\right) - \left(V1(N1) - V1L\right) = 0 \tag{3-93}$$

Collecting like terms

$$-\left(1 + \frac{DKS}{DKI} \cdot \frac{XO}{XH2}\right)\ V1(N1) + \frac{DKS}{DKI}\ \frac{XO}{XH2}\ V1(P) = -V1L \tag{3-94}$$

Multiplying Eq. (3-94) by (-1)

$$\left(1 + \frac{DKS}{DKI}\frac{X_o}{XH2}\right) V1(N1) - \frac{DKS}{DKI}\frac{X_o}{XH2} V1(P) = V1L \qquad (3\text{-}95)$$

Again using a forward difference approximation to Eq. (3-89), (3-90) and multiplying by XH2

$$V_{n1}(P) - V_{n1}(N1) = 0 \qquad (3\text{-}96)$$

$$V_{p1}(P) - V_{p1}(N1) = 0 \qquad (3\text{-}97)$$

or

$$V_{n1}(N1) - V_{n1}(P) = 0 \qquad (3\text{-}98)$$

$$V_{p1}(N1) - V_{p1}(P) = 0 \qquad (3\text{-}99)$$

Therefore, at the interface point, X(N1), three algebraic equations may be derived approximating the three boundary conditions on V1, V_{p1}, and V_{n1}. The equations are (3-95), (3-98) and (3-99). The equations may also be written in matrix form if the ordering of variables takes the following form.

$$\bar{X} = [V1(N1), VN1(N1), VP1(N1), V1(P), VN1(P), VP1(P) \ldots\ldots] \qquad (3\text{-}100)$$

For this ordering Eq. (3-95), (3-98) and (3-99) may be written in the following form:

$$\begin{bmatrix} \left(1 + \frac{DKS}{DKI}\frac{X_o}{XH2}\right) & 0 & 0 & -\frac{DKS}{DKI}\frac{X_o}{XH2} & 0 & 0 \\ 0 & 1 & 0 & 0 & -1 & 0 \\ 0 & 0 & 1 & 0 & 0 & -1 \\ . & . & . & . & . & . \\ . & . & . & . & . & . \\ . & . & . & . & . & . \\ . & . & . & . & . & . \\ . & . & . & . & . & . \\ . & . & . & . & . & . \\ . & . & . & . & . & . \end{bmatrix} \begin{bmatrix} V1(N1) \\ VN1(N1) \\ VP1(N1) \\ V1(P) \\ VN1(P) \\ VP1(P) \\ . \\ . \\ . \\ . \\ . \end{bmatrix} = \begin{bmatrix} V1L \\ 0 \\ 0 \\ 0 \\ 0 \\ 0 \\ . \\ . \\ . \\ . \\ . \end{bmatrix} \quad (3\text{-}101)$$

A summary of the boundary conditions at the I-S interface is given in Figure 3.4.

3.2.2 Finite Difference Approximations within the Epitaxial Layer

In one dimension, Eq. (3-31), (3-41), and (3-42) may be written as:

$$\frac{d^2V_1}{dX^2} - \frac{q}{\varepsilon_s V_T}(N_o+P_o)V_1 + \frac{q}{\varepsilon_s V_T} N_o V_{n1} + \frac{qP_o}{\varepsilon_s V_T} V_{p1} = 0 \quad (3\text{-}102)$$

$$\frac{d^2V_{n1}}{dX^2} - \frac{E_o}{V_T}\frac{dV_{n1}}{dX} + \frac{j\omega}{V_T\mu_n} V_1 - \frac{j\omega}{V_T\mu_n} V_{n1} = 0 \quad (3\text{-}103)$$

$$\frac{d^2V_{p1}}{dX^2} + \frac{E_o}{V_T}\frac{dV_{p1}}{dX} + \frac{j\omega}{V_T\mu_p} V_1 - \frac{j\omega}{V_T\mu_p} V_{p1} = 0 \quad (3\text{-}104)$$

The first point after the insulator for which Eq. (3-102), (3-103) and (3-104) are valid is a point, P = N1+1.

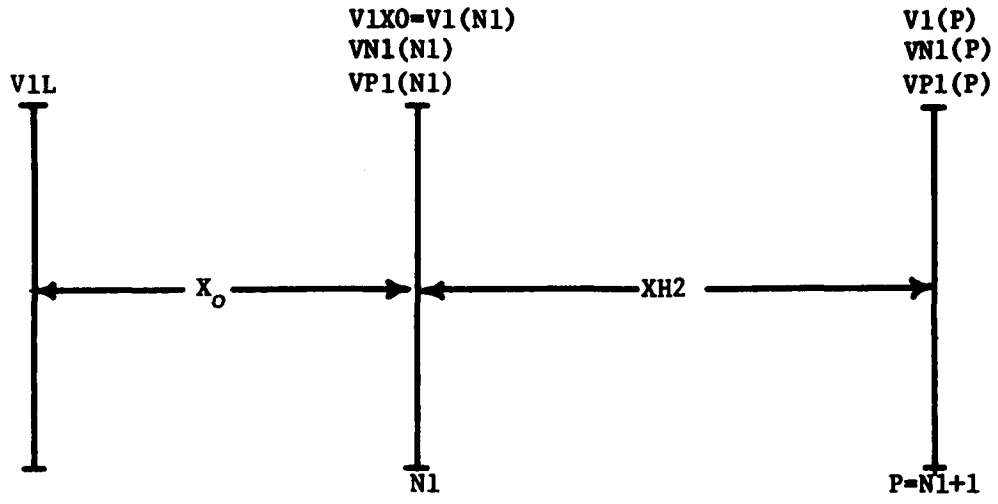

$$\begin{bmatrix} \left(1 + \frac{DKS}{DKI}\frac{X_o}{XH2}\right) & 0 & 0 & -\frac{DKS}{DKI}\frac{X_o}{XH2} & 0 & 0 \\ 0 & 1 & 0 & 0 & -1 & 0 \\ 0 & 0 & 1 & 0 & 0 & -1 \\ & & & & & \\ & & & & & \\ & & & & & \end{bmatrix} \begin{bmatrix} VL(N1) \\ VN1(N1) \\ VP1(N1) \\ V1(P) \\ VN1(P) \\ VP1(P) \end{bmatrix} = \begin{bmatrix} V1L) \\ 0 \\ 0 \\ 0 \\ 0 \\ 0 \end{bmatrix}$$

$$\varepsilon_s\left(\frac{dV_1}{dX}\right)_S - \varepsilon_I\left(\frac{dV_1}{dX}\right)_I = 0$$

$$\left(\frac{dV_{n1}}{dX}\right)_S = 0$$

$$\left(\frac{dV_{p1}}{dX}\right)_S = 0$$

Figure 3.4 Summary of approximate and exact boundary conditions at the insulator-semiconductor surface.

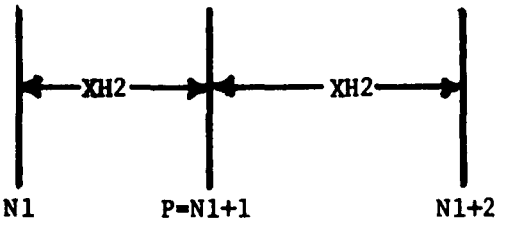

Figure 3.5 Three grid points within the epitaxial layer.

At Point P (Figure 3.5) the uniform finite difference approximations to first and second derivatives are valid. Substituting Eq. (3-76) and (3-77) into (3-102) we get one algebraic equation in three unknowns.

$$\frac{V_1(N1) - 2V_1(P) + V_1(N1+2)}{H2} - \frac{q}{\varepsilon_s V_T}\left(N_o(P)+P_o\right) V_1(P)$$

$$+ \frac{q}{\varepsilon_s V_T} N_o(P) V_{n1}(P) + \frac{qP_o(P)}{\varepsilon_s V_T} V_{p1}(P) \qquad (3\text{-}105)$$

Multiplying through by $H2 = (XH2)^2$

$$V_1(N1) - 2V_1(P) + V_1(N1+2) - \frac{H2}{\varepsilon_s V_T}\left\{N_o(P) + P_o(P)\right\} V_1(P)$$

$$+ \frac{qH2}{\varepsilon_s V_T} N_o(P) V_{n1}(P) + \frac{H2qP_o(P)}{\varepsilon_s V_T} V_{p1}(P) = 0 \qquad (3\text{-}106)$$

Collecting like terms

$$V_1(N1) - \left(2 + \frac{qH2}{\varepsilon_s V_T}\left(N_o(P)+P_o(P)\right)\right) V_1(P) + \frac{qH2}{\varepsilon_s V_T} N_o(P) V_{n1}(P)$$

$$+ \frac{qP_o(P)H2}{\varepsilon_s V_T} V_{p1}(P) + V_1(N1+2) = 0 \qquad (3\text{-}107)$$

Similarly, for Eq. (3-103)

$$\frac{V_{n1}(N1) - 2V_{n1}(P) + V_{n1}(N1+2)}{H2} - \frac{E_o(P)}{V_T}\left(\frac{V_{n1}(N1+2) - V_{n1}(N1)}{2XH2}\right) + \frac{j\omega}{V_T\mu_n} V_1(P)$$

$$- \frac{j\omega}{V_T\mu_n} V_{n1}(P) = 0 \qquad (3\text{-}108)$$

Multiplying by H2

$$V_{n1}(N1) - 2V_{n1}(P) + V_{n1}(N1+2) - \frac{E_o(P)XH2}{2V_T} V_{n1}(N1+2) + \frac{E_o(P)XH2}{2V_T} V_{n1}(N1)$$

$$+ \frac{j\omega H2}{V_T\mu_n} V_1(P) - \frac{j\omega H2}{V_T\mu_n} V_{n1}(P) = 0 \qquad (3\text{-}109)$$

Collecting terms

$$\left(1 + \frac{E_o(P)XH2}{2V_T}\right) V_{n1}(N1) + \frac{j\omega}{\mu_n V_T} V_1(P) - \left(2 + \frac{j\omega}{V_T\mu_n}\right) V_{n1}(P)$$

$$+ \left(1 - \frac{E_o(P)XH2}{2V_T}\right) V_{n1}(N1+2) = 0 \qquad (3\text{-}110)$$

Similarly expanding Eq. (3-104)

$$\frac{V_{p1}(N1) - 2V_{p1}(P) + V_{p1}(N1+2)}{H2} + \frac{XH2E_o(P)}{V_T}\left(\frac{V_{p1}(N1+2) - V_{p1}(N1)}{2XH2}\right)$$

$$+ \frac{j\omega H2}{V_T\mu_p} V_1(P) - \frac{j\omega H2}{V_T\mu_p} V_{p1}(P) = 0 \qquad (3\text{-}111)$$

Collecting like terms

$$\left(1 - \frac{XH2E_o(P)}{2V_T}\right)V_{p1}(N1) + \frac{j\omega H2}{V_T\mu_p}V_1(P) - \left(2 + \frac{j\omega H2}{V_T\mu_p}\right)V_{p1}(P)$$

$$+ \left(1 + \frac{XH2E_o(P)}{2V_T}\right)V_{p1}(N1+2) = 0 \qquad (3\text{-}112)$$

Equations (3-112), (3-110) and (3-107) may be represented in matrix form and is summarized in Figure 3.6. Also in this figure the matrix elements corresponding to the next point, I=N1+2, are listed by inspection. It can be seen from this figure that the matrix can be considered a very sparse matrix of the band type. Specifically, the band width is 7 diagonals and within these bands there are many zeros. The form of the matrix elements continues at every point in the semiconductor in the first uniform grid region (I=P,M). At point K a nonuniform grid situation exists and, therefore, special matrix elements must be derived.

3.2.3 Finite Difference Approximations at the Nonuniform Grid Point, I=K

At the grid point I=K the finite difference approximations for a nonuniform grid previously derives [Eq. (3-79) and (3-80)] may be used. Substituting Eq. (3-79) and (3-78) into (3-102)

$$\frac{2V_1(M)}{H2(1+RS)} - \frac{2V_1(K)}{H2\cdot RS} + \frac{2V_1(P1)}{(H2)(RS)(1+RS)} - \frac{q}{\varepsilon_s V_T}(N_o(K)+P_o(K)V_1(K)$$

$$+ \frac{q}{\varepsilon_s V_T}N_o(K)V_{n1}(K) + \frac{qP_o}{\varepsilon_s V_T}V_{p1}(K) = 0 \qquad (3\text{-}113)$$

1	2	3	4	5	6	7	8	9	10	11	12	J	I
$1+\frac{DKS\ X_o}{DK1\ XH2}$	0	0	$-\frac{DKS\ X_o}{DK1\ XH2}$	0	0							1	
0	1	0	0	-1	0							2	N1
0	0	1	0	0	-1							3	
1	0	0	$-(2+\frac{qH2}{\epsilon_s V_T}(P_o+n_o))$	$\frac{qH2}{\epsilon_s V_T} n_o(P)$	$\frac{qH2 P_o(P)}{\epsilon_s V_T}$	1	0	0				4	
0	$1+\frac{E_o(P)XH2}{2V_T}$	0	$j\frac{\omega H2}{\mu_n V_T}$	$-(2+\frac{j\omega}{\mu_n V_T})$	0	0	$1-\frac{E_o(P)XH2}{2V_T}$	0				5	P= N1+1
0	0	$1-\frac{E_o(P)XH2}{2V_T}$	$j\frac{\omega H2}{V_T \mu_p}$	0	$-(2+\frac{j\omega H2}{V_T \mu_p})$	0	0	$1+\frac{E_o(P)XH2}{2V_T}$				6	
			1	0	0	$-(2+\frac{qH2}{\epsilon_s V_T}(P_o+n_o))$	$\frac{qH2}{\epsilon_s V_T} n_o$	$\frac{qH2}{\epsilon_s V_T} E(N1+2)$	1			7	
				$1+\frac{E_o(N1+2)XH2}{2V_T}$	0	$+j\frac{\omega H2}{\mu_n V_T}$	$-(2+\frac{j\omega}{V_T \mu_n})$	0	0	$1-\frac{E_o(N1+2)XH2}{2V_T}$		8	N1+2
					$1+\frac{E_o(N1+2)XH2}{2V_T}$	$+j\frac{\omega H2}{V_T \mu_p}$	0	$-(2+\frac{j\omega H2}{V_T \mu_p})$	0	0	$1+\frac{E_o(N1+2)XH2}{2V_T}$	9	

Figure 3.6 Summary of first nine rows of the R.F. matrix.

Collecting like terms

$$\left(\frac{2}{H2(1+RS)}\right) V_1(M) - \left(\frac{2}{H2RS} + \frac{q}{\varepsilon_s V_T}\left(N_o(K)+P_o(K)\right)\right) V_1(K) + \frac{q}{\varepsilon_s V_T} N_o(K) V_{ni}(K)$$

$$+ \frac{qP_o}{\varepsilon_s V_T} V_{p1}(K) + \frac{2V_1(P1)}{(H2)(RS)(1+RS)} = 0 \qquad (3\text{-}114)$$

Multiplying by H2

$$\frac{2}{1+RS} V_1(M) - \left\{\frac{2}{RS} + \frac{q\,H2}{\varepsilon_s V_T}\left(N_o(K)+P_o(K)\right)\right\} V_1(K) + \frac{qH2}{\varepsilon_s V_T} N_o(K) V_{n1}(K)$$

$$+ \frac{qH2}{\varepsilon_s V_T} P_o(K) V_{p1}(K) + \frac{2}{RS(1+RS)} V_1(P_1) = 0 \qquad (3\text{-}115)$$

Similarly discretizing Eq. (3-103) with the nonuniform finite difference formulae for the first and second derivative Eq. (3-79) and (3-80).

$$\frac{2V_{n1}(M)}{(1+RS)} - \frac{2V_{n1}(K)}{RS} + \frac{2V_{n1}(P1)}{RS(1+RS)} - \frac{E_o(K)H2}{V_T}\left\{\frac{V_{n1}(P1)}{(1+RS)XH3} + \frac{RS-1}{XH3} V_{n1}(K)\right.$$

$$\left. - \frac{RS}{(1+RS)XH2} V_{n1}(M)\right\} + \frac{j\omega H2}{V_T \mu_n} V_1(K) - \frac{j\omega H2}{V_T \mu_n} V_{n1}(K) = 0 \qquad (3\text{-}116)$$

Collecting terms and multiplying

$$\left\{\left(\frac{2}{1+RS}\right) + \frac{E_o(K)XH2}{V_T}\,\frac{RS}{(1+RS)}\right\} V_{n1}(M) + \frac{j\omega H2}{V_T\mu_n}\,V_1(K)$$

$$-\left\{\frac{2}{RS} + \frac{E_o(K)XH2}{V_T}\,\frac{(RS-1)}{RS} + \frac{j\omega H2}{V_T\mu_n}\right\} V_{n1}(K)$$

$$+\left\{\frac{2}{RS(1+RS)} - \frac{E_o(K)H2}{V_T(1+RS)XH3}\right\} V_{n1}(P_1) = 0 \qquad (3\text{-}117)$$

Note that $RS = \frac{XH3}{XH2}$ so that Eq. (3-117) may be rewritten as

$$\left\{\frac{2}{1+RS} + \frac{E_o(K)XH2}{V_T}\left(\frac{RS}{1+RS}\right)\right\} V_{n1}(M) + \frac{j\omega H2}{V_T\mu_n}\,V_1(K)$$

$$-\left\{\frac{2}{RS} + \frac{E_o(K)XH2}{V_T}\left(\frac{RS-1}{RS}\right) + \frac{j\omega H2}{V_T\,n}\right\} V_{n1}(K)$$

$$+\left\{\frac{2}{RS(1+RS)} - \frac{E_o(K)XH2}{V_T}\left(\frac{1}{(1+RS)RS}\right)\right\} V_{n1}(P_1) = 0 \qquad (3\text{-}118)$$

Similarly, for Eq. (3-104)

$$\frac{2}{(1+RS)}\,V_{p1}(M) - \frac{2}{RS}\,V_{p1}(K) + \frac{2}{RS(1+RS)}\,V_{p1}(P_1)$$

$$+\frac{E_o(K)XH2}{V_T}\left\{\frac{V_{p1}(P_1)}{(1+RS)RS} + \frac{RS-1}{RS}\,V_{p1}(K) - \frac{RS}{(1+RS)}\,V_{p1}(M)\right\}$$

$$+\frac{j\omega H2}{V_T\mu_p}\,V_1(K) - \frac{j\omega H2}{V_T\mu_p}\,V_{p1}(K) = 0 \qquad (3\text{-}119)$$

Collecting terms

$$\left\{\frac{2}{1+RS} - \frac{E_o(K)XH2}{V_T}\ \frac{RS}{(1+RS)}\right\} V_{p1}(M) + \frac{j\omega H2}{V_T\mu_p} V_1(K)$$

$$-\left\{\frac{2}{RS} - \frac{E_o(K)XH2}{V_T}\left(\frac{RS-1}{RS}\right) + \frac{j\omega H2}{V_T\mu_p}\right\} V_{p1}(K)$$

$$+\left\{\frac{2}{RS(1+RS)} + \frac{E_o(K)XH2}{V_T}\ \frac{1}{(1+RS)RS}\right\} V_{p1}(P_1) = 0 \qquad (3\text{-}120)$$

In summary, at point (K) Equations (3-115), (3-118) and (3-120) are the valid algebraic equations. These equations are somewhat complex because the points M, K and P1 constitute a nonuniform grid.

3.2.4 Finite Difference Approximations in the Substrate

After point K the grid size (XH3) becomes relatively large as compared to the grid size in the epitaxial layer. The first point which uses such a grid size is point I=P1. The three points K, P1 and P1+1 of Figure 3.3 are redrawn below for clarity in Figure 3.7.

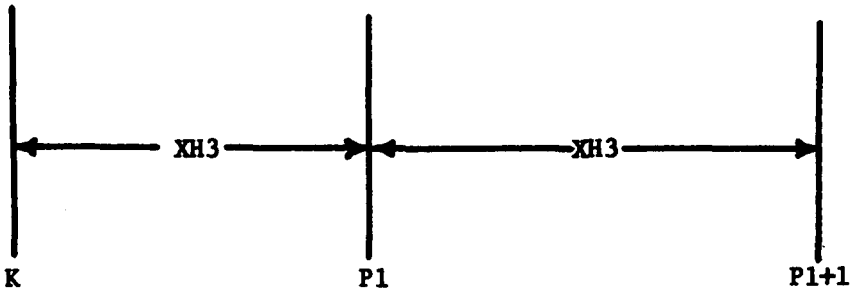

Figure 3.7 Three points within the substrate.

At point P1 the uniform grid formulas previously derived [Eq. (3-107), (3-110) and (3-112)] with the exception that

$$XH2 \rightarrow XH3$$

$$N1 \rightarrow K$$

$$P \rightarrow P1$$

$$N1+2 \rightarrow P1+1$$

Making the above substitutions the three algebraic equations valid at point I=P1 are

$$V_1(K) - \left(2 + \frac{qH3}{\varepsilon_s V_T}\left(N_o(P1)+P_o(P1)\right)\right) V_1(P1) + \frac{qH3}{\varepsilon_s V_T} N_o(P1) V_{n1}(P1)$$

$$+ \frac{qP_o(P1)H3}{\varepsilon_s V_T} V_{p1}(P1) + V_1(P1+1) = 0 \qquad (3\text{-}121)$$

and corresponding to Eq. (3-110)

$$\left(1 + \frac{E_o(P1)XH3}{2V_T}\right)V_{n1}(K) + \frac{j\omega H3}{\mu_n V_T} V_1(P1) - \left(2 + \frac{j\omega H3}{V_T \mu_n}\right)V_{n1}(P1)$$

$$+ \left(1 - \frac{E_o(P1)XH3}{2V_T}\right)V_{n1}(P1+1) = 0 \qquad (3\text{-}122)$$

and also corresponding to Eq. (3-112)

$$\left(1 - \frac{E_o(P1)XH3}{2V_T}\right)V_{p1}(K) + \frac{j\omega H3}{V_T \mu_p} V_1(P1) - \left(2 + \frac{j\omega H3}{V_T \mu_p}\right)V_{p1}(P1)$$

$$+ \left(1 + \frac{XH3E_o(P1)}{2V_T}\right)V_{p1}(P1+1) = 0 \qquad (3\text{-}123)$$

A set of algebraic equations similar to Eq. (3-121), (3-122) and (3-123) must be written up to and including the point I=M1. At the point I=M1 the boundary condition [Eq. (3-75)] is used.

Therefore, at the point I=M1 the following three equations are valid.

$$V_1(L1) - \left(2 + \frac{qH3}{\epsilon_s V_T}\left(N_o(M1)+P_o(M1)\right)\right) V_1(M1)$$

$$+ \frac{qH3}{\epsilon_s V_T} N_o(M1)V_{n1}(M1) + \frac{qP_o(M1)H3}{\epsilon_s V_T} V_{p1}(M1) = 0 \qquad (3\text{-}124)$$

and

$$\left(1 + \frac{E_o(M1)XH3}{2V_T}\right)V_{n1}(L1) + \frac{j\omega H3}{\mu_n V_T} V_1(M1) - \left(2 + \frac{j\omega H3}{V_T\mu_n}\right) V_{n1}(M1) = 0 \qquad (3\text{-}125)$$

and

$$\left(1 - \frac{E_o(M1)XH3}{2V_T}\right)V_{p1}(L1) + \frac{j\omega H3}{V_T\mu_p} V_1(M1) - \left(2 + \frac{j\omega H3}{V_T\mu_p}\right)V_{p1}(M1) = 0 \qquad (3\text{-}126)$$

3.2.5 Summary of Elements of the Band Matrix

The linearized r.f. problem reduces to a set of algebraic equations which is shown (Figure 3.8) to be of the band type (seven bands). Figure 3.6 depicts a full seven-band matrix in which each band has been given a letter (A1, B1, C1, D1, E1, F1, G1). It should be noted that only one element of the matrix may be located by indicating the band letter and a row index (J). J is an integer which takes on any value from J=1 to J=NE.

NE = number of equations

Associated with each element is an index, I, which designates the grid point within the semiconductor at which that coefficient is being evaluated. The integer I varies from N1 to M1. Recall also that

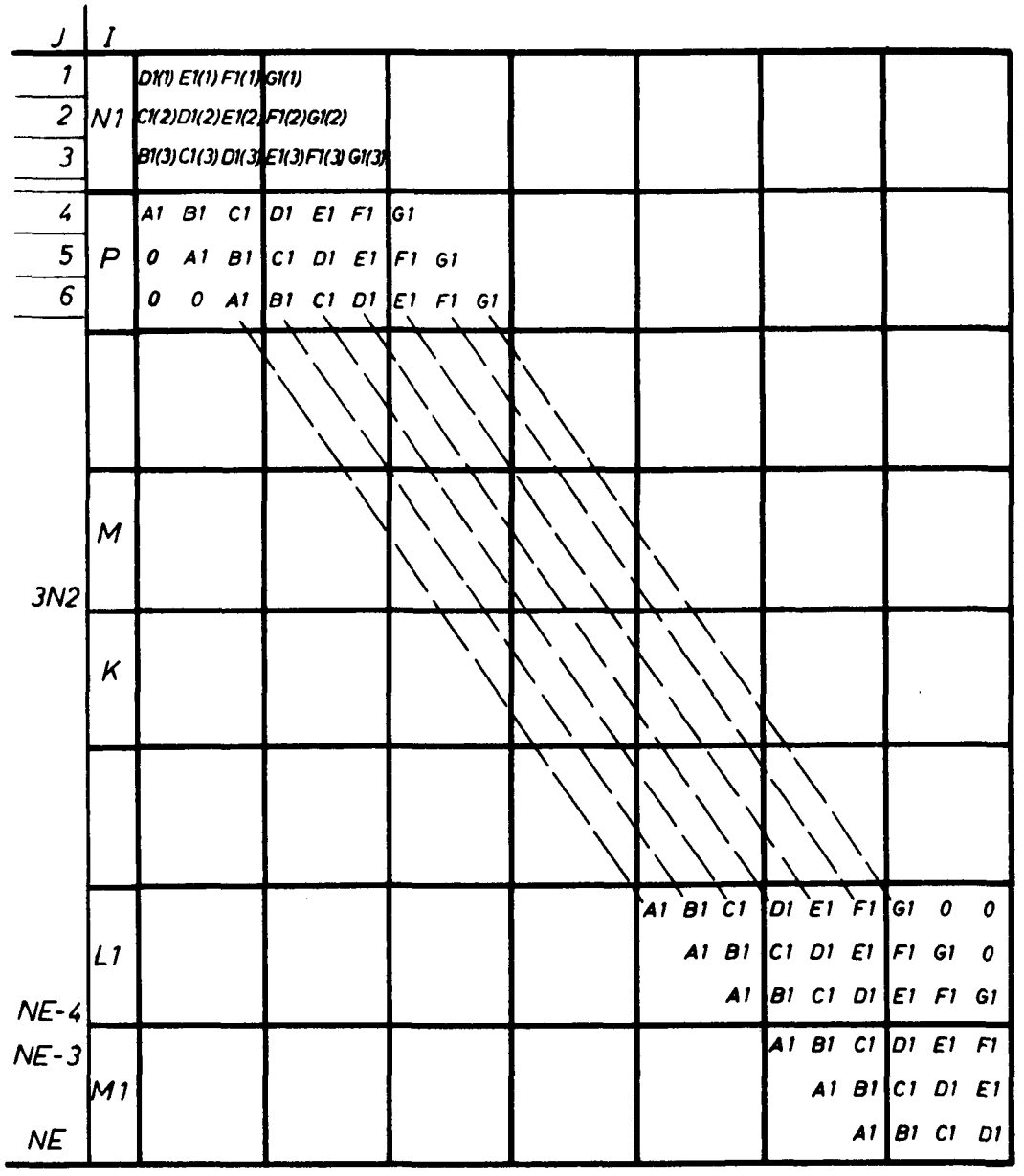

Figure 3.8 Full seven-band matrix.

$$M1 = K1-1 = (N1+N2+N3) - 1 \tag{3-127}$$

The two integers are really related since the matrix represents three algebraic equations in the three unknowns $V_1(J)$, $V_{n1}(J)$, and $V_{p1}(J)$. Therefore, it can be shown that

NE = 3 (number of points in the epitaxial layer and substrate combined)

$$\therefore \quad NE = 3(N2+N3) \tag{3-128}$$

Comparing Figures 3.6 and 3.7 the actual values of the band matrix may be explicitly evaluated. Starting with band $\bar{A}1$:

J	4	A1(4) = 1	(3-129)
I=P=N1+1	5	A1(5) = 1 + $\{E_o(P)XH2/2V_T\}$	(3-130)
	6	A1(5) = 1 - $\{E_o(P)XH2/2V_T\}$	(3-131)
	7	A1(7) = 1	(3-132)
I=N1+2	8	A1(8) = 1 + $\{E_o(N1+2)XH2/2V_T\}$	(3-133)
	9	A1(9) = 1 - $\{E_o(N1+2)XH2/2V_T\}$	(3-134)
		A1(J) = 1	(3-135)
I		A1(J+1) = 1 + $\{E_o(I)XH2/2V_T\}$	(3-136)
		A1(J+2) = 1 - $\{E_o(I)XH2/2V_T\}$	(3-137)
		A1(3N2-2) = 1	(3-138)
I=M		A1(3N2-1) = 1 + $\{E_o(M)XH2/2V_T\}$	(3-139)
		A1(3N2) = 1 - $\{E_o(M)XH2/2V_T\}$	(3-140)

Note that I=K. A nonuniform grid exists and therefore the three values of A are valid at this point change in form. Referring to Eq. (3-115), (3-118), and (3-120), at point I=K

$$A(3N2+1) = \frac{2}{1+RS} \tag{3-141}$$

$$A(3N2+2) = \frac{2}{1+RS} + \frac{E_o(I)XH2}{V_T}\,\frac{RS}{1+RS} \tag{3-142}$$

$$A(3N2+3) = \frac{2}{1+RS} - \frac{E_o(I)XH2}{V_T}\,\frac{RS}{1+RS} \tag{3-143}$$

After point K there exists a uniform grid of spacing XH3.

$$A(3N2+4) = 1 \tag{3-144}$$

I=P1 $$A(3N2+5) = 1 + \{E_o(I)XH3/2V_T\} \tag{3-145}$$

$$A(3N2+6) = 1 - \{E_o(I)XH3/2V_T\} \tag{3-146}$$

$$\vdots$$

$$A(NE-2) = 1 \tag{3-147}$$

I=M1 $$A(NE-1) = 1 + \{E_o(I)XH3/2V_T\} \tag{3-148}$$

$$A(NE) = 1 + \{E_o(I)XH3/2V_T\} \tag{3-149}$$

Note that $E_o = -\frac{dV}{dX}$, which may be expressed as

$$E_o(I) = -\frac{V(I+1) - V(I-1)}{2\Delta X} \tag{3-150}$$

in a uniform grid. In a nonuniform grid such as I=K

$$E_o(K) = -\left\{\frac{V(P_1)}{(1+RS)XH3} + \frac{(RS-1)}{XH3}V(K) - \frac{RS}{(1+RS)(XH2)}V(M)\right\} \quad (3\text{-}151)$$

Using Eq. (3-150) and (3-151) it may be seen that the d.c. electrostatic potential, V, is all that is necessary to completely specify Al. The list of statements which store the elements of Al on the computer are summarized in Figure 3.9. Similarly, Figures 3.10 to 3.15 summarize the elements of each band and the method by which they are stored in the computer.

3.3 High Frequency Simulation of MIS Varactors and Comparison with Experiments

3.3.1 Simplified Mathematical Model

For impurity profiles of one type dopant (n/n^+) minority carrier generation rates are so low that minority carriers may be completely neglected at high frequencies[11]. This assumption implies that minority carriers can be supplied only by the ohmic contact at X=XR. Therefore, if the contact is far enough away from the interface

$$XR >> \sqrt{D/\omega} \quad (3\text{-}152)$$

where D is the minority carrier diffusion coefficient. For an n-type semiconductor the minority carriers are holes and the diffusion coefficient is

$$D_p = V_T \mu_p \quad (3\text{-}153)$$

At room temperature and at 3.5 GHz

$$XR >> .25\ \mu m \quad (3\text{-}154)$$

```
J = 4
DO 22  I = P,M
A(J) = 1
```

$$A(J+1) = 1 + \frac{E_o(I)XH2}{2V_T} = 1 - \frac{V(I+1)-V(I-1)}{4V_T}$$

$$A(J+2) = 1 - \frac{E_o(I)XH2}{2V_T} = 1 + \frac{V(I+1)-V(I-1)}{4V_T}$$

```
J = J+3
22  CONTINUE
```

$$A(J) = \frac{2}{1+RS}$$

$$A(J+1) = \frac{2}{1+RS} + \frac{RS}{1+RS}\ \frac{XH2E_o(K)}{V_T}$$

$$A(J+2) = \frac{2}{1+RS} - \frac{RS}{1+RS}\ \frac{XH2E_o(K)}{V_T}$$

```
J = J+3
DO 23  I = P1,M1
A(J) = 1
```

$$A(J+1) = 1 - \frac{V(I+1)-V(I-1)}{4V_T}$$

$$A(J+2) = 1 + \frac{V(I+1)-V(I-1)}{4V_T}$$

```
J = J+3
23  CONTINUE
```

Figure 3.9 The A1 diagonal

```
B1(3) = 0

J = 4

DO 24  I = P,M

B1(J) = 0

B1(J+1) = 0

B1(J+2) = +j (ωH2 / V_T μ_p)  X 10^-8 = +jXP2

J = J+3

24  CONTINUE

B1(J) = 0

B1(J+1) = 0

B1(J+2) = +j (ωH2 / V_T μ_p)  X10^-8 = +jXP2

J = J+3

DO 26  I = P1,M1

B1(J) = 0

B1(J+1) = 0

                    XH3
B1(J+2) = +j (RS*RS*H2ω / V_T μ_p) X 10^-8 = +jXP3

J = J+3

26  CONTINUE
```

$$\underline{\text{Units}} \quad \frac{\omega H2}{V_T \mu_p} = \frac{(\text{micron})^2}{(\text{cm}^2)} = \left(\frac{\text{micron}}{\text{cm}}\right)^2$$

$$\left.\begin{array}{l} 1 \text{ micron} = 10^{-6}\text{m} \\ 1 \text{ cm} \quad = 10^{-2}\text{m} \end{array}\right\} \left(\frac{\text{micron}}{\text{cm}}\right)^2 = \left(10^{-4}\right)^2 = 10^{-8}$$

Figure 3.10 The B1 diagonal

```
C1(2) = 0

C1(3) = 0

J = 4

DO 27  I = P,M

C1(J) = 0

C1(J+1) = + j (H2)ω / V_T μ_n  X 10^-8 = +jXN2

C(J+2) = 0

J = J+3

27  CONTINUE

C1(J) = 0

C1(J+1) = +j H2ω / V_T μ_n  X 10^-8 = + jXN2

C1(J+2) = 0

J = J+3

DO 28  I = P1,M1

C1(J1) = 0

C1(J+1) = + j H3ω / V_T μ_n  X 10^-8 = + jXN3

C1(J+2) = 0

J = J+3

28  CONTINUE
```

Figure 3.11 The C1 diagonal

$$D1(1) = 1 + \frac{DKS}{DKI}\ \frac{X_o}{XH2}$$

$$D1(2) = 1$$

$$D1(3) = 1$$

$$J = 4$$

$$DO\ 29\quad I = P,M$$

$$D1(J) = -2 - \frac{qH2}{\varepsilon_s V_T}\left(P_o(I)+N_o(I)\right) = -2 - \underbrace{\frac{qH2}{\varepsilon_s V_T}(2n_i)^{x10^{-6}}}_{CS}\ \text{Cosh}\ \frac{V(I)}{V_T}$$

$$D1(J+1) = -2 - j\ \frac{\omega H2}{V_T \mu_n}\ x10^{-8} = -2 - jXN2$$

$$D1(J+2) = -2 - j\ \frac{\omega H2}{V_T \mu_p}\ X10^{-8} = -2 - jXP2$$

$$J = J+3$$

$$29\quad CONTINUE$$

$$D1(J) = -\frac{2}{RS} - \frac{qH2}{\varepsilon_s V_T}\left(N_o(K)+P_o(K)\right) = -\frac{2}{RS} - CS\ \text{Cosh}\ \frac{V(K)}{V_T}$$

$$D1(J+1) = -\frac{2}{RS} - \frac{E_o(K)XH2}{V_T}\ \frac{RS-1}{RS} - j\ \underbrace{\frac{\omega H2}{V_T \mu_n}\ X10^{-8}}_{XN2}$$

$$D1(J+2) = -\frac{2}{RS} + \frac{E_o(K)XH2}{V_T}\left(\frac{RS-1}{RS}\right) - j\ \underbrace{\frac{\omega H2}{V_T \mu_p}\ X10^{-8}}_{XP2}$$

$$J = J+3$$

$$DO\ 31\quad I + P1,M1$$

$$D1(J) = -2 - RS*RS*CS\ \text{Cosh}\ \frac{V(I)}{V_T}$$

$$D1(J+1) = -2 - jXN3$$

$$D1(J+1) = -2 - jXP3$$

$$J = J+3$$

$$31\quad CONTINUE$$

Figure 3.12 The D1 diagonal

```
E(1) = 0
E1(2) = 0
E1(3) = 0
J = 4
DO 32  I = P,M
```

$$E1(J) = \frac{qH2}{\varepsilon_s V_T} N_o(I) = \frac{qH2}{\varepsilon_s V_T} N_i \exp \frac{V(I)}{V_T} = \frac{1}{2} CS \exp \frac{V(I)}{V_T}$$

```
E1(J+1) = 0
E1(J+2) = 0
J = J+3
32  CONTINUE
```

$$E1(J) = \frac{qH2}{\varepsilon_s V_T} N_o(K) = \frac{1}{2} CS \exp \frac{V(K)}{V_T}$$

```
E1(J+1) = 0
E1(J+2) = 0
J = J+3
DO 33  I = P1,L1
```

$$E1(J) = \frac{1}{2} RS*RS*CS*\exp \frac{V(I)}{V_T}$$

```
E1(J+1) = 0
E1(J+2) = 0
J = J+3
33  CONTINUE
```

$$E1(J) = \frac{1}{2} RS*RS*CS*\exp \left(V(M1)/V_T\right)$$

```
E1(J+1) = 0
```

Figure 3.13 The E1 diagonal

F1(1) = 0

F1(2) = 0

F1(3) = 0

J = 4

DO 34 I = P,M

$$F1(J) = \frac{qH2}{\varepsilon_s V_T} P_o(I) = \frac{1}{2} CS \exp - \frac{V(I)}{V_T}$$

F1(J+1) = 0

F1(J+2) = 0

J = J+3

34 CONTINUE

$$F1(J) = \frac{qH2}{\varepsilon_s V_T} P_o(K) = \frac{1}{2} CS \exp - \frac{V(K)}{V_T}$$

F1(J+1) = 0

F1(J+2) = 0

J = J+3

DO 36 I = P1,L1

$$F1(J) = \frac{1}{2} RS*RS*CS \exp - \frac{V(I)}{V_T}$$

F1(J+1) = 0

F1(J+2) = 0

J = J+3

36 CONTINUE

$$F1(J) = \frac{1}{2} RS*RS*CS*\exp - \frac{V(M1)}{V_T}$$

Figure 3.14 The F1 diagonal

LOAD THE G1 BAND

$$G1(1) = -\frac{DKS}{DKI}\ \frac{X_o}{XH2}$$

$$G1(2) = -1$$

$$G1(3) = -1$$

$$J = 4$$

DO 37 I = P,M

$$G1(J) = 1$$

$$G1(J+1) = 1 - \frac{E_o(I)XH2}{2V_T} = 1 + \frac{V(I+1)-V(I-1)}{4V_T}$$

$$G1(J+2) = 1 + \frac{E_o(I)XH2}{2V_T} = 1 - \frac{V(I+1)-V(I-1)}{4V_T}$$

$$J = J+3$$

37 CONTINUE

$$G1(J) = \frac{2}{(1+RS)RS}$$

$$G1(J+1) = \frac{2}{RS(1+RS)} - \frac{1}{(1+RS)}\ \frac{XH2}{RS}\ \frac{E_o(K)}{V_T}$$

$$G1(J+2) = \frac{2}{RS(1+RS)} + \frac{E_o(K)XH2}{(1+RS)RSV_T}$$

$$J = J+3$$

DO 38 I = P1,L1

$$G1(J) = 1$$

$$G1(J+1) = 1 + \frac{V(I+1)-V(I-1)}{4V_T}$$

$$G1(J+2) = 1 - \frac{V(I+1)-V(I-1)}{4V_T}$$

38 CONTINUE

Figure 3.15 The G1 diagonal

For all varactors studied here the n^+ substrate is about 100 μm and, therefore, Eq. (3-154) is easily satisfied. With this simplification, in the small signal mathematical model we may assume

$$V_1 = V_{p1} \tag{3-155}$$

$$J_p = 0 \tag{3-156}$$

The simplified model is fully developed in Appendix III and is summarized in Figure 3.16. This simplification is important in that is reduces the computer storage requirements. The full two-carrier case is a seven-band matrix problem. The simplified solution reduces to a five-band matrix. Also, at every point in the semiconductor the number of variables is reduced by one-third because only V_1 and V_{n1} must be solved for instead of V_1, V_{n1} and V_{p1} for the two-carrier case.

3.3.2 Comparison of Experiments with Computed One-Carrier Results

Figure 3.17 shows a plot of capacitance and resistance versus applied voltage for an MIS varactor. The applied frequency was 3.5 GHz and the material parameters for the epitaxial structure are summarized below.

$$\text{DNE} = 1\text{x}10^{16}\ \text{cm}^{-3}$$

$$\text{DNS} = 1\text{x}10^{19}\ \text{cm}^{-3}$$

$$\text{BX} = 0.1\ \mu\text{m}$$

$$Q_{ss} = 1\text{x}10^{-3}\ \text{coul/m}^3$$

The insulator is SiO_2 which is assumed to have a relative dielectric constant of 4.0. It is assumed that the top electrode is a dot two mils in diameter (50.8 μm). The computed insulator capacitance from the above

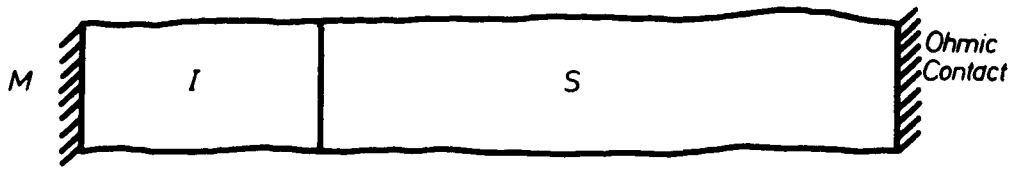

In Semiconductor:

$$\frac{d^2V_i}{dx^2} - \frac{qN_a}{\epsilon_s V_T} V_i + \frac{qN_a}{\epsilon_s V_T} V_n = 0$$

$$\frac{d^2V_n}{dx^2} + \frac{1}{V_T}\frac{dV_b}{dx}\frac{dV_n}{dx} + \frac{j\omega}{V_T \mu_n} V_i - \frac{j\omega}{V_T \mu_n} V_n = 0$$

Boundary Conditions:

(A) *I-S Interface*

$$\epsilon_s \left[\frac{dV_i}{dx}\right]_S - \epsilon_I \left[\frac{dV}{dx}\right]_I = 0$$

$$\frac{dV_n}{dx} = 0$$

(B) *Ohmic Contact*

$$V_i = V_n = 0$$

Figure 3.16 Summary of the high frequency mathematical model

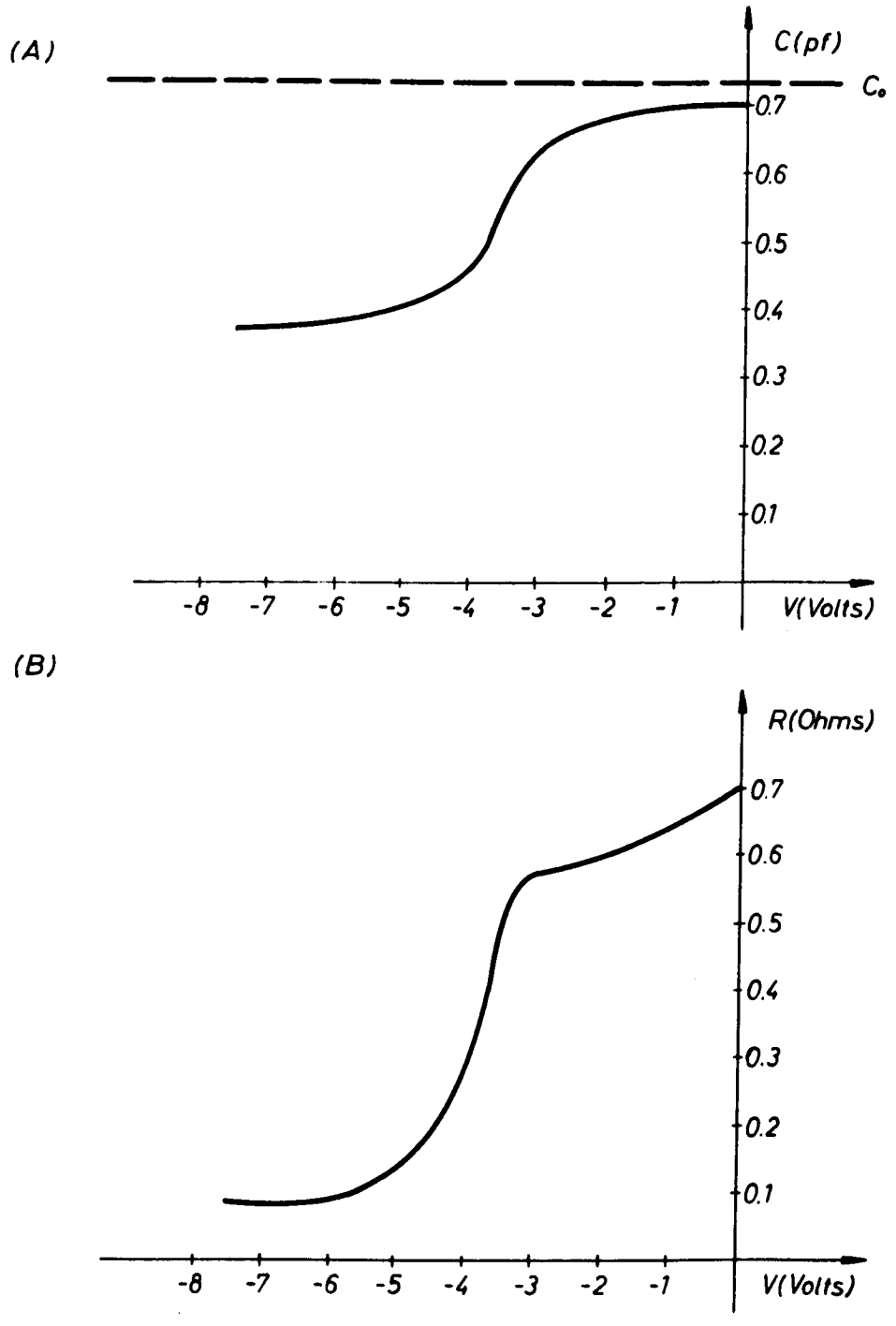

Figure 3.17 One carrier simulation of space charge varactor at 3.5 GHz

data is C_o = 0.717 pf and C/C_o = .975 in the accumulation region. It has been found in running these programs that the denser the grid near the interface point the more accurate the solution becomes. For a dense grid the accumulation capacitance ratio C/C_o approaches unity, and the accumulation resistance anomaly tends to be less pronounced. It is felt that the resistance anomaly is linked to the fact that in accumulation the small signal matrix has very large coefficients which are close to each other. It will be shown later that this anomaly also appears in the inversion region when minority carriers are taken into account. Again, in inversion large exponential terms are present in the small signal matrix.

Figure 3.18 is a reflection coefficient plot (referenced to 50 ohms) of an experimentally fabricated MIS varactor with material parameters very close to those simulated in Figure 3.17. Also appearing in Figure 3.18 are the high and low computed impedance points (Z_H, Z_L). There does not seem to be very good correlation but it must be remembered that the computed results are for the semiconductor chip alone and the experimental result is for device plus package. At microwave frequencies package parasitics must be considered and in many applications dominate performance. A lumped element model for a microwave pill package is shown in Figure 3.19. Assumed values for the model are also tabulated in the figure. A plot of the experimental device is replotted in Figure 3.20. Also in this figure are plotted Z_H and Z_L transformed through the parasitic circuit. A package capacitance of .35 pf was measured at 1 MHz for the microwave package with no chip in it. The additional 0.1 pf is due to stray mounting capacitance.

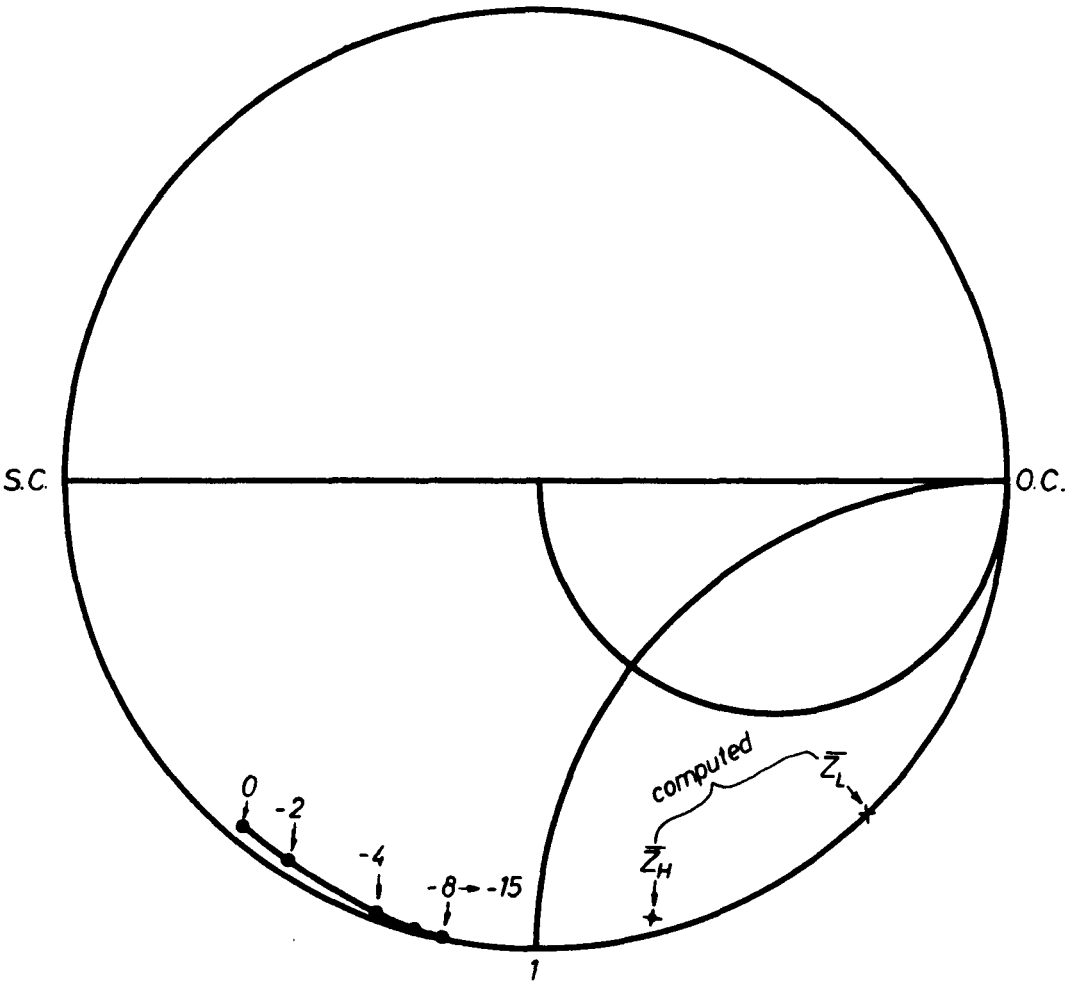

Figure 3.18 Comparison of computed MIS chip and experimental performance

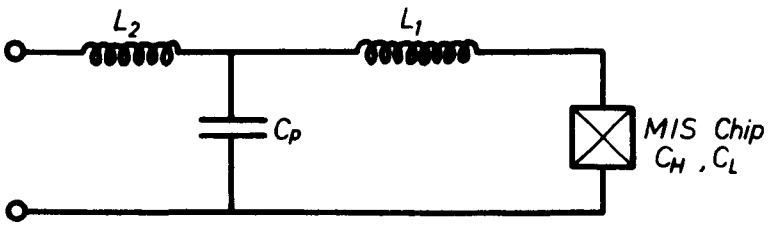

L_1 = bond wire from to the top of ceramic pill package

C_p = package capacitance

L_2 = any lead inductance introduced in mounting the package

Assumed values for parasitics

L_1 = .35 nh
L_2 = .5 nh
C_p = .45 pf

Figure 3.19 **Lumped element model of microwave pill package plus device chip.**

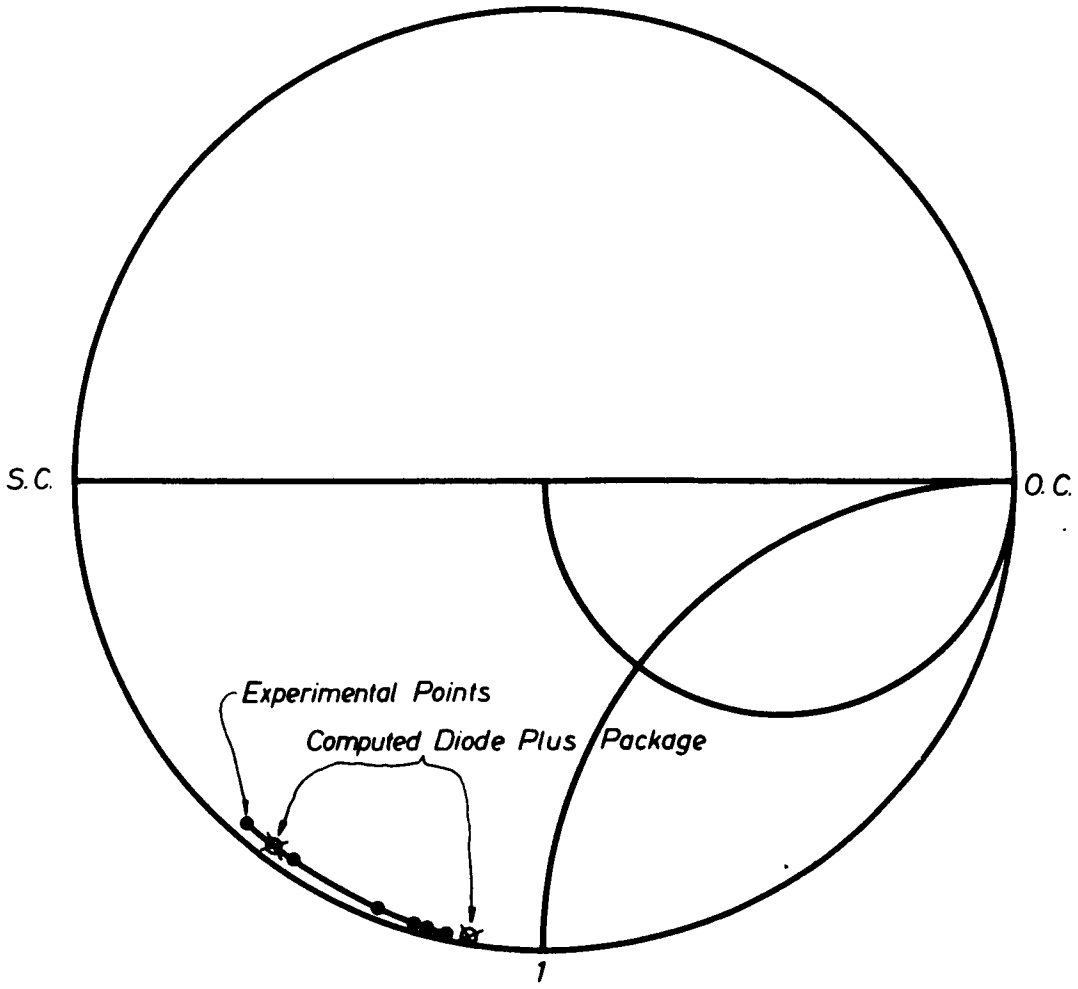

Figure 3.20 Comparison of computed and measured diode plus package.

3.3.3 Comparison of Experiments Computed Two-Carrier Results

Figure 3.21 shows computed high (3.5×10^9Hz) and low frequency (350 Hz) for an M-I-N-N^+-M MIS structure. It is shown here that the inclusion of minority carriers in the analysis predicts the relaxation of the capacitance to its insulator value in the inversion region. The low frequency curve generated by the two-carrier R.F. program compares well with the low frequency curve generated by the D.C. solution in Chapter 2 (Figure 2.11). Figure 3.22 shows computed high frequency curves for the M-I-N-N^+-M structure with the epitaxial (N) layer density (DNE) as a parameter. As the density increases the maximum depletion depth decreases as is predicted from Chapter 2. The two-carrier solution may be used to analyze more general MIS structures. Figures 3.23 and 3.24 show computed normalized capacitance versus voltage curves for M-I-P-N^+-M structures. Figure 3.23 is a plot of normalized capacitance versus voltage, at 350 Hz, for two different P layer densities. Figure 3.24 shows a high frequency capacitance plot for the same structure and densities. In this structure the capacitance versus voltage function is very complicated and requires more detailed investigations to explain the physical mechanisms. Figure 3.25 is a plot of high frequency resistance versus voltage characteristic.

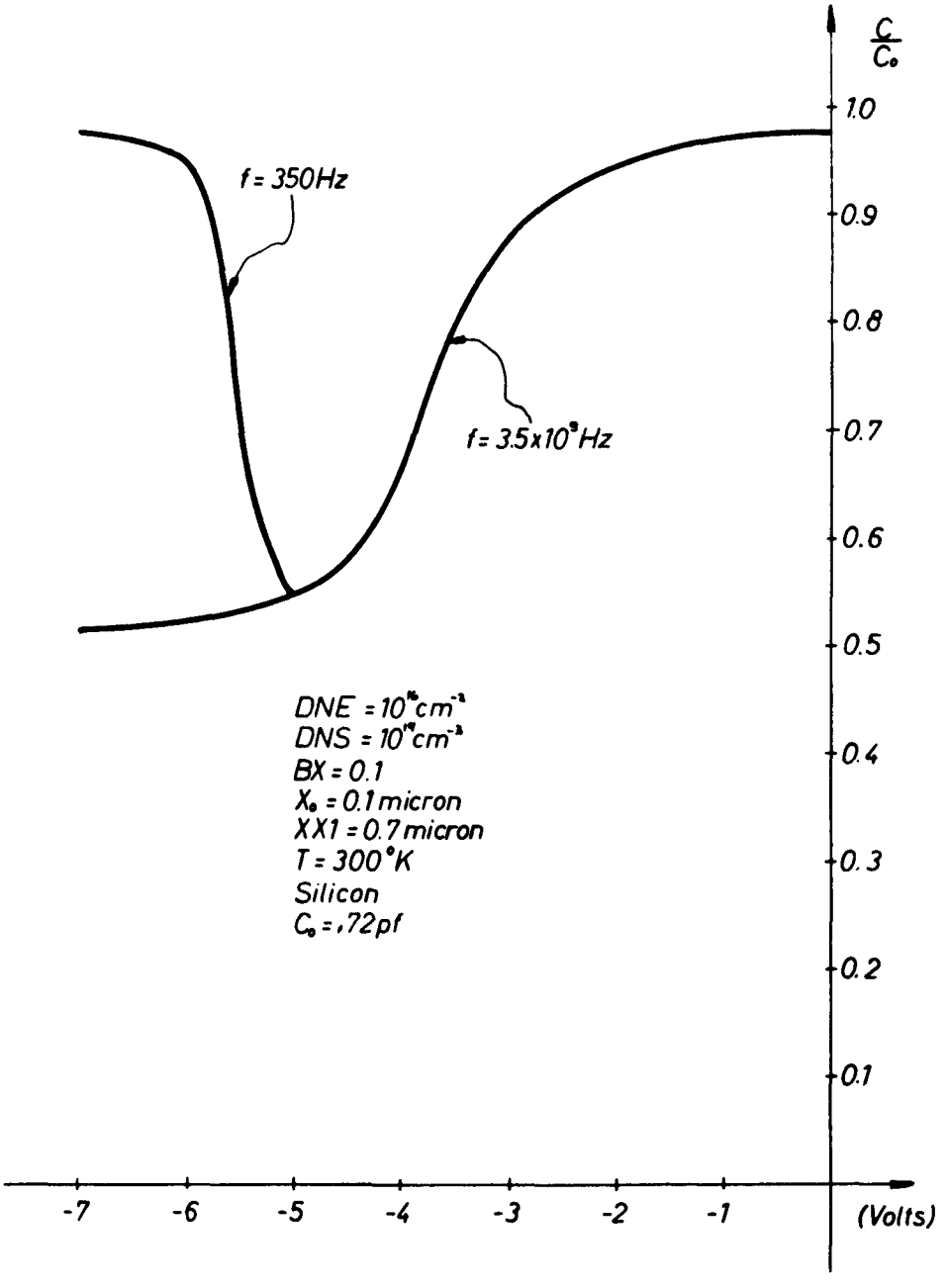

Figure 3.21 Computed low and high frequency normalized capacitance versus voltage curves for an M-I-N-N^+-M structure.

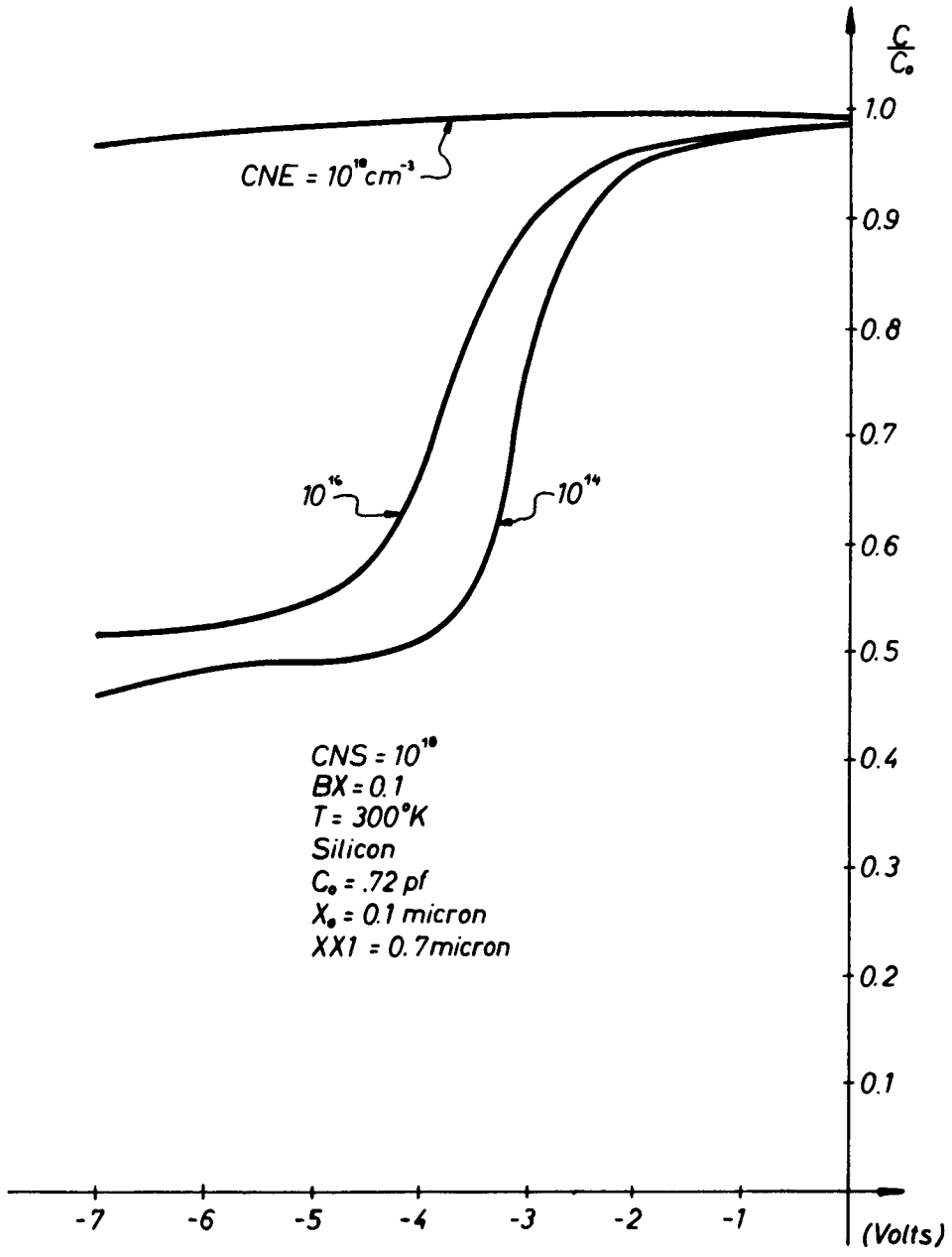

Figure 3.22 Computed high frequency normalized capacitance versus voltage curve with DNE as a parameter.

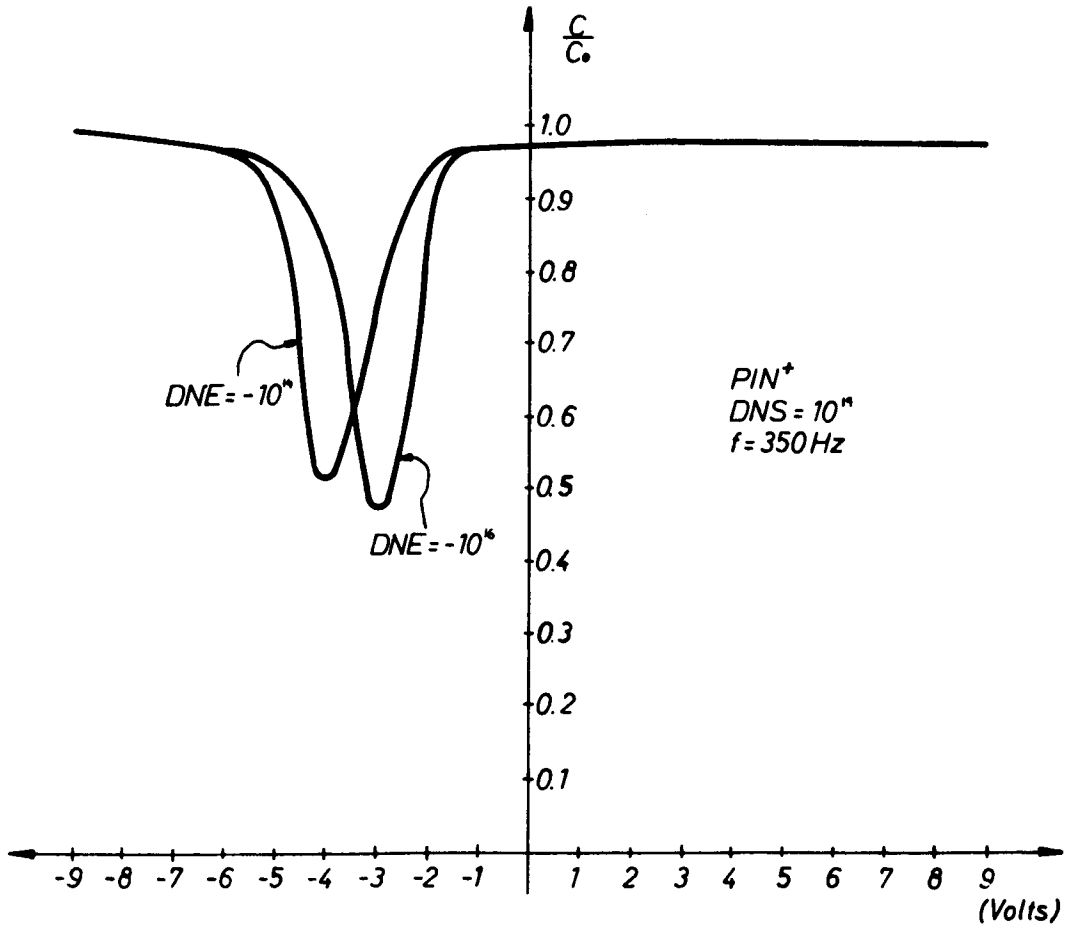

Figure 3.23 Computed low frequency capacitance versus voltage curve for a M-I-P-N^+-M structure.

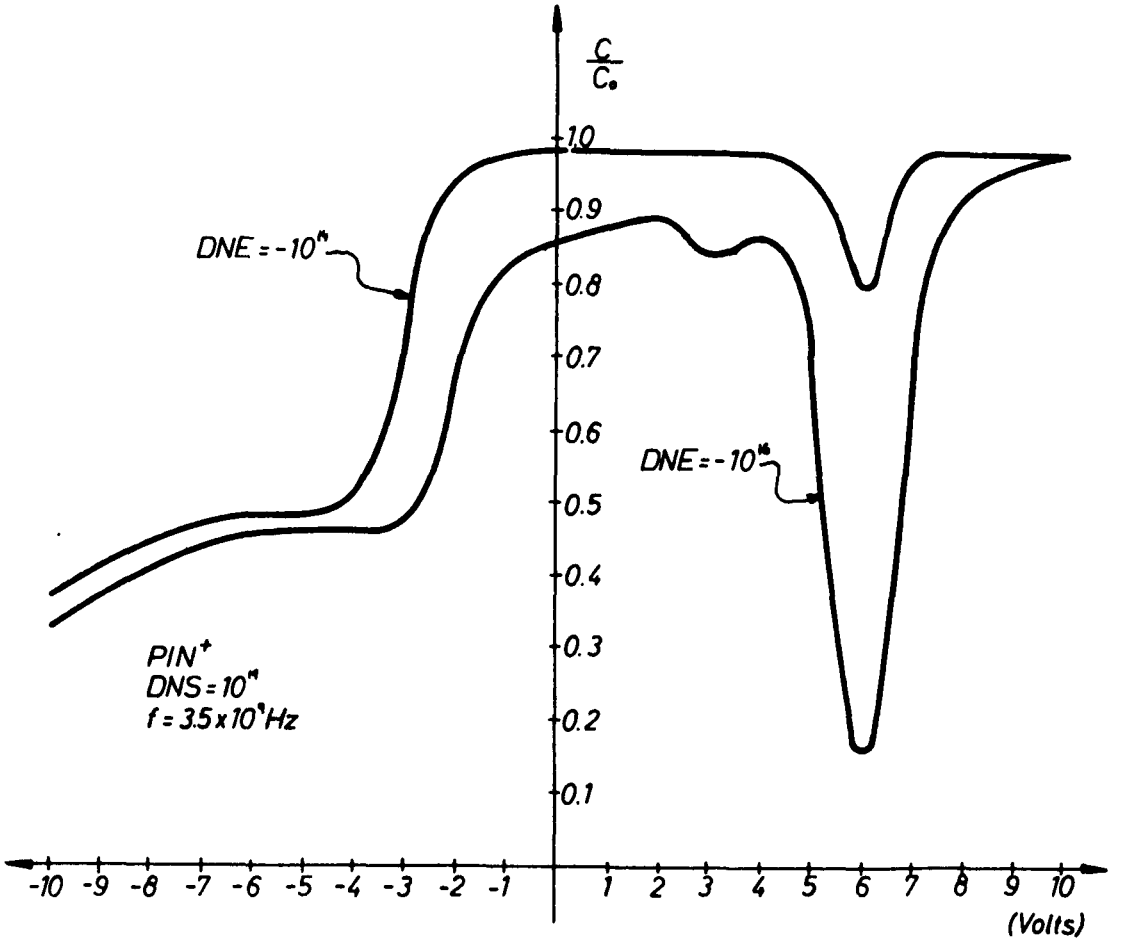

Figure 3.24 Computed high frequency capacitance versus voltage curve for an M-I-P-N^+-M structure.

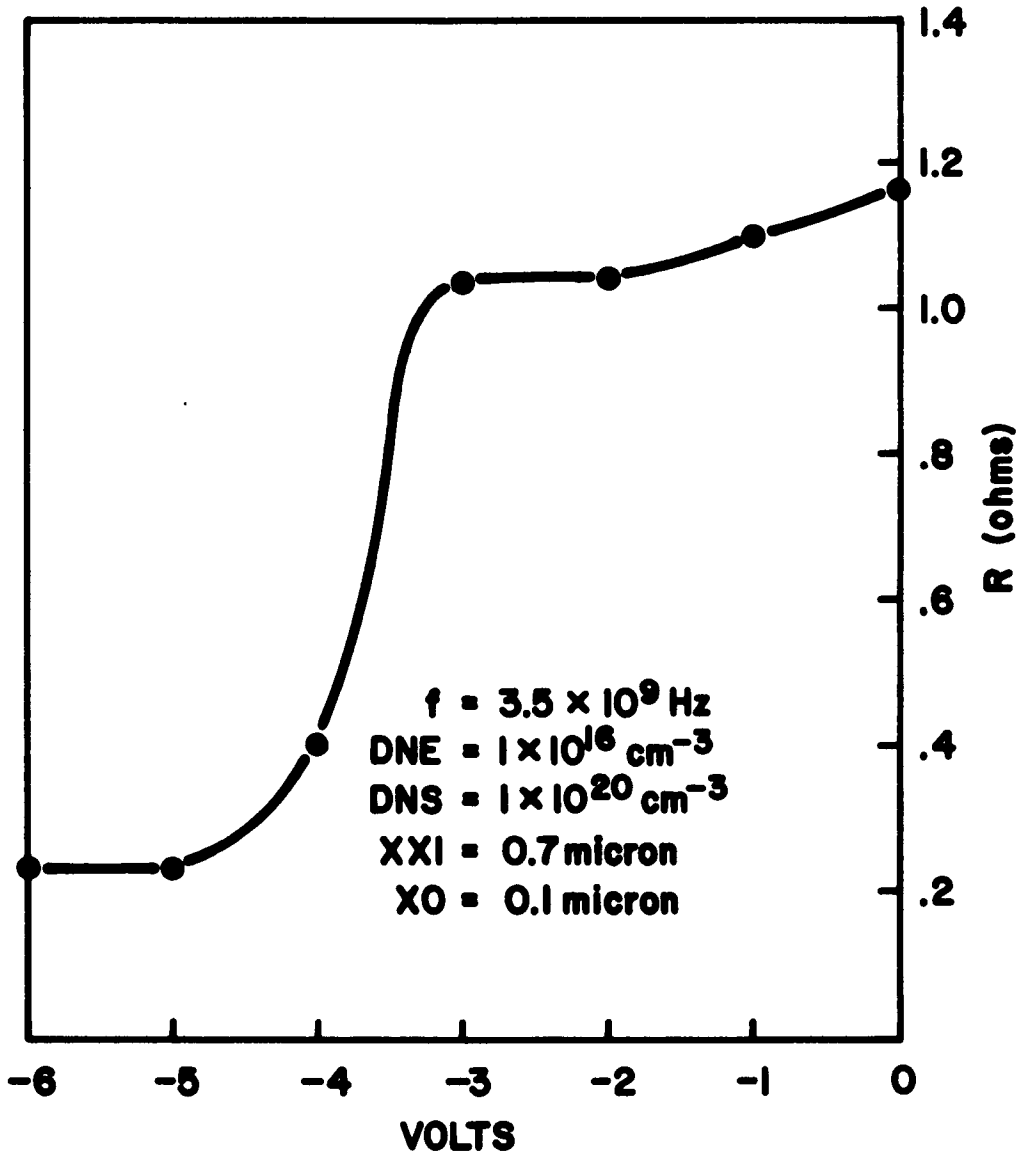

Figure 3.25 Computed resistance versus applied voltage for M-I-N-N^+-M structure.

CHAPTER 4

MIS VARACTOR APPLICATIONS

4.1.1 Principle of Operation of a Reflection Type Phase Shifter[32]

A sketch of a reflection-type phase shifter is shown in Figure 4.1. It consists of a quadrature hybrid, two nonlinear networks terminating the hybrid, and a bias network which is d.c. coupled to the nonlinear element but is r.f. isolated. A signal enters port 1, splits evenly between 3 and 4, and is isolated from 2. There is a 90° phase difference between the wave at 4 and 3. If 3 and 4 are terminated in the same loads (equal reflection coefficients), all power for the ideal hybrid will appear at 2. The phase of the wave at port 2 will equal the sum of the incident phase plus the phase of the reflection coefficient. If there are no losses in the system (hybrid, nonlinear network, bias network) and the hybrid has infinite directivity, then all the power incident will be recovered in port 2.

In general, the nonlinear network will consist of an MIS varactor and a linear phase compensating as stretching network. The MIS device is a voltage variable capacitor which has a unique two-state capacitance characteristic. At first, a nonlinear network consisting of a two-state capacitor (C_H,C_L) will be analyzed. It will be shown for a given phase shift and frequency how to pick the capacitance values for minimum phase variation.

The reflection coefficient for a capacitor terminating a transmission line is

$$\Gamma = \frac{\frac{1}{j\omega c} - Z_o}{\frac{1}{j\omega c} + Z_o} \qquad (4\text{-}1)$$

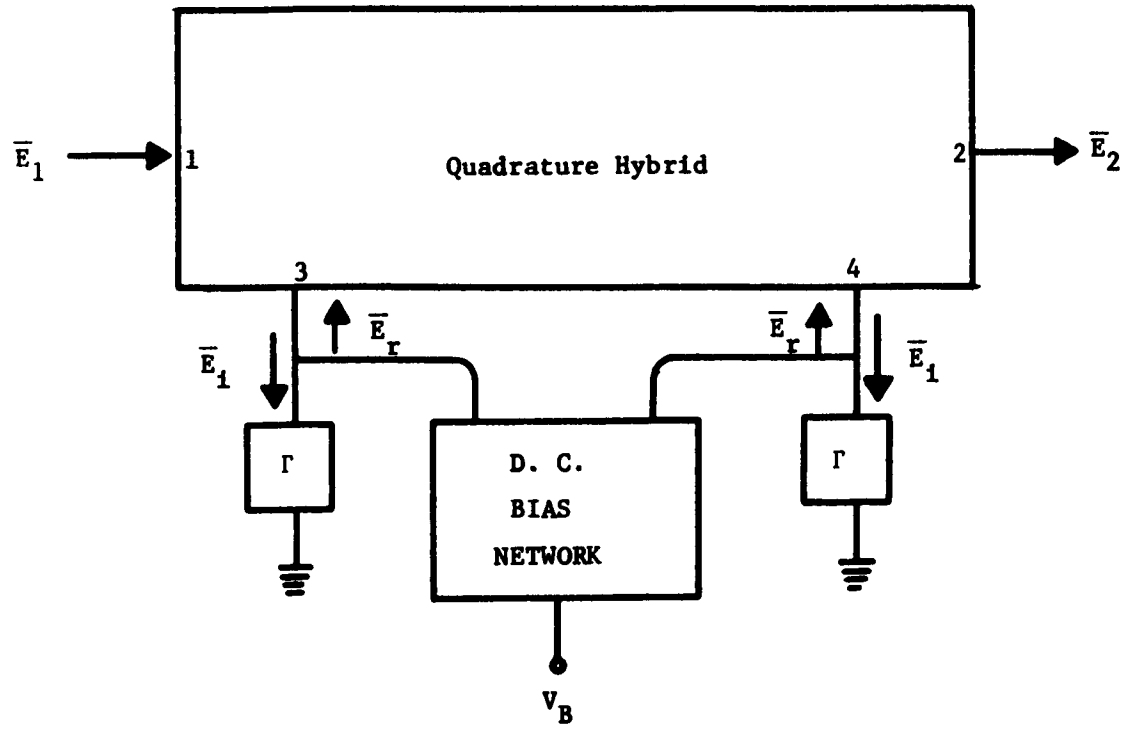

$$\Gamma = \frac{\bar{E}_r}{\bar{E}_i} = \rho \, \underline{|\theta}$$

$$\bar{E}_1 = |E_1| \, \underline{|\phi}$$

$$\bar{E}_2 = |E_2| \, \underline{|\phi+\theta}$$

$$|E_2| = |E_1|$$

$$|E_i| = |E_1/\, 2$$

Figure 4.1 Reflection type phase shifter.

which may be simplified into the form

$$\Gamma = 1 \angle \tan^{-1}\omega cZ_o - \tan^{-1}\omega cZ_o \qquad (4\text{-}2)$$

Using the identity

$$\tan^{-1}(-\phi) = -\tan\phi \qquad (4\text{-}3)$$

then the phase θ of the reflection coefficient may be expressed as

$$\theta = +2\tan^{-1}(\omega cZ_o) \qquad (4\text{-}4)$$

If the capacitor may be switched between two different values (C_1, C_2) by some means, the net differential phase shift is

$$\theta_2 - \theta_1 = 2\tan^{-1}(-\omega c_2 Z_o) - \tan^{-1}(-\omega c_1 Z_o) \qquad (4\text{-}5)$$

Using the identity

$$\tan^{-1}Z_1 \pm \tan^{-1}Z_2 = \tan^{-1}\frac{Z_1 \pm Z_2}{1 \mp Z_1 Z_2} \qquad (4\text{-}6)$$

the expression (4-5) may be shown to be of the form

$$\Delta\theta = \theta_2 - \theta_1 = 2\tan^{-1}\left(\frac{\omega c_2 Z_o - \omega c_1 Z_o}{1 + \omega^2 c_1 c_2 Z_o^2}\right) \qquad (4\text{-}7)$$

In general, it is desired to make the phase variation as small as possible across a given frequency band of interest. This may be done by choosing parameters such that the differential phase shift slope is zero at the design center frequency. Taking the derivative of Eq. (4-7) with respect to ω

$$\frac{d(\Delta\theta)}{d\omega} = \frac{1}{1 + \dfrac{\omega Z_o(c_2 - c_1)}{1 + \omega^2 c_1 c_2 Z_o}} \cdot \frac{(c_2 - c_1)Z_o}{(1+\omega^2 c_1 c_2 Z_o^2)^2} \cdot (1 - \omega^2 Z_o^2 c_1 c_2) \qquad (4\text{-}8)$$

It can be seen that the phase slope will be zero at $\omega = \omega_o$ if

$$1 - \omega_o^2 Z_o^2 c_1 c_2 = 0 \tag{4-9}$$

The values of capacitance for a given differential phase shift may be obtained by solving Eq. (4-9) and (4-7) simultaneously. From Eq. (4-9)

$$c_2 = \frac{1}{\omega_o^2 Z_o^2 c_1} \tag{4-10}$$

Substituting Eq. (4-10) into (4-7)

$$\Delta\theta = 2 \tan^{-1} \frac{\left(\frac{1}{\omega_o^2 Z_o^2 c_1}\right) Z_o - \omega c_1 Z_o}{1 + \omega^2 c_1 \left(\frac{1}{\omega_o^2 Z_o^2 c_1}\right) Z_o^2} \tag{4-11}$$

$$\tan \frac{\Delta\theta}{2} = \frac{\frac{\omega}{\omega_o^2 Z_o c_1} - \omega c_1 Z_o}{1 + \frac{\omega}{\omega_o}^2} \tag{4-12}$$

$$c_1^2 + \frac{1}{\omega Z_o} \left[1 + \left(\frac{\omega}{\omega_o}\right)^2\right] \tan \frac{\Delta\theta}{2} - \frac{1}{(\omega_o Z_o)^2} = 0 \tag{4-13}$$

At $\omega = \omega_o$, the two values which satisfy this equation may be solved for

$$c_1 = \frac{1}{\omega_o Z_o} \left\{ - \tan \frac{\Delta\theta}{2} \pm \sec \frac{\Delta\theta}{2} \right\} \tag{4-14}$$

Since the capacitance cannot be a negative number

$$c_1 = \frac{1}{\omega_o Z_o} \left\{ \sec \frac{\Delta\theta}{2} - \tan \frac{\Delta\theta}{2} \right\} \tag{4-15}$$

is chosen as the solution. Substituting Eq. (4-15) into (4-10)

$$c_2 = \frac{1}{w_o Z_o} \cdot \frac{1}{\sec \frac{\Delta\theta}{2} - \tan \frac{\Delta\theta}{2}} \tag{4-16}$$

and the capacitance ratio is found by dividing Eq. (4-16) by (4-15).

$$\frac{c_2}{c_1} = \frac{1}{\sec \frac{\Delta\theta}{2} - \tan \frac{\Delta\theta}{2}^2} \tag{4-17}$$

Table 4-1 summarizes capacitance ratios and values at a design center frequency of 3.5 GHz, in a 50-ohm system.

$\Delta\theta$	c_2/c_1	c_1(pf)	c_2(pf)
22.5°	1.48	.739	1.09
45.0°	2.06	.627	1.29
90.0°	5.79	.372	2.15
180.0°	∞	0	∞

TABLE 4-1 SUMMARY OF CAPACITANCE RATIOS AND VALUES f_o = 3.5 GHz
Z_o = 50 Ω

It should be noted that the 180° differential phase shift cannot practically be achieved using two capacitors alone. Either an ideal switch is required or additional elements are required in addition to a nonlinear capacitor with a finite capacitance ratio in order to achieve 180° of phase shift. It should also be noted that the values of capacitance obtained have a graphical significance on a reflection chart. Figure 4.2 shows that the optimal reactance values (X_1,X_2), for a given phase shift $\Delta\theta$, fall symmetrically about the -90°

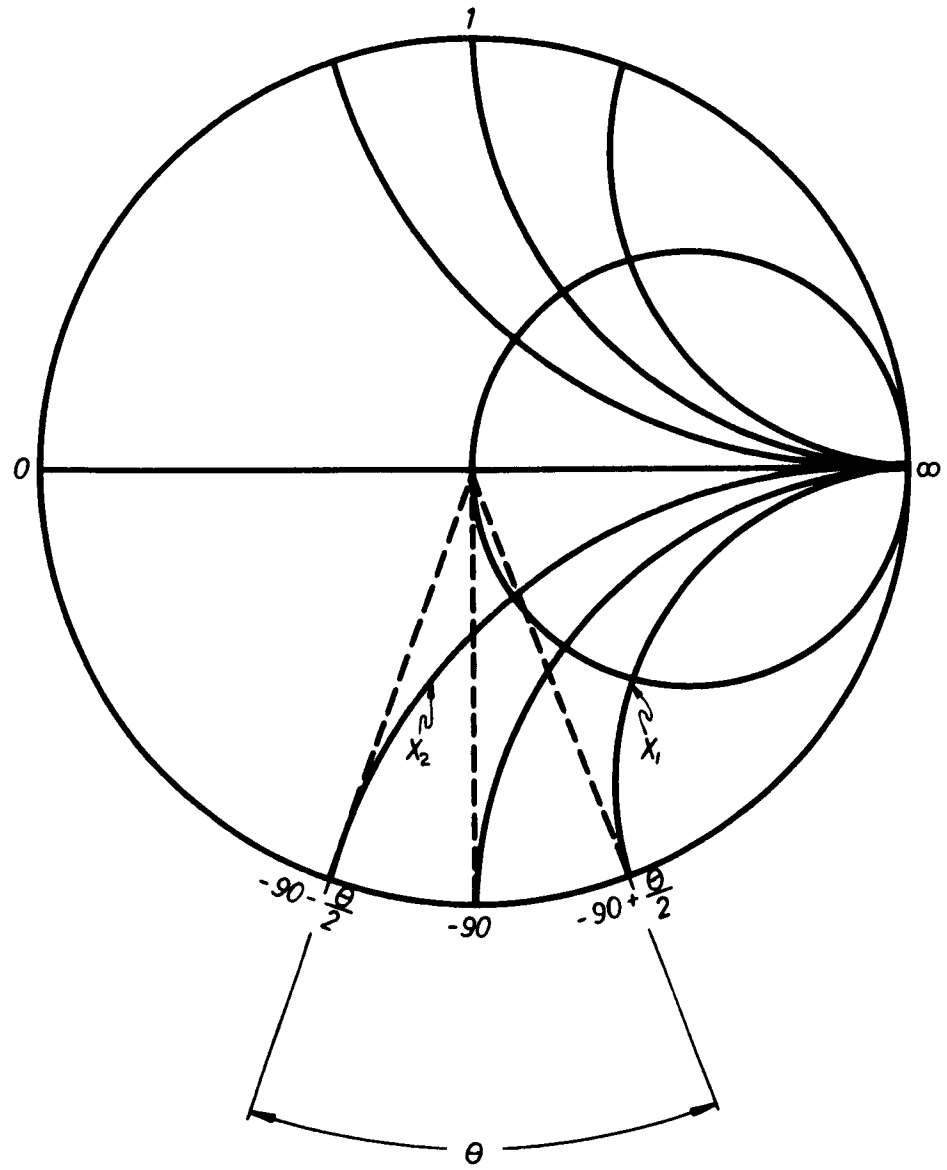

Figure 4.2 Optimal phase shift for two capacitors C_1, C_2.

phase coordinate. For two small capacitance values near the open circuit point, the reactance curves tend to bunch together yielding a small phase shift. For two large capacitors with reactances near the short circuit point, the differential phase shift is small this time because the change in reactance is small. The optimum, therefore, lies halfway between the open circuit and short circuit point.

In order to determine the phase shifter's useful bandwidth, one could plot equation (4-11) and determine phase flatness over the band of interest. Instead, an RCA circuit analysis program (COSMIC) was used to determine phase performance including parasitic series resistance (Figure 4.3). The program allows circuit simulation of the MIS varactor, including chip, parasitics and external tuning elements.

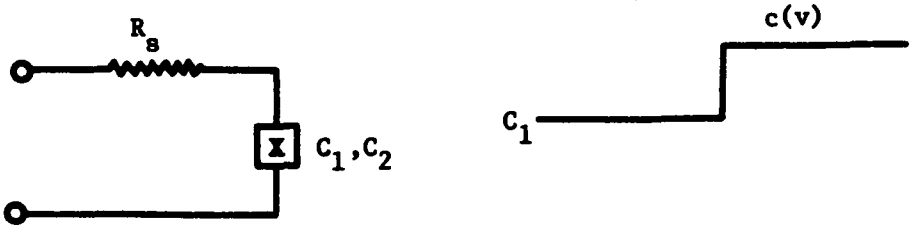

R_s = 1.0 Ω
C_1 = 1.35 pF
C_2 = 0.6 pF

Figure 4.3 Simulation of 45° BIT including parasitic series resistance.

The capacitance values are very close to those previously derived for the 45° BIT summarized in Table 4-1. The program is a linear analysis program so that a value of capacitance is assumed and reflection gain in dB and reflection phase (degrees) is plotted versus frequency. Then, another capacitance value is assumed and the phase shift and gain are calculated. The differential phase shift is obtained by subtracting the phase of reflection coefficient for the two values of capacitance.

Table 4-2 summarizes the results from 3.0 to 4.0 GHz.

Freq. (GHz)	$c = c_2$ Reflection Gain (dB)	$c = c_1$ Reflection Gain	$\Delta\theta$ (degrees)
3.0	-0.215	-0.084	44.685
3.2	-0.225	-0.093	45.028
3.4	-0.235	-0.101	45.200
3.6	-0.243	-0.110	45.225
3.8	-0.251	-0.118	45.128
4.0	-0.258	-0.126	44.927

TABLE 4-2 45° BIT SIMULATION: $R_s = 1.0\ \Omega$

$c_1 = 0.6$ pf

$c_2 = 1.35$ pf

Similar calculations may be done for the 22.5, 90° BITS.

4.1.2 Quadrature Hybrids

One of the most important parts of a reflection type phase shifter is the quadrature hybrid. In order for a hybrid to be useful, its two-way loss should be as low as possible (i.e., loss from 1 to 2 when 3 and 4 are terminated in equal reactances). Also, the phase difference between ports 3 and 4 should be constant over the design bandwidth. Two types of hybrids were investigated:

(1) Branch line[35]

(2) Interdigitated[33]

Branch line hybrids are simple to make, requiring only a one mask photo-etch process. The Lange hybrid also requires a one mask process, but in addition needs bonding straps to interconnect digits. This makes the Lange hybrid less reproducible and more expensive to fabricate.

Both types of hybrid were evaluated.

The branch line hybrid was evaluated for a reflection type phase shifter applications by simulating a phase shift bit using this type hybrid and by building and testing the hybrid itself. A circuit with the topology shown in Figure 4.4 was fed into the COSMIC computer program.

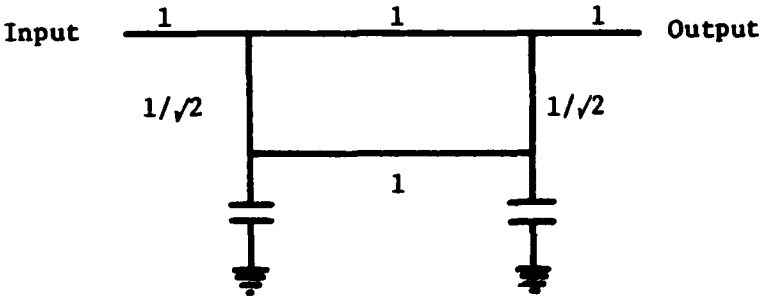

Figure 4.4 Branch line hybrid topology.

All lines were microstrip with a source as reference impedance of 50 ohms. The lengths of all lines were $\lambda g/4$ at the design center frequency of 3.5 GHz. The capacitors were designed to yield approximately the optimum values for a 22.5° bit (c_1 = 1.1, c_2 = .745). The differential phase variation for the capacitors alone can be shown to be less than 0.5° over a ten-percent bandwidth. The differential phase shift for the total circuit above over the same ten percent bandwidth is shown in Table 4.3.

f (GHz)	Δθ°
3.325	27.260
3.500	22.488
3.675	17.45

TABLE 4-3 PHASE SHIFT THROUGH BRANCH LINE HYBRID

The maximum insertion loss occurring in either state is 0.37 dB, which includes microstrip copper losses and mismatch loss. A phase variation of ten degrees is too large, especially for the 22.5° bit. Simultaneous to the hybrid stimulation studies, two 3-dB branch line hybrids were designed, built and tested. Both circuits were fabricated on alumina substrates with chrome-gold metallizations. One substrate was 25 mil thick and the second was 50 mil thick. Theoretically, the thicker substrates should have lower insertion losses. Figures 4.5 to 4.8 summarize the test results. In both hybrids, the designed center frequency is not exactly correct. This is clearly demonstrated in plots of return loss versus frequency (Figures 4.6 and 4.8). This misalignment affects coefficients of coupling and loss variation. The shift of the design center frequency may be explained because the design did not take into account reactances at the junction of the hybrid. A recent paper by Vogel[36] describes how to take into account junction discontinuities and may be used to improve the hybrid performance. When these hybrids were used with varactors to form phase shift bits, the phase variation predicted by simulation was verified. All work on future phase shifters using branch line hybrids stopped at this point. Attention was turned to the Lange type hybrid with the hope of achieving lower loss and smaller phase shift variation.

A photograph and schematic of an experimental Lange hybrid that was designed, fabricated and tested at City College is shown in Figure 4.9.

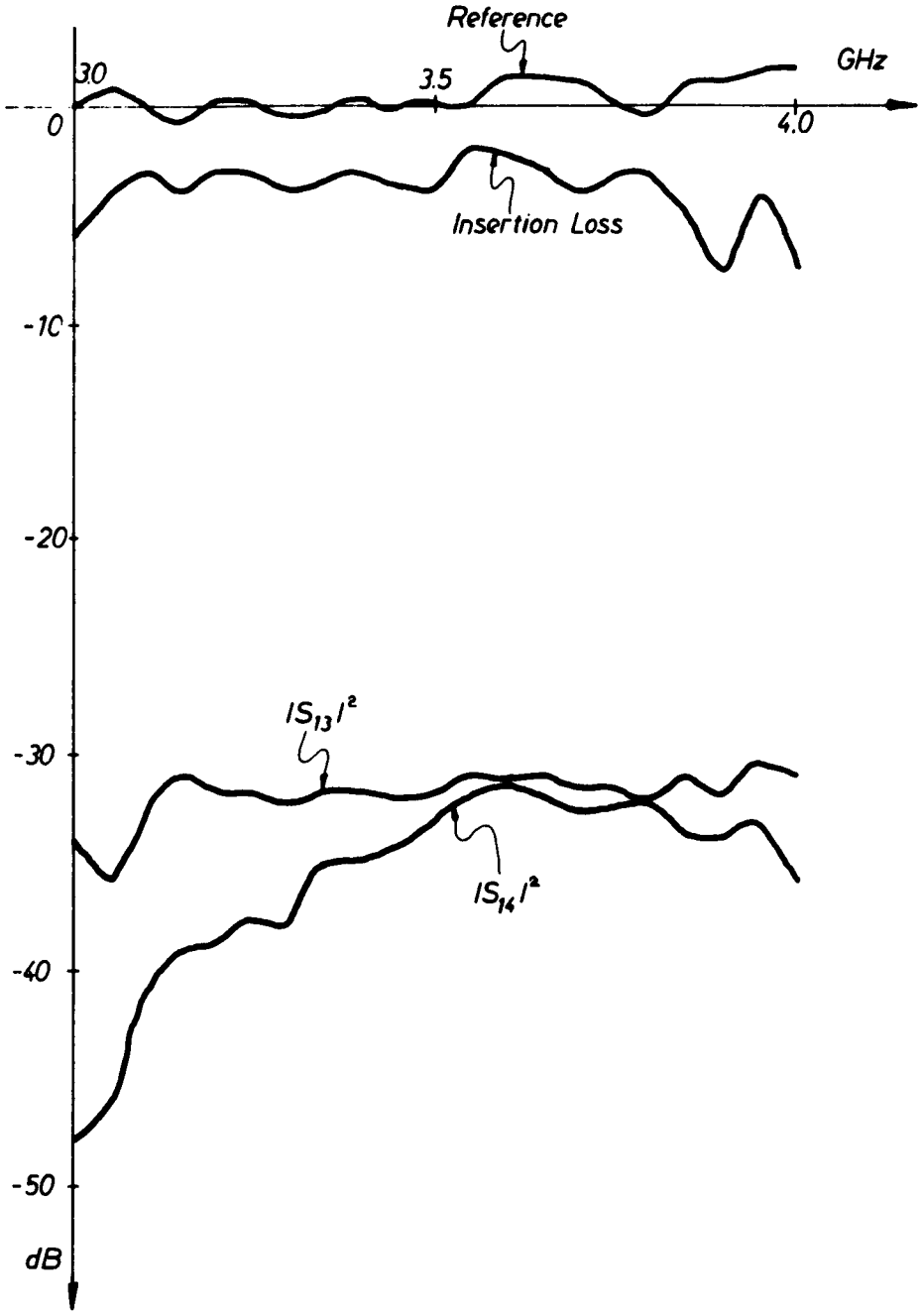

Figure 4.5 Insertion loss and coupling for a 25 mil branch line hybrid.

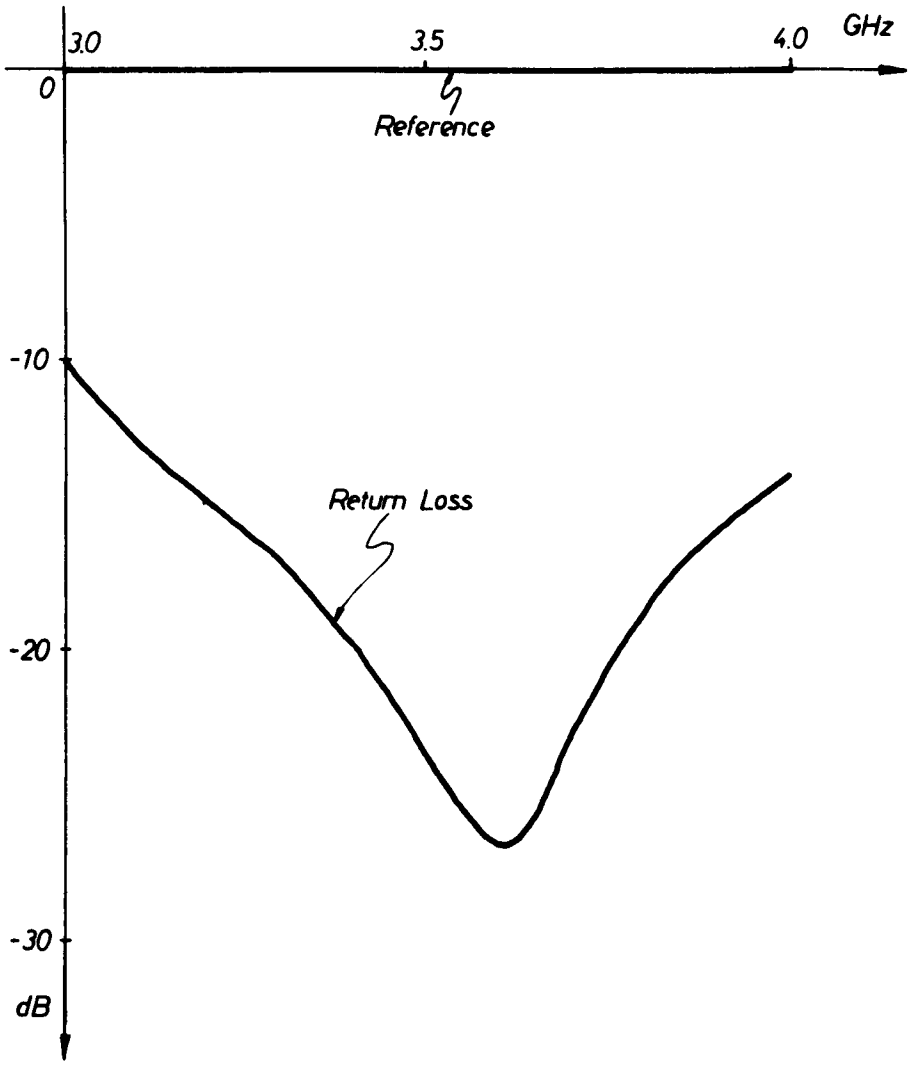

Figure 4.6 Return loss (isolation) for a 25 mil branch line hybrid.

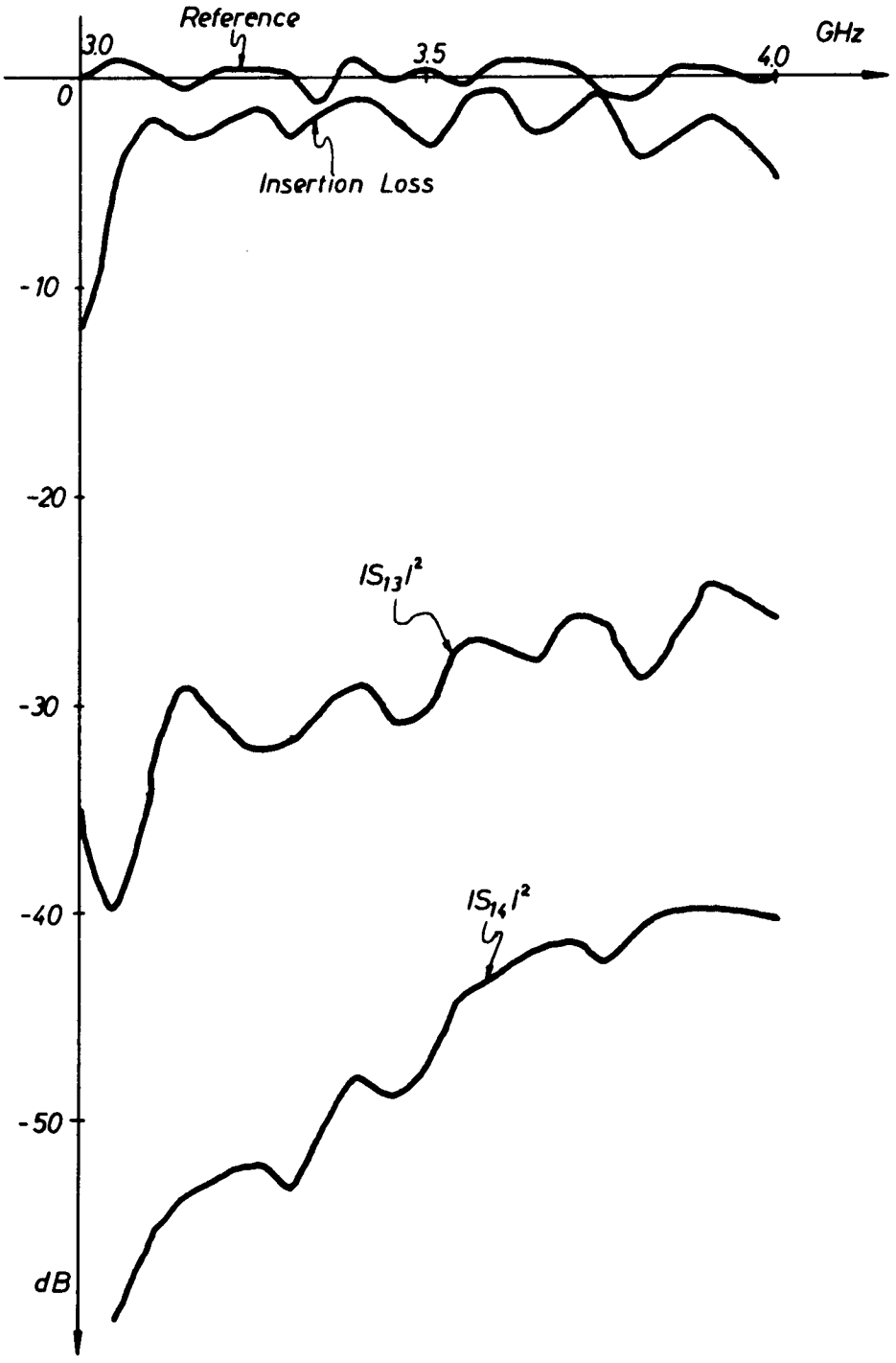

Figure 4.7 Insertion loss and coupling for a 50 mil branch line hybrid.

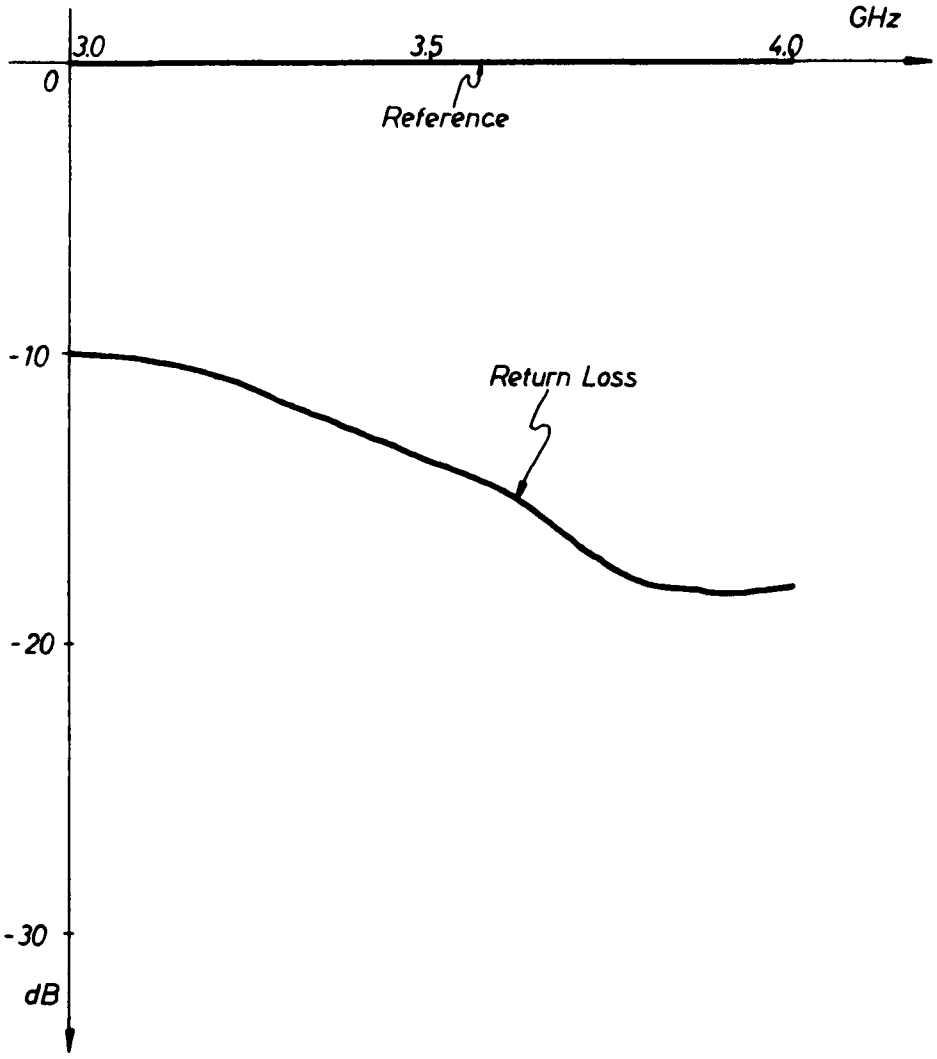

Figure 4.8 Return loss (isolation) for a 50 mil branch line hybrid.

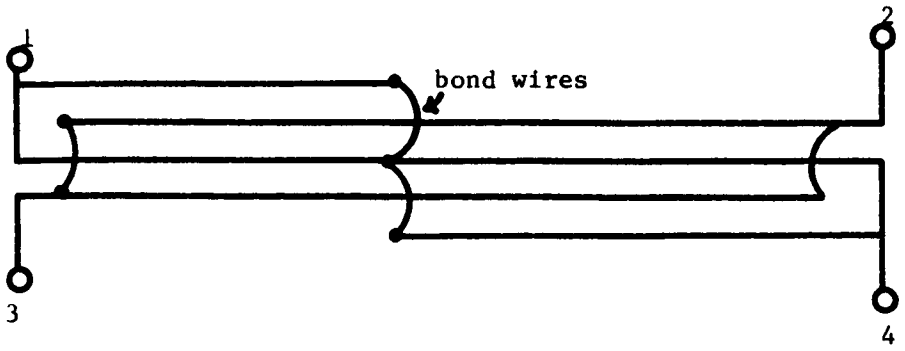

(a)

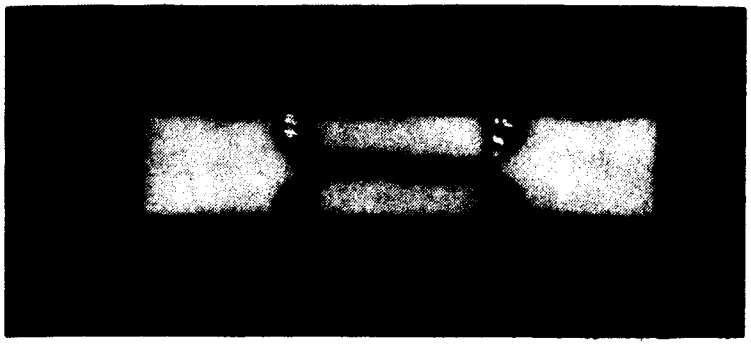

(b)

Figure 4.9 Interdigitated (Lange) hybrid.

It consists of five coupled microstrip lines with four air crossovers. All input and output lines are 50 ohm impedances. The longest line length is a quarter wavelength and the shorter line is an eighth wavelength. The topology shown in Figure 4.4 was simulated by the COSMIC computer program. In Lange's original paper[33] no theory is given, only that the coupling required was determined by an unpublished computer program. Also, Lange's original design was on 40-mil alumina substrates. The widths of the lines are 4.5 mil wide and 3.0 mil spacings. The one-way insertion loss reported was 0.13 dB. We wanted to use thicker substrates (at least 50 mil thick) to try to minimize the losses and also to make dimensions easy to fabricate. Lange's 40-mil alumina design was scaled to determine a design on 50-mil alumina. In this approach, the even and odd mode impedances are kept constant between designs. For microstrip lines, with tight coupling, the even and odd mode impedances have been determined in closed form by Wheeler[34]. Definitions of terms and the closed form expressions are summarized in Figure 4.10.

Scaling the Odd Mode:

Assuming the subscript X denotes an unknown design parameter, then keeping the odd mode constant from Figure 4.10 requires:

$$\sqrt{K_o}\ \ell n\ \frac{4e''}{e} = \sqrt{K_{ox}}\ \ell n\ \frac{4e''_x}{e_x} \qquad (4\text{-}18)$$

Solving Eq. (4-18) for e''/e_x

$$\frac{e''_x}{e_x} = \frac{1}{4}\left(\frac{4e''}{e}\right)^{\sqrt{K_o/K_{ox}}} \qquad (4\text{-}19)$$

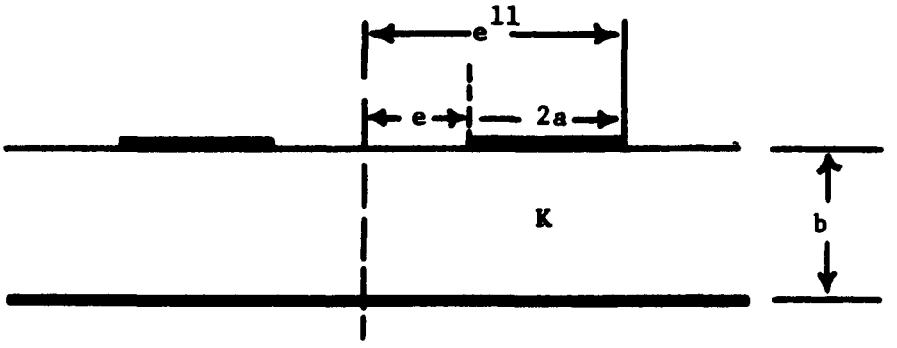

Formula's correct for $e/e'' < 1/4$; $e''/b < 1/2$; $|K\ b/R < 1/8$

$$\frac{4Z_{oo}}{R_o \Pi} = \frac{1}{\sqrt{K_o}\ \ell n\ \frac{4e''}{e}}$$

$$\frac{Z_{oe\Pi}}{R_o} = \frac{\ell n\ 4b/e''}{\sqrt{K_e}}$$

$$K_{o,e} = 1 + q_{o,e}(K-1)$$

Z_{oo}, Z_{oe} - Odd and even mode impedances

K_o, K_e - Effective dielectric constants in odd and even modes

R_o - Wave resistance of free space = 120Π = 377 Ω

$q_{o,e}$ - Odd and even mode filling fraction

Figure 4.10 Odd and even mode impedances for tightly coupled microstrip lines.

where

$$\frac{K_o}{K_{ox}} = \frac{1 + q_o(K-1)}{1 + q_{ox}(K_x-1)} \tag{4-20}$$

Assuming the even and odd mode velocities are approximately the same

$$q_o = q_e = \frac{1}{2} \tag{4-21}$$

and, therefore, the ratio of effective dielectric constants [Eq. (4-20)] may be expressed as

$$\frac{K_o}{K_{ox}} = \frac{\frac{K+1}{2}}{\frac{K_x+1}{2}} = \frac{K+1}{K_x+1} \tag{4-22}$$

Substituting Eq. (4-22) into (4-19)

$$\frac{e''_x}{e_x} = \frac{1}{4}\left(\frac{4e''}{e}\right)\left(\frac{K+1}{K_x+1}\right)^{1/2} \tag{4-23}$$

Similarly, scaling the even mode it may be shown

$$\frac{bx}{e''_x} = \frac{1}{4}\left(\frac{4b}{e''}\right)\left(\frac{K_x+1}{K+1}\right)^{1/2} \tag{4-24}$$

EXAMPLE: Suppose we wish to scale Lange's reported dimensions to a 50-mil alumina substrate. The pertinent data from Lange's paper are summarized below.

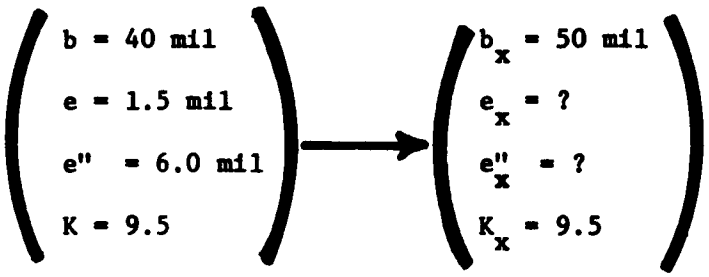

For a scale to a substrate of the same dielectric constant equations (4-23) and (4-24) reduce down to

$$\frac{e''_x}{e_x} = \frac{e''}{e} \tag{4-25}$$

$$\frac{b_x}{e''_x} = \frac{b}{e''} \tag{4-26}$$

$\therefore$ $\frac{e''_x}{e_x} = \frac{6.0}{1.5} = 4.0$, and

$$\frac{b_x}{b''_x} = \frac{40}{6} = 6.68$$

$\therefore$ $e''_x = \frac{50}{6.68} = 7.5$ mil

$$e_x = \frac{7.5}{4} = 1.875 \text{ mil.}$$

On experimental models of the Lange hybrid actual dimensions are slightly smaller than theoretical ones due to undercutting in the etching process. Dimensions may be adjusted by plating up or allowing for undercutting in photomask. Typical dimensions in experimental models are

$e'' = 6.9$ mil

$e = 1.5$ mil

Typical performance for a Lange hybrid is shown in Figures 4.11 and 4.12. Typical phase difference between ports 3 and 4 is less than 3° over the 3 to 4 GHz band, which is much less than the branchline hybrid. The best two-way insertion loss measured with ports 3 and 4 terminated in shorts is 0.35 dB.

4.1.3 Phase Stretching Network and Design of 90° and 180° Phase Shift Bits

It was shown in Section 4.1.1 that the 180° Bit could not be realized with only a nonlinear capacitor. In this section it will be shown how one can increase the phase shift capability of a two-state capacitor using two lumped inductors. The price paid for the increased phase shift is phase variation. But, with a number of iterations on the circuit elements phase variations may be minimized. It should be stressed that the approach presented here is not a direct synthesis and, therefore, optimal solutions cannot be guaranteed.

Figure 4.13(a) shows the phase stretching network which consists of a shunt and series ladder network. A sketch of the effects of each element of the ladder network is shown on a reflection coefficient chart in Figure 4.13(b). The starting point of the design is point a(2) and a(1), which correspond to the points on the chart for the nonlinear capacitor. For a ratio $c_2/c_1 = 2.25$ optimally centered, it was shown in Section 4.1.1 that $\theta = 45°$. A series inductor moves both points toward the short circuit point to b(2), b(1). Because c_1 is a lower value of capacitance the point a(1) is not displaced much by the series L_2. The shunt L_1 moves b(2) to c(2) and b(1) to c(1). Because b(2) is

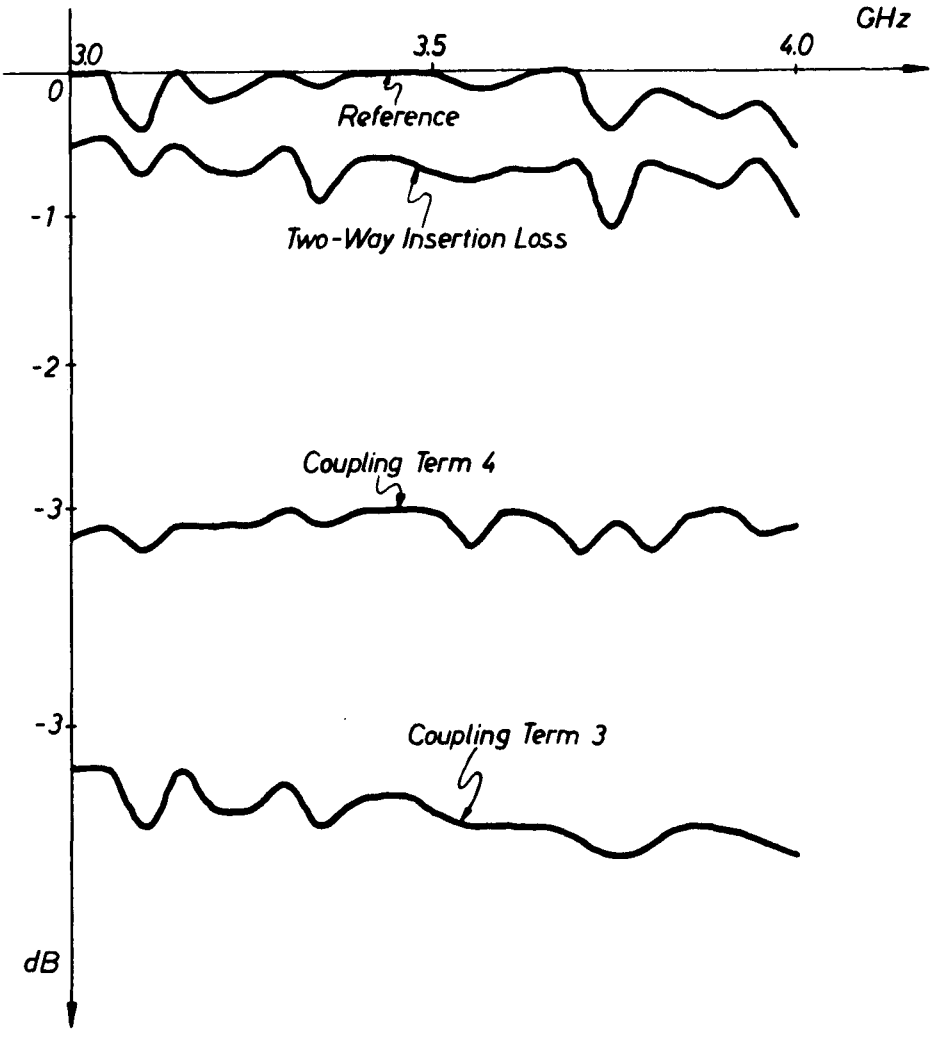

Figure 4.11 50 mil Lange hybrid two-way insertion loss and coupling versus frequency.

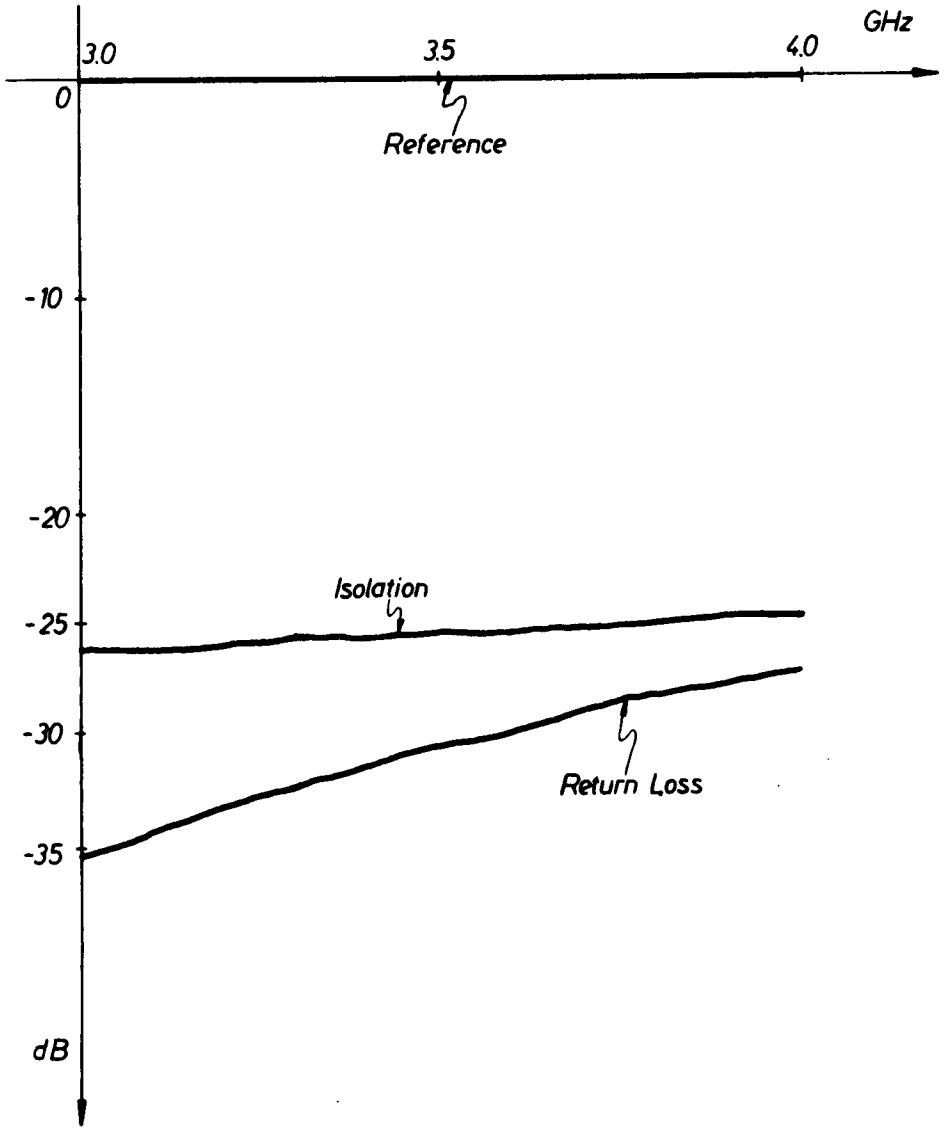

Figure 4.12 50 mil Lange hybrid isolation and input return loss.

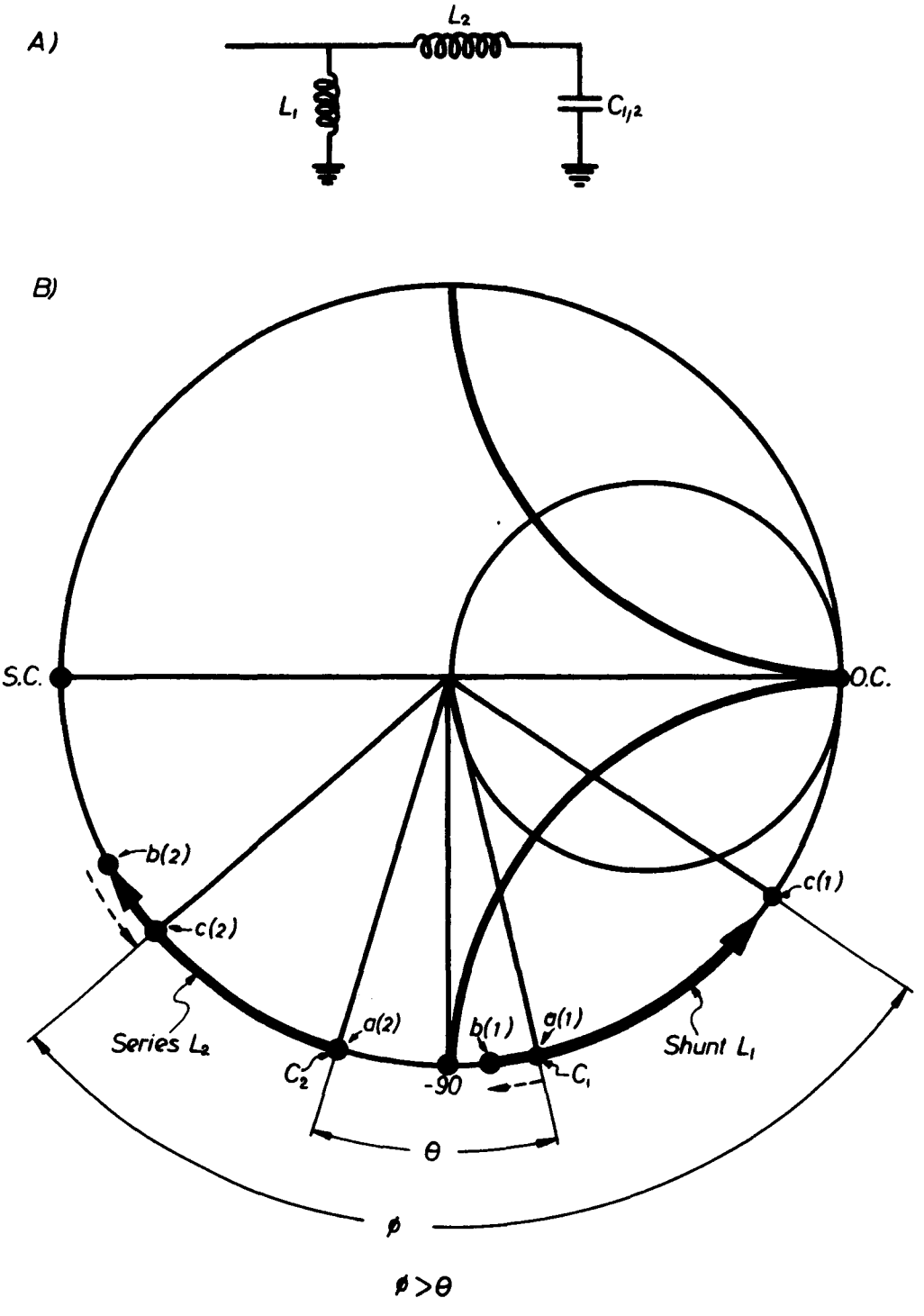

Figure 4.13 Phase shift stretching network and impedance motion on a reflection chart.

closer to the short circuit point a shunt L_1 does not affect it very much in moving it to c(2). But, L_1's effect on the point b(1) is very great, moving it to c(1). The overall effect is to stretch the phase shift from θ to ϕ. Figure 4.14 shows how this technique was used to stretch a 45° phase shift using optimally centered capacitors of ratio $c_2/c_1 = 2.25$ into a 90° phase shift. This network including 1.0 Ω diode series resistance was simulated using COSMIC and the results are tabulated in Figure 4.14. Over the band of interest, 3.3 to 3.7 GHz, the phase variation is 3.5°. Figure 4.15 shows element values and calculated performance of a 180° phase shift Bit using optimally centered capacitors with a ratio $c_2/c_1 = 2.25$. The phase variation over a design 10% bandwidth is approximately 35°. In general, as the ratio c_2/c_1 increases, the phase variation over the band decreases.

4.1.4 Experimental Phase Shifter Performance

Phase shift bits were fabricated in a microwave integrated circuit format. Alumina ceramic substrates with chrome-gold or chrome-copper-gold metallizations were used. A photograph of an early assembly is shown in Figure 4.16. A Lange type hybrid is terminated in two packaged MIS varactors. The varactors are mounted across the alumina substrate. Holes are drilled into the bottom base plate and are fitted with beryllia copper fixtures. The diodes are soldered to the hybrid conductors and the bottom portion of the diode is press-fit into the fixture. In order to test a set of diodes in this fixture, external bias tees are required. Figure 4.17 shows a complete phase shift bit including molybdenum blocking capacitors and d.c. bias network. The d.c. bias network consists of a series high impedance length of line and a shunt

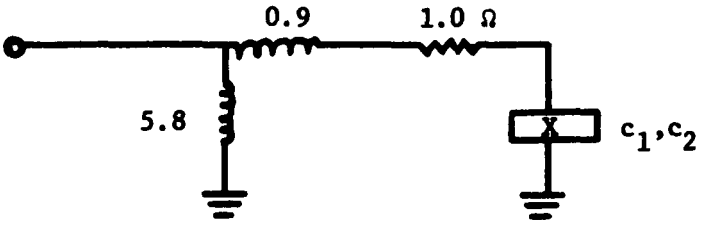

	c_1 = .6 pf	c_2 = 1.35 pf	
f (GHz)	Refl. Loss (dB)	Refl. Loss (dB)	Δθ°
3.1	.175	.418	94.2
3.2	.184	.409	94.0
3.3	.193	.409	93.6
3.4	.211	.400	93.0
3.5	.220	.400	92.2
3.6	.229	.391	91.2
3.7	.247	.391	90.1
3.8	.256	.382	88.9
3.9	.265	.382	87.6

Figure 4.14 Calculated performance of a 90° bit with c_2/c_1 = 2.25.

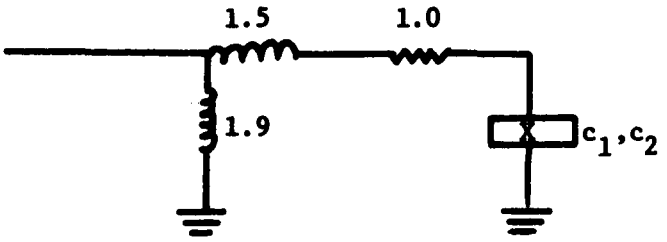

	c_1 = .6 pf	c_2 - 1.35 pf	
f (GHz)	Refl. Loss (dB)	Refl. Loss (dB)	$\Delta\theta°$
3.1	.225	.568	203.85
3.2	.276	.497	201.4
3.3	.336	.441	196.7
3.4	.402	.396	190.11
3.5	.474	.359	181.77
3.6	.545	.329	169.302
3.7	.610	.303	161.1
3.8	.662	.382	159.518
3.9	.697	.264	137.69

Figure 4.15 Calculated performance of 180° bit with c_2/c_1 = 2.25.

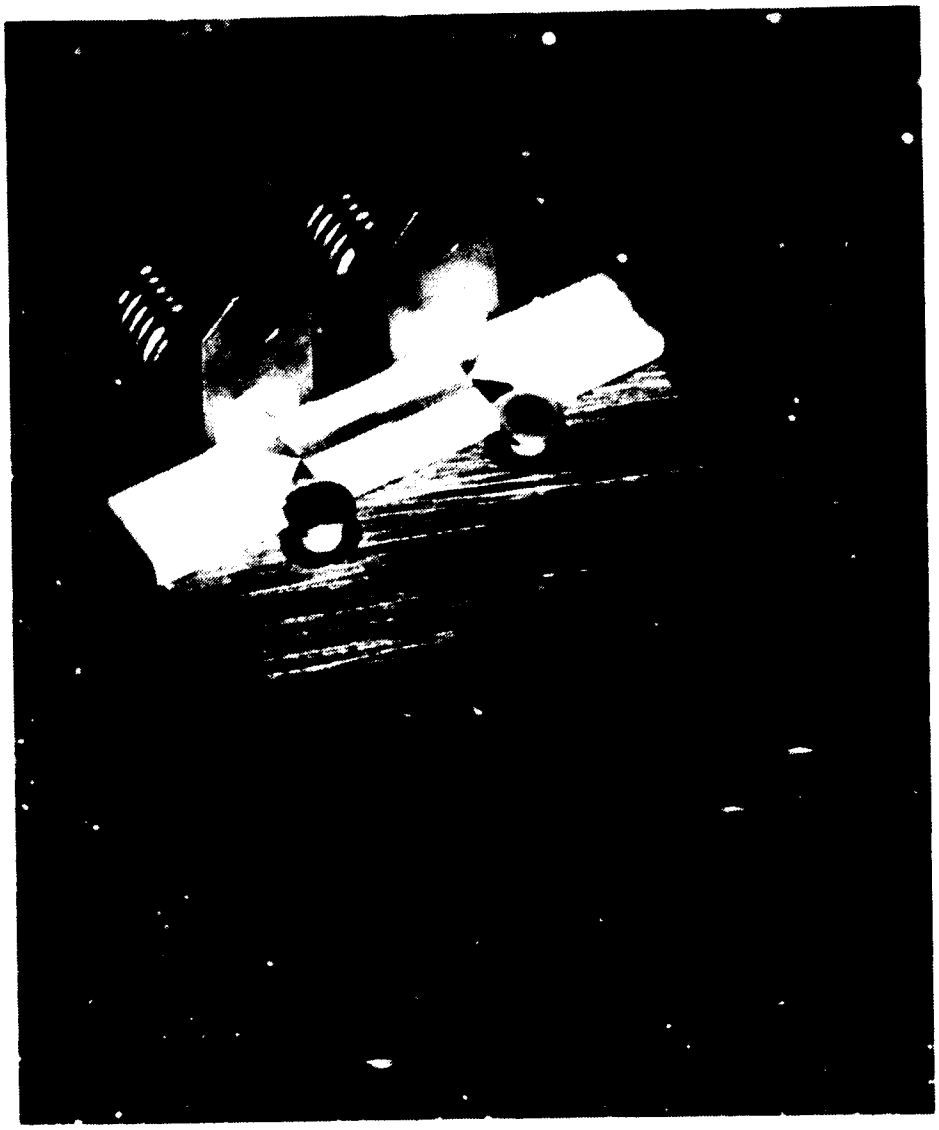

Figure 4.16 Phase shift bit assembly.

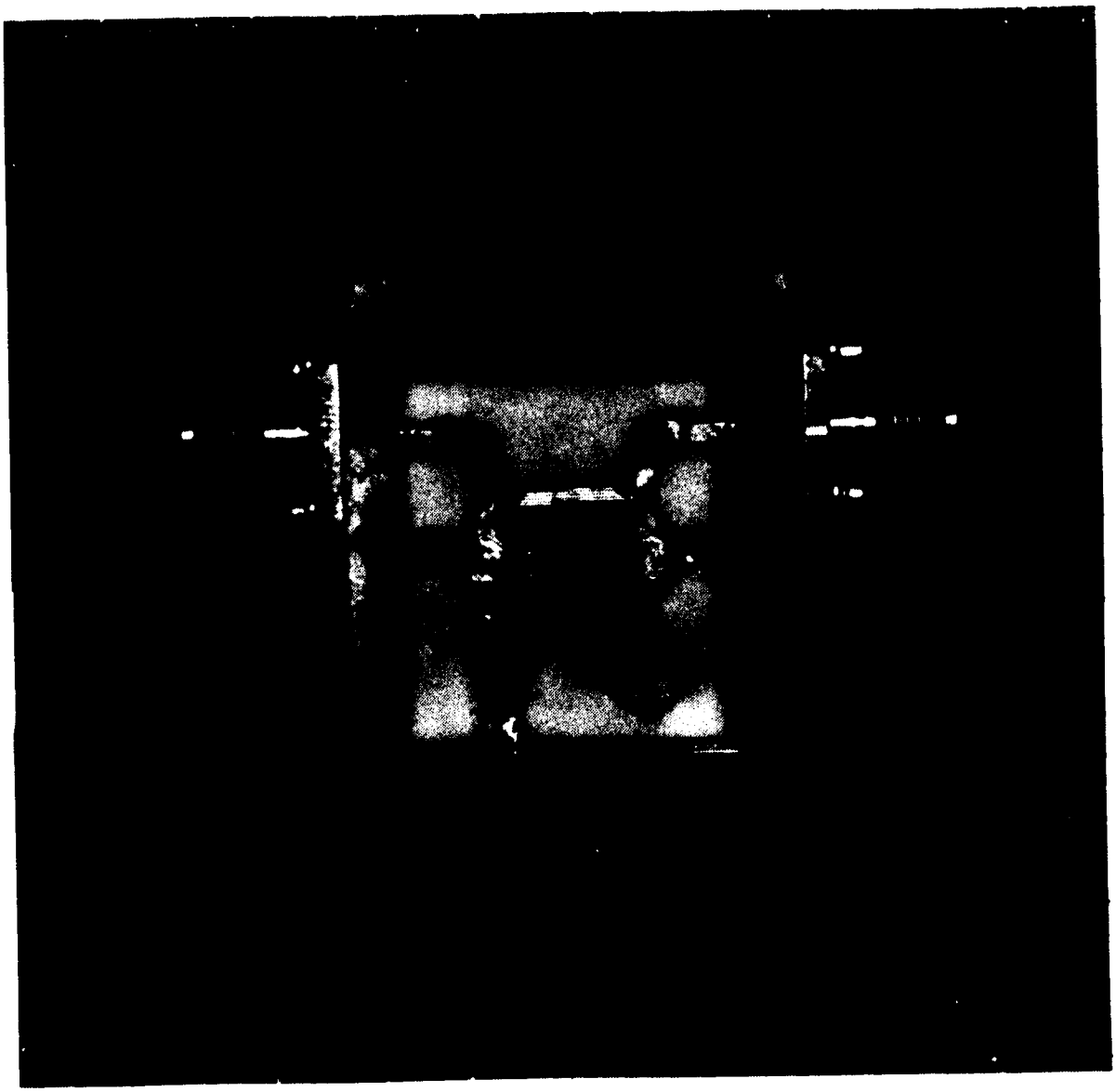

Figure 4.17 Complete phase shift bit.

low impedance line such that the diode over the band of interest sees an open circuit, but at d.c. there is a direct connection. Connections to the outside world are made through coax to microstrip transitions which are commercially available. Bits are made so that it may be cascaded by removing connectors and bolting them together in series.

All phase shifters were measured on an H.P. microwave network analyzer and a typical test setup is shown in Figure 4.18. Small signal performance of 22.5°, 45°, 90° and 180° phase shifters is shown in Figures 4.19, 4.20, 4.21, and 4.22. The insertion loss in each of these figures includes approximately 0.35 to 0.5 dB two-way loss of the Lange hybrid. The loss of the 180° bit is much larger than the other bits because two diodes in series were used which doubles the loss. This was done in order to reduce the phase variation by shifting the diode impeance to a more optimal portion of the chart. The performance of each bit corresponds well with predicted performance.

4.1.5 Large Signal Phase Shifter Effects

In this section, large signal measurements on MIS varactor phase shifters are presented and discussed qualitatively. Specifically, measurements of differential phase shift and switching speed variations versus applied microwave power level will be presented. These effects may be directly attributed to the presence or absence of a minority carrier inversion layer. These effects ultimately limit the usefulness of MIS varactors in accurate, high speed, phase shifting applications. Or at best what may be said, at this point in their development, is that these effects must be minimized in order to make MIS varactors useful phase shifting elements.

Figure 4.23 shows a plot of phase shift versus input applied microwave power, for two different sets of bias. There is a 5° differential

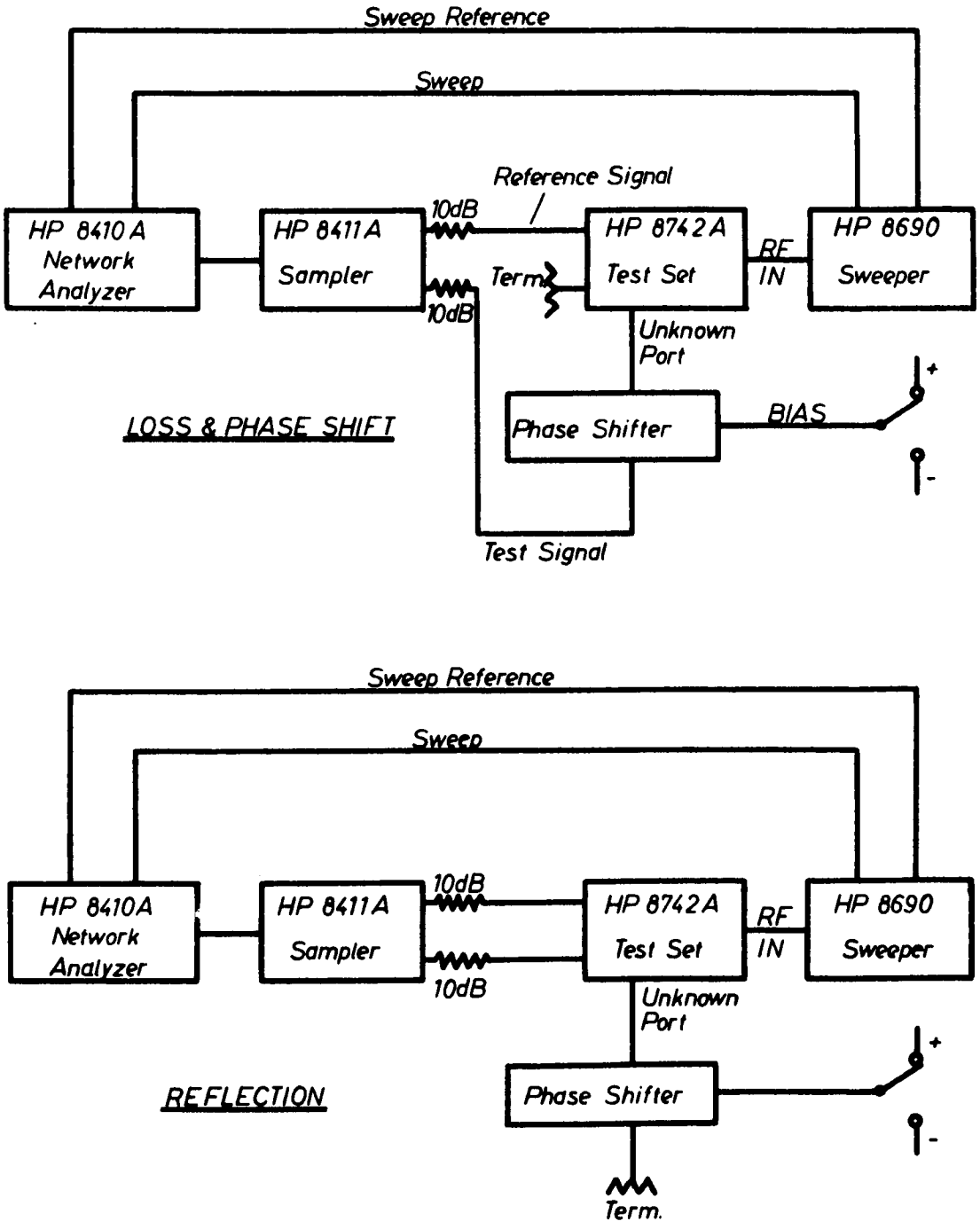

Figure 4.18 Small signal transmission and reflection measurement setup.

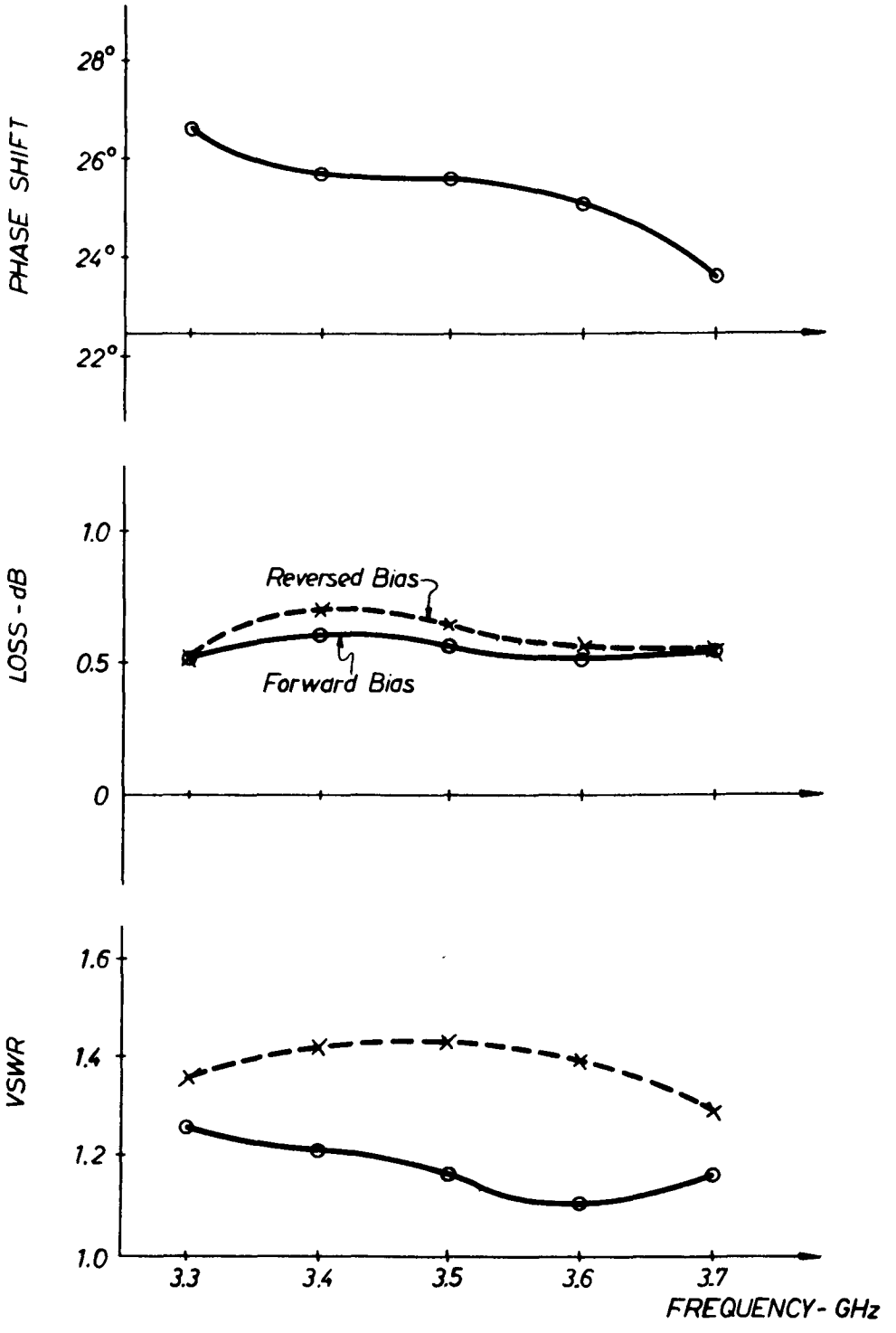

Figure 4.19 22.5° phase shift bit.

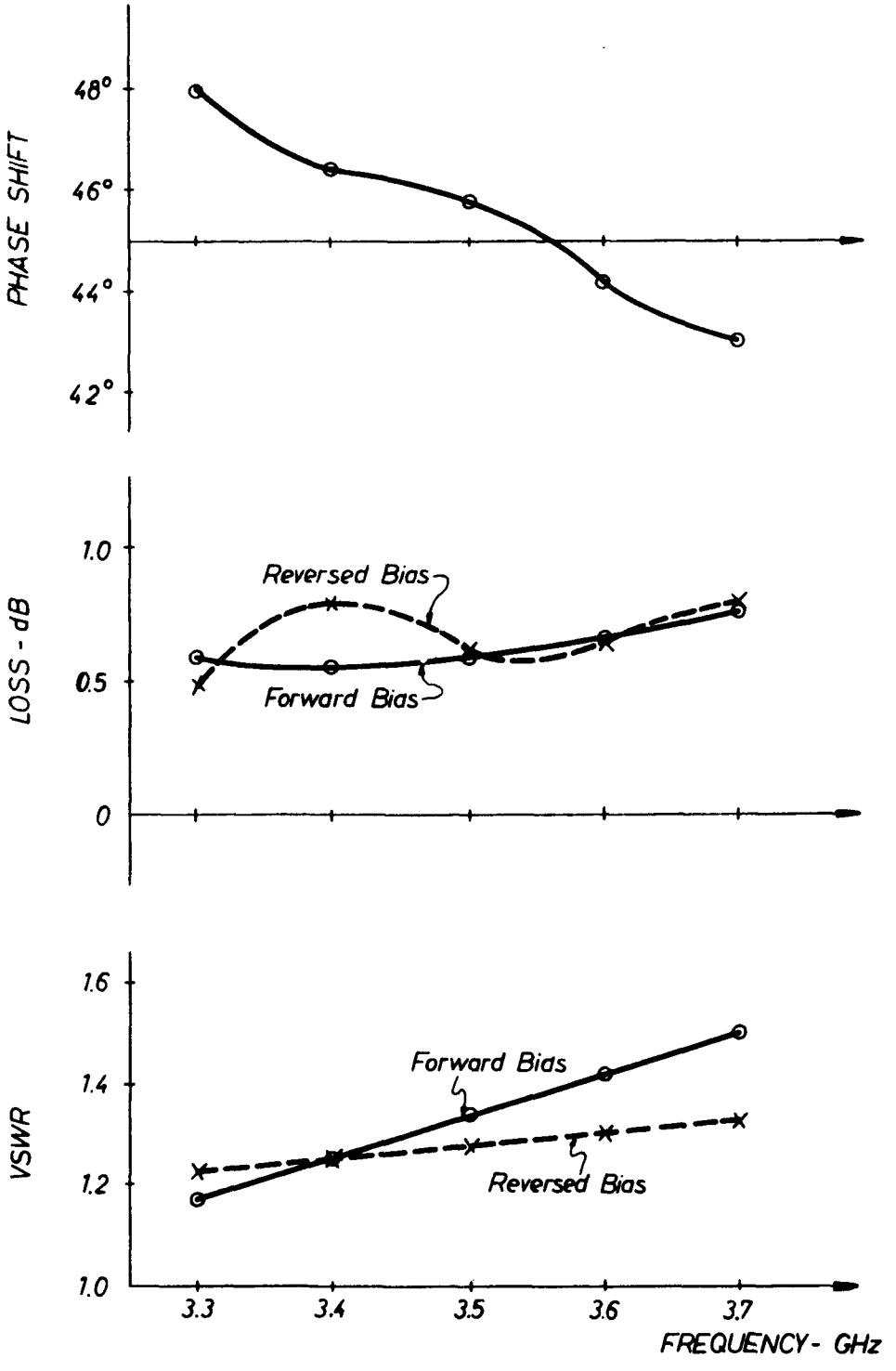

Figure 4.20 45° phase shift bit.

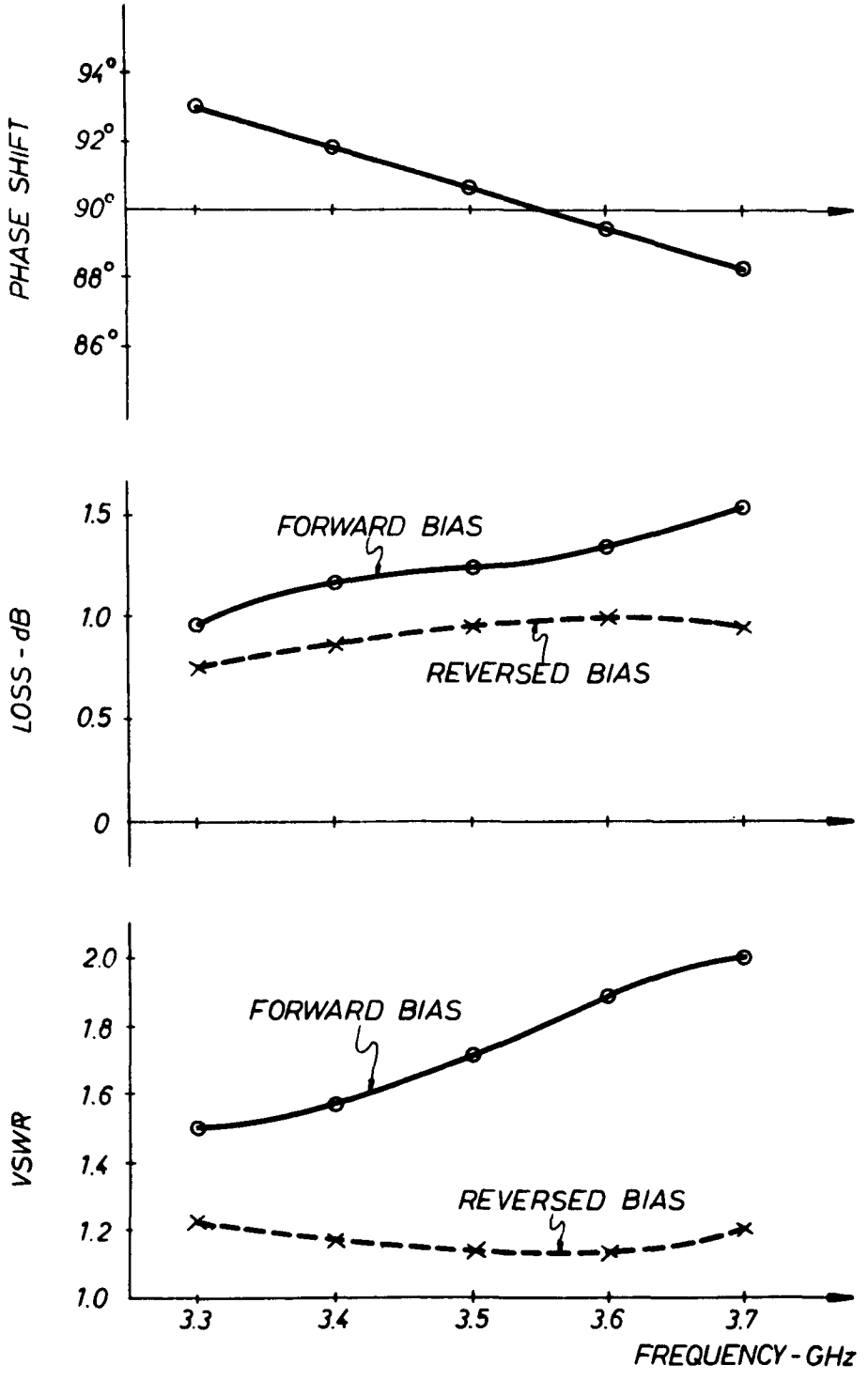

Figure 4.21 90° phase shift bit.

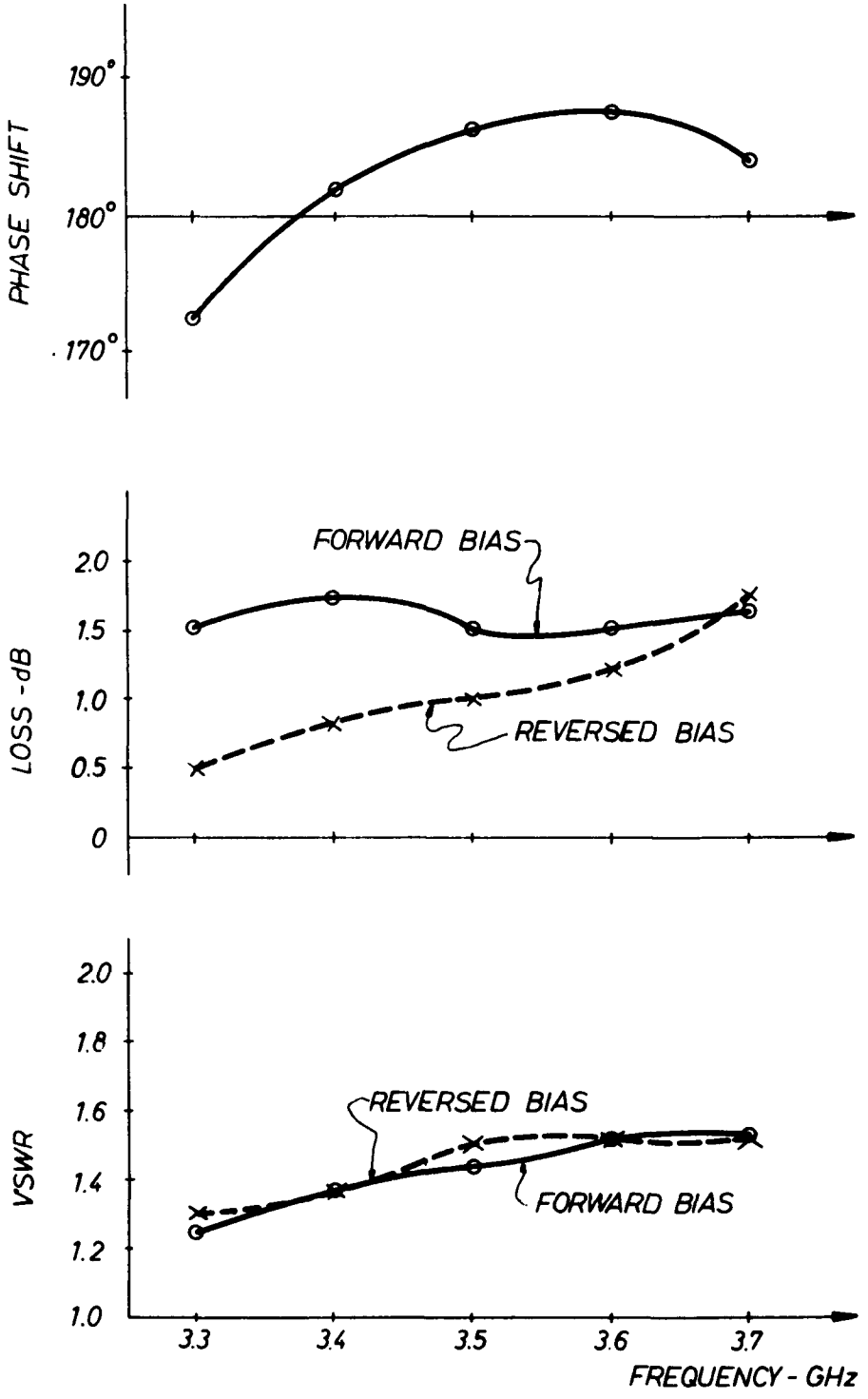

Figure 4.22 180° phase shift bit.

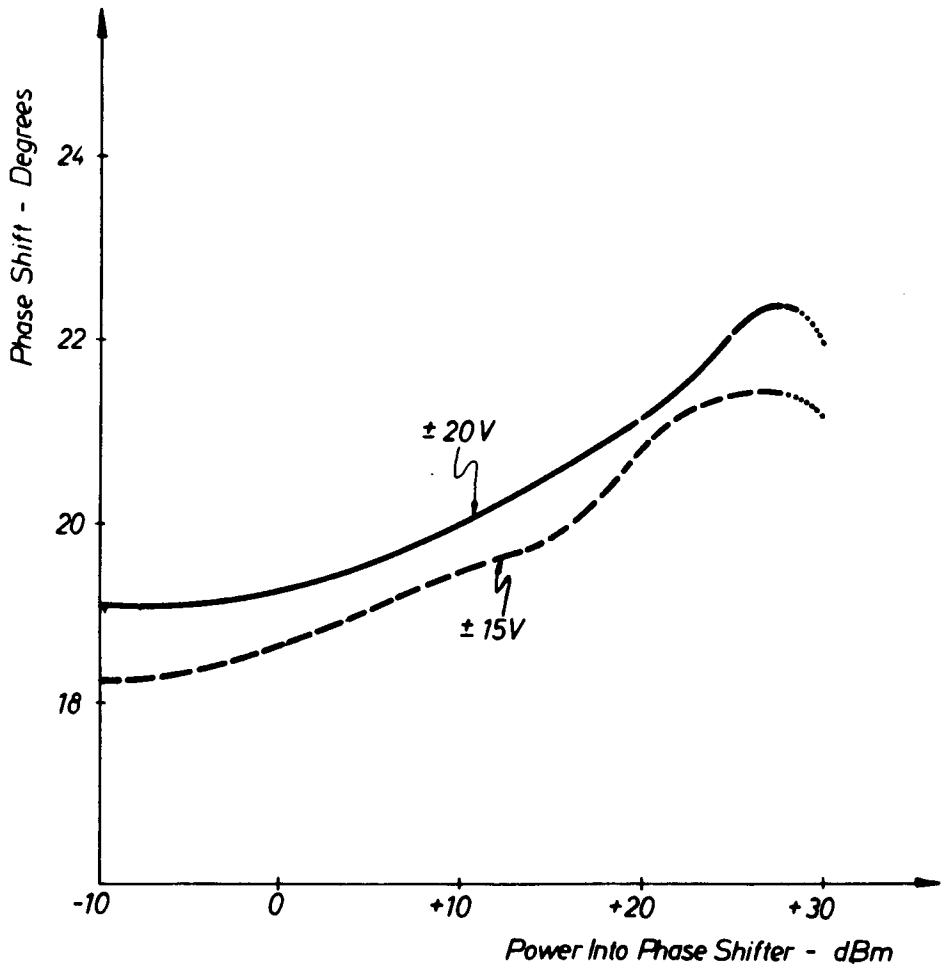

Figure 4.23 Phase shift versus power level.

phase shift variation when the power level is varied from small signals to about 1/2 watt. This variation could be attributed to variation of maximum depth with power. The same effect is shown in Figure 4.24 by plotting phase shift versus applied bias for two different power levels. The large signal transmission phase measurements were made with a setup similar to that of Figure 4.18. The only difference between tests is that in the large signal case the input to the phase shifter was amplified with a TWT and the output was padded so as not to destroy the HP 8411A sampling head.

Another important parameter is the phase shifter switching speed. That is, the time required for the phase to be varied from one state to another. A test setup to measure switching speed is shown in Figure 4.25. In this test setup, the microwave source (3.5 GHz) is split by a 3 dB hybrid. One arm of the hybrid is fed directly into a doubly balanced mixer. The other arm is fed into the mixer through the phase shifter. When the two inputs to a mixer are of the same amplitude and frequency the output is proportional to the phase difference between arms. The output of the mixer is observed on a scope. The bias waveform and phase shift versus time is sketched in Figure 4.26. The rise time (T_n) is of the order of nanoseconds. The settling time depends upon the microwave power level. There is such a thing as a settling time in an MIS varactor, again because of the formation of an inversion layer. The inversion layer is minority carriers which must be thermally generated from within the semiconductor. This generation is a thermal process which is a long process. When the bias voltage is switched suddenly, the surface depletes to a depth X_d in T_n. But then the surface starts to invert and when this occurs, the depletion depth is limited to a maximum value X_{dm}.

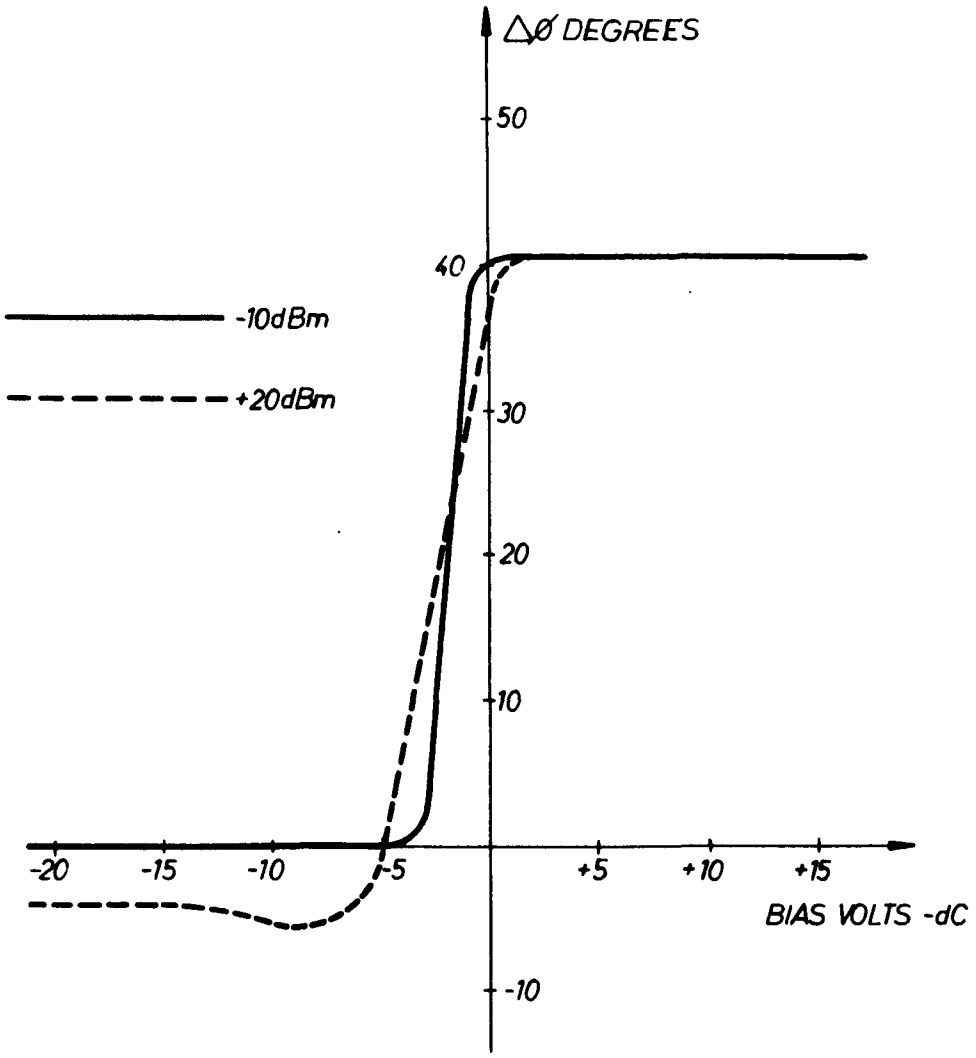

Figure 4.24 Differential phase shift for two different power levels.

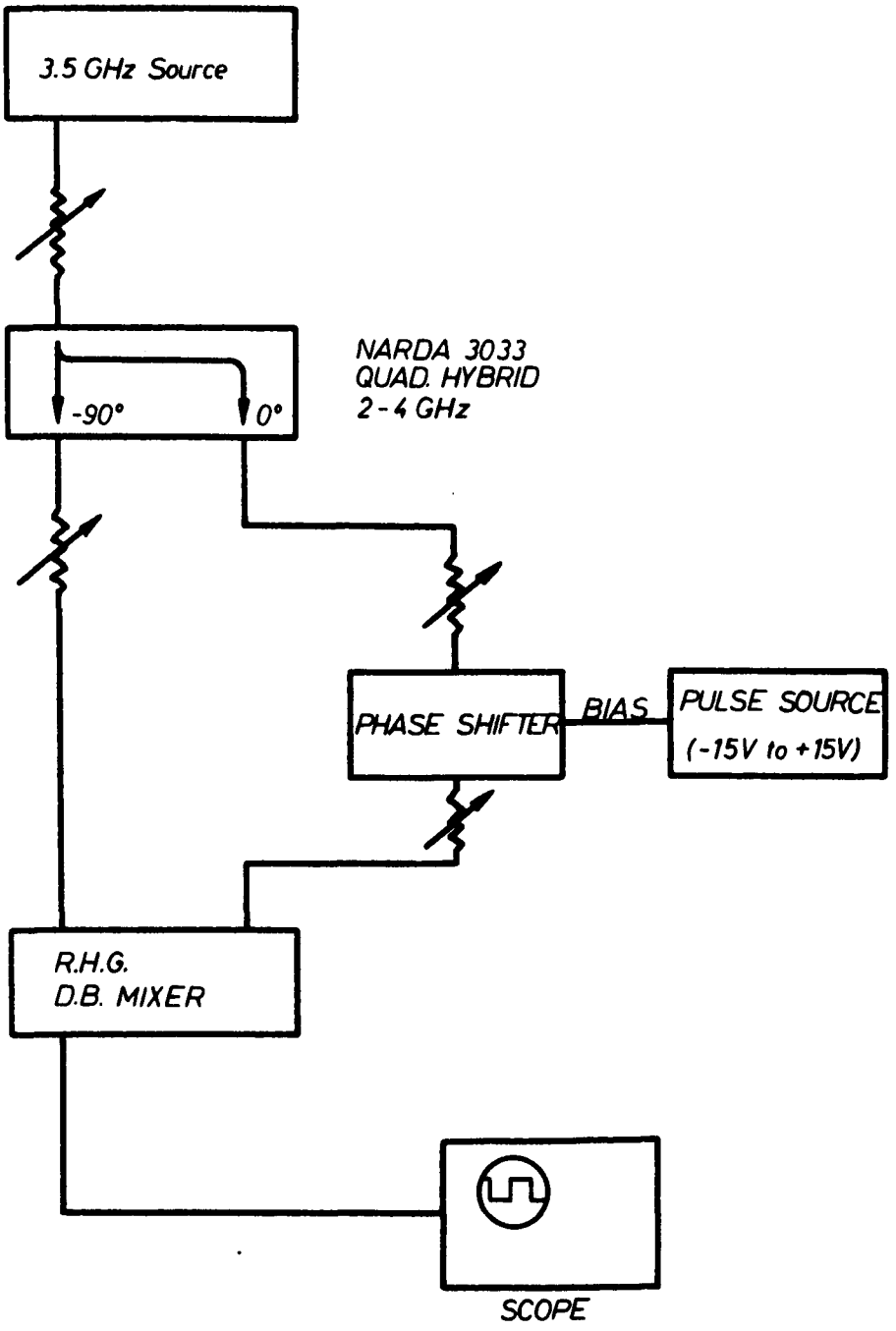

Figure 4.25 Switching time test setup.

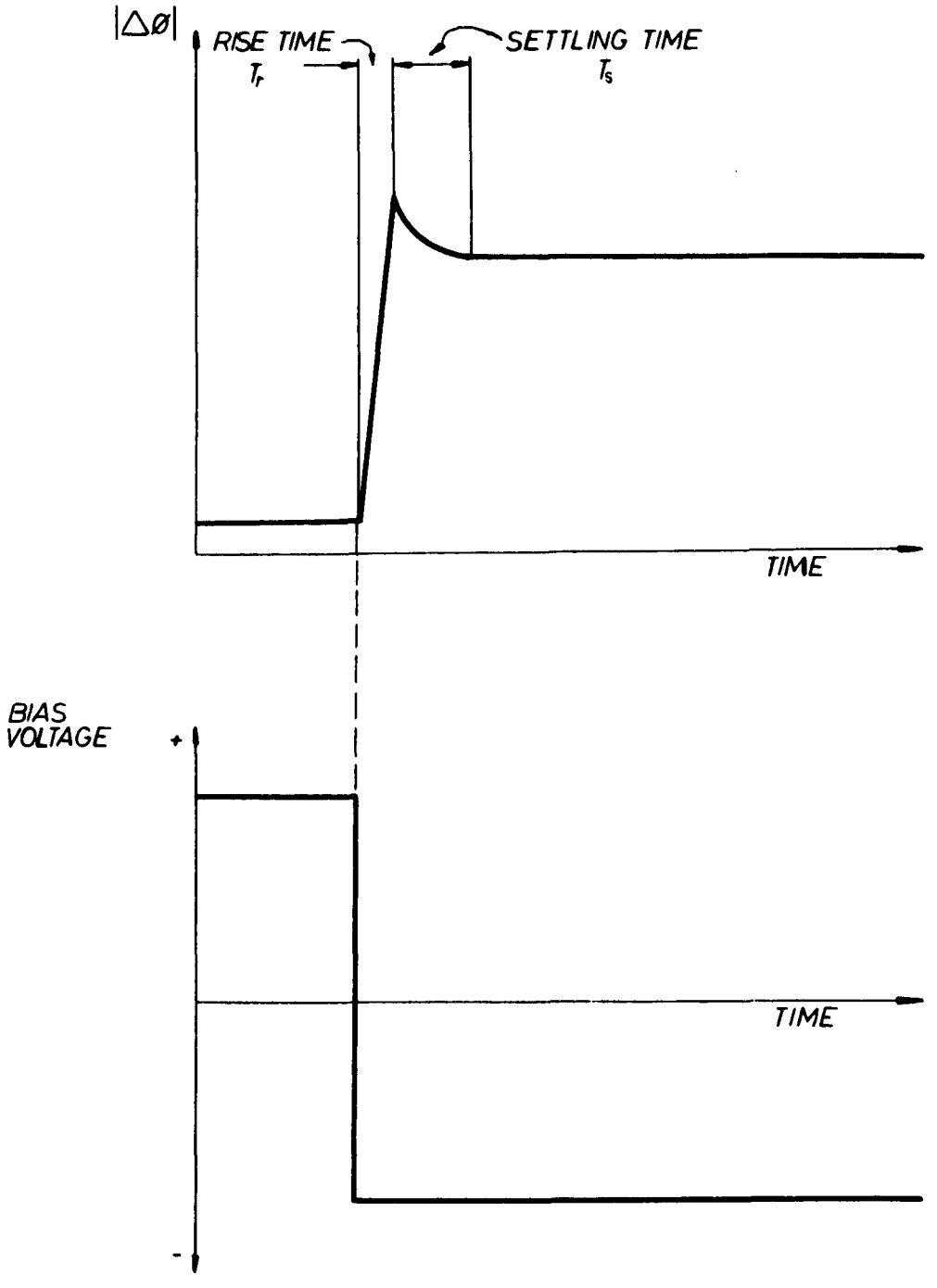

Figure 4.26 Instantaneous phase shift and bias waveforms.

If $X_{dm} < X_d$

The time that it takes to go from X_d to X_{dm} is the settling time T_S. Figure 4.27 shows switching speed versus applied power level for various bias voltages. For small signals, the switching speed is of the order of msec. For +25 dBm the speed is of the order of 0.6 μsec. In general, the larger the bias voltage the faster the switching speed.

4.2 MIS Varactor Parametric Amplifier

In this section important paramp relationships will be briefly reviewed. It will be shown that an important paramp parameter is the nonlinearity ratio c_1/c_o as the dynamic quality factor ($M = f_{co}\, c_1/c_o$). Estimates will be made of c_1/c_o for an MIS varactor using linear approximations. It will be shown that the nonlinearity ratio for an MIS varactor has regions which are relatively insensitive to pump amplitude variations. A rule of thumb for conventional Schottky barriers or pn junction varactor paramps is that for a 0.1 dB change in pump power, the midband gain changes by 0.5 dB. An MIS varactor paramp has been designed, built and tested. The design is in a microwave integrated circuit format similar to that of Bura et al[37].

4.2.1 Parametric Amplifier Review[37]

A typical parametric amplifier system is shown in Figure 4.28. It consists of a circulator, varactor filter and transforming networks, pump source and amplitude leveling loop. The r.f. source is generally a very high microwave frequency (35 to 100 GHz). The value of the pump depends upon the signal frequency f_s and the idler (f_i) required for minimum noise and maximum bandwidth.

$$f_p = f_i + f_s$$

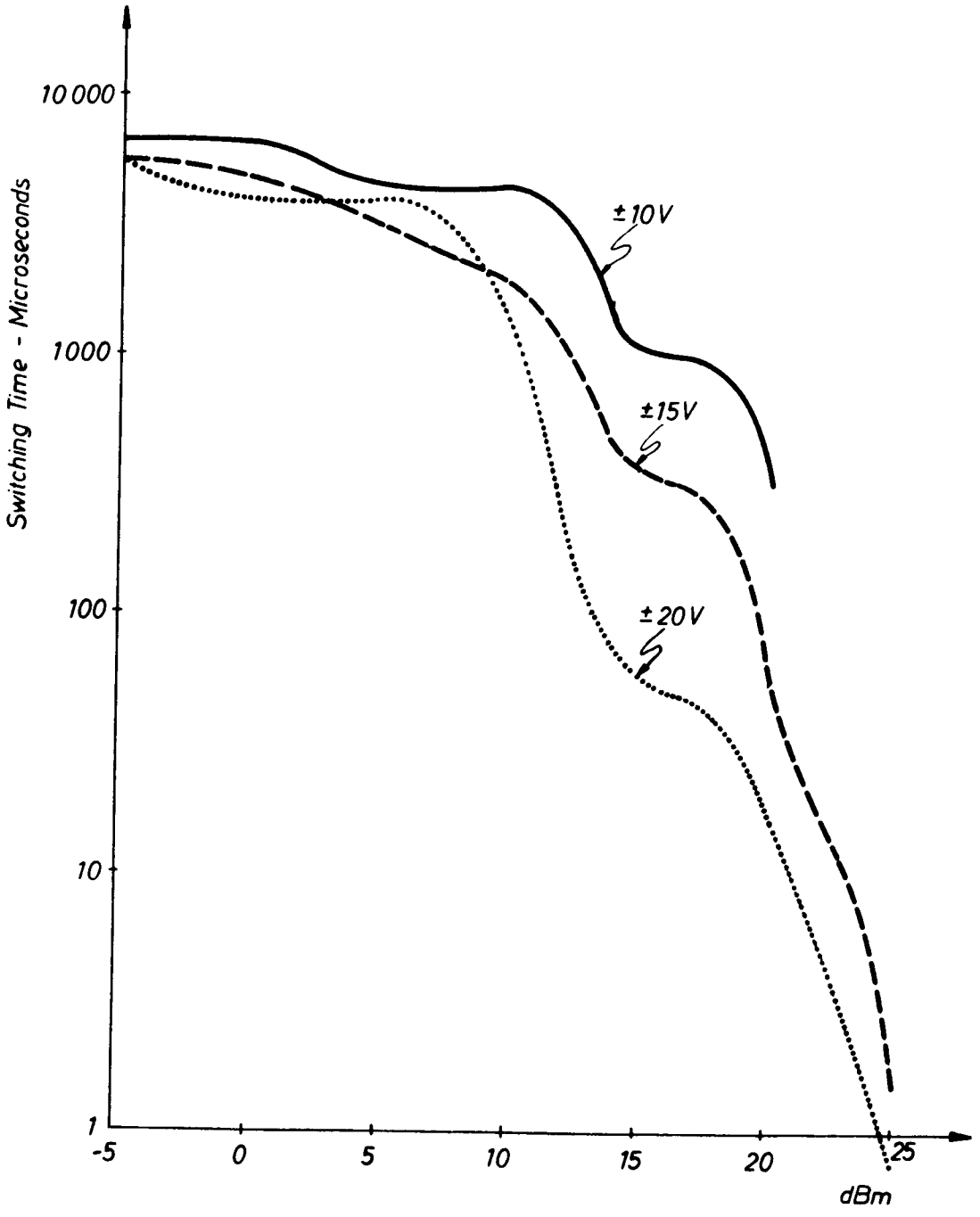

Figure 4.27 Switching time versus power into phase shifter.

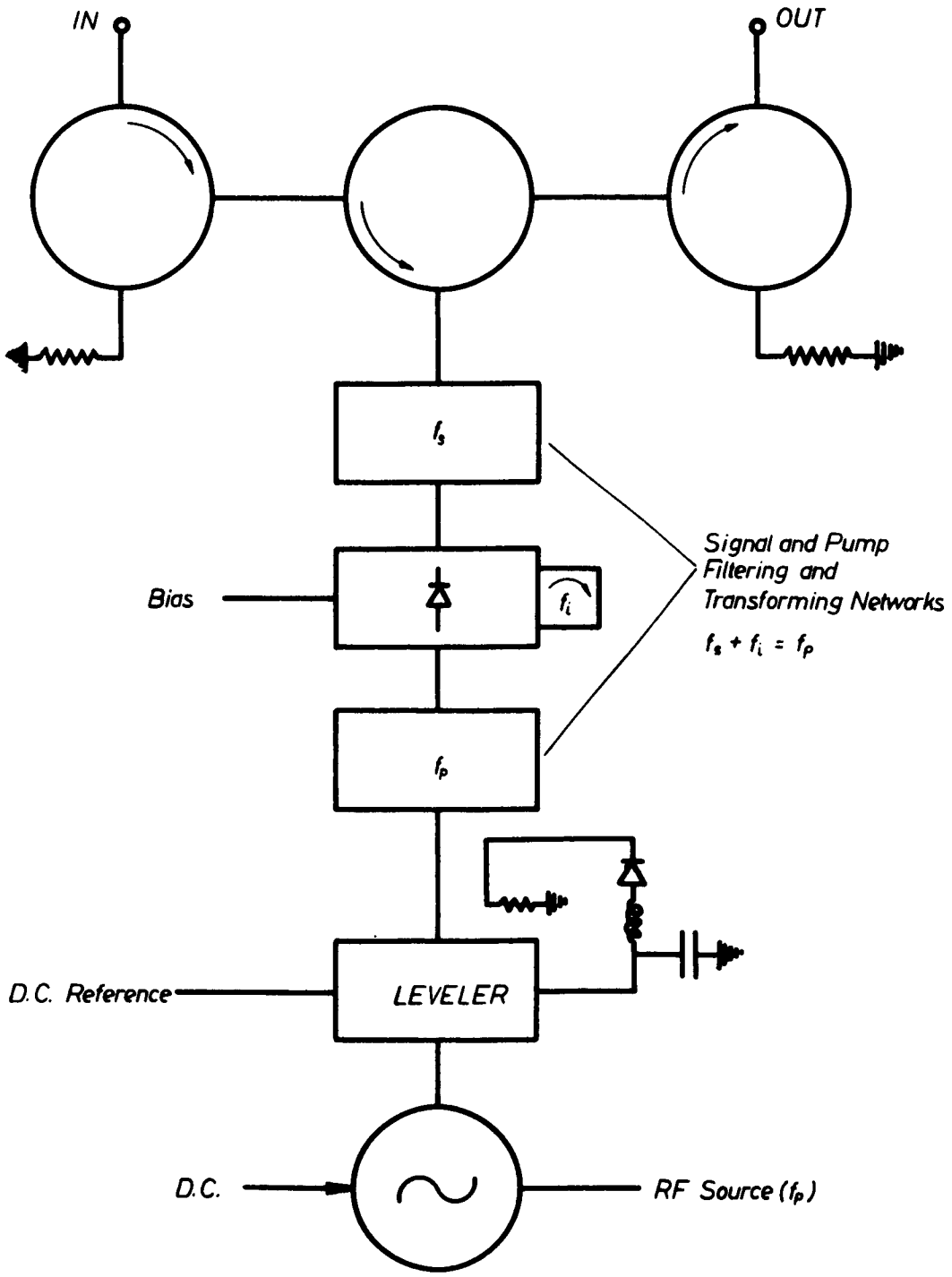

Figure 4.28 Reflection type paramp system.

The pump leveling loop may be fabricated using PIN diodes as ferrite attenuators. Elimination of this loop, without sacrifice to paramp performance, would be desirable in low cost or tactical systems. The filtering and transforming networks are necessary to separate the three frequencies and to establish proper gain and noise conditions.

The hub of the paramp is the varactor itself. Varactors in general must be tailored for each low noise application. Therefore, diode characterization in paramps is extremely important. A varactor is characterized statically and dynamically for parapm's Static (f_c) in the sense that it may be defined in the absence of a large high frequency source (pump). Similarly, dynamic quality factor (M) means that it is defined only when a pump amplitude is present. The static quality factor is the cut off frequency, f_c, and is defined by:

$$f_{cv} = \frac{1}{2\pi R_s c(v)}$$

where R_s = varactor series resistance

$c(v)$ = varactor capacitance at bias v.

Usually, the cutoff frequency is defined as a zero bias which is its lowest value since the capacitance is a maximum. A conventional varactor is never operated in forward bias for fear of drawing current and, therefore, degrading noise performance. Other important varactor parameters are series and parallel resonances which are a function of diode parasitics. The series resonance is generally pushed as high in frequency as possible so that it may be used as the idler resonator. A summary of static diode quality factors is given in Figure 4.29.

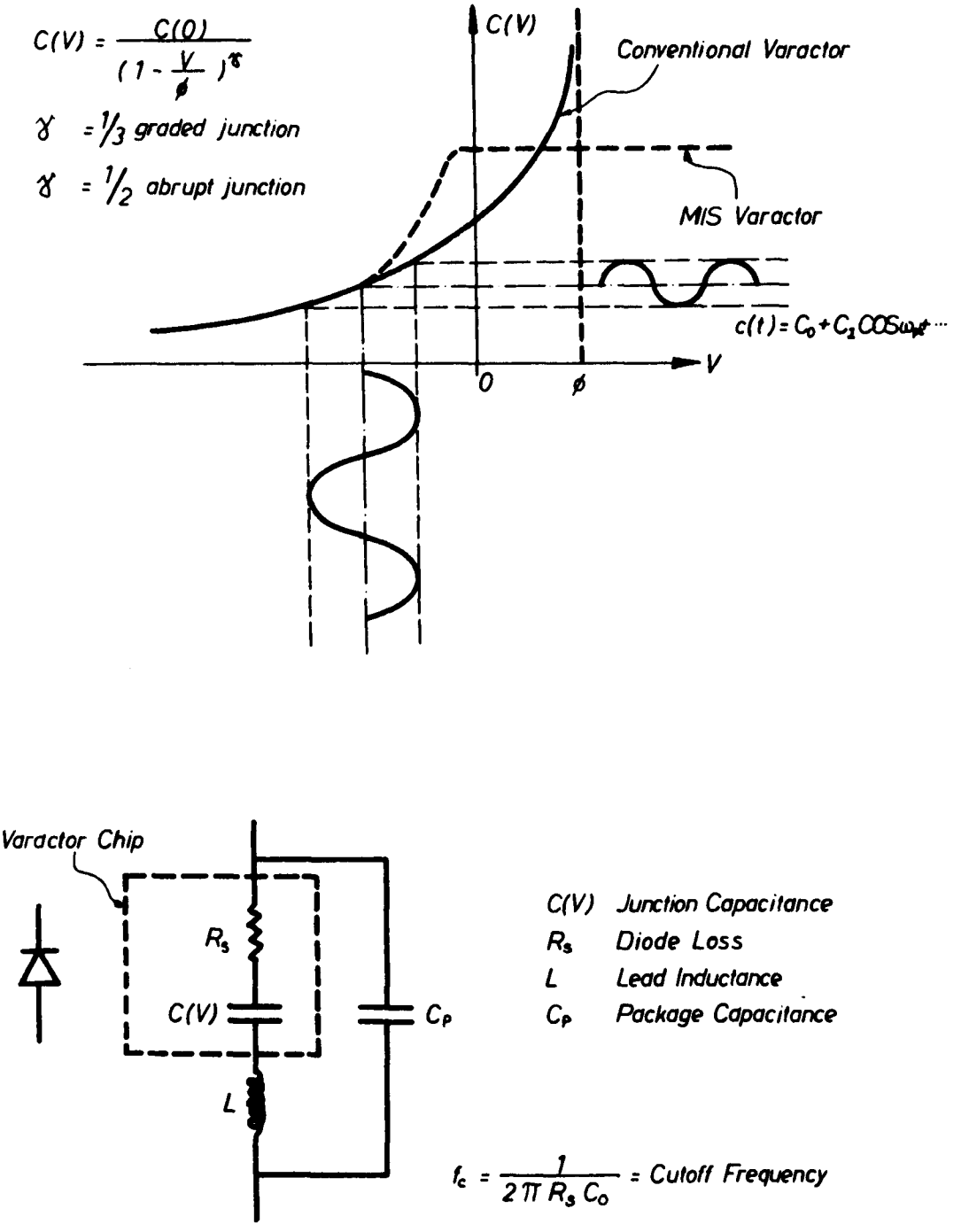

Figure 4.29 Static diode characterization.

The dynamic quality factor, M, is defined as the nonlinearity ratio multiplied by the diode cutoff frequency (i.e., $M = c_1/c_o\ f_c$). c_1 and c_o are the first two terms of a Fourier series expansion of c(t). When no pump is present, $c_1 = 0$ and, therefore, $M = 0$. The ratio c_1/c_o is called the nonlinearity ratio since the more nonlinear the capacitance versus voltage characteristic the greater the ratio becomes. It may be shown that the dynamic quality factor may be used to characterize a pumped varactor (Figure 4.30) which in turn may be used to determine midband gain (Figure 4.31), bandwidth and gain-bandwidth product (Figure 4.32), and effective input noise temperature (Figure 4.33). Each of these important performance parameters may be expressed in terms of f_s, f_i, M and c_1/c_o. The nonlinearity ratio depends upon the varactor capacitance law, and how hard it is driven by the pump amplitude. For conventional varactors, c_1/c_o is in the range of 1/3 to 1/4. Expressions for effective input noise temperature and gain bandwidth have been plotted by Albrecht[38]. These plots are reproduced for reference in Figures 4.34 and 4.35. They show that there is an optimum idler for minimum noise and for maximum gain bandwidth. The optimum idler for minimum noise does not correspond to the optimum idler for maximum gain-bandwidth. It can also be shown the optimum idler for minimum noise is

$$f_{i\ opt} = \sqrt{M^2 + f_s^2} - f_s$$

4.2.2 Estimates of MIS Nonlinearity Ratio

Figure 4.36 is a sketch of a piecewise continuous approximation of an MIS varactor. Also shown is the capacitance versus time waveform resulting from the presence of a large high frequency pump source.

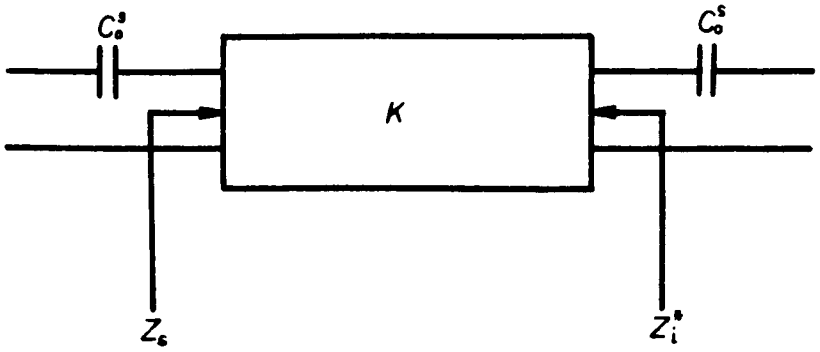

$$I_s = -j\frac{M}{f_i} R_s V_i^*$$

$$I_i^* = j\frac{M}{f_s} R_s V_s$$

$$Z_s Z_i^* = K = \frac{-M^2}{f_s f_i} R_s^2$$

where: $M = \frac{C_1}{C_o} f_c$ = QUALITY FACTOR

C_o, C_1 are first two terms of Fourier Series

$$C_o^2 = C_o \left\{1 - \left(\frac{C_1}{C_o}\right)^2\right\}$$

f_s, f_i Signal and Idler Frequencies

Figure 4.30 Dynamic characterization.

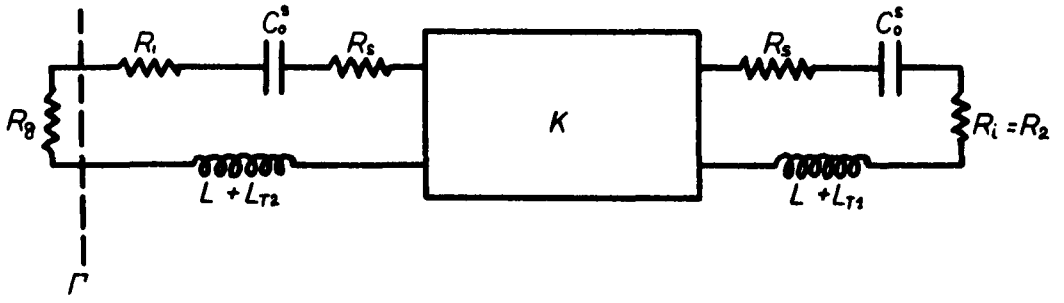

$$\Gamma = \frac{V_r}{V_{in}} = \frac{Z_{in} - R_g}{Z_{in} + R_g} = \text{Voltage Gain}$$

At Midband:

$$\Gamma = \frac{\frac{R_1 + R_s}{R_s} - \frac{R_g}{R_s} - \frac{M^2}{f_s f_i}\,\frac{R_s}{R_s + R_2}}{\frac{R_1 + R_s}{R_s} + \frac{R_g}{R_s} - \frac{M^2}{f_s f_i}\,\frac{1}{\frac{R_s + R_2}{R_s}}}$$

$$\Gamma = \frac{r_i - r_o - \frac{A}{r_f}}{r_i + r_o - \frac{A}{r_2}}; \quad A = \frac{K}{R_s^2}$$

$$G = \Gamma^2 = \text{POWER GAIN}$$

Figure 4.31 Amplifier equivalent and midband gain.

$$b = \frac{BW}{f_s} = \frac{r_1 + r_0 - \frac{A}{r_2}}{Q_1 r_1 + \frac{f_s}{f_i}\frac{A}{r_2} Q_2}$$

Q_1 , Q_2 ⟶ *Unloaded Signal and Idler Circuit Q*

Assuming $R_1 = R_2 = 0$

High Gain $1 + \frac{R_2}{R_6} \cong \frac{M^2}{f_s f_i}$

$$Q_1 = \frac{f_c}{f_s} = \frac{M}{f_s}\frac{C_0}{C_1}$$

$$Q_2 = \frac{f_c}{f_i} = \frac{M}{f_i}\frac{C_0}{C_1}$$

$$G^{1/2} B = 2\frac{C_1}{C_0} f_s \frac{1 - \left(\frac{M}{f_s}\right)^2 \frac{f_s}{f_i}}{\frac{M}{f_s}\left\{1 + \left(\frac{M}{f_s}\right)^2\left(\frac{f_s}{f_i}\right)^3\right\}}$$

Figure 4.32 Bandwidth and voltage-gain bandwidth product.

Assuming $R_1 = R_2 = 0$

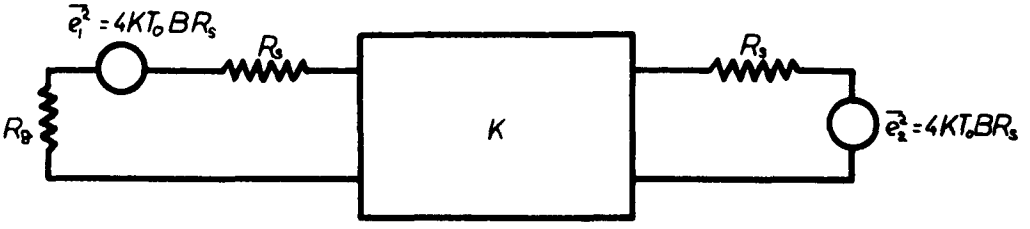

$$T_e \triangleq \frac{N_T}{G\,K\,B}$$

N_T = Total available noise output power due to thermal noise in the signal and idler circuits.

$$\frac{T_e}{T_o} = \frac{f_s}{f_i}\left\{1 + \frac{1 + \frac{f_s}{f_i}}{\left(\frac{M}{f_s}\right)^2\left(\frac{f_s}{f_i}\right)^2 - \frac{f_s}{f_i}}\right\}$$

$$\frac{d(T_e/T_o)}{df_i} = 0; \quad (f_i)_{opt.} = -f_s + \sqrt{M^2 + f_s^2}$$

$$(f_p)_{opt.} = \sqrt{M^2 + f_s^2}$$

Figure 4.33 Noise equivalent circuit.

$$\frac{T_e}{T_o} = \frac{f_s}{f_i}\left(1 + \frac{1 + \frac{f_s}{f_i}}{\left(\frac{M'}{f_s}\right)^2\left(\frac{f_s}{f_i}\right)^2 - \frac{f_s}{f_i}}\right)$$

$$M' = \frac{M}{\sqrt{1 + \frac{R_s}{R_d}}}$$

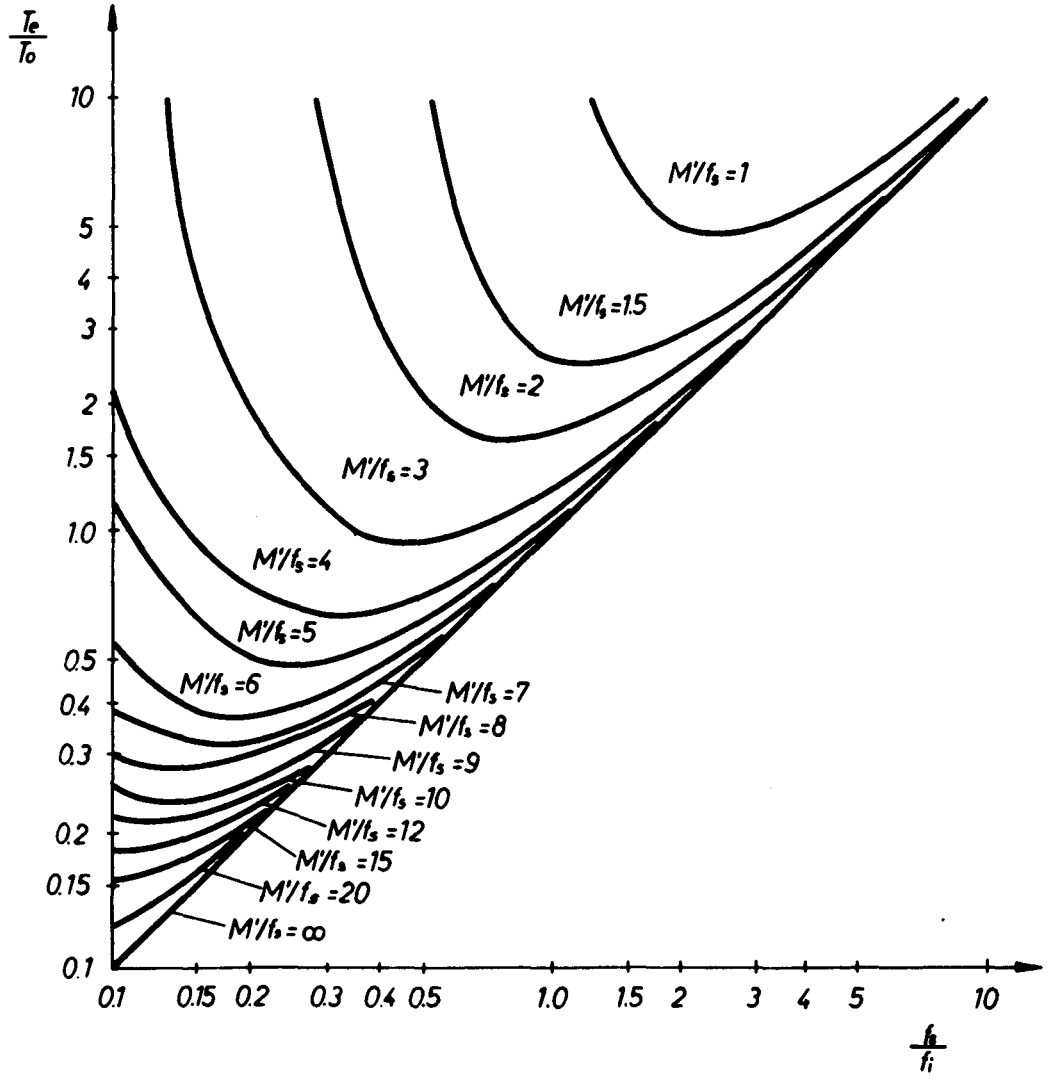

Figure 4.34 Noise ratio (T_e/T_o) versus f_s/f_i with M'/f_s as a parameter.

$$G^{1/2}B = A_1 f_s \frac{C_1}{C_o}$$

$$A_1 = \frac{2\left[\left(\frac{M}{f_s}\right)^2 \frac{f_s}{f_i} - 1\right]}{\frac{M}{f_s}\left[1 + \left(\frac{M}{f_s}\right)^2 \left(\frac{f_s}{f_i}\right)^3\right]}$$

$$M = \frac{C_1}{C_o} f_{co}$$

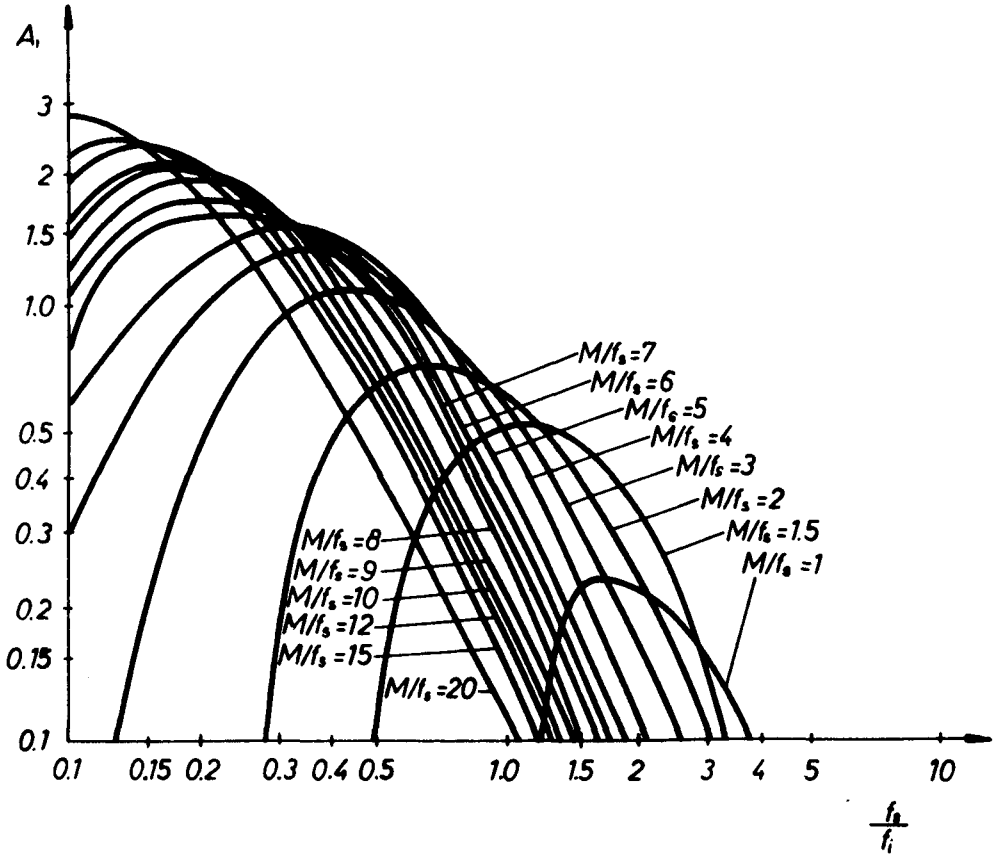

Figure 4.35 Gain bandwidth product versus f_s/f_i for a given diode quality factor.

If c(t) is expanded into a Fourier series, it may be shown that

$$c_o = c_L + \frac{\theta_1}{\pi}(c_H - c_L) + \frac{V_P}{\pi}\,\frac{c_H - c_L}{V_H - V_L}\,(\sin\theta_2 - \sin\theta_1)$$

and

$$c_1 = \frac{c_H - c_L}{\pi}\sin\theta_1 + \frac{V_P}{2\pi}\,\frac{c_H - c_L}{V_H - V_L}\,(\theta_2 - \theta_1)$$

$$+ \frac{V_P}{4\pi}\,\frac{c_H - c_L}{V_H - V_L}\,(\sin 2\theta_2 - \sin 2\theta_1)$$

taking the ratio and manipulating

$$\frac{c_1}{c_o} = \frac{\sin\theta_1 + \frac{1}{2}\,\frac{V_P}{V_H - V_L}(\theta_2 - \theta_1) + \frac{1}{4}\,\frac{V_P}{V_H - V_L}\,(\sin 2\theta_2 - \sin 2\theta_1}{\pi\,\frac{c_L}{c_H - c_L} + \theta_1 + \frac{V_P}{V_H - V_L}(\sin\theta_2 - \sin\theta_1)}$$

Note that θ_1 and θ_2 may be found by

$$V_L + V_P \cos\theta_2 = V_o$$

$$V_H + V_P \cos\theta = V_o$$

An interesting limiting value of nonlinearity ratio is for the abrupt junction case. Letting

$$V_H = V_L = V^+ \quad , \text{ therefore}$$

$$\theta_1 = \theta_2$$

$$c_o = c_2 + \frac{\theta_1}{\pi}\,(c_H - c_L)$$

$$c_1 = \frac{c_H - c_L}{\pi}\sin\theta_1$$

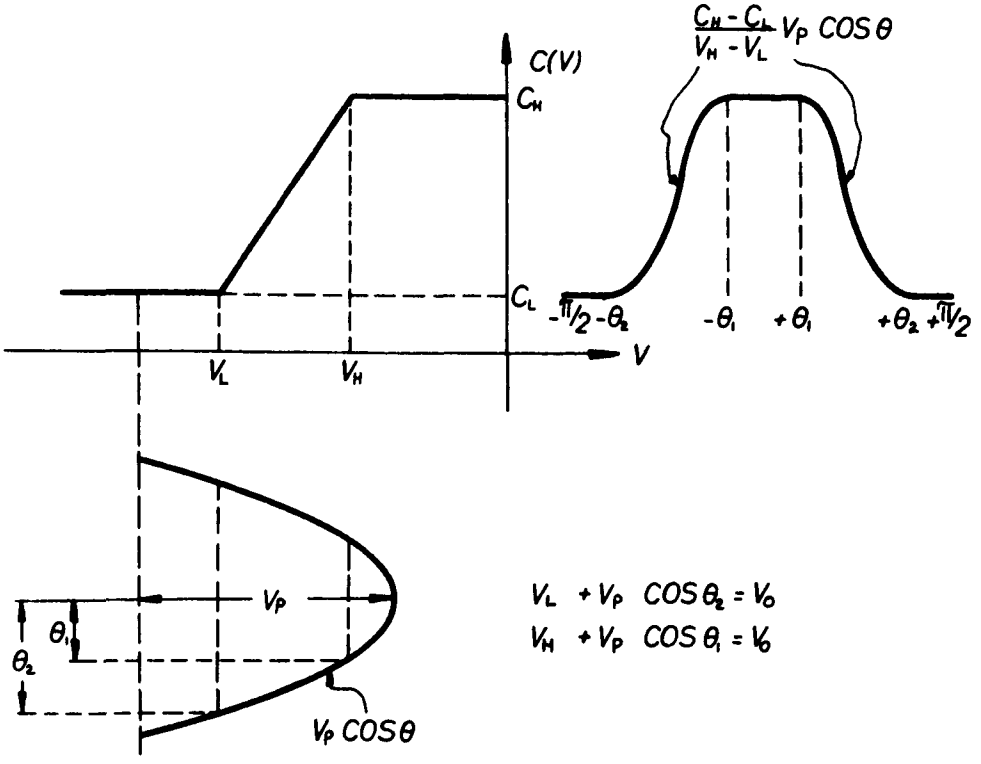

$$\frac{C_1}{C_0} = \frac{\sin\theta_1 + \frac{1}{2}\frac{V_P}{V_H - V_L}\left(\theta_2 - \theta_1\right) + \frac{1}{4}\frac{V_P}{V_H - V_L}\left(\sin 2\theta_2 - \sin 2\theta_1\right)}{\pi\,\frac{C_L}{C_H - C_L} + \theta_1 + \frac{V_P}{V_H - V_L}\left(\sin\theta_2 - \sin\theta_1\right)}$$

Figure 4.36 Nonlinearity ratio for a piecewise linear model.

The nonlinearity ratio for this case is

$$\frac{c_1}{c_o} = \frac{\frac{c_H - c_L}{\Pi} \sin \theta_1}{c_L + \frac{\theta_1}{\Pi} (c_H - c_L)}$$

which may be manipulated into the following form by defining $\theta = \Pi q$ and rearranging terms.

$$\frac{c_1}{c_o} = \frac{q\left(\frac{c_H}{c_L} - 1\right)}{1 + q\left(\frac{c_H}{c_L} - 1\right)} \frac{\sin \Pi q}{\Pi q}$$

where $$\cos \Pi q = \frac{V^t - V_o}{V_P}$$

q may be defined as that fraction of the r.f. cycle when the device is in the high capacitance state. A summary of the abrupt transition two-state capacitor is shown in Figure 4.37. A plot of nonlinearity ratio versus q for various capacitance ratios is shown in Figure 4.38. In this figure it may be seen that there is an optimum value of q for maximum nonlinearity ratio for a given capacitance ratio. This optimum always passes through the curve $c_1/c_o = \cos \Pi q$. This optimum is broad, especially for capacitance ratios less than 10. This effect does not occur in conventional varactors and can have a profound effect on parametric amplifier stability.

4.2.3 Experimental MIS Parametric Amplifier

A microwave parametric amplifier has been designed, built, and tested using a metal insulator semiconductor varactor as the nonlinear

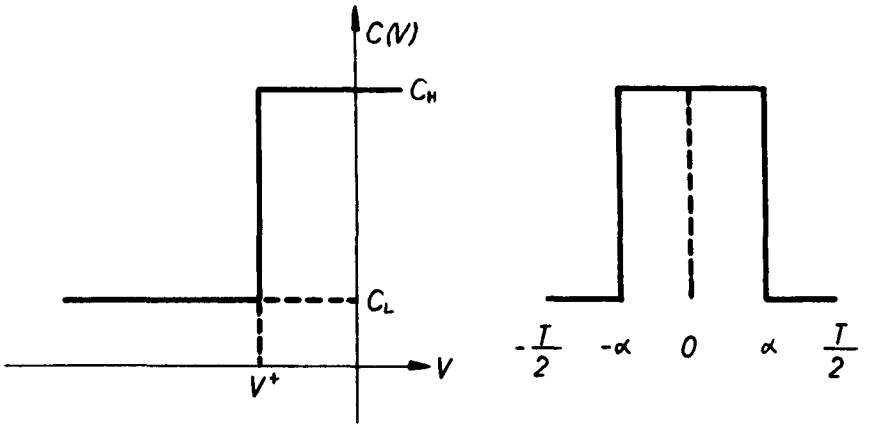

$$c(t) = C_0 + \sum_{n=1}^{\infty} 2C_n \cos n\omega_p t + 2C_n' \sin n\omega_p t$$

$$\frac{C_n}{C_0} = \frac{q\left(\frac{C_H}{C_L} - 1\right)}{1 + q\left(\frac{C_H}{C_L} - 1\right)} \frac{\sin n\pi q}{n\pi q}$$

$$\cos n\pi q = \frac{V^+ - V_0}{V_p} \qquad q = \frac{2\alpha}{T}$$

Figure 4.37 Fourier analysis of an ideal two-state capacitor.

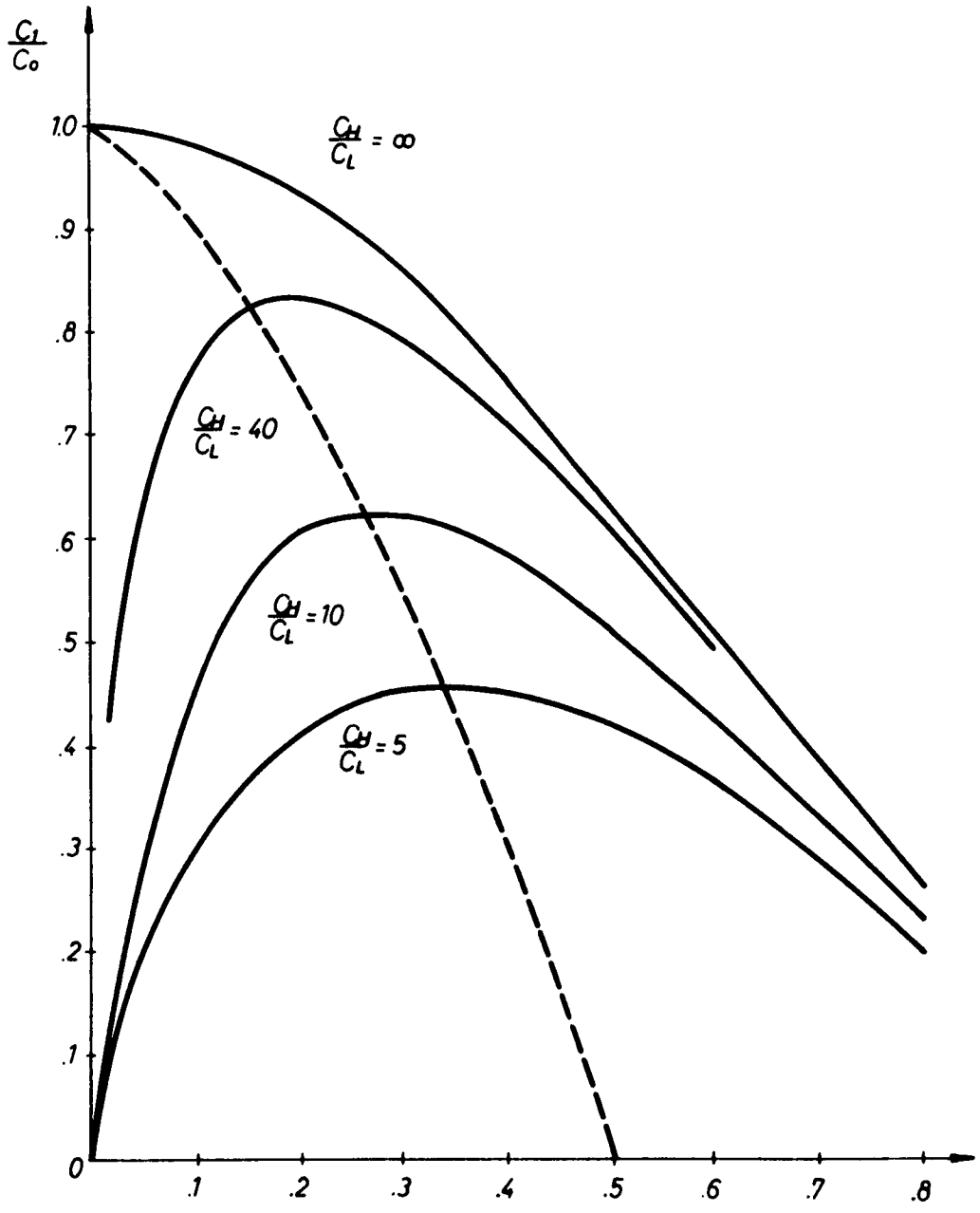

Figure 4.38 Nonlinearity ratio versus q for an ideal two-state capacitor.

capacitor. The amplifier is a microwave hybrid circuit using microstrip as the transmission element. The amplifier was built on an alumina substrate. The transmission lines are formed by thin films of chrome, copper and gold. The chrome promotes adhesion of the copper to the substrate, and the gold prevents the copper from tarnishing. Referring to Figure 4.39, the pump is fed to the diode through a bandpass filter. The idler is formed by the diode parasitics and the last element of the pump filter. Stubs in the signal circuit transform the source impedance to establish the correct gain and also act as a pump reject filter. A commercially available circulator is used to separate input and output signals. Typical paramp performance data is shown below.

f_p	= 7.92 GHz
f_s	= 2.07 GHz
P_p	= 65 mW
V_B	= 3.2 volts
Gain	= 16 dB
3 dB bandwidth	= 38 MHz
NF	= 2.8 dB

Also, measurements of gain variation with pump amplitude change are shown below.

Pump Attenuation Change	Gain (dB)
6.0	15.00
5.9	15.25
5.8	15.50
5.7	15.75

For this amplifier the gain sensitivity was approximately .25 dB better than a conventional parametric amplifier.

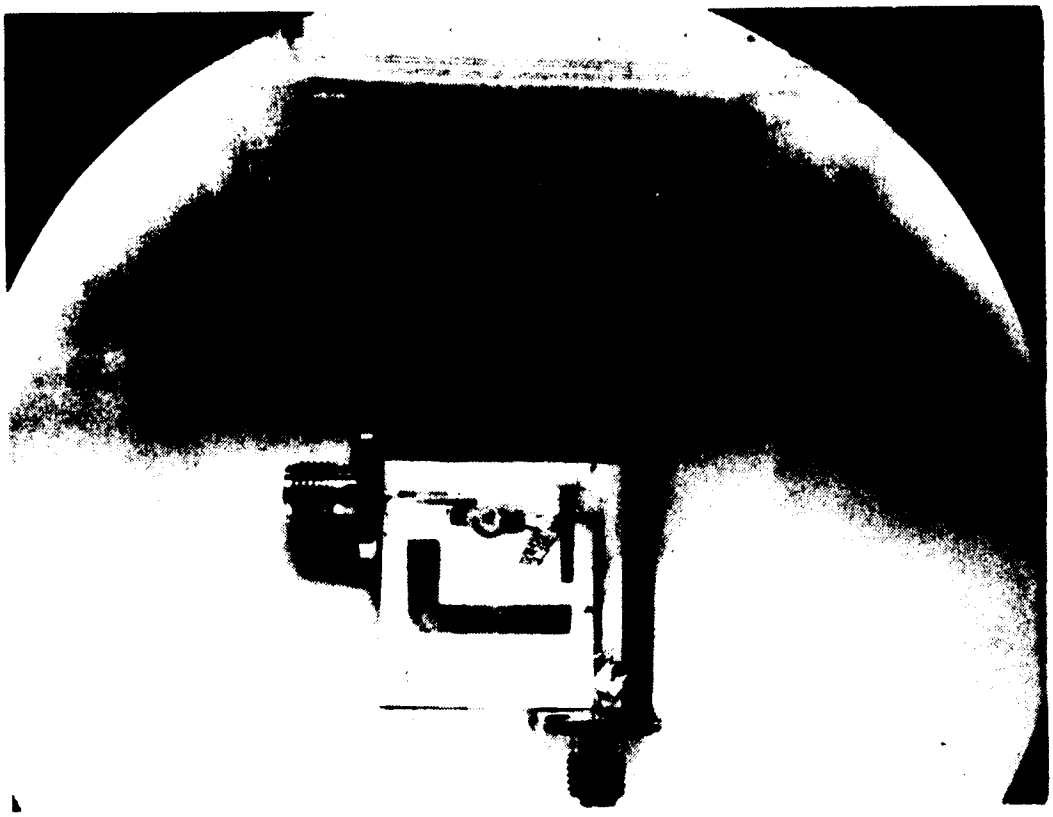

Figure 4.39 Photograph of MIS paramp.

CHAPTER 5

CONCLUSIONS

The purpose of this chapter is to summarize the contributions of this dissertation and to suggest unsolved problem areas for possible future investigation.

In this dissertation high quality MIS varactors have been designed, fabricated and tested. Small signal models valid at microwave frequencies have been developed suitable for high speed digital computation. The devices and models developed were used in two important microwave circuit applications:

(a) low power drain digital phase shifter

(b) low noise parametric amplifier.

The motivation for this work was the need for a low power drain switching device for computer-controlled microwave networks. The major application of such a device is in an electronically scanned phased array antenna. This dissertation shows that the MIS varactor can fulfill this need if minority carrier effects can be overcome. This work also shows that the unique capacitance versus voltage characteristic may be exploited in a low noise parametric amplifier application. MIS varactors are shown to have less gain variation due to pump power fluxuations than conventional varactors.

In Chapter 2 an efficient algorithm for the solution of the d.c. electrostatic potential throughout the semiconductor is given. This problem is solved as a mixed linear-nonlinear boundary value problem. The solution is valid for an arbitrary doping profile and specifically epitaxial profiles were studied extensively. An expression was derived

for the low frequency differential capacitance which requires only the storage of the interface potential. A comparison of experimental results and computer simulation showed good correlation. This is limited in that Boltzmann's statistics are assumed. This assumption excluded exact solusions for degenerate semiconductors. Since, in this work n/n^+ structures are always considered, the solution presented here could be considered approximate by purists. Further work should be done to take into account Fermi statistics simply. It should also be done since in accumulation and inversion majority and minority carrier densities, respectively, obey full Fermi statistics. For the purpose of modeling the MIS structure at microwave frequencies, Boltzmann's statistics were quite adequate.

In Chapter 3 a small signal model suitable for digital computation is described. This model involves the small signal electrostatic potential (V_1) and quasi-potentials (V_{n1}, V_{p1}). Others[11,13] have used these variables to solve MIS small signal problems. Their solution is different from mine in that they first construct a distributed equivalent circuit from the basic equations. Then, the circuit is solved by cascading subsections of the network. Gokhale[27] has used the variables (V_1, V_{n1}, V_{p1}) to solve for the small signal response of bipolar transistors. His solution results in a nine-band matrix which is solved by a special Gauss elimination routine. In this work, the basic equations are manipulated into three coupled linear equations in three unknowns. It is shown here that these equations reduce to a seven-band matrix solution. This system of equations is solved directly using a Gauss elimination routine. Further investigations are required

in this solution to improve computed accuracy in the inversion and accumulation regions. Further work should be done to reduce the amount of computer memory required. It is felt that some type of iterative improvement of the solution using a relaxation technique could solve both problems.

In Chapter 4, 360° digital phase shifter was build at 3.5 GHz. It was found that if these devices are to become practical diode circuit losses must be reduced. Also, a major problem area is the presence and response of minority carriers to large signals and to switching pulses. It was shown that differential phase shift and switching speed were dependent upon microwave signal amplitude. In order to solve these problems, the fabrication of silicon devices on thinner epitaxial layers should be investigated. Layers 0.3 μm thick for $10^{16}cm^{-3}$ densities are suggested. A more forward looking approach to improvement of MIS performance, it is felt, is in the area of new materials. Gallium arsenide for a given density or resistivity has a much larger maximum depletion depth (X_{dm}) than silicon. An approximate expression for X_{dm} is

$$X_{dm} = \alpha\rho^{\beta}$$

where for silicon $\alpha = .44$ μm

$\beta = .465$

GaAs $\alpha = 1.3$ μm

$\beta = .477$

One way of eliminating power sensitivity of phase shift and switching speed is by making the device so that it pushes through the n^+ substrate. Another way of saying that is that maximum depletion depth should be greater than the epitaxial layer thickness (X_1).

$$X_{dm} > X_1$$

This can be achieved easier for GaAs than for Si since the α for GaAs is larger.

The problem with this solution is that very little is understood about insulator-GaAs interfaces. The problem then would be how to put down a high quality insulator on GaAs with a minimum number of surface states.

APPENDIX I

DERIVATION OF FINITE DIFFERENCE APPROXIMATIONS FOR A NONUNIFORM GRID

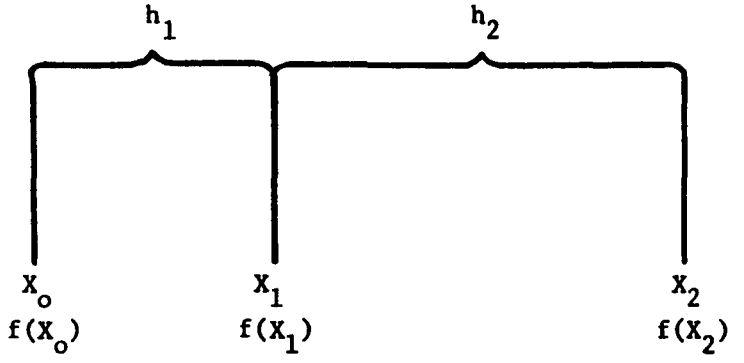

Let us approximate the function f(X) over the interval (X_o, X_1, X_2) by a second order polynomial.*

$$f(X) \simeq f(X_o) + f[X_o,X_1](X-X_o) + f[X_o,X_1,X_2](X-X_o)(X-X_1) \qquad (I\text{-}1)$$

where $f(X_o)$, $f(X_1)$ and $f(X_2)$ are the values of the function in the interval of interest. Also, $f[X_o,X_1]$ and $f[X_o,X_1]$ are the first and second divided differences defined as follows:

$$f[X_o,X_1] = \frac{f(X_o) - f(X_1)}{X_o - X_1} \qquad (I\text{-}2)$$

$$f[X_1,X_2] = \frac{f(X_1) - f(X_2)}{X_1 - X_2} \qquad (I\text{-}3)$$

$$f[X_o,X_1,X_2] = \frac{f[X_o,X_1] - f[X_1,X_2]}{X_o - X_2} \qquad (I\text{-}4)$$

Equation (I-1) may be rewritten by expanding terms into the form

$$f(X) \simeq f(X_o) + f[X_o,X_1](X-X_o) + f[X_o,X_1,X_2]\left(X^2-(X_o+X_1)\ X+X_oX_1\right) \qquad (I\text{-}5)$$

*S. D. Conte and C. DeBoor, "Elementary Numerical Analysis," Second Edition, McGraw Hill, 1972, pp. 195.

Taking the first derivative and second derivative of (I-5)

$$f'(X) \cong f[X_o,X_1] + f[X_o,X_1,X_2](2X - (X_o+X_1)) \tag{I-6}$$

$$f''(X) \cong 2f[X_o,X_1,X_2] \tag{I-7}$$

At point $X=X_1$ both (I-6) and (I-7) may now be evaluated

$$f'(X_1) \cong f[X_o,X_1] + f[X_o,X_1,X_2]\ (X_1-X_o) \tag{I-8}$$

$$f''(X_1) \cong 2f[X_o,X_1,X_2] \tag{I-9}$$

Now, $f'(X_1)$ and $f''(X_1)$ may be expanded in terms of the definitions of divided differences.

$$f''(X_1) = 2\,\frac{\dfrac{f(X_o - f(X_1)}{(X_o-X_1)} - \dfrac{f(X_1) - f(X_2)}{(X_1-X_2)}}{X_o - X_2} \tag{I-10}$$

$$f''(X_1) = \frac{2}{-(h_1+h_2)} \left\{\frac{f(X_o)-f(X_1)}{-h_1} - \frac{f(X_1)-f(X_2)}{-h_2}\right\} \tag{I-11}$$

$$f''(X_1) = \frac{2}{h_1+h_2} \left\{\frac{f(X_o)-f(X_1)}{h_1} - \frac{f(X_1)-f(X_2)}{h_2}\right\} \tag{I-12}$$

$$f''(X_1) = \frac{2}{h_1+h_2} \left\{\frac{f(X_o)}{h_1} - \left(\frac{1}{h_1} + \frac{1}{h_2}\right) f(X_1) + \frac{f(X_2)}{h_2}\right\} \tag{I-13}$$

$$f''(X_1) = \frac{2}{h_1+h_2} \left\{\frac{f(X_o)}{h_1} - \left(\frac{h_1+h_2}{h_1h_2}\right) f(X_1) + \frac{f(X_2)}{h_2}\right\} \tag{I-14}$$

$$f^{11}(X_1) = \frac{2}{(h_1+h_2)h_1} f(X_o) - \frac{2}{h_1h_2} f(X_1) + \frac{2}{(h_1+h_2)h_2} f(X_2) \qquad \text{(I-15)}$$

$$f^{11}(X_1) = \frac{2\ f(X_o)}{h_1^2\ (1+h_2/h_1)} - \frac{2f(X_1)}{h_1h_2} + \frac{2}{h_1h_2(1+h_2/h_1)} f(X_2) \qquad \text{(I-16)}$$

or

$$f^{11}(X_1) = \frac{2f(X_o)}{h_1^2\ (1+h_2/h_1)} - \frac{2f(X_1)}{h_1^2\ h_2/h_1} + \frac{2f(X_2)}{h_1^2\ \ h_2/h_1\ (1+h_2/h_1)} \qquad \text{(I-17)}$$

If we let $H2 = h_1^2 = (XH2)^2$ and $h_2/h_1 = RS = XH3/XH2$

$$X_o \longrightarrow M,\quad X_1 \longrightarrow K,\ X_2 \longrightarrow P1,\ \text{and}\ f \longrightarrow \bar{\gamma}$$

then

$$f''(K) = \frac{2f(M)}{H2(1+RS)} - \frac{2f(K)}{H2RS} + \frac{2f(P1)}{H2RS(1+RS)} \qquad \text{(I-18)}$$

Similarly, starting with equation (I-8) and expanding the divided differences

$$f^1(X_1) = \frac{f(X_o)-f(X_1)}{X_o-X_1} + \frac{\dfrac{f(X_o)-f(X_1)}{X_o-X_1} - \dfrac{f(X_1)-f(X_2)}{X_1-X_2}}{X_o - X_2} (X_1-X_o) \qquad \text{(I-19)}$$

$$f^1(X_1) = \frac{f(X_o-f(X_1)}{-h_1} + \frac{\dfrac{f(X_o)-f(X_1)}{-h_1} - \dfrac{f(X_1)-f(X_2)}{-h_2}}{-(h_1+h_2)} h_1 \qquad \text{(I-20)}$$

$$f^1(X_1) = \frac{f(X_1)-f(X_o)}{h_1} + \frac{\dfrac{f(X_1)-f(X_o)}{h_1} - \dfrac{f(X_2)-f(X_1)}{h_2}}{-(h_1+h_2)}\, h_1 \qquad \text{(I-21)}$$

$$f^1(X_1) = \frac{f(X_1)-f(X_o)}{h_1} + \frac{\dfrac{f(X_2)-f(X_1)}{h_2} - \dfrac{f(X_1)-f(X_o)}{h_1}}{h_1+h_2}\, h_1 \qquad \text{(I-22)}$$

$$f^1(X_1) = \frac{f(X_1)-f(X_o)}{h_1} + \frac{h_1\{f(X_2)-f(X_1)}{h_2(h_1+h_2)} - \frac{f(X_1)-f(X_o)}{(h_1+h_2)} \qquad \text{(I-23)}$$

$$f^1(X_1) = \frac{f(X_1)}{h_1} - \frac{f(X_o)}{h_1} + \frac{f(X_2)}{\frac{h_2}{h_1}(h_1+h_2)} - \frac{f(X_1)}{\frac{h_2}{h_1}(h_1+h_2)} - \frac{f(X_1)}{h_1+h_2} + \frac{f(X_o)}{h_1+h_2} \qquad \text{(I-24)}$$

$$f^1(X_1) = \left(\frac{1}{h_1+h_2} - \frac{1}{h_1}\right) f(X_o) + \left(\frac{1}{h_1} - \frac{1}{\frac{h_2}{h_1}(h_1+h_2)} - \frac{1}{h_1+h_2}\right) f(X_1) \qquad \text{(I-25)}$$

$$+ \frac{f(X_2)}{\frac{h_2}{h_1}(h_1+h_2)}$$

But note that

$$\frac{1}{h_1+h_2} - \frac{1}{h_1} = \frac{h_1 - (h_1+h_2)}{(h_1+h_2)h_1} = \frac{-h_2}{(h_1+h_2)h_1} \quad \text{, and}$$

$$\frac{1}{h_1} - \frac{1}{\frac{h_2}{h_1}(h_1+h_2)} - \frac{1}{h_1+h_2} = \frac{\frac{h_2}{h_1}(h_1+h_2)-h_1-h_2}{h_1\,\frac{h_2}{h_1}\,(h_1+h_2)} = \frac{\frac{h_2^2}{h_1} - h_1}{h_2(h_1+h_2)}$$

and, therefore, (I-25) may be simplified to (I-26).

$$f'(X_1) = \frac{-h_2}{(h_1+h_2)h_1} f(X_o) + \frac{\left(\frac{h_2}{h_1}\right)^2 - h_1}{h_2(h_1+h_2)} f(X_1) + \frac{f(X_2)}{\frac{h_2}{h_1}(h_1+h_2)} \qquad \text{(I-26)}$$

$$f'(X_1) = \frac{f(X_2)}{h_1\left(\frac{h_2}{h_1}\right)\left(1+\frac{h_2}{h_1}\right)} + \frac{\left(\frac{h_2}{h_1}\right)^2 - 1}{\left(\frac{h_2}{h_1}\right)\left(1+\frac{h_2}{h_1}\right)} f(X_1) - \frac{h_2/h_1}{h_1(1+h_2/h_1)} f(X_o) \qquad \text{(I-27)}$$

Let, as before, $H2 = h_1^2 = (XH2)^2$

$$RS = \frac{h_2}{h_1} = \frac{XH3}{XH2}$$

$X_o \longrightarrow M$

$X_1 \longrightarrow K$

$X_2 \longrightarrow P1$

Then

$$f'(K) = \frac{f(P1)}{XH2RS(1+RS)} + \frac{(RS)^2-1}{XH2RS(1+RS)} f(K) - \frac{RS}{(1+RS)XH2} f(M) \qquad \text{(I-28)}$$

When $h_1 = h_2 = h$, the nonuniform grid formula corresponds to the well-known uniform grid formula.

$$f'(X_1) = \frac{f(X_2)}{2h} - \frac{f(X_o)}{2h} \qquad \text{(I-29)}$$

$$= \frac{f(X_2) - f(X_o)}{2h} \quad \checkmark \qquad \text{(I-30)}$$

Note equation (I-28) may be rewritten in the form

$$f'(K) = \frac{f(P1)}{XH3(1+RS)} + \frac{RS-1}{XH3} f(K) - \frac{RS}{(1+RS)XH2} f(M) \qquad (I-31)$$

Therefore, the derivative of electrostatic potential with respect to distance at point K is

$$\left.\frac{dV}{dX}\right]_K = \frac{V(P1)}{XH3(1+RS)} + \frac{(RS-1)}{XH3} V(K) - \frac{RS}{(1+RS)XH2} V(M)$$

$$E_o(K) = -\frac{dV}{dX} = EOK$$

and the electric field is

$$EOK = \frac{RS}{(1+RS)XH2} V(M) - \frac{(RS-1)}{XH3} V(K) - \frac{V(P1)}{XH3(1+RS)}$$

If

$$XRS = 1+RS$$

$$XRT = RS-1$$

then

$$EOK = \frac{RS}{(XRS)(XH2)} V(M) - \frac{XRT}{XH3} V(K) - \frac{V(P1)}{(XH3)(XRS)}$$

APPENDIX II

DIRECT INVERSION BY GAUSS ELIMINATION - A 7-BAND DIAGONAL MATRIX

We wish to solve the linear system of equations of the form:

$$\overline{A} \cdot \overline{X}_n = \overline{h}$$

where $\overline{A}$ is a 7-band matrix of the form:

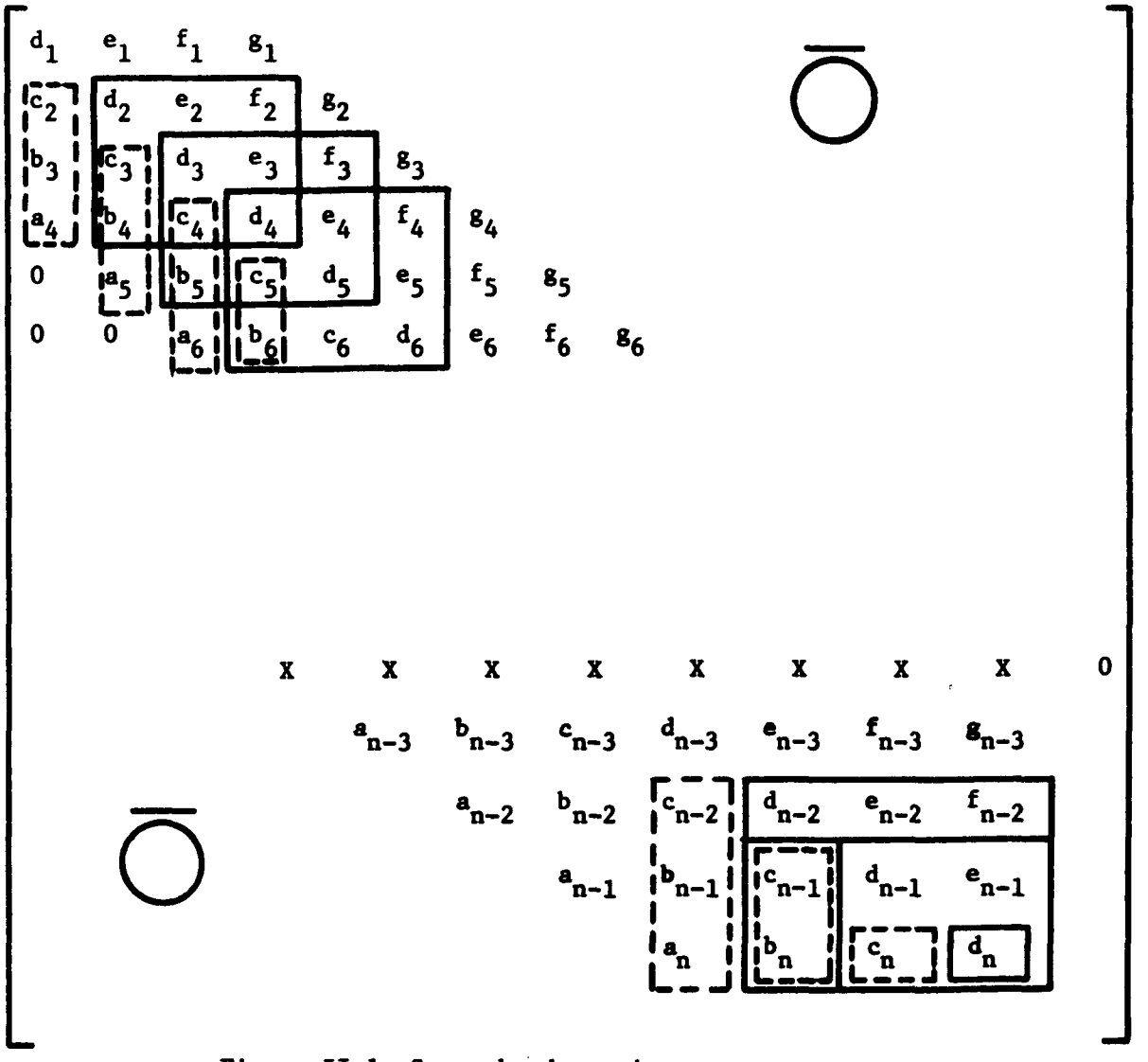

Figure II.1 Seven-band matrix.

The first step in a Gauss elimination routine is to convert the existing matrix into an upper triangularized matrix. This corresponds to eliminating the elements dotted in Figure II.1. It should be noted that because of the band nature of the matrix below the main diagonal three eliminations in each column are necessary except the last three columns which correspond to elements below d_{n-2} (two eliminations), d_{n-1} (one elimination), and d_n (no elimination).

The set of equations of interest may be written as:

$$d_1X_1+e_1X_2+f_1X_3+g_1X_4 = h_1 \qquad \text{(II-1)}$$

$$c_2X_1+d_2X_2+e_2X_3+f_2X_4+g_2X_5 = h_2 \qquad \text{(II-2)}$$

$$b_3X_1+c_3X_2+d_3X_3+e_3X_4+f_3X_5+g_3X_6 = h_3 \qquad \text{(II-3)}$$

$$a_4X_1+b_4X_2+c_4X_3+d_4X_4+e_4X_5+f_4X_6+g_4X_7 = h_4 \qquad \text{(II-4)}$$

$$0 \quad a_5X_2+b_5X_3+c_5X_4+d_5X_5+e_5X_6+f_5X_7+g_5X_8 = h_5 \qquad \text{(II-5)}$$

$$\vdots \qquad \vdots \qquad \vdots \qquad \vdots \qquad \vdots \qquad \vdots$$

$$a_{n-3}X_{n-6}+b_{n-3}X_{n-5}+c_{n-3}X_{n-4}+d_{n-3}X_{n-3}+e_{n-3}X_{n-2}+f_{n-3}X_{n-1}+g_{n-3}X_n = h_{n-3}$$

$$a_{n-2}X_{n-5}+b_{n-2}X_{n-4}+c_{n-2}X_{n-3}+d_{n-2}X_{n-2}+e_{n-2}X_{n-1}+f_{n-2}X_n = h_{n-2}$$

$$a_{n-1}X_{n-4}+b_{n-1}X_{n-3}+c_{n-1}X_{n-2}+d_{n-1}X_{n-1}+e_{n-1}X_n = h_{n-1}$$

$$a_nX_{n-3}+b_nX_{n-2}+c_nX_{n-1}+d_nX_n = h_n \qquad \text{(II-n)}$$

Let

$$R1 = \frac{c_2}{d_1} \qquad R2 = \frac{b_3}{d_1} \qquad R3 = \frac{a_4}{d_1}$$

Multiplying Eq. (II-1) by R1

$$c_2X_1 + R1*e_1X_2 + R1*f_1X_3 + R1*g_1X_4 = R1*h_1 \qquad \text{(II-2')}$$

Subtracting Eq. (II-2') from (II-2), an equation (II-2") results, and the coefficients of (II-2") may be considered to replace the coefficients of (II-2).

$$\underbrace{(d_2-R1*e_1)}_{d_2}X_2 + \underbrace{(e_2-R1*f_1)}_{e_2}X3 + \underbrace{(f_2-R_1*g_1)}_{f_2}X4 + g_2X_5 = \underbrace{h_2-R1*h_1}_{h_2} \qquad \text{(II-2")}$$

Multiplying Eq. (II-1) by R2 we get (II-3').

$$b_3X_1 + R2*e_1X_2 + R2*f_1X_3 + R2*g_1X_4 = R2*h_1 \qquad \text{(II-3')}$$

Subtracting Eq. (II-3') from (II-3), Eq. (II-3") results.

$$\underbrace{(c_3-R2*e_1)}_{c_3}X_2 + \underbrace{(d_3-R2*f_1)}_{d_3}X_3 + \underbrace{(e_3-R2*g_1)}_{e_3}X_4 + f_3X_5+g_cX_6 = \underbrace{(h_3-R2*h_1)}_{h_3} \qquad \text{(II-3")}$$

Similarly, multiplying Eq. (II-1) by R3 we get Eq. (II-4').

$$a_4X_1 + R3*e_1X_2 + R3*f_1X_3 + R3*g_1X_4 = R3*h_1 \qquad \text{(II-4')}$$

Subtracting Eq. (II-4') from (II-4), Eq. (II-4") results.

$$\underbrace{(b_4-R3*e_1)}_{b_4}X_2 + \underbrace{(c_4-R3*f_1)}_{c_4}X_3 + \underbrace{(d_4-R3*g_1)}_{d_4}X_4$$

$$+ e_4X_5+f_4X_6+g_4X_7 = \underbrace{(h_4-R3*h_1)}_{h_4} \qquad \text{(II-4")}$$

That completes the first column of eliminations.

For Eq. (II-1) the above procedure may be generalized to

$$\text{If } d_i = 0$$

$$R1 = \frac{c_{i+1}}{d_i}$$

$$R2 = \frac{b_{i+2}}{d_i}$$

$$R3 = \frac{a_{i+3}}{d_i}$$

Then calculate

$$d_{i+1} = d_{i+1} - R1*e_i$$

$$e_{i+1} = e_{i+1} - R1*f_i$$

$$f_{i+1} = f_{i+1} - R1*g_i$$

$$h_{i+1} = h_{i+1} - R1*h_i$$

Then calculate

$$c_{i+2} = c_{i+2} - R2*e_i$$

$$d_{i+2} = d_{i+2} - R2*f_i$$

$$e_{i+2} = e_{i+2} - R2*g_i$$

$$h_{i+2} = h_{i+2} - R2*h_i$$

Then calculate

$$b_{i+3} = b_{i+3} - R3*e_i$$

$$c_{i+3} = c_{i+3} - R3*f_i$$

$$d_{i+3} = d_{i+3} - R3*g_i$$

$$h_{i+3} = h_{i+3} - R3*h_i$$

At this point it should be noted that when eliminating the first column (c_2, b_3, a_4) then a 3x3 block is changed or affected.

$$\begin{bmatrix} d_2 & e_2 & f_2 \\ c_3 & d_3 & e_3 \\ b_4 & c_4 & d_4 \end{bmatrix}$$

This procedure may be continued until i=n-3, which corresponds to the last 3x3 block available.

After the i=n-3 elimination procedure, the following situation should exist:

$$\begin{bmatrix} & \cdot & \cdot & \cdot & \cdot & \cdot \\ & \cdot & \cdot & \cdot & \cdot & \cdot \\ & \cdot & \cdot & \cdot & \cdot & \cdot \\ \cdots & 0 & d_{n-3} & e_{n-3} & f_{n-3} & g_{n-3} \\ \cdots & 0 & 0 & d_{n-2} & e_{n-2} & f_{n-2} \\ \cdots & 0 & 0 & c_{n-1} & d_{n-1} & e_{n-1} \\ \cdots & 0 & 0 & b_n & c_n & d_n \end{bmatrix} \begin{bmatrix} \cdot \\ \cdot \\ \cdot \\ X_{n-3} \\ X_{n-2} \\ X_{n-1} \\ X_n \end{bmatrix} = \begin{bmatrix} \cdot \\ \cdot \\ \cdot \\ h_{n-3} \\ h_{n-2} \\ h_{n-1} \\ h_n \end{bmatrix}$$

The algorithm continues by letting

$$i = n-2$$

$$R1 = \frac{c_{i+1}}{d_i} \qquad R2 = \frac{b_{i+2}}{d_i}$$

$$d_{i+1} = d_{i+1} - R1*e_i$$

$$e_{i+1} = e_{i+1} - R1*f_i$$

$$h_{i+1} = h_{i+1} - R1*h_i$$

$$c_{i+2} = c_{i+2} - R2*e_i$$

$$d_{i+2} = d_{i+2} - R2*f_i$$

$$h_{i+2} = h_{i+2} - R2*h_i$$

Then let

$$i = n-1$$

$$R1 = \frac{c_{i+1}}{d_i}$$

$$d_{i+1} = d_{i+1} - R1*e_i$$

$$h_{i+1} = h_{i+1} - R1*h_i$$

After the above procedure the original matrix is converted to one which has all zero's below the main diagonal.

$$\begin{bmatrix} d_1 & e_1 & f_1 & g_1 & & & & & & & \\ 0 & d_2 & e_2 & f_2 & g_2 & & & & & & \\ 0 & 0 & d_3 & e_3 & f_3 & g_3 & & & & & \\ 0 & 0 & 0 & d_4 & e_4 & f_4 & g_4 & & & & \\ & & & & & & & & & & \\ & & & & & & & & & & \\ & & & & & & & d_{n-3} & c_{n-3} & f_{n-3} & g_{n-3} \\ & & & & & & & 0 & d_{n-2} & e_{n-2} & f_{n-2} \\ & & & & & & & 0 & 0 & d_{n-1} & e_{n-1} \\ & & & & & & & 0 & 0 & 0 & d_n \end{bmatrix} \begin{bmatrix} X_1 \\ X_2 \\ X_3 \\ X_4 \\ \\ \\ X_{n-3} \\ X_{n-2} \\ X_{n-1} \\ X_n \end{bmatrix} = \begin{bmatrix} h_1 \\ h_2 \\ h_3 \\ h_4 \\ \\ \\ h_{n-3} \\ h_{n-2} \\ h_{n-1} \\ h_n \end{bmatrix}$$

Back substituting

$$X_n = \frac{h_n}{d_n}$$

$$X_{n-1} = \frac{h_{n-1} - e_{n-1} X_n}{d_{n-1}}$$

$$X_{n-2} = \frac{h_{n-2} - f_{n-2} X_n - e_{n-2} X_{n-1}}{d_{n-2}}$$

Then for

$$i = 3, n-1$$

let

$$K = n-i$$

$$X_k = \frac{h_k - g_k * X_{k+3} - f_k * X_{k+2} - e_k * X_{k+1}}{d_k}$$

for instance, for i = n-1, k=1 and

$$X_1 = \frac{h_1 - g_1 * X_4 - f_1 * X_3 - e_1 * X_2}{d_1}$$

7-DIAGONAL BAND MATRIX ALGORITHM SUMMARY

DO 16 I=1, N-3

1 IF $D_1(I) = 0$ continue

2 $R_1 = C_1(I+1)/D_1(I)$

3 $R_2 = B_1(I+2)/D_1(I)$

4 $R_3 = A_1(I+3)/D_1(I)$

5 $D_1(I+1) = D_1(I+1) - R_1*E_1(I)$

6 $E(I+1) = E(I+1) - R_1*F(I)$

7 $F(I+1) = F(I+1) - R_1*G(I)$

8 $H(I+1) = H(I+1) - R_1*H(I)$

9 $C(I+2) = C(I+2) - R_2*E(I)$

10 $D(I+2) = D(I+2) - R_2*F(I)$

11 $E(I+2) = E(I+2) - R_2*G(I)$

12 $H(I+2) = H(I+2) - R_2*H(I)$

13 $B(I+3) = B(I+3) - R_3*E(I)$

14 $C(I+3) = C(I+3) - R_3*F(I)$

15 $D(I+3) = D(I+3) - R_3*G(I)$

16 $H(I+3) = H(I+3) - R_3*H(I)$

17 I = N-2

18 $R_1 = C(I+1)/D(I)$

19 $R_2 = B(I+2)/D(I)$

20 $D(I+1) = D(I+1) - R_1*E(I)$

21 $E(I+1) = E(I+1) - R_1*F(I)$

22 $H(I+1) = H(I+1) - R_1*H(I)$

23 $C(I+2) = C(I+2) - R_2*E(I)$

24 $D(I+2) = D(I+2) - R_2*F(I)$

25 $H(I+2) = H(I+2) - R_2*H(I)$

```
26                  I = N-1
27                  R1 = C(I+1)/D(I)
28                  D(I+1) = D(I+1) - R1*E(I)
29                  H(I+1) = H(I+1) - R1*H(I)
```

Now we solve for X(N) by back substitution

```
29                  X(N) = H(N)/D(N)
30                  X(N-1) = (H(N-1)-E(N-1)*H(N))/D(N-1)
31                  X(N-2) = (H(N-2)-F(N-2)*X(N)-E(N-2)*X(N-1))/D(N-2)
32                  DO ---- I = 3, N-1
33                  K = N-I
34                  X(K) = (H(K)-G(K)*X(K+3)-F(K)*X(K+2)-E(K)*X(K+1))/D(K)

RETURN
END
```

APPENDIX III

HIGH FREQUENCY SIMPLIFICATION FOR ONE TYPE CARRIER[11]

The valid linearized equations assuming no surface states and no doped deep level impurities are:

$$\nabla\cdot\bar{J}_p + \frac{qP_o}{V_T}(\dot{V}_p - \dot{V}_i) = 0 \qquad \text{(III-1)}$$

$$\nabla\cdot\bar{J}_n + \frac{qN_o}{V_T}(\dot{V}_n - \dot{V}_i) = 0 \qquad \text{(III-2)}$$

$$\bar{J}_p = -q\mu_p P_o \nabla V_p \qquad \text{(III-3)}$$

$$\bar{J}_n = -q\mu_n N_o \nabla V_n \qquad \text{(III-4)}$$

$$\varepsilon_s \nabla^2 V_i = \frac{qP_o}{V_T}(V_i - V_p) + \frac{qN_o}{V_T}(V_i - V_n) \qquad \text{(III-5)}$$

$$\bar{J}_T = \bar{J}_p + \bar{J}_n - \varepsilon_s \nabla\dot{V}_i \qquad \text{(III-6)}$$

The above authors have also shown that for high frequencies minority carriers need not be considered and, therefore, for an n-type semiconductor

$$V_i = V_p \qquad \text{(III-7)}$$

$$\bar{J}_p = 0 \qquad \text{(III-8)}$$

Using Eq. (III-7) and (III-8) in (III-1 through III-6) and assuming sinusoidal steady state $d/dt \rightarrow j\omega$

$$\nabla\cdot\bar{J}_n + j\omega\frac{qN_o}{V_T}(\dot{V}_n - \dot{V}_i) = 0 \qquad \text{(III-9)}$$

$$\bar{J}_n = - q\mu_n N_o \nabla V_n \tag{III-10}$$

$$\varepsilon_s \nabla^2 V_i = \frac{qN_o}{V_T}(V_i - V_n) \tag{III-11}$$

Substituting Eq. (III-10) into (III-9)

$$-q\mu_n \nabla\cdot(N_o \nabla V_n) + j\omega \frac{qN_o}{V_T}(V_n - V_i) = 0 \tag{III-12}$$

$$\nabla\cdot(N_o V_n) + j\omega \frac{N_o}{\mu_n V_T}(V_i - V_n) = 0 \tag{III-13}$$

It may be shown that

$$N_o = n_i \exp V_o/V_T \tag{III-14}$$

$$\nabla\cdot(N_o \nabla V_n) = N_o \nabla^2 V_n + \nabla N_o \cdot \nabla V_n \tag{III-15}$$

$$\nabla N_o = n_i \exp \frac{V_o}{V_T}\left(\frac{1}{V_T}\right) \nabla V_o \tag{III-16}$$

$$\nabla N_o = \frac{N_o \nabla V_o}{V_T} \tag{III-17}$$

Substituting Eq. (III-17 and 15) into (III-13)

$$N_o \nabla^2 V_n + \frac{N_o \nabla V_o}{V_T} \cdot \nabla V_n + \frac{j\omega N_o}{V_T \mu_n}(V_i - V_n) = 0 \tag{III-18}$$

$$\nabla^2 V_n + \frac{\nabla V_o}{V_T} \cdot \nabla V_n + j\frac{\omega}{V_T \mu_n}(V_i - V_n) = 0 \tag{III-19}$$

Equations (III-11) and (III-19) may be written in one dimension.

$$\frac{d^2 V_i}{dX^2} - \frac{qN_o}{\varepsilon_s V_T}(V_i - V_n) = 0 \tag{III-20}$$

$$\frac{d^2V_n}{dX^2} + \frac{1}{V_T}\frac{dV_o}{dX}\frac{dV_n}{dX} + j\frac{\omega}{V_T\mu_n}(V_i - V_n) = 0 \qquad \text{(III-21)}$$

The boundary conditions are:

at $X = X_o$ (Insulator-Semiconductor Interface)

$$D_s - D_I = 0 \qquad \text{(III-22)}$$

$$J_n = 0 \qquad \text{(III-23)}$$

But
$$D = \varepsilon E = -\varepsilon\frac{dV}{dX} \qquad \text{(III-24)}$$

$\therefore$ substituting Eq. (III-24) into (III-22)

$$\varepsilon_s\left(-\frac{dV_i}{dX}\right)_s - \varepsilon_I\left(-\frac{dV_i}{dX}\right)_I = 0 \qquad \text{(III-25)}$$

$\therefore$

$$\varepsilon_s\left.\frac{dV_i}{dX}\right]_s - \varepsilon_I\left(\frac{dV}{dX}\right)_I = 0 \qquad \text{(III-26)}$$

Also using the definition of hole r.f. current [Eq. (III-10)] in (III-23)

$$\frac{d}{dX}V_n = 0 \qquad \text{(III-27)}$$

At the ohmic contact:

$$V_i = V_n = 0 \qquad \text{(III-28)}$$

Equations (III-20, 21, 26, 27, 28) may be solved by replacing derivatives by finite difference approximations. Starting at the interface between the insulator and semiconductor Eq. (III-26) is reduced to

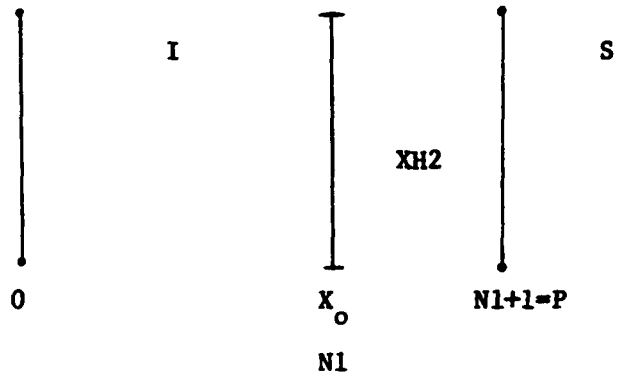

an algebraic equation.

$$\left.\frac{dV_i}{dX}\right]_s = \frac{V_i(P) - V_i(N1)}{XH2} \qquad \text{(III-29)}$$

$$\left.\frac{dV_i}{dX}\right]_I = \frac{V_i(N1) - V1L}{X_o} \qquad \text{(III-30)}$$

$$\varepsilon_s \left\{\frac{V_i(P) - V_i(N1)}{XH2}\right\} - \varepsilon_I \left\{\frac{V_i(N1) - V1L}{X_o}\right\} = 0 \qquad \text{(III-31)}$$

or

$$\frac{DKS}{DKI}\ \frac{X_o}{XH2}\ \left\{V_i(P) - V_i(N1)\right\} - \left\{V_i(N1) - V1L\right\} = 0 \qquad \text{(III-32)}$$

$$-\left\{1 + \frac{DKS}{DKI}\ \frac{X_o}{XH2}\right\} V_i(N1) + \frac{DKS}{DKI}\ \frac{X_o}{XH2}\ V_i(P) = -V1L \qquad \text{(III-33)}$$

Multiplying by (-1)

$$\left\{1 + \frac{DKS}{DKI}\ \frac{X_o}{XH2}\right\} V_i(N1) - \frac{DKS}{DKI}\ \frac{X_o}{XH2}\ V_i(P) = V1L \qquad \text{(III-34)}$$

Expanding Eq. (III-27)

$$V_n(P) - V_n(N1) = 0 \qquad \text{(III-35)}$$

or

$$V_n(N1) - V_n(P) = 0 \qquad \text{(III-36)}$$

Next, since point P is the first point within the semiconductor, Eq. (III-20) and (III-21) are the valid expressions to expand.

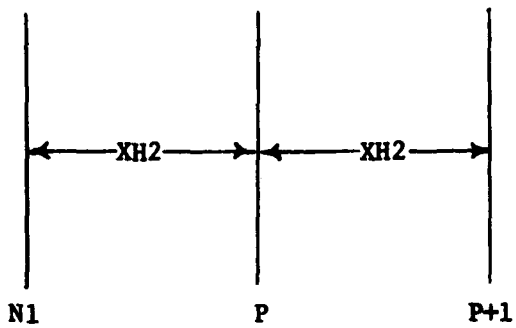

$$\frac{V_i(N1)-2V_i(P)+V_i(P+1)}{(XH2)^2} - \frac{qN_o(P)}{\varepsilon_s V_T} V_i(P) + \frac{qN_o(P)}{\varepsilon_s V_T} V_n(P) = 0 \qquad \text{(III-37)}$$

Multiplying through by $H2=(XH2)^2$

$$V_i(N1)-2V_i(P)+V_i(P+1) - \frac{qH2}{\varepsilon_s V_T} N_o(P)V_i(P) + \frac{qH2N_o(P)}{\varepsilon_s V_T} V_n(P) = 0 \qquad \text{(III-38)}$$

Collecting terms

$$V_i(N1) - \left\{ 2 + \frac{qH2}{\varepsilon_s V_T} N_o(P) \right\} V_i(P) + \frac{qH2}{\varepsilon_s V_T} N_o(P)V_n(P)$$

$$+ V_i(P+1) = 0 \qquad \text{(III-39)}$$

Similarly, expanding Eq. (III-21)

$$\frac{V_n(N1)-2V_n(P)+V_n(P+1)}{H2}+\left(\frac{1}{V_T}\ \frac{dV_o}{dX}\right)\left(\frac{V_n(P+1)-V_n(N1)}{2XH2}\right)+\frac{j\omega}{V_T\mu_n}V_i(P)$$

$$-j\frac{\omega}{V_T\mu_n}V_n(P)=0 \qquad \text{(III-40)}$$

Multiplying through by H2

$$V_n(N1)-2V_n(P)+V_n(P+1)+\left(\frac{XH2}{2V_T}\ \frac{dV_o}{dX}\right)\left(V_n(P+1)-V_n(N1)\right)+j\frac{\omega H2}{V_T\mu_n}V_i(P)$$

$$-j\frac{\omega H2}{V_T\mu_n}V_n(P)=0 \qquad \text{(III-41)}$$

Collecting terms

$$\left(1-\frac{XH2}{2V_T}\ \frac{dV_o}{dX}\right)V_n(N1)+j\frac{\omega H2}{V_T\mu_n}V_i(P)-\left(2+\frac{j\omega H2}{V_T\mu_n}\right)V_n(P)$$

$$+\left(1+\frac{XH2}{2V_T}\ \frac{dV_o}{dX}\right)V_n(P+1)=0 \qquad \text{(III-42)}$$

At Point K we have a nonuniform grid and therefore

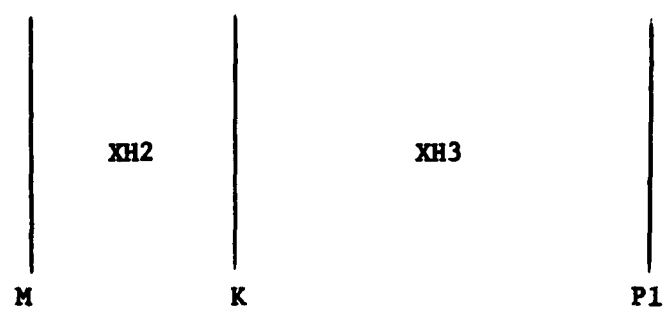

nonuniform grid formulas must be used (Appendix I).

$$\left[\frac{dY}{dX}\right]_K = \frac{Y(P1)}{XH3(1+RS)} + \frac{(RS-1)}{XH3}\,Y(K) - \frac{RS}{(1+RS)XH2}\,Y(M) \qquad \text{(III-43)}$$

$$\left[\frac{d^2Y}{dX^2}\right]_K = \frac{2Y(M)}{H2(1+RS)} - \frac{2Y(K)}{(H2)RS} + \frac{2Y(P1)}{(H2)RS(1+RS)} \qquad \text{(III-44)}$$

where

$$RS = \frac{XH3}{XH2} \qquad \text{(III-45)}$$

$$H2 = (XH2)^2 \qquad \text{(III-46)}$$

Substituting the expression (III-44) into (III-20)

$$\frac{2V_i(M)}{(1+RS)} - \frac{2V_i(K)}{RS} + \frac{2V_i(P)}{RS(1+RS)} - \frac{qH2N_o(K)}{\epsilon_s V_t}\,V_i(K) + \frac{qN_o(K)H2}{\epsilon_s V_T}\,V_n(K) = 0 \qquad \text{(III-47)}$$

Multiplying by H2 and collecting terms

$$\frac{2}{(1+RS)}\,V_i(M) - \left\{\frac{2}{RS} + \frac{qH2N_o(K)}{\epsilon_s V_T}\right\}V_i(K) + \frac{qH2N_o(K)}{\epsilon_s V_T}\,V_n(K) + \frac{2}{RS(1+RS)}\,V_i(P1) = 0 \qquad \text{(III-48)}$$

Substituting Eq. (III-43) and (III-44) into (III-21)

$$\frac{2V_n(M)}{(1+RS)} - \frac{2V_n(K)}{(RS)} + \frac{2V_n(P1)}{RS(1+RS)} + \frac{XH2}{V_T}\left[\frac{dV_o}{dX}\right]_K \left\{\frac{V_n(P1)}{RS(1+RS)} + \frac{RS-1}{RS}\,V_n(K) - \frac{RS}{(1+RS)}\,V_n(M)\right\} + j\,\frac{\omega H2V_i(K)}{V_T\mu_n} - j\,\frac{\omega H2V_n(K)}{V_T\mu_n} = 0 \qquad \text{(III-49)}$$

Collecting terms

$$\left\{\frac{2}{(1+RS)} - \frac{XH2}{V_T}\left.\frac{dV_o}{dX}\right]_K \frac{RS}{1+RS}\right\} V_n(M) + j\frac{\omega H2}{V_T \mu_n} V_i(K)$$

$$- \left\{\frac{2}{RS} + \frac{XH2}{V_T}\left.\frac{dV_o}{dX}\right]_K \frac{RS-1}{RS} + j\frac{\omega H2}{V_T \mu_n}\right\} V_n(K)$$

$$+ \left\{\frac{2}{RS(1+RS)} + \frac{XH2}{V_T}\left.\frac{dV_o}{dX}\right]_K \frac{1}{RS(1+RS)}\right\} V_n(p1) = 0 \qquad \text{(III-50)}$$

After point K, P1 → L1, M1 replace XH2 by XH3 and the form of the coefficients should be the same.

```
LOAD THE A1 DIAGONAL

      J = 3
      DO 22  I = P,M
      A1(J) = (0., 0.)
      A1(J+1) = (0.,0.)
      J = J+2
    2 2 CONTINUE
      A1(J) = (0., 0.)
      A1(J+1) = (0., 0.)
      J = J+2
      DO 23  I + P1,M1
      A1(J) = (0., 0.)
      A1(J+1) = (0., 0.)
      J = J+2
   23  CONTINUE
```

LOAD THE B1 DIAGONAL

J = 3

DO 24 I = P,M

B1(J) = (1., 0.)

$$B1(J=1) = 1 - \frac{XH2}{2V_T}\left[\frac{dV_o}{dX}\right]_I = 1 - \underbrace{\left(\frac{V_o(I+1) - V_o(I-1)}{4V_T}\right)}_{RV}$$

J = J+2

24 CONTINUE

$$B1(J) = \frac{2}{1+RS} = (2./XRS, 0)$$

$$B1(J+1) = \frac{2}{1+RS} - \frac{XH2}{V_T}\left[\frac{dV_o}{dX}\right]_K \frac{RS}{1+RS} = \left(\frac{2}{1+RS} + \frac{XH2}{V_T}\,EOK\,\frac{RS}{1+RS}\,,\ 0.\right)$$

J = J+2

DO 26 I + P1, M1

B1(J) = (1., 0.)

$$B1(J+1) = 1. - \frac{XH3}{2V_T}\left[\frac{dV_o}{dX}\right]_I = 1 - \underbrace{\left(\frac{V_o(I+1)-V_o(I-1)}{4V_T}\right)}_{RV}$$

J = J+2

26 CONTINUE

$$\left[\frac{dV_o}{dX}\right]_I = \frac{V_o(I+1)-V_o(I-1)}{2\Delta X}$$

where

$$\Delta X \rightarrow \begin{Bmatrix} XH2 \\ XH3 \end{Bmatrix}$$, depending upon if we are in region 2 or 3.

LOAD THE C1 DIAGONAL

C1(2) = 0

J = 3

DO 27 I = P,M

C1(J) = 1.

$C1(J+1) = +j \frac{\omega H2}{V_T \mu_n} \times 10^{-8} = +jXN2$

J = J+2

27 CONTINUE

C1(J) = 0

$C1(J+1) = j \frac{\omega H2}{V_T \mu_n} = + jXN2$

J = J+2

D) 28 I = P1,M1

C1(J) = 0

$C1(J+1) = j \frac{\omega H3}{V_T \mu_n} = + jXN3$

J = J+2

28 CONTINUE

$$XN2 = \frac{\omega H2}{V_T \mu_n} \times 10^{-8}$$

$$RS = \frac{XH3}{XH2} \; ; \quad H2 = (XH2)(XH2)$$

$$XN3 = RS * RS * XN2$$

Units

$$\frac{\omega H2}{V_T \mu_n} = \frac{(1/sec)(micron)^2}{(volt)(cm^2/volt \cdot sec)} = \left(\frac{micron}{cm}\right)^2 = \left(\frac{10^{-6}_m}{10^{-2}_m}\right)^2 - (10^{-4})^2 = 10^{-8}$$

LOAD THE D1 DIAGONAL

$$D1(1) = 1 + \frac{DKS}{DKI}\ \frac{X_o}{XH2}$$

$$D1(2) = 1.$$

$$J = 3$$

DO 29 I = P,M

$$D1(J) = -\left\{2. + \frac{qH2}{\varepsilon_s V_T} N_o(I)\right\} = -\left\{2. + \frac{1}{2}\, cs \exp \frac{V_o(I)}{V_T}\right\}$$

$$D1(J+1) = -\left\{2. + j\,\frac{\omega H2}{V_T \mu_n}\right\} = -\left\{2. + j\ XN2\right\}$$

$$J = J+2$$

29 CONTINUE

$$D1(J) = -\left\{\frac{2}{RS} + \frac{qH2 N_o(K)}{\varepsilon_s V_T}\right\} = -\left\{\frac{2}{RS} + \frac{1}{2}\, cs \exp\ \frac{V_o(K)}{V_T}\right\}$$

$$D1(J+1) = -\left\{\frac{2}{RS} + \frac{XH2}{V_T}\ EOK\ \frac{RS-1}{RS} + j\ \underbrace{\frac{\omega H2}{V_T \mu_n}}_{XN2}\right\}$$

$$J = J+2$$

DO 31 I = P1,M1

$$D1(J) = -\left\{2. + \frac{qH3}{\varepsilon_s V_T} N_o(I)\right\} = -\left\{2. + RS*RS*\frac{1}{2} cs \exp\ \frac{V_o(I)}{V_T}\right\}$$

$$D1(J+1) = -\left\{2. + j\,\frac{\omega H3}{V_T \mu_n}\right\} = -\left\{2. + jXN3\right\}$$

$$J = J+2$$

31 CONTINUE

$$N_o = N_i \exp \frac{V_o}{V_T}$$

$$EOK = -\left.\frac{dV_0}{dX}\right]_K$$

LOAD THE E1 DIAGONAL

E1(1) = 0

E1(2) = 0

J = 3

D) 32 I = P,M

$$E1(J) = \frac{qH2}{\varepsilon_s V_T} N_o(I) = \frac{1}{2} cs \exp \frac{V_o(I)}{V_T}$$

E1(J+1) = 0

J = J+2

32 CONTINUE

$$E1(J) = \frac{qH2}{\varepsilon_s V_T} N_o(K) = \frac{1}{2} cs \exp \frac{V_o(K)}{V_T}$$

E1(J+1) = 0

J = J+2

DO 33 I = P1,L1

$$E1(J) = \frac{qH3}{\varepsilon_s V_T} N_o(I) = RS * RS * \frac{1}{2} * cs * \exp \frac{V_o(I)}{V_T}$$

E1(J+1) = 0

J = J+2

33 CONTINUE

$$E1(J) = \frac{qH3}{\varepsilon_s V_T} N_o(M1) = RS * RS * \frac{1}{2} * cs \exp \frac{V_o(M1)}{V_T}$$

LOAD THE F1 COEFFICIENT

$$F1(1) = -\frac{DKS}{DKI}\ \frac{X_o}{XH2}$$

F1(2) =-1

J = 3

DO 34 I = P,M

F1(J) = 1

$$F1(J+1) = 1. + \frac{XH2}{2V_T}\left[\frac{dV_o}{dX}\right]_I = 1 + RV$$

34 CONTINUE

$$F(J) = \frac{2}{RS(1+RS)}$$

$$F(J+1) = \frac{2}{RS(1+RS)} - \frac{XH2}{V_T}\underbrace{\left[\frac{dV_o}{dX}\right]_K}_{EOK}\frac{1}{RS(1+RS)}$$

J = J+2

DO 36 I = P1,L1

F1(J) = 1

$$F1(J+1) = 1. + \frac{XH3}{2V_T}\left[\frac{dV_o}{dX}\right]_I = 1 + RV$$

36 CONTINUE

$$RF = \frac{V_o(I+1) - V_o(I-1)}{4V_T}$$

```
LOAD THE G1 DIAGONAL


G1(1) = 0

G1(2) = 0

J = 3

DO 37  I = P,M

G1(J) = 0

G1(J+1) = 0

J = J+2

37  CONTINUE

G1(J) = 0

G1(J+1) = 0

J = J+1

DO 38  I = P1,L1

G1(J) = 0

G1(J+1) = 0

J = J+2

38  CONTINUE
```

APPENDIX IV

MIS TWO-CARRIER PROGRAM

```
FORTRAN IV G LEVEL  21                MAIN              DATE = 74277          15/31/44

0001                  COMPLEX A1(1500),B1(1500),C1(1500),D1(1500)
0002                  COMPLEX E1(1500),F1(1500),G1(1500),V1(1500),H1(1500)
0003                  COMPLEX R1,R2,R3,R4,R5,XIMPED,V1X1(26),CMPLX,V1LN
0004                   DIMENSION A(500),B(500),C(500),D(500)
0005                   DIMENSION V(500),X(500),CC(500),DELTA(500),D2V(500)
0006                  DIMENSION VX1(26),VX2(26),VX3(26),VX4(26)
0007                 DIMENSION CAP(26),RES(26),VB(26),EX1(26),EX2(26)
0008                  INTEGER P1,P2,P3,P4,P5
0009                  COMMON A1,B1,C1,D1,E1,F1,G1,H1,A,B,C,D
                C  DATA REQUIRED IN FORMAT0 INTEGERS  I5,  ALL OTHERS  E10.2
                C  DATA LINE 1)N1,N2,N3,N4,N5
                C  DATA LINE 2)XL,X1,X2,X3,X4,XR      (MICRONS)
                C  DATA LINE 3)UPM,UNM(CM**2/VOLT/SEC),EGAP(EV),DOT(MILS)
                C  DATA LINE 4)CNE,CNS(1/CM**3),XXL,RX(MICRONS)
                C  DATA LINE 5)T(DEG K),DKI,DKS,COSS(COUL/M**2)
                C  DATA LINE 6)CNC,CNV(1/CM**3)
                C  DATA LINE 7)VIN,DV,NV
                C  DATA LINE 8)RREG,EN2,EP2(MOBILITY REDUCTION FACTORS)
                C      SEVERAL CASES MAY BE RUN ON ONE JOB BUT ALL IO DATA LINES
                C           MUST BE LISTED FOR EACH CASE
0010           700    CONTINUE
0011                  READ(5,901) N1,N2,N3,N4,N5
0012           901    FORMAT(5I5)
0013                  IF (N1-0) 701,701,703
0014           701    WRITE(6,909)
0015           909    FORMAT('1')
0016                  STOP
0017           703    CONTINUE
0018                  WRITE(6,910)
0019           910    FORMAT('1',' DATA FOR MIS 5-REGION 2-CARRIER FORTRAN PROGRAM')
0020                  WRITE(6,902)N1,N2,N3,N4,N5
0021           902    FORMAT('0','N1 =',I4,'  N2 =',I4,'  N3 =',I4,'  N4 =',I4,
                     1  '  N5 =',I4)
0022                  READ (5,9)4) XML,XM1,XM2,XM3,XM4,XMR
0023                  WRITE(6,904) XML,XM1,XM2
0024           903    FORMAT (6E10.2)
0025           904    FORMAT('0','XL  =',E10.2,'  X1  =',E10.2,'  X2  =',E10.2)
0026                   WRITE(6,937)XM3,XM4,XMR
0027           937     FORMAT('0','X3  =',E10.2,'  X4  =',E10.2,'  XR  =',E10.2)
0028                  X0=XML*1.E-6
0029                  X1=XM1*1.E-6
0030                  X2=XM2*1.E-6
0031                  X3=XM3*1.E-6
0032                  X4=XM4*1.E-6
0033                  X5=XMR*1.E-6
0034                  XL=X0
0035                  XR=X5
0036                  READ(5,980)UPM,UNM,EGAP,DOT
0037           980    FORMAT(4E10.2)
0038                  WRITE(6,982)UPM,UNM,EGAP,DOT
0039           982    FORMAT('0','MUP =',E10.2,'  MUN =',E10.2,'  EGAP=',E10.2,
                     1    '  DOT =',E10.2)
0040                  UN=UNM*1.E-4
0041                  UP=UPM*1.E-4
0042                  DIA=25.4*DOT*1.E-6
0043                  AREA =3.141594*DIA**2/4
```

```
FORTRAN IV G LEVEL  21                  MAIN                    DATE = 74277          15/31/44

0044                  XH1=(X1-X0)/N1
0045                  XH2=(X2-X1)/N2
0046                  XH3=(X3-X2)/N3
0047                  XH4=(X4-X3)/N4
0048                  XH5=(X5-X4)/N5
0049                  N=N1+N2+N3+N4+N5
0050                  K1=N1
0051                  K2=N1+N2
0052                  K3=N1+N2+N3
0053                  K4=N1+N2+N3+N4
0054                  K5=N1+N2+N3+N4+N5
0055                  P1=1
0056                  P2=K1+1
0057                  P3=K2+1
0058                  P4=K3+1
0059                  P5=K4+1
0060                  M1=K1-1
0061                  M2=K2-1
0062                  M3=K3-1
0063                  M4=K4-1
0064                  M5=K5-1
0065                  MM5=M5-1
0066                  MMM5=MM5-1
0067                  JC=3*(M5-N1)+1
0068                  DO 101 I=P1,K1
0069          101     X(I)=XL+I*XH1
0070                  DO 102 I=P2,K2
0071          102     X(I)=X1+(I-K1)*XH2
0072                  DO 103 I=P3,K3
0073          103     X(I)=X2+(I-K2)*XH3
0074                  DO 104 I=P4,K4
0075          104     X(I)=X3+(I-K3)*XH4
0076                  DO 105 I=P5,K5
0077          105     X(I)=X4+(I-K4)*XH5
0078                  READ (5,905)ONE,ONS,XMX1,RMX
0079          905     FORMAT(4F1 .2)
0080                 XX1=XMX1*1.E-6
0081                 RX=RMX*1.E-6
0082                  ONE=ONE*1.E6
0083                  ONS=ONS*1.E6
0084                  WRITE (6,906)ONE,ONS,XMX1,RMX
0085          906     FORMAT(1H0,'ONE =',F10.2,'  ONS =',F10.2,'  XX1 =',F10.2,
                     1            '  RX  =',F10.2)
0086                  AX=(ONS-ONE)/2.
0087                  CX=(ONS+ONE)/2.
0088                  DO 106 I=K1,K5
0089          106     CC(I)=AX*TANH((X(I)-XX1)/RX)+CX
0090                  READ(5,907)T,DKT,DKS,QSS
0091          907     FORMAT(4F10.2)
0092                  RK=8.625E-5
0093                  READ(5,941)CNC,CNV
0094          941     FORMAT(2F10.2)
0095                  QSS=QSS
0096                  VT=T*R.616E-05
0097                  CUI=SQRT(QC*CNV)*EXP(-EGAP/(2*RK*T))*1.E6
0098                  CCUI=CUI*1.E-6
```

```
FORTRAN IV G LEVEL  21                  MAIN                    DATE = 74277          15/31/44

0029                  YO= CC(K5)/2./CC1
0030                  VR=1.0*VI*ALOG(YO+SQRT(YO*YO+1))
0031                  WRITE(6,920)VI,VR,CC1
0032           920    FORMAT('0','VI  =',E10.2,'  VR  =',E10.2,'  CC1 =',E10.2)
0033                  H21=XH1*XH1
0034                  H2=XH2*XH2
0035                  H3=XH3*XH3
0036                  H4=XH4*XH4
0037                  H5=XH5*XH5
0038                  WRITE(6,915)T, CROSS,DKI,DKS
0039           915    FORMAT('0','T   =',E10.2,2X,'CROSS=',E10.2,
                     1            '  DKI =',E10.2,'  DKS =',E10.2)
0040                  EPO=8.845-12
0041                  EPI=DKI*EPO
0042                  EPS=DKS*EPO
0043                  Q=1.602E-19
0044                  GE=G/EPS
0045                  CO=(EPI*AREA)/(XI-XO)
0046                  READ(5,911)VIN,DV,NV
0047           911    FORMAT(2E1 .2,I5)
0048                  WRITE(6,912)VIN,DV,NV,CO
0049           912    FORMAT('0','VIN =',E10.2,'  DV  =',E10.2,'  NV  =',I5,
                     1    5X, '  CO  =',E10.2)
0050                  READ(5,913)ERPO,EN2,EP2
0051           913    FORMAT(3E10.2)
0052                  WRITE(6,914)ERPO,EN2,EP2
0053           914    FORMAT('0','ERPO=',E10.2,'  EN2 =',E10.2,'  EP2 =',E10.2)
               C
               C          CALCULATION OF POTENTIAL
               C
0054                  DO 221 IP=1,NV
0055                  VL=VIN+V2+DV*(IP-1)
               C
               C              INITIALIZATION
               C
0056                  VR(IP)=VL-VR
               C  ALTERNATE INITIALIZATION
               C       QQQ=1-2*(EPI**2)*VR(IP)/EPS/Q/DNE/(XI)**2)
               C       QQ=(DKS/DKI)**2*(-XO)**(-DNE)*(-1+SQRT(QQQ))
               C       VX1(IP)=VR(IP)+QQ**2)/EPI
               C       VX2(IP)=VX1(IP)+(QQ**2)/2/EPS/Q/DNE
               C       VX3(IP)=VR
               C       VX4(IP)=VR
               C   END OF ALTERNATE
0057                  VX1(1)=VR
0058                  VX2(1)=VR
0059                  VX3(1)=VR
0060                  VX4(1)=VR
0061                  VVX1=VX1(IP)
0062                  DO 220 I=P1,K1
0063           220    V(I)=VL+((VX1(IP)-VL)*((X(I)-XO)/(X1-XO)))
0064                  DO 221 I=P2,K2
0065           221    V(I)=VX1(IP)+((VX2(IP)-VX1(IP))*((X(I)-X1)/(X2-X1)))
0066                  DO 222 I=P3,K3
0067           222    V(I)=VX2(IP)+((VX3(IP)-VX2(IP))*((X(I)-X2)/(X3-X2)))
0068                  DO 223 I=P4,K4
```

```
FORTRAN IV G LEVEL  21                 MAIN                DATE = 74277          15/31/44

0139          223     V(I)=VX3(IP)+((VX4(IP)-VX3(IP))*((X(I)-X3)/(X4-X3)))
0140                  DO 224 I=P5,K5
0141          224     V(I)=VX4(IP)+((V9-VX4(IP))*((X(I)-X4)/(X5-X4)))
0142                  DO 2039 I=1,M5
0143          2039    DELTA(I)=0.
                C               ITERATION
0144                  J=1
0145          204     D2V(1)=(VL-2*V(1)+V(2))/H21
0146                  DO 205 I=2,M1
0147          205     D2V(I)=(V(I-1)-2.*V(I)+V(I+1))/H21
0148                   D2V(K1)=((V(P2)-V(K1))/XH2 -(V(K1)-V(M1))/XH1) /((XH1+XH2)/2)
0149                  DO 206 I=P2,M2
0150          206     D2V(I)=(V(I-1)-2.*V(I)+V(I+1))/H2
0151                 D2V(K2)=((V(P3)-V(K2))/XH3 -(V(K2)-V(M2))/XH2) /((XH2+XH3)/2)
0152                  DO 207 I=P3,M3
0153          207     D2V(I)=(V(I-1)-2.*V(I)+V(I+1))/H3
0154                 D2V(K3)=((V(P4)-V(K3))/XH4 -(V(K3)-V(M3))/XH3 )/((XH3+XH4)/2)
0155                  DO 208 I=P4,M4
0156          208     D2V(I)=(V(I-1)-2.*V(I)+V(I+1))/H4
0157                 D2V(K4)=((V(P5)-V(K4))/XH5 -(V(K4)-V(P4))/XH4 )/((XH4+XH5)/2)
0158                  DO 209 I=P5,M5
0159          209     D2V(I)=(V(I-1)-2.*V(I)+V(I+1))/H5
0160                  D2V(K5)=0
                C
                C     CALCULATE ELEMENTS OF TRIDIAGONAL MATRIX
                C
                C
0161                  DO 210 I=1,M1
0162                  A(I)=1.
0163                  B(I)=-2.
0164                  C(I)=1.
0165                  D(I)=-H21*D2V(I)
0166          210     CONTINUE
0167                  EK1=(DKS/DKI)*(XH1/XH2)
0168                  FK1=QSS*XH1/EPI
0169                  A(K1)=1.
0170                  B(K1)=-(1+EK1)
0171                  C(K1)=EK1
0172                  D(K1)=-(FK1+EK1*V(P2)+V(M1))+(1+EK1)*V(K1)
0173                  GG=2.*CNI*QE/VT
0174          941     FORMAT('0','V(',I4,')=',E13.2,4X,'X(I)=',F14.6)
0175                  DO 211 I=P2,M2
0176          2511    VIT=V(I)/VT
0177                  IF(ABS(VIT)-170.)251,252,252
0178          252     WRITE(6,941)I,VIT,X(I)
0179                  V(I)=V(I)-0.1*DELTA(I)
0180                  GO TO 2511
0181          251     CONTINUE
0182                  A(I)=1.
0183                  B(I)=-(2.+H2*GG*COSH(VIT))
0184                  C(I)=1.
0185                  D(I)=-H2*(D2V(I)+Q*CC(I)/EPS-2.*CNI*QE*SINH(VIT))
0186          211     CONTINUE
0187                  EK2=XH2/XH3
0188                  FK2=(XH2/2.)*(XH2+XH3)
0189          2512    VIT=V(K2)/VT
```

```
FORTRAN IV G LEVEL 21                MAIN                DATE = 74277          15/31/44

0195                  IF(ABS(VIT)-17.)253,254,254
0196           254    WRITE(6,941)I,VIT,X(I)
0197                  V(K2)=V(K2)-.1*DELTA(K2)
0198                  GO TO 2512
0199           253    CONTINUE
0200                  A(K2)=1.
0201                  B(K2)=-(1.+EK2+EK2*((2.)*CNI)/(EPS*VT))*COSH(V(K2)/VT)
0202                  C(K2)=EK2
0203                  D(K2)=-EK2*(D2V(K2)+Q*GG(K2)/EPS-2.*CNI*Q*SINH(VIT)/EPS)
0204                  DO 212 I=P4,M3
0205           2513   VIT=V(I)/VT
0206                  IF(ABS(VIT)-17.)255,256,256
0207           256    WRITE(6,941)I,VIT,X(I)
0208                  V(I)=V(I)-.1*DELTA(I)
0209                  GO TO 2513
0210           255    CONTINUE
0211                  A(I)=1.
0212                  B(I)=-(2.+H3*GG*COSH(VIT))
0213                  C(I)=1.
0214                  D(I)=-H3*(D2V(I)+Q*GG(I)/EPS-2.*CNI*QE*SINH(VIT))
0215           212    CONTINUE
0216                  EK3=XH3/XH4
0217                  EK3=(XH3/2.)*(XH3+XH4)
0218           2514   VIT=V(K3)/VT
0219                  IF(ABS(VIT)-17.)257,258,258
0220           258    WRITE(6,941)I,VIT,X(I)
0221                  V(K3)=V(K3)-.1*DELTA(K3)
0222                  GO TO 2514
0223           257    CONTINUE
0224                  A(K3)=1.
0225                  B(K3)=-(1.+EK3+EK3*((2.)*CNI)/(EPS*VT))*COSH(V(K3)/VT))
0226                  C(K3)=EK3
0227                  D(K3)=-EK3*(D2V(K3)+Q*GG(K3)/EPS-2.*CNI*Q*SINH(VIT)/EPS)
0228                  DO 213 I=P4,M4
0229           2515   VIT=V(I)/VT
0230                  IF(ABS(VIT)-17.)259,260,260
0231           260    WRITE(6,941)I,VIT,X(I)
0232                  V(I)=V(I)-.1*DELTA(I)
0233                  GO TO 2515
0234           259    CONTINUE
0235                  A(I)=1.
0236                  B(I)=-(2.+H4*GG*COSH(VIT))
0237                  C(I)=1.
0238                  D(I)=-H4*(D2V(I)+Q*GG(I)/EPS-2.*CNI*QE*SINH(VIT))
0239           213    CONTINUE
0240                  EK4=XH4/XH5
0241                  EK4=(XH4/2.)*(XH4+XH5)
0242           2516   VIT=V(K4)/VT
0243                  IF(ABS(VIT)-17.)261,262,262
0244           262    WRITE(6,941)I,VIT,X(I)
0245                  V(K4)=V(K4)-.1*DELTA(K4)
0246                  GO TO 2516
0247           261    CONTINUE
0248                  A(K4)=1.
0249                  B(K4)=-(1.+EK4+EK4*((2.)*CNI)/(EPS*VT))*COSH(V(K4)/VT))
0250                  C(K4)=EK4
```

```
FORTRAN IV G LEVEL  21                  MAIN                DATE = 74277          15/31/44

 0246                 D(K4)=-FK4*(D2V(K4)+Q*CC(K4)/EPS-2.*CNI*Q*SINH(VIT)/EPS)
 0247                 DO 214 I=P5,M5
 0248          2517   VIT=V(I)/VT
 0249                 IF(ABS(VIT)-170.)263,264,264
 0250           264   WRITE(6,941)I,VIT,X(I)
 0251                 V(I)=V(I)-0.1*DELTA(I)
 0252                 GO TO 2517
 0253           263   CONTINUE
 0254                 A(I)=1.
 0255                 B(I)=-(2.+H5*GG*COSH(VIT))
 0256                 C(I)=1.
 0257                 D(I)=-H5*(D2V(I)+Q*CC(I)/EPS-2.*CNI*QE*SINH(VIT))
 0258           214   CONTINUE
                C
                C          INVERSION OF TRIDIAGONAL MATRIX
                C
 0259                  CALL DIAGM3(M5,DMAX,IMAX,DELTA)
 0260                 IF(ABS(DMAX)-0.001*VT)216,216,215
 0261           215   J=J+1
 0262                 IF((J.EQ.40).OR.(J.EQ.40)
                     1            .OR.(J.EQ.50))WRITE(6,900)DMAX,IMAX,J
 0263           900   FORMAT('0','DMAX=',1PE10.2,'  AT I =',0PI5,'  FOR ITER=',I4)
 0264                 IF(J-50) 217,217,219
 0265           217   DO 218 I=1,M5
 0266           218   V(I)=V(I)+1.00*DELTA(I)
 0267                 GO TO 204
 0268           216   CONTINUE
 0269                VX1(IP+1)=V(K1)
 0270                VX2(IP+1)=V(K2)
 0271                VX3(IP+1)=V(K3)
 0272                VX4(IP+1)=V(K4)
 0273                 EX1(IP)=-(V(P2)-V(K1))/XH2
 0274                 EX2(IP)=-(V(P3)-V(K2))/XH3
                C          CALCULATION OF RF POTENTIALS
 0275                 OMEGN=2.*3.14159*FREQ/VT/UN
 0276                 OMEGP=2.*3.14159*FREQ/VT/UP
 0277                 XN2=H2*OMEGN/EN2
 0278                 XN3=H3*OMEGN
 0279                 XN4=H4*OMEGN
 0280                 XN5=H5*OMEGN
 0281                 XP2=H2*OMEGP/EP2
 0282                 XP3=H3*OMEGP
 0283                 XP4=H4*OMEGP
 0284                 XP5=H5*OMEGP
 0285                 RS2=XH3/XH2
 0286                 RS3=XH4/XH3
 0287                 RS4=XH5/XH4
 0288                 XT2=RS2-1.
 0289                 XT3=RS3-1.
 0290                 XT4=RS4-1.
 0291                 XS2=RS2+1.
 0292                 XS3=RS3+1.
 0293                 XS4=RS4+1.
 0294                 EK2=((RS2*V(M2))/(XS2*XH2))-((XT2*V(K2))/XH3)-V(P3)/(XS2*XH3)
 0295                 EK3=((RS3*V(M3))/(XS3*XH3))-((XT3*V(K3))/XH4)-V(P4)/(XS3*XH4)
 0296                 EK4=((RS4*V(M4))/(XS4*XH4))-((XT4*V(K4))/XH5)-V(P5)/(XS4*XH5)
```

```
FORTRAN IV G LEVEL  21                  MAIN                    DATE = 74277          15/31/44

0297                    CS2=H2*2.*PI*CNI/VT/EPS
0298                    CS3=H3*2.*PI*CNI/VT/EPS
0299                    CS4=H4*2.*PI*CNI/VT/EPS
0300                    CS5=H5*2.*PI*CNI/VT/EPS
                C           LOAD THE A1 DIAGONAL
0301                    J=1
0302                    A1(J  )=(1.,0.)
0303                    A1(J+1)=(0.,0.)
0304                    A1(J+2)=(0.,0.)
0305                    J=J+3
0306                    DO 301 I=P2,M2
0307                    A1(J  )=(1.,0.)
0308                    RV=(V(I+1)-V(I-1))/4./VT
0309                    A1(J+1)=CMPLX(1.,-RV,0.)
0310                    A1(J+2)=CMPLX(1.,+RV,0.)
0311                    J=J+3
0312                301 CONTINUE
                C K2
0313                    A1(J  )=CMPLX(2./XS2,0.)
0314                    A1(J+1)=CMPLX((2./XS2)+((RS2*EK2*XH2)/(XS2*VT)),0.)
0315                    A1(J+2)=CMPLX((2./XS2)-((RS2*EK2*XH2)/(XS2*VT)),0.)
0316                    J=J+3
0317                    DO 302 I=P3,M3
0318                    A1(J  )=(1.,0.)
0319                    RV=(V(I+1)-V(I-1))/4./VT
0320                    A1(J+1)=CMPLX(1.,-RV,0.)
0321                    A1(J+2)=CMPLX(1.,+RV,0.)
0322                    J=J+3
0323                302 CONTINUE
                C K3
0324                    A1(J  )=CMPLX(2./XS3,0.)
0325                    A1(J+1)=CMPLX((2./XS3)+((RS3*EK3*XH3)/(XS3*VT)),0.)
0326                    A1(J+2)=CMPLX((2./XS3)+((RS4*EK3*XH3)/(XS3*VT)),0.)
0327                    J=J+3
0328                    DO 303 I=P4,M4
0329                    A1(J  )=(1.,0.)
0330                    RV=(V(I+1)-V(I-1))/4./VT
0331                    A1(J+1)=CMPLX(1.,-RV,0.)
0332                    A1(J+2)=CMPLX(1.,+RV,0.)
0333                    J=J+3
0334                303 CONTINUE
                C K4
0335                    A1(J  )=CMPLX(2./XS4,0.)
0336                    A1(J+1)=CMPLX((2./XS4)+((RS4*EK4*XH4)/(XS4*VT)),0.)
0337                    A1(J+2)=CMPLX((2./XS4)+((RS4*EK4*XH4)/(XS4*VT)),0.)
0338                    J=J+3
0339                    DO 304 I=P5,M5
0340                    A1(J  )=(1.,0.)
0341                    RV=(V(I+1)-V(I-1))/4./VT
0342                    A1(J+1)=CMPLX(1.,-RV,0.)
0343                    A1(J+2)=CMPLX(1.,+RV,0.)
0344                    J=J+3
0345                304 CONTINUE
                C           LOAD THE B1 DIAGONAL
0346                   J=1
0347                   B1(J)=(0.,0.)
```

```
FORTRAN IV G LEVEL  21                  MAIN                    DATE = 74277          15/31/44

0348                  B1(J+1)=(0.,0.)
0349                  B1(J+2)=(0.,0.)
0350                  J=J+3
0351                  DO 315 I=P2,M2
0352                  B1(J)=(0.,0.)
0353                  B1(J+1)=(0.,0.)
0354                  B1(J+2)=CMPLX(0.,XP2)
0355                  J=J+3
0356           315    CONTINUE
              C M2
0357                  B1(J)=(0.,0.)
0358                  B1(J+1)=(0.,0.)
0359                  B1(J+2)=CMPLX(0.,XP2)
0360                  J=J+3
0361                  DO 306 I=P3,M3
0362                  B1(J)=(0.,0.)
0363                  B1(J+1)=(0.,0.)
0364                  B1(J+2)=CMPLX(0.,XP3)
0365                  J=J+3
0366           306    CONTINUE
              CM3
0367                  B1(J)=(0.,0.)
0368                  B1(J+1)=(0.,0.)
0369                  B1(J+2)=CMPLX(0.,XP3)
0370                  J=J+3
0371                  DO 307 I=P4,M4
0372                  B1(J)=(0.,0.)
0373                  B1(J+1)=(0.,0.)
0374                  B1(J+2)=CMPLX(0.,XP4)
0375                  J=J+3
0376           307    CONTINUE
              CM4
0377                  B1(J)=(0.,0.)
0378                  B1(J+1)=(0.,0.)
0379                  B1(J+2)=CMPLX(0.,XP4)
0380                  J=J+3
0381                  DO 308 I=P5,M5
0382                  B1(J)=(0.,0.)
0383                  B1(J+1)=(0.,0.)
0384                  B1(J+2)=CMPLX(0.,XP5)
0385                  J=J+3
0386           308    CONTINUE
              C             LOAD THE C1 DIAGONAL
0387                  J=1
0388                  C1(J)=(0.,0.)
0389                  C1(J+1)=(0.,0.)
0390                  C1(J+2)=(0.,0.)
0391                  J=J+3
0392                  DO 315 I=P2,M2
0393                  C1(J)=(0.,0.)
0394                  C1(J+1)=CMPLX(0.,XN2)
0395                  C1(J+2)=(0.,0.)
0396                  J=J+3
0397           315    CONTINUE
              C M2
0398                  C1(J)=(0.,0.)
```

```
FORTRAN IV G LEVEL  21                  MAIN                DATE = 74277          15/31/44

0399                C1(J+1)=CMPLX(0.,XN2)
0400                C1(J+2)=(0.,0.)
0401                J=J+3
0402                DO 316 I=P3,M3
0403                C1(J)=(0.,0.)
0404                C1(J+1)=CMPLX(0.,XN3)
0405                C1(J+2)=(0.,0.)
0406                J=J+3
0407             316  CONTINUE
                    CK3
0408                C1(J)=(0.,0.)
0409                C1(J+1)=CMPLX(0.,XN3)
0410                C1(J+2)=(0.,0.)
0411                J=J+3
0412                DO 317 I=P4,M4
0413                C1(J)=(0.,0.)
0414                C1(J+1)=CMPLX(0.,XN4)
0415                C1(J+2)=(0.,0.)
0416                J=J+3
0417             317  CONTINUE
                    CK4
0418                C1(J)=(0.,0.)
0419                C1(J+1)=CMPLX(0.,XN4)
0420                C1(J+2)=(0.,0.)
0421                J=J+3
0422                DO 318 I=P5,M5
0423                C1(J)=(0.,0.)
0424                C1(J+1)=CMPLX(0.,XN5)
0425                C1(J+2)=(0.,0.)
0426                J=J+3
0427             318  CONTINUE
                    C       LOAD THE D1 DIAGONAL
0428                  J=1
0429                  D1(J)=  CMPLX((1.+DKS*X1/DK1/XH2),0.)
0430                  D1(J+1)=(1.,0.)
0431                  D1(J+2)=(1.,0.)
0432                  J=J+3
0433                DO 325 I=P2,M2
0434                  VIT=V(I)/VT
0435                D1(J)=CMPLX(-2.-CS2*COSH(VIT),0.)
0436                D1(J+1)=CMPLX(-2.,-XN2)
0437                D1(J+2)=CMPLX(-2.,-XP2)
0438                J=J+3
0439             325  CONTINUE
                    C K2
0440                   VIT=V(K2)/VT
0441                D1(J)=CMPLX((-2./RS2)-CS2*COSH(VIT),0.)
0442                D1(J+1)=CMPLX((-2./RS2)-(XT2*XH2*EK2/RS2/VT),-XN2)
0443                D1(J+2)=CMPLX((-2./RS2)+(XT2*XH2*EK2/RS2/VT),-XP2)
0444                J=J+3
0445                DO 326 I=P3,M3
0446                  VIT=V(I)/VT
0447                D1(J)=CMPLX(-2.-CS3*COSH(VIT),0.)
0448                D1(J+1)=CMPLX(-2.,-XN3)
0449                D1(J+2)=CMPLX(-2.,-XP3)
0450                J=J+3
```

```
FORTRAN IV G LEVEL  21                MAIN                DATE = 74277          15/31/44

0451          326  CONTINUE
             C K3
0452                  VIT=V(K3)/VT
0453                D1(J)=CMPLX((-2./RS3)-CS3*COSH(VIT),0.)
0454                D1(J+1)=CMPLX((-2./RS3)-(XT3*XH3*EK3/RS3/VT),-XN3)
0455                D1(J+2)=CMPLX((-2./RS3)+(XT3*XH3*EK3/RS3/VT),-XP3)
0456                J=J+3
0457                DO 327 I=P4,M4
0458                  VIT=V(I)/VT
0459                D1(J)=CMPLX(-2.-CS4*COSH(VIT),0.)
0460                D1(J+1)=CMPLX(-2.,-XN4)
0461                D1(J+2)=CMPLX(-2.,-XP4)
0462                J=J+3
0463          327   CONTINUE
             C K4
0464                  VIT=V(K4)/VT
0465                D1(J)=CMPLX((-2./RS4)-CS4*COSH(VIT),0.)
0466                D1(J+1)=CMPLX((-2./RS4)-(XT4*XH4*EK4/RS4/VT),-XN4)
0467                D1(J+2)=CMPLX((-2./RS4)+(XT4*XH4*EK4/RS4/VT),-XP4)
0468                J=J+3
0469                DO 328 I=P5,M5
0470                  VIT=V(I)/VT
0471                D1(J)=CMPLX(-2.-CS5*COSH(VIT),0.)
0472                D1(J+1)=CMPLX(-2.,-XN5)
0473                D1(J+2)=CMPLX(-2.,-XP5)
0474                J=J+3
0475          328   CONTINUE
             C          LOAD THE E1 DIAGONAL
0476                J=1
0477                E1(J)=(0.,0.)
0478                E1(J+1)=(0.,0.)
0479                E1(J+2)=(0.,0.)
0480                J=J+3
0481                DO 335 I=P2,M2
0482                  VIT=V(I)/VT
0483                  E1(J)=CMPLX(0.5*CS2*EXP(VIT),0.)
0484                E1(J+1)=(0.,0.)
0485                E1(J+2)=(0.,0.)
0486                J=J+3
0487          335   CONTINUE
             C K2
0488                  VIT=V(K2)/VT
0489                  E1(J)=CMPLX(0.5*CS2*EXP(VIT),0.)
0490                E1(J+1)=(0.,0.)
0491                E1(J+2)=(0.,0.)
0492                J=J+3
0493                DO 336 I=P3,M3
0494                  VIT=V(I)/VT
0495                  E1(J)=CMPLX(0.5*CS3*EXP(VIT),0.)
0496                E1(J+1)=(0.,0.)
0497                E1(J+2)=(0.,0.)
0498                J=J+3
0499          336   CONTINUE
             CK3
0500                  VIT=V(K3)/VT
0501                  E1(J)=CMPLX(0.5*CS3*EXP(VIT),0.)
```

```
FORTRAN IV G LEVEL  21                  MAIN                    DATE = 74277          15/31/44

0532                E(J+1)=(0.,0.)
0533                E(J+2)=(0.,0.)
0534                J=J+3
0535                DO 347 I=P4,M4
0536                  VIT=V(I)/VT
0537                    E(J)=CMPLX(0.5*CS4*EXP(VIT),0.)
0538                E(J+1)=(0.,0.)
0539                E(J+2)=(0.,0.)
0540                J=J+3
0541           347  CONTINUE
               CK4
0542                    VIT=V(K4)/VT
0543                    E(J)=CMPLX(0.5*CS4*EXP(VIT),0.)
0544                E(J+1)=(0.,0.)
0545                E(J+2)=(0.,0.)
0546                J=J+3
0547                DO 348 I=P5,M5
0548                  VIT=V(I)/VT
0549                    E(J)=CMPLX(0.5*CS5*EXP(VIT),0.)
0550                E(J+1)=(0.,0.)
0551                E(J+2)=(0.,0.)
0552                J=J+3
0553           348  CONTINUE
               C          LOAD THE EL DIAGONAL
0554                J=1
0555                E(J)=(0.,0.)
0556                E(J+1)=(0.,0.)
0557                E(J+2)=(0.,0.)
0558                J=J+3
0559                DO 345 I=P2,M2
0560                  VIT=V(I)/VT
0561                    E(J)=CMPLX(0.5*CS2*EXP(-VIT),0.)
0562                E(J+1)=(0.,0.)
0563                E(J+2)=(0.,0.)
0564                J=J+3
0565           345  CONTINUE
               C K2
0566                    VIT=V(K2)/VT
0567                    E(J)=CMPLX(0.5*CS2*EXP(-VIT),0.)
0568                E(J+1)=(0.,0.)
0569                E(J+2)=(0.,0.)
0570                J=J+3
0571                DO 346 I=P3,M3
0572                  VIT=V(I)/VT
0573                    E(J)=CMPLX(0.5*CS3*EXP(-VIT),0.)
0574                E(J+1)=(0.,0.)
0575                E(J+2)=(0.,0.)
0576                J=J+3
0577           346  CONTINUE
               CK3
0578                    VIT=V(K3)/VT
0579                    E(J)=CMPLX(0.5*CS3*EXP(-VIT),0.)
0580                E(J+1)=(0.,0.)
0581                E(J+2)=(0.,0.)
0582                J=J+3
0583                DO 347 I=P4,M4
```

```
FORTRAN IV G LEVEL  21                  MAIN                DATE = 74277          15/31/44

0554                  VIT=V(I)/VT
0555                   F1(J)=CMPLX(0.5*CS4*EXP(-VIT),0.)
0556                 F1(J+1)=(0.,0.)
0557                 F1(J+2)=(0.,0.)
0558                 J=J+3
0559          347    CONTINUE
             CK4
0560                   VIT=V(K4)/VT
0561                   F1(J)=CMPLX(0.5*CS4*EXP(-VIT),0.)
0562                 F1(J+1)=(0.,0.)
0563                 F1(J+2)=(0.,0.)
0564                 I=J+3
0565                 DO 348 I=P5,M5
0566                   VIT=V(I)/VT
0567                    F1(J)=CMPLX(0.5*CS5*EXP(-VIT),0.)
0568                 F1(J+1)=(0.,0.)
0569                 F1(J+2)=(0.,0.)
0570                 J=J+3
0571          348    CONTINUE
             C              LOAD THE G1 DIAGONAL
0572                   J=1
0573                   G1(J  )=CMPLX(-DKS*X1/DKI/XH2,0.)
0574                   G1(J+1)=(-1.,0.)
0575                   G1(J+2)=(-1.,0.)
0576                   J=J+3
0577                   DO 351 I=P2,M2
0578                   G1(J  )=(1.,0.)
0579                   RV=(V(I+1)-V(I-1))/4./VT
0580                   G1(J+1)=CMPLX(1.,RV,0.)
0581                   G1(J+2)=CMPLX(1.,-RV,0.)
0582                   J=J+3
0583          351      CONTINUE
             C K2
0584                   G1(J  )=CMPLX(2./XS2/RS2,0.)
0585                 G1(J+1)=CMPLX(2./XS2/RS2-XH2*EK2/RS2/XS2/VT,0.)
0586                 G1(J+2)=CMPLX(2./XS2/RS2+XH2*EK2/RS2/XS2/VT,0.)
0587                   J=J+3
0588                   DO 352 I=P3,M3
0589                   G1(J  )=(1.,0.)
0590                   RV=(V(I+1)-V(I-1))/4./VT
0591                   G1(J+1)=CMPLX(1.,RV,0.)
0592                   G1(J+2)=CMPLX(1.,-RV,0.)
0593                   J=J+3
0594          352      CONTINUE
             C K3
0595                   G1(J  )=CMPLX(2./XS3,0.)
0596                 G1(J+1)=CMPLX(2./XS3/RS3-XH3*EK3/RS3/XS3/VT,0.)
0597                 G1(J+2)=CMPLX(2./XS3/RS3+XH3*EK3/RS3/XS3/VT,0.)
0598                   J=J+3
0599                   DO 353 I=P4,M4
0600                   G1(J  )=(1.,0.)
0601                   RV=(V(I+1)-V(I-1))/4./VT
0602                   G1(J+1)=CMPLX(1.,RV,0.)
0603                   G1(J+2)=CMPLX(1.,-RV,0.)
0604                   J=J+3
0605          353      CONTINUE
```

```
FORTRAN IV G LEVEL  21                MAIN                DATE = 74277          15/31/44

            C K4
0606                  G1(J  )=CMPLX(2./XS4,0.)
0607                G1(J+1)=CMPLX(2./XS4/XS4-XM4*EK4/RS4/XS4/VT,0.)
0608                G1(J+2)=CMPLX(2./XS4/XS4+XM4*EK4/RS4/XS4/VT,0.)
0609                  J=J+3
0610                  DO 354 I=M5,M5
0611                  G1(J  )=(1.,0.)
0612                  RV=(V(I+1)-V(I-1))/4./VT
0613                  G1(J+1)=CMPLX(1.*RV,0.)
0614                  G1(J+2)=CMPLX(1.-RV,0.)
0615                  I=I+3
0616           354    CONTINUE
0617                  VIL=VT
0618                  H1(1)=CMPLX(VIL,0.)
0619                  DO 355 J=2,JJ
0620           355    H1(J)=(0.,0.)
0621                  CALL DIAGM7(JJ,VILN,K1,K2,K3,K4)
0622                  VIX1(IP)=VILN
0623                  Y=REAL(VIX1(IP)/VIL)
0624                  Z=AIMAG(VIX1(IP)/VIL)
0625                  BBAR=1.-Y
0626                  CF=2.*3.14159*FREQ*CO
0627                  XIMPED=(0.,-1.)/CMPLX(CF*BBAR,-CF*Z)
0628                  RR1=REAL(XIMPED)
0629                  CAP(IP)=BBAR
0630                  RES(IP)=RR1
0631           201    CONTINUE
0632                  WRITE (6,335)
0633           335  FORMAT('1','VB',10X,'CAP',7X,'RES',11X,'VX1',9X,'EX1',9X,'EX2')
0634                  DO 356 IP=1,JV
0635           356    WRITE(6,334)VB(IP),CAP(IP),RES(IP),VX1(IP),EX1(IP),EX2(IP)
0636           334    FORMAT(' ',6(E10.3,2X))
0637                  GO TO 700
0638           219    WRITE(6,921)
0639           921    FORMAT('0','IT RATION PROCESS FAILED TO CONVERGE')
0640                  WRITE (6,935)
0641                  DO1356 JP=1,IP
0642          1356    WRITE(6,934)VB(JP),CAP(JP),RES(JP),VX1(JP),EX1(JP),EX2(JP)
0643                  GO TO 700
0644                  END
```

```
FORTRAN IV G LEVEL  21                  DIAGM3          DATE = 74277          15/31/44

0001                  SUBROUTINE DIAGM3(MM5,DMAX,IMAX,DELTA)
0002                  COMPLEX A1(1500),B1(1500),C1(1500),D1(1500)
0003                  COMPLEX E1(1500),F1(1500),G1(1500),V1(1500),H1(1500)
0004                  COMPLEX R1,R2,R3,R4,R5,XIMPED,V1X1(26),CMPLX,V1LN
0005                   DIMENSION A(500),B(500),C(500),D(500)
0006                   DIMENSION V(500),X(500),CC(500),DELTA(500),D2V(500)
0007                  DIMENSION VX1(26),VX2(26),VX3(26),VX4(26)
0008                 DIMENSION CAP(26),RES(26),VB(26),EX1(26),EX2(26)
0009                  INTEGER P1,P2,P3,P4,P5
0010                  COMMON A1,B1,C1,D1,E1,F1,G1,H1,A,B,C,D
0011                  MM5=M5-1
                C     ELIMINATION OF THE A DIAGONAL
0012                  DO 401 I=1,MM5
0013                  B(I+1)=B(I+1)-C(I)*A(I+1)/B(I)
0014                  D(I+1)=D(I+1)-D(I)*A(I+1)/B(I)
0015           401    CONTINUE
                C     BACK SUBSTITUTION
0016                  DELTA(M5)=D(M5)/B(M5)
0017                  DMAX=0.
0018                  IMAX=1
0019                  DO 402 K=1,MM5
0020                  I=MM5-K+1
0021                  DELTA(I)=(D(I)-C(I)*DELTA(I+1))/B(I)
0022                  IF(ABS(DELTA(I))-ABS(DMAX))  402,402,403
0023           403    DMAX=DELTA(I)
0024                  IMAX=I
0025           402    CONTINUE
0026                  RETURN
0027                  END
```

```
FORTRAN IV G LEVEL  21                  DIAG47              DATE = 74277          15/31/44

0001                  SUBROUTINE DIAG47(JQ,VILN,K1,K2,K3,K4)
0002                  COMPLEX A1(1500),B1(1500),C1(1500),D1(1500)
0003                  COMPLEX E1(1500),F1(1500),G1(1500),V1(1500),H1(1500)
0004                  COMPLEX X1,X2,X3,X4,X5,XIMPED,VIX1(26),CMPLX,VILN
0005                   DIMENSION A(500),B(500),C(500),D(500)
0006                  DIMENSION V(500),X(500),CC(500),DELTA(500),D2V(500)
0007                  DIMENSION VX1(26),VX2(26),VX3(26),VX4(26)
0008                 DIMENSION CIP(26),RES(26),VB(26),EX1(26),EX2(26)
0009                  INTEGER P1,P2,P3,P4,P5
0010                  COMMON A1,B1,C1,D1,E1,F1,G1,H1,A,B,C,D
                C     ELIMINATION OF THE A1 DIAGONAL
0011                  JQ1=JQ-1
0012                  JQ2=JQ-2
0013                  JQ3=JQ-3
0014                  JK2=3*(K2-K1)
0015                  JK3=3*(K3-K1)
0016                  JK4=3*(K4-K1)
0017                  DO 501 I=1,JQ3
0018                  A1R=REAL(A1(I))
0019                  A1I=AIMAG(A1(I))
0020                  IF(ABS(A1R).LT.1.E-30)A1R=10.*A1R
0021                  IF(ABS(A1I).LT.1.E-30)A1I=10.*A1I
0022                  A1(I)=CMPLX(A1R,A1I)
0023                  B1R=REAL(B1(I))
0024                  B1I=AIMAG(B1(I))
0025                  IF(ABS(B1R).LT.1.E-30)B1R=10.*B1R
0026                  IF(ABS(B1I).LT.1.E-30)B1I=10.*B1I
0027                  B1(I)=CMPLX(B1R,B1I)
0028                  C1R=REAL(C1(I))
0029                  C1I=AIMAG(C1(I))
0030                  IF(ABS(C1R).LT.1.E-30)C1R=10.*C1R
0031                  IF(ABS(C1I).LT.1.E-30)C1I=10.*C1I
0032                  C1(I)=CMPLX(C1R,C1I)
0033                  D1R=REAL(D1(I))
0034                  D1I=AIMAG(D1(I))
0035                  IF(ABS(D1R).LT.1.E-30)D1R=10.*D1R
0036                  IF(ABS(D1I).LT.1.E-30)D1I=10.*D1I
0037                  D1(I)=CMPLX(D1R,D1I)
0038                  E1R=REAL(E1(I))
0039                  E1I=AIMAG(E1(I))
0040                  IF(ABS(E1R).LT.1.E-30)E1R=10.*E1R
0041                  IF(ABS(E1I).LT.1.E-30)E1I=10.*E1I
0042                  E1(I)=CMPLX(E1R,E1I)
0043                  F1R=REAL(F1(I))
0044                  F1I=AIMAG(F1(I))
0045                  IF(ABS(F1R).LT.1.E-30)F1R=10.*F1R
0046                  IF(ABS(F1I).LT.1.E-30)F1I=10.*F1I
0047                  F1(I)=CMPLX(F1R,F1I)
0048                  G1R=REAL(G1(I))
0049                  G1I=AIMAG(G1(I))
0050                  IF(ABS(G1R).LT.1.E-30)G1R=10.*G1R
0051                  IF(ABS(G1I).LT.1.E-30)G1I=10.*G1I
0052                  G1(I)=CMPLX(G1R,G1I)
0053                  H1R=REAL(H1(I))
0054                  H1I=AIMAG(H1(I))
0055                  IF(ABS(H1R).LT.1.E-30)H1R=10.*H1R
```

```
FORTRAN IV G LEVEL  21                  DIAGM7              DATE = 74277          15/31/44

0056                    IF(ABS(H1I).LT.1.E-30)H1I=10.*H1I
0057                    H1(I)=CMPLX(H1R,H1I)
0058                    R1=C1(I+1)/D1(I)
0059                    R1R=REAL(R1)
0060                    R1I=AIMAG(R1)
0061            5013    IF(ABS(R1R)-1.E-30)5011,5012,5012
0062            5011    J=1
0063                    R1R=1.E10*(R1R+1.E-30)
0064                    J=J+1
0065                    IF(J.GT.2)GO TO 5012
0066                    GO TO 5013
0067            5012    CONTINUE
0068            5113    IF(ABS(R1I)-1.E-30)5111,5112,5112
0069            5111    J=1
0070                    R1I=1.E10*(R1I+1.E-30)
0071                    J=J+1
0072                    IF(J.GT.2)GO TO 5112
0073                    GO TO 5113
0074            5112    CONTINUE
0075                    R1=CMPLX(R1R,R1I)
0076                    R2=B1(I+2)/D1(I)
0077                    R2R=REAL(R2)
0078                    R2I=AIMAG(R2)
0079            5213    IF(ABS(R2R)-1.E-30)5211,5212,5212
0080            5211    J=1
0081                    R2R=1.E10*(R2R+1.E-30)
0082                    J=J+1
0083                    IF(J.GT.2)GO TO 5212
0084                    GO TO 5213
0085            5212    CONTINUE
0086            5313    IF(ABS(R2I)-1.E-30)5311,5312,5312
0087            5311    J=1
0088                    R2I=1.E10*(R2I+1.E-30)
0089                    J=J+1
0090                    IF(J.GT.2)GO TO 5312
0091                    GO TO 5313
0092            5312    CONTINUE
0093                    R2=CMPLX(R2R,R2I)
0094                    R3=A1(I+3)/D1(I)
0095                    R3R=REAL(R3)
0096                    R3I=AIMAG(R3)
0097            5413    IF(ABS(R3R)-1.E-30)5411,5412,5412
0098            5411    J=1
0099                    R3R=1.E10*(R3R+1.E-30)
0100                    J=J+1
0101                    IF(J.GT.2)GO TO 5412
0102                    GO TO 5413
0103            5412    CONTINUE
0104            5513    IF(ABS(R3I)-1.E-30)5511,5512,5512
0105            5511    J=1
0106                    R3I=1.E10*(R3I+1.E-30)
0107                    J=J+1
0108                    IF(J.GT.2)GO TO 5512
0109                    GO TO 5513
0110            5512    CONTINUE
0111                    R3=CMPLX(R3R,R3I)
```

```
FORTRAN IV G LEVEL  21                  DIAGM7              DATE = 74277          15/31/44

0112                  D1(I+1)=D1(I+1)-R1*E1(I)
0113                  E1(I+1)=E1(I+1)-R1*E1(I)
0114                  F1(I+1)=F1(I+1)-R1*G1(I)
0115                  H1(I+1)=H1(I+1)-R1*H1(I)
0116                  C1(I+2)=C1(I+2)-R2*E1(I)
0117                  D1(I+2)=D1(I+2)-R2*F1(I)
0118                  E1(I+2)=E1(I+2)-R2*G1(I)
0119                  H1(I+2)=H1(I+2)-R2*H1(I)
0120                  R1(I+3)=R1(I+3)-R3*E1(I)
0121                  C1(I+3)=C1(I+3)-R3*F1(I)
0122                  D1(I+3)=D1(I+3)-R3*G1(I)
0123                  H1(I+3)=H1(I+3)-R3*H1(I)
                C     IF(I-JK2)1,2,1
                C     IF (I-JK3)1,2,1
                C     IF(I-JK4)1,2,1
                C 2     WRITE(6,940)I
                940     FORMAT('0','VALUES OF THE ELEMENTS AT I =',I5)
                C     WRITE(6,927)A1(I),A1(I+1),A1(I+2)
                C     WRITE(6,928)R1(I),R1(I+1),R1(I+2)
                C     WRITE(6,929)C1(I),C1(I+1),C1(I+2)
                C     WRITE(6,930)D1(I),D1(I+1),D1(I+2)
                C     WRITE(6,931)E1(I),E1(I+1),E1(I+2)
                C     WRITE(6,932)F1(I),F1(I+1),F1(I+2)
                C     WRITE(6,933)G1(I),G1(I+1),G1(I+2)
                C     WRITE(6,934)H1(I),H1(I+1),H1(I+2)
                C     WRITE(6,935)R1,R2,R3
                C 1     CONTINUE
0124             531    CONTINUE
0125                    I=JQ2
0126                    R1=C1(I+1)/D1(I)
0127                    R2=B1(I+2)/D1(I)
0128                    D1(I+1)=D1(I+1)-R1*E1(I)
0129                    F1(I+1)=F1(I+1)-R1*F1(I)
0130                    H1(I+1)=H1(I+1)-R1*H1(I)
0131                    C1(I+2)=C1(I+2)-R2*E1(I)
0132                    D1(I+2)=D1(I+2)-R2*F1(I)
0133                    H1(I+2)=H1(I+2)-R2*H1(I)
0134                    I=JQ1
0135                    R1=C1(I+1)/D1(I)
0136                    D1(I+1)=D1(I+1)-R1*E1(I)
0137                    H1(I+1)=H1(I+1)-R1*H1(I)
                C     BACK SUBSTITUTIONV
0138                    V1(JQ3)=H1(JQ1)/D1(JQ3)
0139                    V1(JQ1)=(H1(JQ1)-F1(JQ1)*V1(JQ1))/D1(JQ1)
0140                   V1(JQ2)=(H1(JQ2)-E1(JQ2)*V1(JQ1)-F1(JQ2)*V1(JQ3))/D1(JQ2)
0141                    DO 534 K=1,JQ3
0142                    I=JQ3-K+1
0143                    V1(I)= (H1(I)-C1(I)*V1(I+1)-F1(I)*V1(I+2)-G1(I)*V1(I+3))/
                       1D1(I)
0144             534    CONTINUE
0145                    V1LN=V1(1)
0146                    RETURN
0147                    END
```

REFERENCES

1. J. L. Moll, "Variable Capacitance with Large Capacity Change," 1959 IRE WESCON Convention Record, pt-3, pp. 32-36.

2. W. G. Pfann and C. G. B. Garrett, "Semiconductor Varactors Using Surface Space-Charge Layers," Proc. IRE, vol. 47, pp. 2011-2012, Nov. 1959.

3. D. R. Frankl, "Some Effects of Material Parameters on the Design of Surface Space-Charge Varactors," Solid State Electronics, vol. 2, pp. 71-76, No. 1, 1961.

4. R. Lindner, "Semiconductor Surface Varactor," Bell Sys. Tech. J., vol. 16, pp. 803-831, May 1962.

5. A. E. Feursanger and D. R. Frankl, "High Frequency Surface Varactors," IEEE Transactions on Electron Devices, ED-10, May 1963, No. 3.

6. A. S. Grove et. al., "Investigation of Thermally Oxidized Semiconductor Structures," Solid State Electronics, vol. 8, pp. 913-921, 1965.

7. D. P. Howson, B. Owen and G. T. Wright, "The Space Charge Varactor," Solid State Electronics, 1965, vol. 8, pp. 913-921.

8. J. Marquart and B. Schick, "An Even C.V. Characteristic Parametric Amplifier Using MIS Varactors," Proc. IEEE, pp. 2076-2077, vol. 57, 1969.

9. J. Nigrin, "Exact Small Signal Study of Space Charge Varactors," Solid State Electronics, 1970, vol. 13, pp. 1267-1281.

10. B. Siegal, "The Binary Varactor - A New Microwave Device," Microwave Journal, May 1970.

11. C. T. Sah, R. F. Pierret and A. B. Tole, "Exact Analytical Solution of High Frequency Lossless MOS Capacitance-Voltage Characteristics and Validity of Charge Analysis," Solid State Electronics, 1969, vol. 12, pp. 681-688.

12. R. F. Pierret and G. Panigrahi, "Solution of Poissons' Equation Appropriate for Semiconductors with Nonconstant Impurity Profiles," Journal of Applied Physics, vol. 41, 1970.

13. V. Temple and J. Shewchun, "Exact Frequency Dependent Complex Admittance of the MOS Diode Including Surface States, Shockley-Hall-Read (SRH) Impurity Effects, and Low Temperature Dopant Impurity Response," Solid State Electronics, 1973, vol. 16, pp. 93-113.

REFERENCES (Continued)

14. G. Panigraki, "Numerical Calculation of Low Frequency Capacitance/ Voltage Curves of MOS Capacitors with Nonconstant Doping Profiles," Electronics Letters, 25th January 1973, vol. 9, No. 2.

15. L. Fox, Numerical Solution of Two Point Boundary Problems," Claredon Press, Oxford, 1957, pp. 87-89.

16. R. E. Bellman and R. E. Kalaba, "Quasilinearization and Nonlinear Boundary Value Problems," American Elsevier Publishing Co., New York, 1965.

17. H. K. Gummel, IEEE Transactions on Electron Devices, 1964, vol. ED-11, No. 10, pp. 455-465.

18. H. Wolfe, "Semiconductors," Wiley-Interscience, 1972.

19. Isaacson and Keller, "Analysis of Numerical Methods," Wiley, 1966.

20. S. D. Conte and C. de Boer, "Elementary Numerical Analysis, Sec. Ed., McGraw Hill, 1965.

21. C. T. Sah, "The Equivalent Circuit Model in Solid State Electronics," pt. I, The Single Energy Level Defect Centers, Proc. IEEE, vol. 55, No. 5, pp. 654-671, May 1967.

22. F. Hennig and C. T. Sah, "Matrix Analysis of Distributed Semiconductor Circuit Models," Solid State Electronics, 1973, vol. 16, pp. 1081-1083.

23. J.Mueller, "An Upper-Sideband Upconverter Using MIS Varactors," 1971 IEEE ISCC Digest, pp. 28-29.

24. R. L. Camisa, "Digital Tuning of Microwave Solid State Oscillators," Solid State Electronics Research Seminar, C.U.N.Y., June 21, 1971.

25. R. L. Camisa and J.Nadan , "M-ary MOS Varactor," N.Y. Chapter of Electron Devices, MOS Symposium, C.U.N.Y., 1972.

26. R. W. Burns, E. L. Holden and R. Tang, "Driverless Phase Shifter," 1973 IEEE G-MIT International Microwave Symposium, University of Colorado, June 4-6, IEEE Cat. No. 73 CHO 736-9 MTT.

27. B. V. Gokhale, "Numerical Solutions for a One-Dimensional Silicon NPN Transistor," IEEE Trans. Electron Devices, vol. ED-17, No. 8, pp. 594-602, August 1970.

28. G. Hachtel, R. C. Jay and J. W. Coaley, "A New Efficient One-Dimensional Analysis Program for Junction Device Modeling," Proc. of IEEE, Vol. 60, No. 1, Jan. 1972, pp. 86-98.

REFERENCES (Continued)

29. R. N. Hall, "Electron-Hole Recombination in Germanium," Phys. Rev., 87, 387, 1952.

30. W. Shockly and W. T. Read, "Statistics of the Recombination of Holes and Electrons," Phys. Rev., 87, 835, 1952.

31. J. Lange, "Interdigitated Strip Line Quadrature Hybrid," 1969 International Symposium Digest, IEEE Cat. No. 69C6.

32. R. E. Fisher, M. R. Barber, and J. E. Morris, "Digital-Reflection-Type Microwave Phase Shifter," Microwave Journal, Vol. 12, No. 5, May 1969, pp. 63-68.

33. J. Lange, "Interdigitated Strip Line Quadrature Hybrid," 1969 G-MTT Symposium Digest, May 1969, pp. 10-13.

34. H. A. Wheeler, "Handbook of Electromagnetics," unpublished.

35. J. Reed and G. J. Wheeler, "A Method of Analysis of Four Port Networks," IRE Trans. Microwave Theory Tech., Vol. MTT-4, pp. 246-252, Oct.

36. R. W. Vogel, "Effects of the T-junction Discontinuity on the Design of Microstrip Directional jCouplers," March 1973, IEEE Trans. on Microwave Theory and Techniques, March 1973, Vol. MTT-21, No. 3.

37. Bura et al., "Design Considerations for a 1.8 GHz Parametric Amplifier," Special issue on Microwave Integrated Circuits, IEEE Trans. on Microwave Theory and Techniques, July 1968, Vol. MTT-16, No. 7

AUTOBIOGRAPHICAL STATEMENT

Mr. Camisa received his B.E.E. and M.E.E. degrees from the City College of the City University of New York in 1965 and 1969, respectively.

From 1965 to 1967 he was a Member of the Technical Staff at the RCA Advanced Communications Laboratory, New York. While there he worked on microwave filters, low noise parametric amplifiers and microwave integrated circuit techniques.

From 1967 to 1970 he was a Member of the Technical Staff at Wheeler Laboratories, Inc., Great Neck, L.I., where he was part of a group developing a microwave integrated circuit receiver for IFF applications. Specifically, he developed various MIC components including low noise transistor amplifiers, frequency multipliers and filters.

From 1970 to 1974 he was a part time lecturer teaching courses in electromagnetic theory, electronics and microwave measurements. At the University he also worked as a graduate research assistant investigating the use of MIS varactors in microwave networks.

From 1970 to 1974 he was a consultant to Wheeler Laboratories and the RCA Advanced Communications Laboratory.

In 1974 Mr. Camisa joined the Microwave Technology Center at RCA Laboratories. His responsibilities include research on GaAs field effect transistors device technology and linear amplifier development.

Mr. Camisa has published papers on low noise parametric amplifiers, microwave integrated circuits and MIS varactors.